THE ROLES OF PI3K AND MAPK PATHWAY MUTATIONS IN GLIOMAGENESIS AND RESPONSE TO TARGETED INHIBITION

Robert Shawn McNeill

A dissertation submitted to the faculty at the University of North Carolina at Chapel Hill in partial fulfillment of the requirements for the degree of Doctor of Philosophy in the Department of Pathology and Laboratory Medicine in the School of Medicine.

Chapel Hill
2017

Approved by:

C. Ryan Miller

William B. Coleman

Cyrus Vaziri

Albert S. Baldwin

William Y. Kim

ABSTRACT

Robert Shawn McNeill: The Roles of PI3K and MAPK Pathway Mutations in Gliomagenesis and Response to Targeted Inhibition
(Under the direction of C. Ryan Miller)

Glioblastoma (GBM) is the most common malignant primary brain tumor in adults, and even with treatment, its median survival is only 12-15 months. Molecular analyses by The Cancer Genome Atlas and others have identified the genetics underlying GBM pathogenesis, but this knowledge has yet to influence therapy. The receptor tyrosine kinase (RTK) pathway is frequently mutated in GBM, including its phosphoinositide-3-kinase (PI3K) and mitogen activated protein kinase (MAPK) effector arms. Because of their mutational frequency and established role in GBM pathogenesis, these pathways are important therapeutic targets. However, results from clinical investigations of inhibitors targeting RTK/PI3K/MAPK signaling in GBM have been disappointing.

The primary aim of this dissertation was to determine how PI3K and MAPK pathway mutations influence response to targeted inhibition. We previously developed a series of non-germline genetically engineered mouse (nGEM) models in which PI3K and/or MAPK signaling were activated in immortalized astrocytes (T) by deletion of *Pten* (P) and expression of a constitutively active *Kras* mutant (R), respectively. We used these models to define how PI3K/MAPK mutations and drug potency influence signaling dynamics, efficacy, and synergism of PI3K and MEK inhibitors. We found that

PI3K/MAPK signaling are alternate bypass pathways that promote resistance to inhibition of either pathway alone. *Pten*/*Kras* mutation status and drug potency interacted to influence single agent efficacy and PI3K/MEK inhibitor synergism. Subcutaneous TRP allografts were most sensitive to dual PI3K/MEK inhibitor treatment, but target inhibition and efficacy were limited in orthotopic allografts.

PIK3CA missense mutations frequently occur in GBM, but their role in disease pathogenesis had not been experimentally validated. We therefore transduced immortalized, normal human astrocytes with lentiviral vectors encoding wild-type or mutant *PIK3CA*. We showed that mutations in the helical or kinase domains of *PIK3CA* activate PI3K signaling and cooperate with mutant *RAS* to potentiate gliomagenesis in orthotopic xenografts. *PIK3CA* mutations did not affect PI3K inhibitor efficacy, but they influenced synergism with MEK inhibition. Taken together, the work described here explored how PI3K and MAPK mutations altered response to targeted inhibition, and will inform future research into predictive biomarkers and rationale combination therapies.

ACKNOWLEDGMENTS

First, I would like to thank my advisor, Dr. C. Ryan Miller, for his support and guidance. Ryan has been a great mentor and friend over the years. He was always available to offer both scientific and career advice. Moreover, he has provided an excellent learning environment and constantly pushed me to grow as a researcher. His support has enabled me to become the scientist that I am today. I would also like to thank my past and current lab mates, particularly Ryan Bash, David Irvin, and Brian Constance. They have been excellent friends, and have helped make the Miller lab a fun place to work. I would like to acknowledge my co-authors for the previously published works described in Chapters II and III. I would also like to acknowledge the current and former undergraduates and BBSP rotation students in the Miller lab who have contributed to the data described in Chapters IV and V: Emily Stroobant, Demitra Canoutas, Madison Butler, Shrey Patel, Erin Smithberger, Juanita Limas, and Kasey Skinner.

I would like to thank Drs. Bill Coleman and Cyrus Vaziri. They have been amazing mentors over the years and have always been willing to offer me guidance in scientific and career endeavors. I greatly appreciate their help, and they have both helped me become the scientist that I am today. I would also like to acknowledge the rest of my committee, Drs. Albert Baldwin and William Kim. They have challenged me to think critically and creatively, and I have appreciated their guidance while performing my dissertation research. I am also grateful for the support that I have received from

the Department of Pathology & Laboratory Medicine, particularly Dr. Charles Jennette, Dr. Jon Homeister, Brenda Brock, and Cyndi Taylor. I am very happy I matriculated into the Pathology department after completion of my first year in BBSP. Everyone within the department has been very supportive, and I enjoyed my time as a graduate student. Also, thanks to the Wagner Scholars Program and the UNC Graduate Training Program in Translational Medicine for providing my funding.

Lastly, I would like to thank my wonderful family for their support. Thanks to my brother, Tim, for always believing in me and preventing me from becoming too serious. Thanks to my mom, Laura, for her unconditional love and support throughout my life. She has always been there to support me, and I would not have been able to accomplish everything that I have without her. I would like to thank my dad, David, for helping me become the man that I am today, and I wish he was still here to share this great accomplishment with me. Finally, I want to thank my wife and best friend Megan. She has given me so much love, support, and strength over the years. She has been by my side during the ups and downs of graduate school and I could not have done this without her.

PREFACE

Chapter II is a pre-copyedited, author-produced version of an article accepted for publication in in *Neuro-Oncology* following peer review. The version of record "McNeill RS, Vitucci M, Wu J, Miller CR. Contemporary murine models in preclinical astrocytoma drug development. Neuro Oncol. 2015;17(1):12-28" is available online at: https://doi.org/10.1093/neuonc/nou288. Doi:10.1093/neuonc/nou288.

Chapter III is a pre-copyedited, author-produced version of an article accepted for publication in in *Neuro-Oncology* following peer review. The version of record "McNeill RS, Canoutas DA, Stuhlmiller TJ, Dhruv HD, Irvin DM, Bash RE, Angus SP, Herring LE, Simon JM, Skinner KR, Limas JC, Chen X, Schmid RS, Siegel MB, Van Swearingen AED, Hadler MJ, Sulman EP, Sarkaria JN, Anders CK, Graves LM, Berens ME, Johnson GL, and Miller CR. Combination therapy with potent PI3K and MAPK inhibitors overcomes adaptive kinome resistance to single agents in preclinical models of glioblastoma. Neuro Oncol. 2017;nox044" is available online at: https://doi.org/10.1093/neuonc/nox044. Doi: 10.1093/neuonc/nox044.

TABLE OF CONTENTS

LIST OF TABLES

LIST OF FIGURES

LIST OF ABBREVIATIONS

ANOVA	Analysis of variance
ABD	Adaptor-binding domain
BBB	Blood brain barrier
BCNU	Carmustine, bis-chloroethylnitrosourea
CCNU	Lomustine, 1-(2-chloroethyl)-3-cyclohexyl-1-nitrosourea
CI	Combination index
DMEM	Dulbecco's Modified Eagle Medium
DMF	N,N-Dimethylformamide
DMSO	Dimethyl sulfoxide
ECL	Established cell lines
EGFR	Epidermal growth factor receptor
FA	Fraction affected
FBS	Fetal bovine serum
FDA	US Food and Drug Administration
GBM	Glioblastoma
geHC	Genetically-engineered human cells
GEM	Genetically-engineered mice
GEMM	Genetically-engineered mouse model
GFAP	Glial fibrillary acidic protein
GPCR	G-protein-coupled receptors
GSC	Glioma stem cell

H&E	hematoxylin and eosin
LGA	Low-grade astrocytoma
MAPK	Mitogen activated protein kinase
MEK	Mitogen-active protein kinase kinase
MEKi	Mitogen-active protein kinase kinase 1/2 inhibitor(s)
MGMT	Methylguanine-DNA methyltransferase
MIB	Multiplexed inhibitor beads
MS	Mass spectrometry
mTOR	Mechanistic target of rapamycin
mTORi	Mechanistic target of rapamycin inhibitor
NF1	Neurofibromatosis type 1
nGEM	Non-germline genetically engineered mouse
NSC	Neural stem cell
OPC	Oligodendrocyte precursor cells
P	Pten
p110α	The protein encoded by PIK3CA
p110β	The protein encoded by PIK3CB
PDX	Patient derived xenografts
PI3K	Phosphoinositide-3-kinase
PI3Ki	Phosphoinositide-3-kinase inhibitor(s)
PIK3CA	Phosphatidylinositol-4,5-bisphosphate 3-kinase catalytic subunit alpha
$PIK3CA^{mut}$	PIK3CA missense mutation
PIK3CB	Phosphatidylinositol-4,5-bisphosphate 3-kinase catalytic subunit beta

PIK3R1	Phosphoinositide-3-kinase regulatory subunit 1
PIP_2	Phosphatidylinositol (4,5)-bisphosphate
PIP_3	Phosphatidylinositol (3,4,5)-trisphosphate
PTEN	Phosphatase and tensin homolog
R	$Kras^{G12D}$
RB	Retinoblastoma
RTK	Receptor tyrosine kinase
T	N-terminal 121 amino acid truncation mutant of SV40 large T antigen
TCGA	The Cancer Genome Atlas
TMZ	Temozolomide
TP53	Tumor protein p53
T(RP)	T, TP, TR, and TRP astrocytes
WHO	World Health Organization
WT	Wild type

CHAPTER I: INTRODUCTION

The promise of precision medicine

Systematic genomic analyses of cancers, such as the NCI's precision medicine initiative, seek to individualize patient care by screening for "actionable" alterations in oncogenic pathways in order to direct treatment with targeted inhibitors.[1,2] Successful implementation of precision medicine relies upon identifying mutations which drive tumorigenesis and are predictive of drug efficacy.[3] A straightforward approach to precision medicine makes important simplifications and assumes that within a signaling pathway, activating mutations in oncogenes and loss-of-function mutations in tumor suppressor genes are equivalent for tumorigenesis and drug response. It also assumes that mutations within the same gene have equivalent effects. However, this approach does not account for potential biologic differences between loss of tumor suppressors and activation of oncogenes. It also does not reflect the potential for divergent effects of multiple mutations within the same gene.

A more nuanced and realistic approach to precision medicine accounts for the gene mutated and the specific mutation within a gene. Whether a straightforward or nuanced approach to precision medicine is required remains unclear, and may be disease and pathway specific.[3] Preclinical studies can aid in answering these questions by defining how multiple mutations within the same gene and pathway impact tumorigenesis and drug response. Furthermore, results of these studies may help

guide clinical investigations of targeted inhibitors and accelerate the clinical implementation of precision medicine.

Glioblastoma histology and molecular pathology

Diffuse gliomas are a histologically and molecularly diverse group of malignant primary brain tumors.[4,5] Glioblastoma (GBM) is the most common and aggressive glioma in adults.[6,7] Traditional diagnosis has relied purely on histology, but now histological and molecular criteria have been included in the updated WHO 2016 classification.[4,6] However, this updated classification does not reflect an improvement in GBM standard-of-care. GBM is currently treated empirically and uniformly with radiation and concurrent and adjuvant temozolomide chemotherapy, yielding a median survival of only 12-15 months and 10% 5-year survival.[8,9] Recurrence is inevitable, and alternative treatments are limited. Thus, therapies that improve GBM patient outcomes are desperately needed. Despite uniform treatment, and the absence of approved targeted inhibitors, the molecular characteristics of GBM have been well defined.[10-12] GBM is genetically heterogeneous with frequent mutations occurring in three "core" pathways: RB mediated G_1/S cell cycle checkpoint, TP53, and receptor tyrosine kinase (RTK)/ mitogen activated protein kinase (MAPK)/ phosphoinositide-3-kinase (PI3K).[10,12] Large scale transcriptome analyses have shown that GBM is composed of four molecular subtypes with distinct clinical outcomes: proneural, classical, mesenchymal, and neural.[12] Moreover, alterations in specific genes are enriched in each molecular subtype of GBM, particularly *NF1* deletions in mesenchymal, *PDGFRA* amplifications in proneural, and *EGFR* amplifications/truncations in classical.[10,12]

RTK and MAPK signaling are prime therapeutic targets in GBM, due to their

frequent activation and the myriad of drugs designed to inhibit them.[13,14] Mutations in the RTK/MAPK pathways have an established role in cancer biology, including GBM. RTK are mutated in ~67% of GBM, and their activation promotes many downstream pathways, including MAPK and PI3K.[10,15-17] MAPK signaling is frequently activated in GBM via upstream RTK mutations or by mutations in canonical MAPK genes, particularly the proto-oncogenes *KRAS* and *BRAF* and the tumor suppressor *NF1*. Moreover, activation of RTK or mutations in canonical MAPK genes cooperate with RB and/or TP53 pathway mutations to promote tumorigenesis in preclinical glioma models.[18-30]

The role of PI3K signaling in GBM pathogenesis

PI3K are a diverse group of kinases that are divided into three classes based on their structural features and lipid substrates.[31,32] Class IA PI3K (hereafter just PI3K), regulate many of the hallmarks of cancer, including proliferation and migration, and has a well-established role in cancer biology.[31-34] In contrast, the role of class II and III PI3K in cancer are less clear. PI3K are heterodimeric proteins composed of a catalytic subunit encoded by *PIK3CA*, *PIK3CB*, or *PIK3CD*, and a regulatory subunit encoded by *PIK3R1*, *PIK3R2*, or *PIK3R3*.[31,32] Regulatory subunits stabilize and constitutively inhibit the catalytic subunit in the absence of upstream activating signals. Upon activation, catalytic subunits produce the phosphatidylinositol (3,4,5)-trisphosphate (PIP_3) secondary messenger from membrane bound phosphatidylinositol (4,5)-bisphosphate (PIP_2). Furthermore, the lipid phosphatase *PTEN* antagonizes PI3K signaling via the conversion of PIP_3 to PIP_2. The PI3K pathway is activated by numerous upstream proteins that specifically interact with either the catalytic or regulatory subunit.[31,32,35] For

example, RTK interact with the regulatory subunit to activate signaling, while RAS stimulates activity by directly binding to the catalytic subunit. Moreover, catalytic isoforms differentially respond to upstream proteins.[32] Current evidence suggests that RTK preferentially activate PI3K signaling via p110α compared to p110β, the proteins encoded by *PIK3CA* and *PIK3CB* respectively. Moreover, GPCR have been shown to activate p110β, but inhibit p110α.

The canonical PI3K pathway genes *PIK3CA, PIK3R1,* and *PTEN* are mutated in 46% of GBM, with individual frequencies of 10%, 11%, and 31% respectively.[10,15,16] Mutations in these genes tend to be mutually exclusive, suggesting that they have similar roles in GBM pathogenesis. The role of *PTEN* in GBM tumorigenesis has been well-established using multiple preclinical models.[19,36-38] For instance, we found that *Pten* deletion alone is not sufficient for gliomagenesis, but it cooperates with oncogenic RAS in immortalized astrocytes to activate PI3K signaling and potentiate malignant progression.[19,37] This is consistent with the observation that somatic *PTEN* mutations often occur later in the course of GBM pathogenesis in patients, suggesting that they function in disease progression, but not initiation.[39,40] Similarly, loss-of-function *PIK3R1* mutations were recently shown to activate signaling and promote tumorigenesis in preclinical GBM models.[41] Based on the mutational frequency of *PIK3CA* and its established role in other cancers, *PIK3CA* mutations are presumed to active PI3K signaling and drive gliomagenesis.[10,32,42] However, these assumptions have not been validated in GBM models until now.

Recurrent *PIK3CA* missense mutations in GBM are restricted to three of its protein domains: helical, kinase, and adaptor binding (ABD).[15,16] Structural analyses

predict that *PIK3CA* missense mutations activate signaling via distinct mechanisms based upon the location within the mutated protein.[35,43-47] Helical domain mutations disrupt the inhibitory interactions between p110α and the nSH2 domain of p85α, a regulatory subunit encoded by *PIK3R1*. Kinase domain mutations alter the conformation of p110α activation loop, resulting in increased binding to the cellular membrane and catalytic efficiency. ABD mutations, specifically R88Q, alter the conformation of the kinase domain increasing its enzymatic activity. These predicted structural changes translate into distinct biologic effects in experimental models of non-brain tissues. For instance, helical domain mutations require RAS for activation of PI3K signaling, but not the p85α regulatory subunit.[48] Furthermore, the converse was true for kinase domain mutations. Helical and kinase domain *PIK3CA* mutations also initiate tumorigenesis and promote malignant progression in non-brain tissues, such as the breast.[42,49,50] Not as much is known about the role of the less frequent ABD domain mutations in cancer pathogenesis.[15,16] The R88Q ABD mutation has been shown to induce PI3K signaling *in vitro*, but its requirement for RAS or p85α and its role in tumorigenesis remains unclear.[51]

Targeting the RTK/MAPK/PI3K pathways in GBM

The RTK/MAPK/PI3K pathways are prime therapeutic targets in GBM because they are frequently mutated and promote gliomagenesis in preclinical models. Kinase inhibitors targeting these pathways have been clinically investigated as single agents in GBM, but results have been disappointing.[14,52,53] One reason for this is the poor brain penetrance of many targeted kinase inhibitors. For example, *EGFR* is the most frequently mutated RTK in GBM, and the success of the EGFR inhibitors gefitinib and

erlotinib in *EGFR*-mutant non-small cell lung cancer fueled clinical investigations of these inhibitors in GBM.[3,10,54] However, they do not effectively cross the blood brain barrier (BBB), limiting their therapeutic benefit in GBM.[55,56]

Drug resistance mediated by adaptive kinome reprogramming is another potential reason for the lack of efficacy of the kinase inhibitors tested in GBM. Kinase inhibitors can induce widespread kinome changes that promote drug resistance via re-activation of the targeted pathway or activation of alternate pro-tumorigenic pathways.[14,57,58] For instance, preclinical studies suggested that sensitivity to mTOR inhibitors was increased by *PTEN* loss in multiple cancer types.[59-61] The mTOR inhibitor rapamycin was therefore investigated in *PTEN*-deficient GBM patients.[62] Interestingly, rapamycin led to increased activation of the upstream kinase AKT in several patients. Moreover, AKT activation correlated with a decreased time to disease progression, suggesting that rapamycin-induced AKT activity may promote malignancy in these patients. Taken together, these clinical results highlight some of the challenges in effectively targeting the RTK/MAPK/PI3K pathways in GBM and suggest that a nuanced approach to precision medicine will be required. Furthermore, they exemplify the necessity for preclinical research that evaluates drug efficacy, determines mechanisms of drug resistance, and validates putative predictive biomarkers in a specific disease context.

Genetically engineered models enable determination of direct genotype to phenotype relationships in preclinical studies.[3,63] In contrast, tumor-derived models have more complex genomic profiles that may obscure the phenotypic consequences of individual mutations. We leveraged this advantage of genetically engineered models to characterize how PI3K and MAPK activation via *Pten* loss and a constitutively active

Kras mutant in immortalized mouse astrocytes influenced response to single agent and combination treatments with PI3K and MAPK inhibitors.[19,64] Additionally, we used genetically engineered human astrocytes to characterize the role of *PIK3CA* missense mutations in gliomagenesis and sensitivity to PI3K and MAPK inhibitors.[18] Taken together, the results described in the following chapters may aid in the design of future preclinical and clinical studies investigating predictive biomarkers and resistance mechanisms for single agent and combination treatments with targeted kinase inhibitors.

REFERENCES

1. Mendelsohn J. Personalizing oncology: perspectives and prospects. *J Clin Oncol.* 2013;31(15):1904-1911.

2. Tomczak K, Czerwinska P, Wiznerowicz M. The Cancer Genome Atlas (TCGA): an immeasurable source of knowledge. *Contemp Oncol (Pozn).* 2015;19(1A):A68-77.

3. McNeill RS, Vitucci M, Wu J, Miller CR. Contemporary murine models in preclinical astrocytoma drug development. *Neuro Oncol.* 2015;17(1):12-28.

4. Louis DN, Perry A, Reifenberger G, et al. The 2016 World Health Organization Classification of Tumors of the Central Nervous System: a summary. *Acta Neuropathol.* 2016;131(6):803-820.

5. Ceccarelli M, Barthel FP, Malta TM, et al. Molecular profiling reveals biologically discrete subsets and pathways of progression in diffuse glioma. *Cell.* 2016;164(3):550-563.

6. Louis DN, Ohgaki H, Wiestler OD, Cavenee WK, eds. *WHO classification of tumours of the central nervous system.* 4th ed. Lyon: IARC; 2007. WHO Classification of Tumours.

7. Ostrom QT, Gittleman H, Fulop J, et al. CBTRUS statistical report: primary brain and central nervous system tumors diagnosed in the United States in 2008-2012. *Neuro Oncol.* 2015;17 Suppl 4:iv1-iv62.

8. Stupp R, Hegi ME, Mason WP, et al. Effects of radiotherapy with concomitant and adjuvant temozolomide versus radiotherapy alone on survival in glioblastoma in a randomised phase III study: 5-year analysis of the EORTC-NCIC trial. *Lancet Oncol.* 2009;10(5):459-466.

9. Stupp R, Mason WP, van den Bent MJ, et al. Radiotherapy plus concomitant and adjuvant temozolomide for glioblastoma. *N Engl J Med.* 2005;352(10):987-996.

10. Brennan CW, Verhaak RG, McKenna A, et al. The somatic genomic landscape of glioblastoma. *Cell.* 2013;155(2):462-477.

11. Cancer Genome Atlas Research Network. Comprehensive genomic characterization defines human glioblastoma genes and core pathways. *Nature.* 2008;455(7216):1061-1068.

12. Verhaak RG, Hoadley KA, Purdom E, et al. Integrated genomic analysis identifies clinically relevant subtypes of glioblastoma characterized by abnormalities in PDGFRA, IDH1, EGFR, and NF1. *Cancer Cell.* 2010;17(1):98-110.

13. Roberts PJ, Der CJ. Targeting the Raf-MEK-ERK mitogen-activated protein kinase cascade for the treatment of cancer. *Oncogene.* 2007;26(22):3291-3310.

14. Cloughesy TF, Cavenee WK, Mischel PS. Glioblastoma: from molecular pathology to targeted treatment. *Annu Rev Pathol.* 2014;9:1-25.

15. Cerami E, Gao J, Dogrusoz U, et al. The cBio cancer genomics portal: an open platform for exploring multidimensional cancer genomics data. *Cancer Discov.* 2012;2(5):401-404.

16. Gao J, Aksoy BA, Dogrusoz U, et al. Integrative Analysis of Complex Cancer Genomics and Clinical Profiles Using the cBioPortal. Vol 62013.

17. Mendoza MC, Er EE, Blenis J. The Ras-ERK and PI3K-mTOR pathways: cross-talk and compensation. *Trends Biochem Sci.* 2011;36(6):320-328.

18. Sonoda Y, Ozawa T, Hirose Y, et al. Formation of intracranial tumors by genetically modified human astrocytes defines four pathways critical in the development of human anaplastic astrocytoma. *Cancer Res.* 2001;61(13):4956-4960.

19. Vitucci M, Karpinich NO, Bash RE, et al. Cooperativity between MAPK and PI3K signaling activation is required for glioblastoma pathogenesis. *Neuro Oncol.* 2013;15(10):1317-1329.

20. Holland EC, Celestino J, Dai C, Schaefer L, Sawaya RE, Fuller GN. Combined activation of Ras and Akt in neural progenitors induces glioblastoma formation in mice. *Nat Genet.* 2000;25(1):55-57.

21. Galvao RP, Kasina A, McNeill RS, et al. Transformation of quiescent adult oligodendrocyte precursor cells into malignant glioma through a multistep reactivation process. *Proc Natl Acad Sci U S A.* 2014;111(40):E4214-4223.

22. Bachoo RM, Maher EA, Ligon KL, et al. Epidermal growth factor receptor and Ink4a/Arf: convergent mechanisms governing terminal differentiation and transformation along the neural stem cell to astrocyte axis. *Cancer Cell.* 2002;1(3):269-277.

23. Uhrbom L, Dai C, Celestino JC, Rosenblum MK, Fuller GN, Holland EC. Ink4a-Arf loss cooperates with KRas activation in astrocytes and neural progenitors to generate glioblastomas of various morphologies depending on activated Akt. *Cancer Res.* 2002;62(19):5551-5558.

24. Holland EC, Hively WP, DePinho RA, Varmus HE. A constitutively active epidermal growth factor receptor cooperates with disruption of G1 cell-cycle arrest pathways to induce glioma-like lesions in mice. *Genes Dev.* 1998;12(23):3675-3685.

25. Dai C, Celestino JC, Okada Y, Louis DN, Fuller GN, Holland EC. PDGF autocrine stimulation dedifferentiates cultured astrocytes and induces oligodendrogliomas and oligoastrocytomas from neural progenitors and astrocytes in vivo. *Genes Dev.* 2001;15(15):1913-1925.

26. Alcantara Llaguno S, Chen J, Kwon CH, et al. Malignant astrocytomas originate from neural stem/progenitor cells in a somatic tumor suppressor mouse model. *Cancer Cell.* 2009;15(1):45-56.

27. Robinson JP, VanBrocklin MW, Guilbeault AR, Signorelli DL, Brandner S, Holmen SL. Activated BRAF induces gliomas in mice when combined with Ink4a/Arf loss or Akt activation. *Oncogene.* 2010;29(3):335-344.

28. Shin CH, Grossmann AH, Holmen SL, Robinson JP. The BRAF kinase domain promotes the development of gliomas in vivo. *Genes Cancer.* 2015;6(1-2):9-18.

29. Zou H, Feng R, Huang Y, et al. Double minute amplification of mutant PDGF receptor alpha in a mouse glioma model. *Sci Rep.* 2015;5:8468.

30. Liu KW, Feng H, Bachoo R, et al. SHP-2/PTPN11 mediates gliomagenesis driven by PDGFRA and INK4A/ARF aberrations in mice and humans. *J Clin Invest.* 2011;121(3):905-917.

31. Vanhaesebroeck B, Guillermet-Guibert J, Graupera M, Bilanges B. The emerging mechanisms of isoform-specific PI3K signalling. *Nat Rev Mol Cell Biol.* 2010;11(5):329-341.

32. Thorpe LM, Yuzugullu H, Zhao JJ. PI3K in cancer: divergent roles of isoforms, modes of activation and therapeutic targeting. *Nat Rev Cancer.* 2015;15(1):7-24.

33. Fruman DA, Rommel C. PI3K and cancer: lessons, challenges and opportunities. *Nat Rev Drug Discov.* 2014;13(2):140-156.

34. Hanahan D, Weinberg RA. Hallmarks of cancer: the next generation. *Cell.* 2011;144(5):646-674.

35. Vadas O, Burke JE, Zhang X, Berndt A, Williams RL. Structural basis for activation and inhibition of class I phosphoinositide 3-kinases. *Sci Signal.* 2011;4(195):re2.

36. Chow LM, Endersby R, Zhu X, et al. Cooperativity within and among Pten, p53, and Rb pathways induces high-grade astrocytoma in adult brain. *Cancer Cell.* 2011;19(3):305-316.

37. Song Y, Zhang Q, Kutlu B, et al. Evolutionary etiology of high-grade astrocytomas. *Proc Natl Acad Sci U S A.* 2013;110(44):17933-17938.

38. Schmid RS, Vitucci M, Miller CR. Genetically engineered mouse models of diffuse gliomas. *Brain Res Bull.* 2012;88(1):72-79.

39. Endersby R, Baker SJ. PTEN signaling in brain: neuropathology and tumorigenesis. *Oncogene.* 2008;27(41):5416-5430.

40. Sottoriva A, Spiteri I, Piccirillo SG, et al. Intratumor heterogeneity in human glioblastoma reflects cancer evolutionary dynamics. *Proc Natl Acad Sci U S A.* 2013;110(10):4009-4014.

41. Quayle SN, Lee JY, Cheung LW, et al. Somatic mutations of PIK3R1 promote gliomagenesis. *PLoS One.* 2012;7(11):e49466.

42. Koren S, Bentires-Alj M. Mouse models of PIK3CA mutations: one mutation initiates heterogeneous mammary tumors. *FEBS J.* 2013;280(12):2758-2765.

43. Zhao L, Vogt PK. Class I PI3K in oncogenic cellular transformation. *Oncogene.* 2008;27(41):5486-5496.

44. Huang CH, Mandelker D, Schmidt-Kittler O, et al. The structure of a human p110alpha/p85alpha complex elucidates the effects of oncogenic PI3Kalpha mutations. *Science.* 2007;318(5857):1744-1748.

45. Carson JD, Van Aller G, Lehr R, et al. Effects of oncogenic p110alpha subunit mutations on the lipid kinase activity of phosphoinositide 3-kinase. *Biochem J.* 2008;409(2):519-524.

46. Hon WC, Berndt A, Williams RL. Regulation of lipid binding underlies the activation mechanism of class IA PI3-kinases. *Oncogene.* 2012;31(32):3655-3666.

47. Gkeka P, Evangelidis T, Pavlaki M, et al. Investigating the structure and dynamics of the PIK3CA wild-type and H1047R oncogenic mutant. *PLoS Comput Biol.* 2014;10(10):e1003895.

48. Zhao L, Vogt PK. Helical domain and kinase domain mutations in p110alpha of phosphatidylinositol 3-kinase induce gain of function by different mechanisms. *Proc Natl Acad Sci U S A.* 2008;105(7):2652-2657.

49. Hanker AB, Pfefferle AD, Balko JM, et al. Mutant PIK3CA accelerates HER2-driven transgenic mammary tumors and induces resistance to combinations of anti-HER2 therapies. *Proc Natl Acad Sci U S A.* 2013;110(35):14372-14377.

50. Bader AG, Kang S, Vogt PK. Cancer-specific mutations in PIK3CA are oncogenic in vivo. *Proc Natl Acad Sci U S A.* 2006;103(5):1475-1479.

51. Oda K, Okada J, Timmerman L, et al. PIK3CA cooperates with other phosphatidylinositol 3'-kinase pathway mutations to effect oncogenic transformation. *Cancer Res.* 2008;68(19):8127-8136.

52. De Witt Hamer PC. Small molecule kinase inhibitors in glioblastoma: a systematic review of clinical studies. *Neuro Oncol.* 2010;12(3):304-316.

53. Mellinghoff IK, Schultz N, Mischel PS, Cloughesy TF. Will kinase inhibitors make it as glioblastoma drugs? *Curr Top Microbiol Immunol.* 2012;355:135-169.

54. Pao W, Chmielecki J. Rational, biologically based treatment of EGFR-mutant non-small-cell lung cancer. *Nat Rev Cancer.* 2010;10(11):760-774.

55. de Vries NA, Buckle T, Zhao J, Beijnen JH, Schellens JH, van Tellingen O. Restricted brain penetration of the tyrosine kinase inhibitor erlotinib due to the drug transporters P-gp and BCRP. *Invest New Drugs.* 2012;30(2):443-449.

56. Togashi Y, Masago K, Masuda S, et al. Cerebrospinal fluid concentration of gefitinib and erlotinib in patients with non-small cell lung cancer. *Cancer Chemother Pharmacol.* 2012;70(3):399-405.

57. Duncan JS, Whittle MC, Nakamura K, et al. Dynamic reprogramming of the kinome in response to targeted MEK inhibition in triple-negative breast cancer. *Cell.* 2012;149(2):307-321.

58. Stuhlmiller TJ, Miller SM, Zawistowski JS, et al. Inhibition of lapatinib-induced kinome reprogramming in ERBB2-positive breast cancer by targeting BET family bromodomains. *Cell Rep.* 2015;11(3):390-404.

59. Shi Y, Gera J, Hu L, et al. Enhanced sensitivity of multiple myeloma cells containing PTEN mutations to CCI-779. *Cancer Res.* 2002;62(17):5027-5034.

60. Neshat MS, Mellinghoff IK, Tran C, et al. Enhanced sensitivity of PTEN-deficient tumors to inhibition of FRAP/mTOR. *Proc Natl Acad Sci U S A.* 2001;98(18):10314-10319.

61. Yu K, Toral-Barza L, Discafani C, et al. mTOR, a novel target in breast cancer: the effect of CCI-779, an mTOR inhibitor, in preclinical models of breast cancer. *Endocr Relat Cancer.* 2001;8(3):249-258.

62. Cloughesy TF, Yoshimoto K, Nghiemphu P, et al. Antitumor activity of rapamycin in a Phase I trial for patients with recurrent PTEN-deficient glioblastoma. *PLoS Med.* 2008;5(1):e8.

63. Sharpless NE, Depinho RA. The mighty mouse: genetically engineered mouse models in cancer drug development. *Nat Rev Drug Discov.* 2006;5(9):741-754.

64. Schmid RS, Simon JM, Vitucci M, et al. Core pathway mutations induce de-differentiation of murine astrocytes into glioblastoma stem cells that are sensitive to radiation but resistant to temozolomide. *Neuro Oncol.* 2016;18(7):962-973.

CHAPTER II: CONTEMPORARY MURINE MODELS IN PRECLINICAL ASTROCYTOMA DRUG DEVELOPMENT[1]

Introduction

Oncology drug development is an inherently long and expensive process. The average time required from the initial filing of an investigational new drug application to marketing approval by the US Food and Drug Administration (FDA) is ~9 years.[1] Most oncology drugs fail late in the clinical trials process from lack of efficacy. Only 5% ultimately receive FDA approval, after a typical cost of $400 million.[2] In addition to length and cost, this inefficiency significantly limits the number of drugs with proven clinical benefit. Since nitrogen mustard (mechlorethamine) became the first cytotoxic anti-cancer agent in 1949, only 138 oncology drugs have received FDA approval – an average of 1.4 per year. The approval rate was even lower (~1 drug per year) during the era of empirical therapy with cytotoxic drugs (1949-1996). However, the rate of new drug approvals has increased dramatically (~4 per year) since the dawn of the precision medicine era of oncology,[3] marked by the 1996 approval of rituximab, the first targeted anti-cancer agent.

---

[1]A version of this work appeared as an article in *Neuro-Oncology*. The original citation is as follows: McNeill RS, Vitucci M, Wu J, Miller CR. Contemporary murine models in preclinical astrocytoma drug development. *Neuro Oncol*. 2015;17(1):12-28.

Targeted agents now constitute 36% of all FDA-approved oncology drugs. Twenty-three were approved in the last four year alone (**Fig 2.1**). Dozens more are currently in clinical trials and hundreds are in preclinical development at pharmaceutical companies and academic centers worldwide.

However, only three drugs have been approved specifically for the treatment of astrocytomas, the most common malignant primary brain tumors.[4] These include two cytotoxic agents, carmustine wafers and temozolomide (TMZ), and one targeted agent, bevacizumab. Carmustine wafers were approved for recurrent and newly diagnosed glioblastoma (GBM), a WHO grade IV astrocytoma, in 1997 and 2003. TMZ was approved for recurrent anaplastic astrocytomas (WHO grade III) and newly diagnosed GBM in 1999 and 2005. The targeted agent bevacizumab, a humanized monoclonal antibody directed against VEGF, was approved for recurrent GBM in 2009. Thus, despite the accelerated pace of oncology drug development over the past two decades, the therapeutic armamentarium for astrocytomas remains severely limited.

Histopathological classification has served as the foundation for diagnosis and management of astrocytomas for nearly a century.[5] Periodic refinement of the initial 1926 classification culminated in the current scheme, published in 2007 by the World Health Organization.[6,7] This system utilizes cytological evidence of astrocytic differentiation and the presence of morphological features, including mitotic activity, angiogenesis, and necrosis, to stratify patients into prognostically distinct diagnostic entities with increasingly poor survival. Low grade (WHO grade II) astrocytomas have a 10-year median overall survival. High-grade astrocytomas, including anaplastic astrocytomas and GBM, feature elevated mitotic activity and angiogenesis and/or

necrosis. These tumors have dismal prognoses of ~3 years and 15 months, respectively.[7] Despite their classification into distinct diagnostic entities, comprehensive genomic analyses have shown that astrocytomas of all grades are molecularly diverse.[8,9] Recognition of this fact has fueled efforts to develop a molecular classification scheme to further accelerate the shift from empirical, cytotoxic therapies to precision medicine with targeted agents in molecularly-defined tumor subsets (**Fig 2.2**).[3,8]

Although astrocytomas significantly contribute to cancer-related death and disability, they are relatively rare. GBM accounts for 86% of all astrocytomas, but only affects 3.2 in 100,000 individuals in the United States. Its incidence is age-dependent, ranging from 0.14 in children to a peak of 14.9 in 100,000 75-84 year olds.[4] Moreover, less than 20% of adult astrocytoma patients enroll in clinical trials.[10] The low prevalence and limited clinical trial participation represent significant challenges for astrocytoma drug development.

As the diagnostic and treatment landscape evolves from empirical to precision medicine, now is an opportune time to reassess the way drugs are developed for adult patients with astrocytomas (**Fig 2.2**). The reality that, relative to other cancer types, astrocytomas are rare and that trial participation is limited makes this issue even more acute. A number of innovative approaches to clinical trial design, including adaptive, biomarker-based trials, are currently under investigation and will not be the focus of this chapter.[11,12] Rather, we focus on the role of murine models in preclinical drug development for adult astrocytoma patients and will argue that fundamental changes in

their use are required to expand the therapeutic armamentarium and improve outcomes for these devastating malignancies.

Given the number of promising targeted agents that deserve clinical testing, preclinical astrocytoma modeling will be critical in validating drug targets and prioritizing candidates for clinical studies. These models will also be critical in discovery and development of novel predictive biomarkers that can be used to stratify patients into biologically meaningful disease subtypes and identify likely responders. Finally, these models will be critical in defining the molecular mechanisms of drug sensitivity and resistance so that rational combination therapies, and molecular diagnostic tests to guide their use, can be developed.

The last twenty years have witnessed major improvements in the preclinical modeling of astrocytomas. A number of recent reviews have described these in detail.[13-24] Here we examine the role of conventional mouse models in the development of cytotoxic drugs commonly used to treat adult astrocytoma patients. We then examine their use in the development of select targeted agents that have recently failed in late stage clinical trials. We will then describe contemporary mouse models and how they may be best utilized to improve clinical drug development in the future.

Development of DNA alkylating agents for GBM

Three cytotoxic, DNA alkylating agents, carmustine (bis-chloroethylnitrosourea, BCNU), lomustine (1-(2-chloroethyl)-3-cyclohexyl-1-nitrosourea, CCNU), and TMZ have been the cornerstones of astrocytoma chemotherapy for the past five decades. The nitrosoureas, BCNU and CCNU, entered clinical practice in the 1960s and were studied in a number of clinical trials through the 1990s. TMZ was developed in the late 1980s

and entered clinical practice in the mid-1990s. Here we describe the clinical development of these drugs and how animal model studies were utilized to inform their development.

Randomized phase III clinical trials of nitrosoureas in adult astrocytoma patients were published in the late 1970s.[25,26] BCNU and CCNU were initially chosen for clinical development based on their excellent ability to cross the blood-brain barrier (BBB) and their efficacy in multiple preclinical models. However, individual trial results from 1976 to 2001 were inconclusive and a meta-analysis of over 3,000 patients from twelve trials was required to definitively demonstrate their efficacy, specifically a ~2 month increase in median survival and a 5% increase in 2-year survival.[27] Although this study established chemotherapy as a valuable adjuvant to surgical resection and radiation therapy, the clinical benefits of nitrosoureas were marginal and systemic toxicity was common.

The successful culture of spontaneous tumors from chemically mutagenized rodents as established cell lines (ECL) transformed the cancer research landscape in the 1940s (**Fig 2.3A**). Development of the P388 and L1210 models of leukemia in particular were critical in development of dozens of cytotoxic drugs by the Developmental Therapeutics Program at the National Cancer Institute from the 1950s through the 1980s.[28,29] Their rapid, reproducible growth, high penetrance, and short latency when injected into syngeneic hosts made these models particularly attractive for preclinical drug studies. It is therefore not surprising, in retrospect, that the nitrosoureas were first tested and found to have efficacy in intracranial leukemia models.[30] While chemical mutagenesis had been shown to produce gliomas in rodents during the

1940s,[31] ECL and allograft models of murine gliomas, including GL26, GL261, 9L, and C6, became widespread during the late 1960s and early 1970s.[13,19,31-34] ECL cultures from human astrocytomas and xenotransplantation in immunodeficient mice were developed contemporaneously.[19,35-39] Thus, preclinical testing of nitrosoureas in glioma models occurred much later during their clinical development, with the first results published in 1973.[33] A meta-analysis of preclinical studies employing either murine allograft or human xenograft ECL models showed highly variable efficacy significantly influenced by experimental design. Overall effect sizes were small (0.19-fold and 0.43-fold increases in median survival for BCNU and CCNU, respectively) and no statistically significant beneficial effect was found.[40]

TMZ, a mono-alkylating agent developed in the 1980s, was clinically investigated due to its broad anti-tumor activity and favorable toxicity profile in preclinical models, particularly L1210 leukemias (**Fig 2.4**).[41] It was found to have excellent oral bioavailability in a phase I study. Fortunately, this trial included several high-grade astrocytoma patients who experienced partial sustained responses.[42] Subsequent clinical experience in recurrent and newly diagnosed high-grade astrocytoma patients was similarly favorable.[43] Phase II trials in recurrent high-grade astrocytomas and in combination with radiation in newly diagnosed GBM patients showed 58% radiographic response rates and 16 month median survival, respectively.[44,45] The definitive phase III trial published in 2005 established adjuvant TMZ in combination with fractionated radiation as standard-of-care for newly diagnosed GBM based on a 21% increase in median survival and a 5-fold increase in 5-year survival compared to radiation alone, which produced only 12.1 month median and 1.9% 5-year survivals.[46,47]

The first preclinical study of TMZ efficacy in GBM ECL models was published in 1994, seven years after its first description and two years after entering clinical trials.[48] A 2013 meta-analysis of TMZ in murine allograft and human xenograft ECL models of GBM showed that it was consistently efficacious in both, producing 50% decreases in tumor volume and ~2-fold increases in median survival on average.[49] This contrasts with the meta-analysis of nitrosoureas in similar preclinical models that showed far smaller and inconsistent effect sizes.[40]

The biological effects of TMZ are largely mediated by its ability to methylate the O^6 position of guanine.[50] Repair of this lesion is carried out by a single enzyme, encoded by the methylguanine-DNA methyltransferase (*MGMT*) gene. MGMT expression is regulated through promoter methylation and ~50% of GBM have methylated *MGMT*.[51] Based upon this knowledge, a retrospective companion study to the definitive phase III trial that established TMZ as standard-of-care for GBM showed that MGMT promoter methylation was a favorable prognostic and likely predictive marker for TMZ benefit in GBM patients.[52] Subsequent studies using more contemporary human GBM models whereby patient-derived tumors are directly xenografted into immunodeficient mice without prior serum-based culture showed that *MGMT* promoter methylation was an important predictor of TMZ efficacy.[53,54] TMZ given concurrently with radiation produced a survival benefit only in a subset of GBM patient-derived xenografts (PDX) models with methylated *MGMT*.[55] Moreover, TMZ showed a wider response range in PDX (0.2 to 5.9-fold increases in median survival) than in human ECL models (0.3 to 2.5-fold) of GBM, suggesting that these newer

models may more accurately reflect its clinical efficacy, particularly in molecularly defined subsets of tumors.[49,54,55]

Based on the role of MGMT in TMZ resistance and the fact that protracted, dose-dense TMZ depleted MGMT activity in peripheral blood mononuclear cells, the hypothesis that dose-dense TMZ would enhance its therapeutic benefits, particularly in GBM with unmethylated *MGMT*, was explored in a randomized, phase III clinical trial.[56-58] Although this recently published trial prospectively confirmed the prognostic significance of *MGMT* promoter methylation, dose-dense TMZ failed to improve survival in either MGMT unmethylated or methylated GBM. These results are consistent with a preclinical study in GBM PDX models that showed that TMZ induced MGMT expression, even in MGMT unmethylated GBM.[59] A similar lack of efficacy and correlation with *MGMT* methylation status was found in a preclinical study of dose-dense TMZ with seven GBM PDX models published during trial accrual.[60]

Development of targeted agents for GBM

The promise of small molecule inhibitors that target the dysregulated signaling pathways driving gliomagenesis has fueled neuro-oncology drug development since the late 1990s. The epidermal growth factor receptor (*EGFR*) had long been known to be a mutated target in GBM, where amplifications and activating truncation mutations are among the most common genetic abnormalities.[61-64] Based upon this knowledge, their anti-tumor activity in preclinical models,[65-69] and their efficacy in *EGFR*-mutant non-small-cell lung cancers (NSCLC),[70] the first generation EGFR tyrosine kinase inhibitors (TKI) gefitinib and erlotinib entered clinical trials in the 2000s (**Fig 2.5A**). However, no significant activity was found in a number of phase II GBM studies and no reliable

biomarkers to predict their efficacy could be identified in retrospective molecular analyses.[71-81] Reasons for their failure remain poorly understood, but signaling pathway redundancy and molecular heterogeneity likely contributed.[82] Subsequent pharmacokinetic (PK) studies in patients with NSCLC brain metastases showed limited CSF penetration of both gefitinib and erlotinib.[83] Moreover, expression of ABC transporters, including P-glycoprotein and breast cancer resistance protein (BRCP), were shown to significantly limit brain penetration of erlotinib.[84]

Newer EGFR TKI showed broader activity spectra and targeted multiple EGFR family receptors. Whereas first generation EGFR TKI bound only the active conformation of the EGFR TK domain, second generation TKI such as lapatinib bound the inactive conformation. It was subsequently shown using GBM ECL and neurosphere culture models that, unlike EGFR TK domain mutations characteristic of NSCLC, GBM-specific extracellular domain mutations were poorly inhibited by first-generation TKI, but effectively inhibited by lapatinib.[82] However, lapatinib showed minimal activity in recurrent GBM clinical trials.[85] Subsequent retrospective PK studies using NABTC 04-01 trial material showed intratumoral lapatinib concentrations well below its predicted therapeutic threshold.[82]

In contrast to EGFR TKI, data from preclinical glioma models significantly influenced the design of clinical trials with cilengitide, an alpha v-integrin antagonist and putative anti-angiogenic agent (**Fig 2.5B**). Cilengitide showed efficacy in subcutaneous GBM ECL xenografts in a 2001 study.[86] A subsequent phase I trial in recurrent GBM patients reported promising biological activity and demonstrated a correlation between PK parameters and radiographic response.[87] Moderate antitumor activity in the

recurrent setting was confirmed in a single-agent phase II trial, supporting its continued investigation in combination regimens.[88] Prior to those trials, preclinical studies in GBM ECL xenograft models demonstrated the radiosensitization effects of cilengitide and revealed an unanticipated dependence on schedule.[89] These preclinical data informed the design of subsequent phase I-III trials of cilengitide in combination with chemoradiation in newly diagnosed GBM.[90-92] Retrospective molecular analysis of phase II specimens suggested that *MGMT* methylation was associated with cilengitide benefit in this clinical setting.[90] However, cilengitide failed to prolong survival in newly diagnosed GBM patients with methylated *MGMT* in a randomized phase III trial.[92]

Lessons from the development of cytotoxic and targeted agents for GBM

What lessons can be gleaned from the development of alkylating and targeted agents for GBM that might improve future drug development efforts? Clinical trials of nitrosoureas and TMZ were initiated based on preclinical data from murine leukemia models. Data from glioma models came later. With the benefit of hindsight and decades of research that have conclusively demonstrated that neoplasms from different tissues are molecularly and biologically distinct, it is now clear that the decision to initiate clinical studies should be based on preclinical data in the tumor type of interest. Preclinical data from models that do not accurately reflect the tumor histology or its native organ-based microenvironmental interactions are likely to produce misleading results.[28,93]

However, comparison of alkylating agent efficacy in preclinical glioma models and clinical studies demonstrates striking similarities. Nitrosoureas produced small, but significant benefits in some murine models and astrocytoma patients. In contrast, TMZ

was consistently effective in both ECL model studies and clinical trials, with relatively large effect sizes. These data suggest that large effect sizes in multiple preclinical models may be required to accurately predict efficacy in clinical trials, particularly those that enroll molecularly heterogeneous, unselected patient populations. We therefore recommend that the bar for future preclinical drug studies be set well beyond small, but statistically significant prolongations of survival in single model systems, particularly ECL models. Rather, consistent demonstration of large effect sizes in newer model systems that more accurately recapitulate the genomic and biological properties of human astrocytomas may have increased ability to predict clinical efficacy in unselected patient populations.

How do newer model systems, such as PDX, fare in predicting clinical success relative to conventional ECL models? Preclinical studies with nitrosoureas and cilengitide were only conducted in ECL models (**Table 2.1**). Many of the same ECL models were also used in the initial preclinical development of TMZ (**Fig 2.4**), as well as the EGFR TKI gefitinib and erlotinib (**Fig 2.5**). However, the more recent preclinical TMZ and EGFR TKI studies utilized PDX models to characterize genetic mechanisms of response and resistance, and discover predictive biomarkers.[53-55,59,60,68,69,94-96] Thus, the fact that TMZ succeeded clinically, while EGFR TKI and cilengitide failed, cannot be attributed simply to use of newer model systems in preclinical development. Comprehensive comparison of drug efficacy in newer PDX versus conventional ECL models is limited to TMZ. Such data suggest that PDX models may more accurately reflect the heterogeneity of response seen in GBM patients. Therefore, systematic drug efficacy screening in multiple genomically characterized PDX models might be useful for

prospective identification of molecularly-defined subsets of tumors that are likely to respond.[18,97] In order to evaluate the predictive accuracy of these models and maximize their utility for biomarker discovery and development, preclinical studies in PDX models should be performed earlier in the drug development process, ideally prior to initiating clinical trials or concurrently as "co-clinical trials."[98]

Rather than relying on data from preclinical models, predictive biomarker discovery for TMZ and EGFR TKI was largely conducted by retrospective molecular analyses of clinical trial specimens. Of the above examples, only the phase III cilengitide trial utilized prospective molecular stratification of *MGMT*-methylated GBM to increase molecular homogeneity and enrich for likely responders. While this approach is critical for clinical biomarker validation and required for their eventual incorporation as an inclusion criterion in prospective trials, retrospective analyses are inefficient because they require completion of the trial. Given the limited incidence and trial participation of astrocytoma patients, we would argue that a more efficient approach for the discovery of predictive biomarkers would be an increased reliance on preclinical drug studies in genomically and biologically faithful murine models. Such markers could then be validated in retrospective molecular studies of clinical trial specimens. Indeed, this approach has been applied to investigate the ability of a prognostic gene expression signature to predict bevacizumab efficacy in mesenchymal GBM.[99-102] Increased use of this approach for future drug development is likely to reduce time and costs and improve the efficiency of clinical trials.

Nitrosoureas and TMZ were attractive clinical candidates due to their lipophilic chemical structures and favorable brain PK profiles. Indeed, their ability to penetrate

the BBB and reach diffusely infiltrative tumor cells is likely one reason for their clinical efficacy.[103] In contrast, the failure of first and second generation TKI to fulfill the promise of EGFR targeted therapy was likely due in part to their poor brain PK and the activity of BBB drug efflux pumps. Unfortunately, CNS neoplasms are a frequent exclusion criterion in phase I studies and brain PK is not routinely analyzed during early development of many targeted agents. The unfortunate failure of EGFR TKI clearly demonstrates the importance of such data. Preclinical PK studies in both glioma models and mice with genetically engineered defects in BBB efflux pumps have the potential to predict clinical failure on the basis of poor PK if used prior to, or concurrent with, the initiation of advanced clinical trials.

In addition to poor brain PK, receptor tyrosine kinase (RTK) signaling pathway redundancy and inter-tumoral molecular heterogeneity likely contributed to the clinical failures of first-generation EGFR TKI. Although they share *EGFR* mutations in common, the divergent efficacy of these drugs in NSCLC and GBM demonstrates that mutation status of a biologically attractive target gene alone is insufficient to predict efficacy of inhibitors that specifically target its activity. Rather, preclinical and clinical data with these drugs in NSCLC and GBM demonstrate that mutation location, within specific functional domains, and its impact on protein structure and catalytic activity is equally important in determining efficacy. Moreover, these data suggest that current precision medicine initiatives that utilize next generation sequencing to identify "actionable" somatic mutations in oncogenic kinases may require more nuance to fulfill their potential of targeted therapy. Indeed, success of such efforts rests on three critical assumptions: 1) that the identified mutation activates downstream signaling and

promotes tumorigenesis in the specific tumor type in which it is found; 2) that the mutated kinase is sensitive to drug inhibition in the appropriate anatomical context (e.g. lung versus brain); and 3) that inhibition results in clinical benefit in the specific tumor type of interest. Because the biological function and druggability of mutational targets are likely tissue specific, it stands to reason that experimental evidence, such as that provided by contemporary preclinical model studies, is necessary to prove the "actionability" of drug-targetable gene mutations in the specific clinical context to be investigated.

Astrocytoma genomic heterogeneity and its impact on drug development

Over the last 15 years, advances in genomics and DNA sequencing technologies have revolutionized cancer research. Studies have conclusively demonstrated that significant inter-tumoral heterogeneity exists on multiple molecular levels, both within and among the three diagnostic categories of astrocytomas.[9,104,105] The transcriptome profiles of lower grade astrocytomas (WHO grades II and III) and GBM are distinct[102,103] and each consists of three or four transcriptomal subtypes.[61,64,106,107] Particular patterns of somatic mutations, chromosomal alterations, and DNA methylation are evident not only within each grade, but also within grade-specific subtypes.[61,64,108] For example, the *IDH1* and *IDH2* genes are mutated in ~60-80% of lower grade astrocytomas and ~50-80% of the secondary GBM into which they inevitably progress, but only ~3-7% of primary GBM that arise *de novo* without a clinically detectable, lower grade antecedent.[109] Lower grade astrocytomas that lack IDH mutations have transcriptome and copy number profiles similar to GBM. A molecular classification system that supplements histological classifiers with layers of molecular information promises to

provide a diagnostic framework that not only reflects the inter-tumoral heterogeneity present in these neoplasms, but facilitates more accurate prognostic stratification and prediction of therapeutic response to targeted therapies.[8,9]

Many of the putative oncogenic driver mutations in astrocytomas occur in genes that comprise three core signaling pathways – the G1/S cell cycle checkpoint controlled by the Rb family of pocket proteins, RTK and their downstream RAS-mitogen activated protein kinase (MAPK) and phosphoinositide 3-kinase (PI3K) effector pathways, and the *TP53* pathway.[63] Dozens of drugs are currently in development to inhibit kinases in these pathways and many are actively being investigated in astrocytoma clinical trials. However, given limited trial participation, low disease prevalence, and the number of promising targeted agents that deserve clinical testing, a more rational approach to preclinical drug development for astrocytomas is required.

In addition to inter-tumoral heterogeneity, genomics studies have shown significant molecular heterogeneity within individual astrocytomas as well.[110-113] Sequencing data from multiple samples of individual tumors has demonstrated coexistence of spatially distinct clones with divergent mutational and transcriptomal profiles. Phylogenetic reconstruction showed patient-specific patterns of evolution within each tumor.[111,112] Moreover, treatment of lower grade astrocytomas with DNA damaging agents such as TMZ may modify the evolutionary path to high-grade disease by inducing alternative mutational spectra.[112] Similarly, comprehensive fluorescence *in situ* hybridization studies have shown that multiple RTK genes, including *EGFR*, *MET*, and *PDGFRA*, can be simultaneously amplified not only within spatially distinct subpopulations of tumor cells, but within individual tumor cells as well.[114] This mosaic

gene amplification can lead to coactivation of multiple redundant RTK signaling pathways, limiting the effectiveness of inhibitors targeting individual kinases and suggesting the need to develop rational combination therapies.[115]

In addition to molecular heterogeneity, murine modeling studies of human GBM have suggested that individual cells within the tumor may be functionally heterogeneous.[116] The cancer stem hypothesis posits that a small subpopulation of tumor cells, termed cancer stem cells (CSC), are uniquely capable of tumor maintenance and hierarchical differentiation into multiple tumor cell lineages.[117-119] CSC have been proposed as a cause of therapeutic resistance and tumor recurrence.[120] Their implications in astrocytoma biology and drug development have been previously reviewed in detail.[121-125]

GBM subtypes may have distinct treatment responses.[64] Although transcriptome profiling was recently evaluated in the trial of bevacizumab in combination with standard-of-care therapy for newly diagnosed GBM,[99,102] it is remains unclear how this measure of inter-tumoral genomic heterogeneity should be incorporated in future clinical trials. It is likely that novel drug efficacy will be restricted to specific molecular subtypes with unique mutational, epigenetic, or CSC profiles. However, the ideal molecular diagnostic approach to prospectively identify likely responders has yet to be developed. How should molecular profiles be incorporated into clinical trial design to account for the heterogeneity present in astrocytomas? In the absence of definitive data on their prognostic and predictive significance, a prudent approach would be to retrospectively characterize genomic heterogeneity in clinical trial specimens on as many molecular levels as is economically feasible. An even more cost-effective approach may be to

conduct preclinical drug studies, either before or in parallel with clinical trials, using biologically diverse panels of contemporary murine models that have also been comprehensively profiled.

Conventional and contemporary murine models of astrocytomas

Like diagnosis and therapy, the last two decades have witnessed major improvements in preclinical modeling of astrocytomas (**Figs 2.2**, **2.3**). A number of recent reviews have described these improvements in detail.[13-24] Here, we compare contemporary with conventional ECL models and discuss how they may be utilized to improve preclinical astrocytoma drug development.

Established cell line (ECL) models

ECL cultured from rodent astrocytomas induced by chemical mutagenesis transformed the preclinical drug development landscape in the late 1960s (**Fig 2.3A**).[13,19,31-38] These technically straightforward, highly penetrant models were widely disseminated and developed tumors with rapid, uniform growth kinetics, and short latency when transplanted subcutaneously or orthotopically in the brains of murine hosts (**Table 2.2**). Many recapitulated the histopathological features of human high-grade astrocytomas, including their diffuse invasion of normal brain. Orthotopic murine allograft models were particularly attractive for the development of drugs targeting tumor-stroma interactions or immune-modulatory therapies because tumorigenesis could be induced in the native brain microenvironment in immunocompetent, syngeneic mice.[13,19]

Developed in the late 1960s through the 1980s, xenograft models using ECL cultured from human astrocytomas shared many of the attractive features of murine

allograft models. Because ECL originated from human tumors, extrapolation of experimental results were uncomplicated by molecular and physiological differences between mice and humans. However, many failed to recapitulate the brain invasive histopathology of human astrocytomas.[20,126,127] The requirement for immunodeficient hosts also rendered examination of microenvironmental and immune influences on drug response impossible.

Comprehensive genomics analyses of both murine and human ECL models identified a number of additional limitations. Phenotypic and genotypic drift due to clonal selection upon serial culture of adherent cells in serum-containing media rendered ECL markedly different from their original tumor.[19] ECL cultured under these non-physiological conditions adapted to the presence of abundant nutrients by increasing metabolic and proliferation programs and to their artificial micro-environment by decreasing cell adhesion. Thus, ECL frequently developed uncharacteristic and complex chromosomal abnormalities and their molecular profiles differed significantly from acutely-isolated GBM samples.[128-131] Although genomic analyses have defined the mutational landscapes of many astrocytoma ECL, their abundance of mutations and complex chromosomal alterations render genotype-phenotype comparisons difficult.

Subcutaneous ECL models remain a popular method of assessing both *in vivo* tumorigenesis and drug efficacy due to the technical ease of monitoring growth kinetics in this anatomic compartment. Nevertheless, these models fail to account for native microenvironmental influences on tumor pathogenesis and drug response and do not accurately model PK effects of the BBB. Targeted agents, such as palbociclib, that show efficacy in subcutaneous xenografts have failed when tested in orthotopic models

due to drug efflux pumps at the BBB.[132] The molecular profiles of ECL xenografted subcutaneously markedly differ from corresponding orthotopic xenografts.[133] Tumor location can also significantly impact molecular and biological responses to cytotoxic therapies, such as radiation.[134] Because subcutaneous ECL models can over-estimate the therapeutic potential of novel agents, their use should be restricted to validation of therapeutic targets in biological proof-of-principle experiments and their role in prioritizing drugs for clinical investigation should be minimized.

Patient-derived xenograft (PDX) models

Many of the shortcomings of ECL models can be directly attributed to their serial culture as adherent cells in serum-containing media. Some of these have subsequently been overcome through development of PDX (**Fig 2.3B**), whereby fresh tumor tissue fragments are directly injected into the brain or serially passaged subcutaneously in immunodeficient mice. Alternatively, PDX can be cultured as non-adherent spheroids in growth factor-defined, serum-free medium prior to orthotopic transplantation.[15,19,135] Development of these techniques have been critical in defining the functional heterogeneity present in human astrocytoma cells and exploring the biological and therapeutic implications of the CSC hypothesis in these tumors.[121-125]

PDX share many of the advantages of ECL models for preclinical drug development, including high penetrance, short latency, and rapid, uniform growth kinetics *in vivo*. However, unlike ECL, PDX maintain the genomic features of the tumors from which they were derived and faithfully recapitulate the molecular profiles and histopathological features of GBM, including diffuse brain invasion.[19,136-141] Although their cellular origin is undefined and their genomic complexity renders

elucidating the phenotypic consequences of individual oncogenic mutations difficult, when studied in multi-model panels, PDX more broadly recapitulate the inter-tumoral genomic heterogeneity evident in GBM.[137] As such, systematic drug screening in these models has the potential to more accurately reflect clinical activity of novel drugs and to more readily identify predictive molecular characteristics. The multi-institutional Ivy Genomics-based Medicine Project is currently utilizing this approach to investigate both novel and conventional cytotoxic agents and develop predictive biomarkers in a genomically diverse panel of PDX models.[18,97]

Genetically engineered human cell (geHC) models

Models using genetically engineered normal human brain cells (geHC) have been recently developed to overcome some of the limitations of human astrocytoma ECL and PDX models (**Fig 2.3C**). These models were generated by purifying specific cell types, such as astrocytes or neural stem cells, from normal human brains and using standard molecular biology techniques to engineer their expression of specific oncogenic mutations.[142-145] By virtue of their design, these genetically-defined models permit direct determination of the phenotypic consequences of astrocytoma associated mutations in specific neural cell types. Their serial culture *in vitro* is generally unaccompanied by additional genomic abnormalities.[144] While penetrance, growth kinetics, and latency vary based on mutations and cellular origin, many geHC models give rise to diffusely infiltrative astrocytomas when orthotopically injected into the brains of immunodeficient mice.

Genetically engineered mouse (GEM) models

Genetically engineered mouse (GEM) models revolutionized basic cancer research in the 1990s. Over the past two decades, dozens of astrocytoma GEM models have been developed to dissect the genetics of *de novo* tumorigenesis in the native brain microenvironment (**Fig 2.3D**).[19,20] Because knockout and transgenic GEM harbored engineered mutations in all cell types, embryonic lethality precluded study of genes critical for development.[20] GEM that utilized conditional alleles were subsequently developed to overcome this limitation and to spatially restrict oncogenic mutations to defined cell types within the brain. Conditional, inducible and somatic gene transfer GEM, including the RCAS-tva system, were designed to facilitate temporal as well as spatial control of mutations. The value of these models in basic astrocytoma research has been reviewed extensively elsewhere.[16-24] Here we focus on their use in astrocytoma drug development.

A number of factors inherent in the design of astrocytoma GEM models has limited their use in preclinical drug development, particularly for studies evaluating drug efficacy by conventional clinical endpoints – radiographic response and overall survival.[146-149] Whereas single oncogenic alleles are sufficient to induce tumorigenesis in medulloblastoma models, multiple mutations are typically required to induce astrocytoma tumorigenesis in GEM.[20,150,151] Conditional GEM models require complex and often inefficient breeding schemes to generate sufficiently large cohorts for preclinical drug studies. RCAS/tva GEM are much more amenable because multiple pre-defined, oncogenic alleles can be simultaneously introduced into specific neural cell types using a single transgenic mouse line engineered to express tva receptors.[20,152]

However, because RCAS retroviral vectors are required, these models are limited to the transformation of endogenously proliferative cell types.[152] High-grade astrocytoma tumorigenesis typically occurs with variable penetrance after relatively long periods of latency in these model systems. Moreover, GBM develop in a temporally heterogeneous, stochastic manner. Therefore, the presence and location of tumors in individual mice must be confirmed by radiographic imaging prior to treatment initiation and intermittently thereafter in order to monitor drug response *in vivo*.[20,152-154] Taken together, these features make preclinical drug studies in astrocytoma GEM long, cumbersome, and expensive.

Non-germline genetically engineered mouse (nGEM) models

Non-germline GEM (nGEM) models overcome many of the limitations of GEM and may be more amenable to preclinical drug studies. Like geHC, nGEM models utilize cultures of specific cell types harvested from GEM brains, including astrocytes and neural stem cells (**Fig 2.3D**).[127,155-159] They harbor defined genetic mutations and their serial culture is generally unaccompanied by additional genomic abnormalities (unpublished observations). While penetrance and latency vary with mutations and cellular origin, nGEM astrocytomas developed with uniform growth kinetics *in vivo* when injected into syngeneic, immunocompetent hosts, precluding the need for radiographic screening.[127] Like ECL, PDX, and geHC, these cells can be readily modified genetically to express luminescence proteins to facilitate monitoring of disease burden and drug response with bioluminescence imaging.[53,160] Both geHC and nGEM models enable direct determination of genotype-phenotype relationships. Unlike ECL and PDX, these models can be used to define the oncogenic roles of single mutations and the

cooperative roles of multiple mutations during tumorigenesis. They are thus uniquely suited for the systematic validation of putative oncogenic "driver" mutations identified in large-scale genome characterization projects.[161] Because geHC and nGEM grow *in vitro* and *in vivo* and feature defined genomic landscapes, these models can also be used to unambiguously define the genetics of drug response and resistance.

Moreover, nGEM may be useful in dissecting the role of individual mutations and their cellular origin in generating genomic diversity of human astrocytomas. As such, subtype-specific nGEM models of GBM may be developed for drug development. We have recently published an nGEM model derived from G1/S-defective astrocytes with activated MAPK and PI3K signaling that molecularly mimics proneural human GBM.[64,127] However, in contrast to ECL, PDX, and geHC models, nGEM models utilize syngeneic, immunocompetent hosts and may be useful in development of drugs targeting tumor-stroma interactions or immune-modulatory therapies.

Modeling low grade astrocytomas

Despite advances in modelling techniques, murine models that mimic the natural history of low grade astrocytomas (WHO grade II) in humans have been difficult to develop. These tumors generally fail to become established when cultured *in vitro* or grow when transplanted into immunodeficient mice. In fact, *in vivo* tumorigenesis has long been known to correlate with histological grade and poor prognosis.[162] Thus, human ECL and PDX models of low grade astrocytomas are virtually non-existent. Their absence has significantly impeded study of the genetics of malignant progression and the development of effective drugs for these tumors. However, several GEM models have recently been described that develop clinically silent, but

histopathologically detectable low grade astrocytomas.[154,163] These tumors progressively expand over time, spontaneously acquire additional mutations, and undergo malignant progression to lethal, high-grade disease.[164] Despite their initiation by a limited number of oncogenic mutations, malignant progression in these GEM results in GBM with transcriptomes that recapitulate the full spectrum of human subtypes.[153,154] Moreover, we have genomically characterized multiple, spatially distinct GBM that developed in different brain regions of individual mice and found that their genomic landscapes differ, suggesting that divergent genetic evolution occurs in these models (Vitucci et al, submitted).[164] These GEM models therefore may be uniquely suited to define the genetics of malignant progression, the prognostic impact of TMZ-induced hypermutation in low grade astrocytomas,[112,165] and the development of novel treatments to prevent or delay their progression.

IDH1 and *IDH2* mutations are subtype-defining genetic features of lower grade astrocytomas (The Cancer Genome Atlas Research Network, manuscript submitted).[107,109] However, effective preclinical models for the development of IDH-mutant astrocytoma therapies are scarce. Most studies published to date have used stably transfected ECL or geHC to investigate the biological effects of IDH mutations *in vitro*.[166-174] Adherent, serum cultures of IDH-mutant astrocytomas have been shown to lose the mutant allele upon serial passage and mutant-containing clones fail to become ECL.[175] In contrast, four *IDH1*^{R132H}-mutant anaplastic gliomas (WHO grade III) have been successfully cultured as neurospheres *in vitro*.[176-179] However, only two of these, both from anaplastic oligodendroglial neoplasms, formed serially transplantable gliomas

in the immunodeficient mouse brain. Thus, only two potential PDX models are currently available for preclinical IDH-mutant glioma drug development.[178,179]

The initial attempt to develop a GEM model of IDH-mutant gliomas was also disappointing.[180] Conditional activation of a heterozygous, floxed IDH1^{R132H} mutant allele using Nestin-cre or Gfap-cre drivers failed to elicit tumorigenesis in the developing mouse brain, despite production of the oncometabolite D-2-hydroxyglutarate (D2HG). Rather, D2HG blocked collagen maturation and altered vascular basement membranes, leading to brain hemorrhage and embryonic lethality. These results suggest that IDH1 mutations alone are not sufficient to induce tumorigenesis, at least in the developing mouse brain. However, the effects of IDH1^{R132H} have not been examined in the adult brain. It therefore remains possible that temporal control of IDH1^{R132H} induction in the adult mouse brain using drug-inducible Cre drivers may be more successful in modeling IDH-mutant gliomas.

Alternatively, successful culture and xenografting of IDH-mutant human gliomas, as well as GEM modeling, may require the presence of cooperative oncogenic mutations. geHC and nGEM represent attractive model systems to explore this hypothesis. In this regard, the IDH1^{R132H} mutation has been shown to impair histone demethylation in immortalized normal human astrocytes (NHA).[173] IDH1^{R132H} also remodeled the DNA methylome of these cells and was sufficient to induce the glioma CpG island methylator (G-CIMP) phenotype.[174] Moreover, IDH1^{R132H} blocked astrocytic differentiation in neurosphere cultures of neural stem cells harvested from neonatal *Ink4a*/*Arf* null GEM.[173] When engineered to express mutations in the RAS-MAPK and PI3K pathways, immortalized human and murine astrocytes have been shown to induce

tumorigenesis upon transplantation into mouse brains.[127,143,144,181] Thus, IDH-mutant geHC or nGEM brain cells with additional engineered mutations may represent promising preclinical systems for development of IDH targeted therapies.

Contemporary murine models in preclinical astrocytoma drug development

Murine models can address a number of issues important in the clinical drug development for astrocytomas. These include validation of molecular targets, defining the role of cellular origin in drug response, prioritizing drugs for clinical development, and developing predictive markers to identify potential responders (**Table 2.3**). The ideal model(s) to address these issues differs based on the inherent strengths and weaknesses of their design.

GEM have established roles in the validation of molecular targets, particularly in defining the role of putative oncogenic drivers in the initiation and progression of tumorigenesis. Because of their genetic tractability, nGEM and geHC models are poised to supplement GEM in future target validation efforts. Indeed, we utilized nGEM models to establish that cooperativity between MAPK and PI3K signaling is required for GBM pathogenesis *in vivo*, suggesting that simultaneous inhibition of both pathways may be required for effective therapeutic design.[127] Moreover, geHC models with human astrocytes proved critical in defining the effects of IDH mutations on the epigenetic control of tumor cell differentiation.[173]

In addition to target validation, GEM, nGEM, and geHC models may be useful in defining the impact of cellular origin on astrocytoma tumorigenesis and drug sensitivity.[20] Like high-grade astrocytomas, multiple genomic subtypes of medulloblastoma with distinct mutations exist.[182] GEM models have shown that

different oncogenic mutations in specific cells of origin in the developing mouse cerebellum lead to distinct genomic subtypes of medulloblastoma that mimic their human counterparts. GEM models of sonic hedgehog-associated medulloblastoma in particular are currently being utilized for the preclinical evaluation of subtype-specific targeted therapies.[150]

PDX and GEM models with defective ABC transporters have established roles in characterizing CNS PK.[132,183] The advantages of PDX, nGEM, and geHC over ECL models promise to replace their use in defining dose and schedule dependencies of combination therapies for GBM.[89] Due to the redundancies of RTK signaling, mosaic amplification of multiple RTK in GBM, and significant inter- and intratumoral molecular heterogeneity, mono-therapy with single targeted agents will likely prove ineffective for GBM.[105] Increasing use of contemporary PDX, nGEM, and geHC models in preclinical development of these agents is likely to aid in defining and further characterizing these mechanisms of drug resistance. Because these cells can be cultured *in vitro*, synthetic lethality screens or kinome profiling promises to aid definition of rational combination therapies to combat drug resistance.[184] Moreover, more systematic use of multiple genomically diverse models in preclinical drug efficacy screens promises to aid development of predictive genomic biomarkers.[18,97]

Conclusion

Despite decades of research, the therapeutic armamentarium of approved drugs for astrocytomas remains limited. The field of neuro-oncology has yet to benefit from the accelerated pace of oncology drug development due to issues of prevalence, trial participation, and biological complexity of the disease. However, comprehensive

genomic characterization and changes in clinical trial design promise to improve disease classification and increase the number of targeted agents that can be clinically evaluated. Improvements in preclinical murine models and their systematic integration by the neuro-oncology community during early drug development promises to further accelerate therapeutic advances for these devastating malignancies.

Table 2.1. GBM models used in preclinical development of alkylating and targeted agents

Chemotherapeutic agent		Conventional ECL models		Contemporary models	
		Murine allografts	Human xenografts	PDX	nGEM
Alkylating agents	Carmustine (BCNU)	9L [40] GL26, GL261 VMDk 497-P(1)	D54MG [40] U251MG		
	Lomustine (CCNU)	G XII [40] G XIII GL26, GL261 VMDk 497-P(1)	U251MG [40]		
	Temozolomide (TMZ)	9L [49] C6 F98 T98	A172 [49] D54MG, Hs683 SNB-75, SF295 U251MG, U373MG U87MG	GBM6 [49,53-55,59,60,94-96] GBM8, GBM10, GBM12 GBM14, GBM22, GBM 26 GBM34, GBM36, GBM39 GBM43, GBM44	TRP [127,185,186]
Targeted agents	Gefitinib		U87MG [67]	ODA-4-GEN [69] GBM-1-HAM, GBM-17-ROM GBM-14-RAV, TG-17-GIR GBM-9-THI	
	Erlotinib		U87MG [66]	GBM6, GBM8 [68] GBM12, GBM14, GBM15 GBM22, GBM 28 GBM34, GBM36, GBM39 GBM44	
	Lapatinib			GS676, GS600 [82]	
	Celingitide		U87MG [86] U251MG [89]		

Table 2.2. Comparison of conventional and contemporary murine astrocytoma models

Characteristic		Conventional ECL models		Contemporary models			
				Human xenografts		Engineered mice	
		Mouse allografts	Human xenografts	PDX	geHC	GEM	nGEM
Host	Intact immune system	Y [a]				Y	Y
	Faithful microenvironment	Y				Y	Y
	Intact DNA repair	Y	Y [b]	Y [b]	Y [b]	Y	Y
	Host and tumor genomes differ		Y	Y	Y		
Tumor	*In vitro* culture possible	Y	Y	Y	Y		Y
	Subcutaneous growth	Y	Y	Y	Y		Y
	Orthotopic growth	Y	Y	Y	Y	Y	Y
	Histologically faithful	Y [c]		Y	Y	Y	Y
	Rapid growth kinetics	Y	Y	Y	Y	[d]	[d]
	High penetrance	Y	Y	Y	Y	[d]	[d]
	Short latency	Y	Y	Y	Y	[d]	[d]
	Defined oncogenic mutations	[e]	[e]	[e]	Y	Y	Y
	Straightforward genotype-phenotype comparisons				Y	Y	Y
	Complex genome landscapes	Y [f]	Y	Y		Y [f]	
	Defined cellular origin				Y	Y [g]	Y
	Low grade astrocytomas develop			[h]		Y	Y
	Stochastic malignant progression					Y	

NOTES

a. Some murine ECL are immunogenic and xenografting requires immunodeficient hosts.[19]
b. Immunodeficient scid, but not nude mice have genetic DNA repair defects.[187]
c. Some murine ECL fail to invade normal brain.[19]
d. Growth kinetics, penetrance, and latency in GEM and nGEM models vary greatly depending on oncogenic mutations and targeted cell type.
e. Mutational profiles can be defined by genomic analyses, but genomic complexity renders direct genotype-phenotype correlations difficult.
f. Complex gene rearrangements occur less frequently in murine compared to human tumors.
g. Conventional knockout GEM models do not have a defined cellular origin.
h. IDH mutant PDX models of anaplastic oligodendrogliomas, not astrocytomas, have recently been described.[177,179]

Table 2.3. The role of contemporary murine models in preclinical astrocytoma drug development

Clinical issue	Role of preclinical models	Ideal model(s)	References
Target validation	Define role in tumorigenesis	GEM, nGEM, geHC	127,143,144,154,188
Cellular origin	Define role in tumorigenesis	GEM, nGEM, geHC	127,143,145,153,154,189, 190
Drug prioritization	Characterize CNS penetration	PDX, GEM	132,183
	Define effective dose and schedule	PDX, nGEM, geHC	53,60,89
	Define resistance mechanisms	PDX, nGEM, geHC	82,191,192
	Test combination therapies	PDX, nGEM, geHC	95,156,193-195
Patient selection	Developing predictive biomarkers	PDX, nGEM	53-55,59,60,68,69,94-96

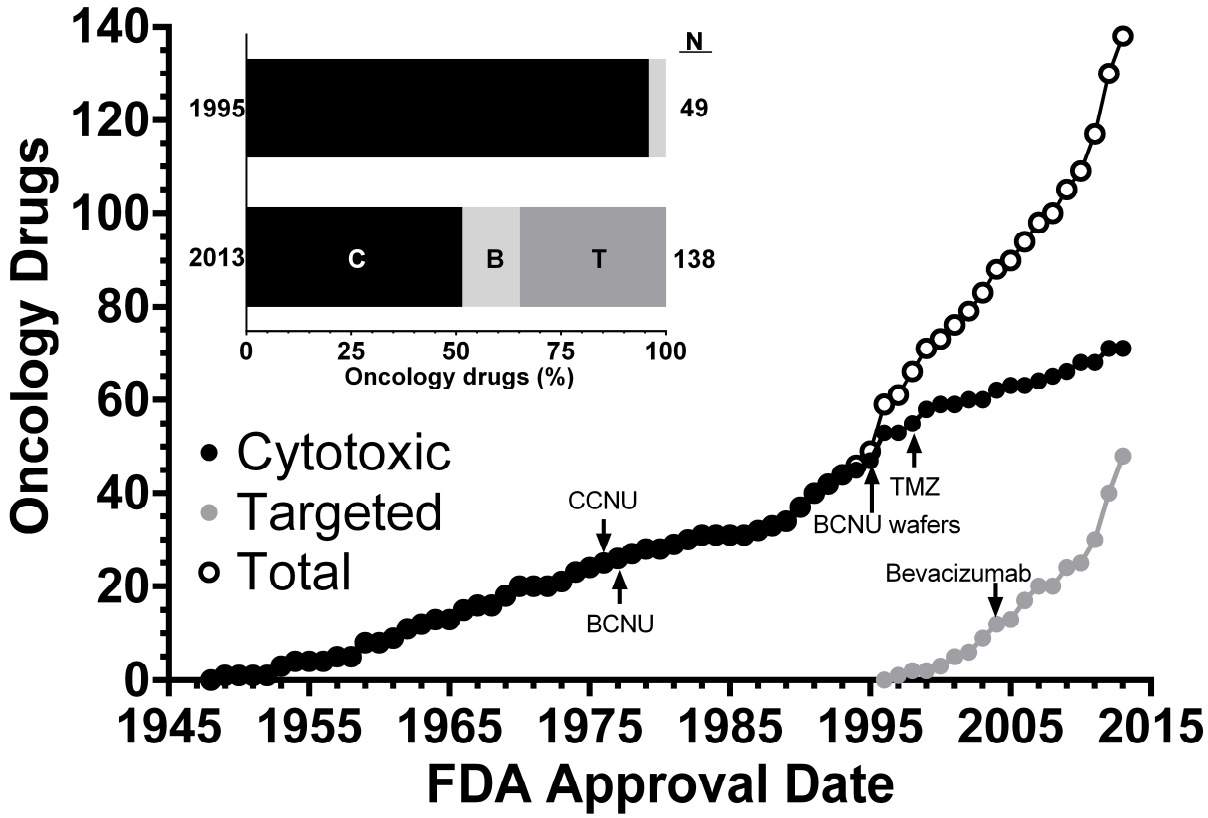

Figure 2.1. **FDA approved oncology drugs**. The cumulative number of cytotoxic (C), biological (B), and targeted (T) drugs approved by the FDA is shown. Dates correspond to the first indication approved. Approvals for subsequent indications are not shown. Drugs used for astrocytomas are indicated. Data were compiled from http://www.drugs.com and http://www.medilexicon.com/drugs-list/cancer.php.

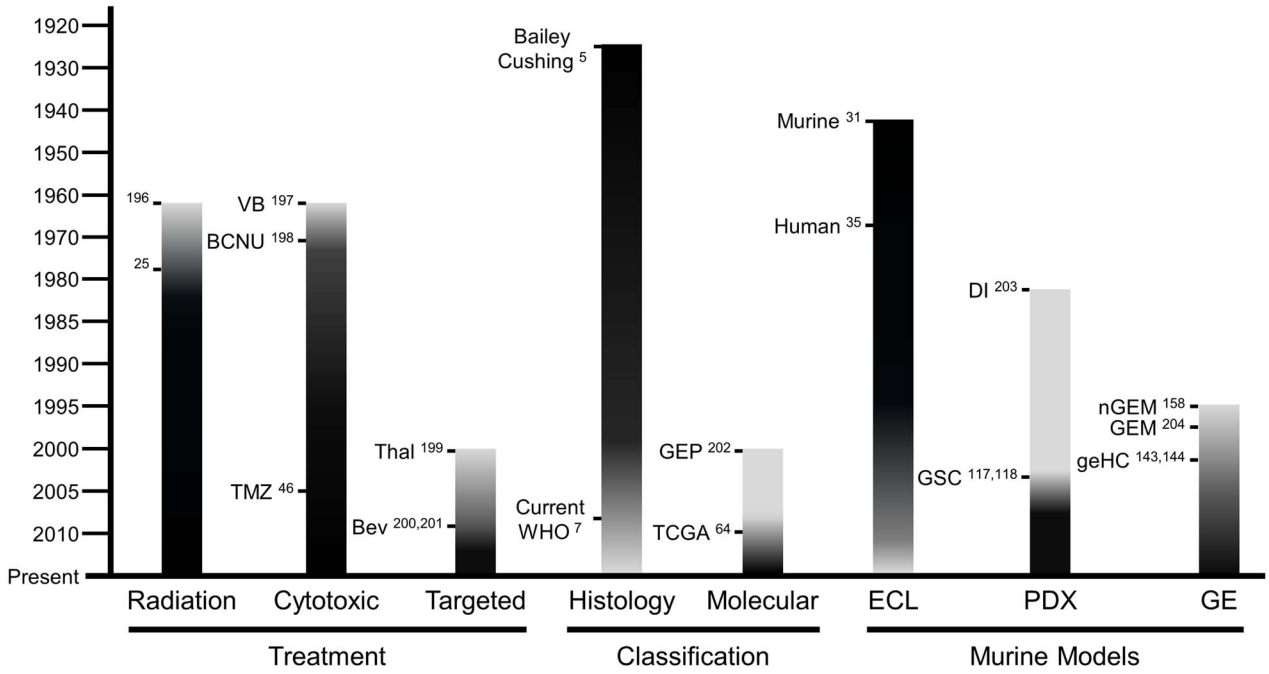

Figure 2.2. **Evolution of astrocytoma treatment, classification, and murine models**. Shading in black depicts increased emphasis over time. Major developments in each category are noted.[5,7,25,31,35,46,64,117,118,143,144,158,196-204] Abbreviations: BCNU, bis-chloroethylnitrosourea; Bev, bevacizumab; DI, direct injection; ECL, established cell line; GE, genetically engineered; geHC, genetically engineered human cells; GEM, genetically engineered mice; GEP, gene expression profiling; GSC, glioma stem cell; nGEM, non-germline genetically engineered mice; PDX, patient derived xenografts; TCGA, The Cancer Genome Atlas; Thal, thalidomide; TMZ, temozolomide; VB, vinblastine; WHO, World Health Organization.

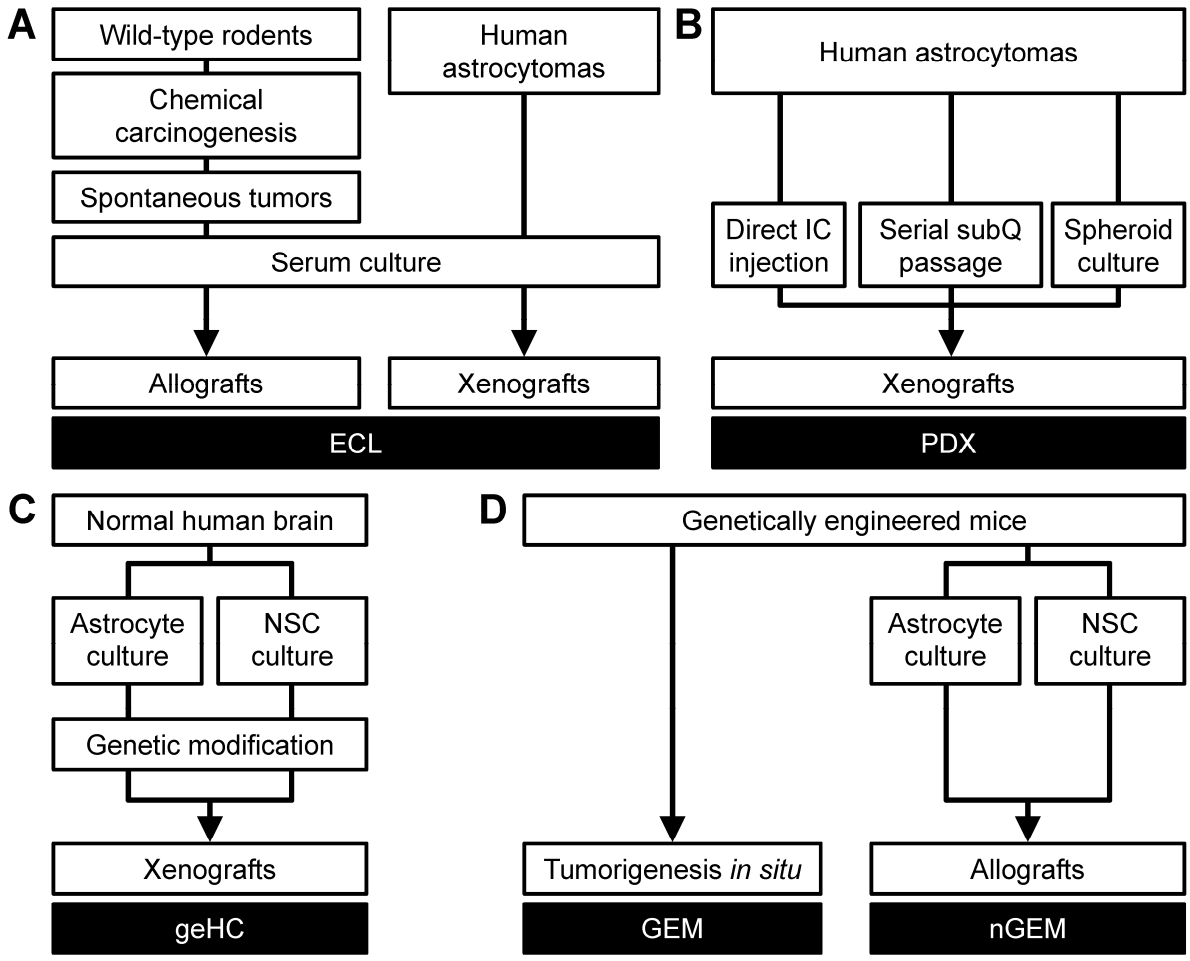

Figure 2.3. **Conventional and contemporary murine astrocytoma models**. Conventional murine and human astrocytoma models utilized established cell lines (ECL) (**A**). Murine ECL models were generated by serum culture of cells harvested from spontaneous rodent astrocytomas induced by chemical carcinogens and transplantation into immunocompetent rodents. Human ECL were similarly generated from human astrocytomas and xenografted into immunodeficient mice. Contemporary human models (**B**) consist of patient-derived xenografts (PDX) whereby tumor cells harvested from human astrocytomas are directly injected or culture as non-adherent spheroids in defined, serum-free media prior to engraftment in immunodeficient mice. Genetically engineered models include genetically-engineered human cells (geHC), whereby astrocytes or neural

stem cells (NSC) are harvested from normal human brains, genetically modified with oncogenic mutations, and xenografted into immunodeficient mice (**C**); GEM, whereby induction of oncogenic mutations produces tumorigenesis *in situ* (**D**); and non-germline genetically-engineered mouse (nGEM) models, whereby astrocytes or NSC are harvested from GEM, cultured *in vitro*, and allografted into immunocompetent or immunodeficient mice (**D**).

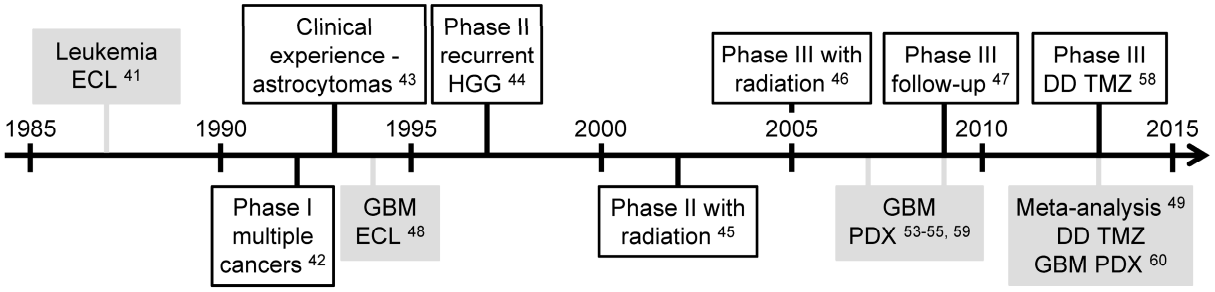

Figure 2.4. **Developmental timeline for temozolomide (TMZ)**. Clinical studies outlined in black were conducted with newly diagnosed GBM patients, unless otherwise noted.[41-49,53-55,58-60] Preclinical studies are highlighted in gray. Abbreviations: DD, dose-dense; ECL, established cell line models; HGG, high-grade gliomas; PDX, patient-derived xenograft models.

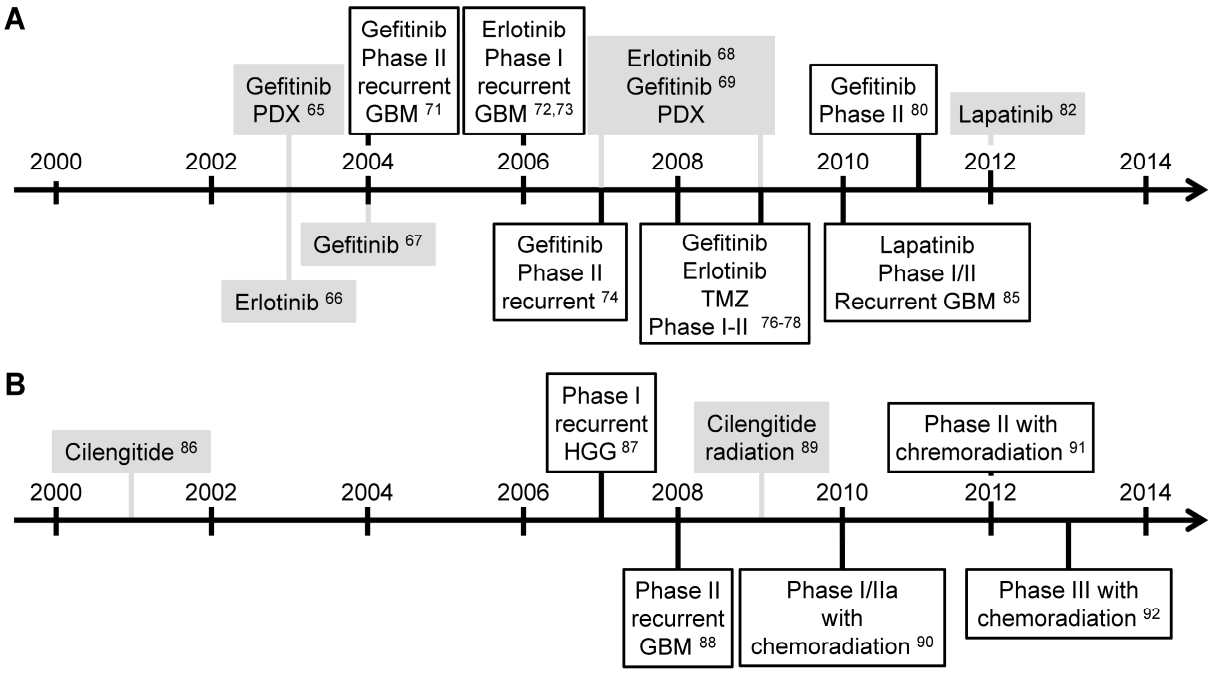

Figure 2.5. **Developmental timelines for EGFR tyrosine kinase inhibitors (A) and cilengitide (B)**. Clinical studies outlined in black were conducted with newly diagnosed GBM patients, unless otherwise noted. Preclinical studies are highlighted in gray and were performed with established GBM xenograft models, unless otherwise noted.[65-69,71-74,76-78,80,82,85-92]

REFERENCES

1. DiMasi JA, Grabowski HG. Economics of new oncology drug development. *J Clin Oncol.* 2007;25(2):209-216.

2. Sharpless NE, Depinho RA. The mighty mouse: genetically engineered mouse models in cancer drug development. *Nat Rev Drug Discov.* 2006;5(9):741-754.

3. Mendelsohn J. Personalizing oncology: perspectives and prospects. *J Clin Oncol.* 2013;31(15):1904-1911.

4. Ostrom QT, Gittleman H, Farah P, et al. CBTRUS statistical report: Primary brain and central nervous system tumors diagnosed in the United States in 2006-2010. *Neuro Oncol.* 2013;15 Suppl 2:ii1-56.

5. Bailey P, Cushing H. *A classification of the tumors of the glioma group on a histogenetic basis with a correlated study of prognosis*. Philadelphia: J.B. Lippincott; 1926.

6. Miller CR, Perry A. Glioblastoma. *Arch Pathol Lab Med.* 2007;131(3):397-406.

7. Louis DN, Ohgaki H, Wiestler OD, Cavenee WK, eds. *WHO classification of tumours of the central nervous system.* 4th ed. Lyon: IARC; 2007.

8. Riemenschneider MJ, Louis DN, Weller M, Hau P. Refined brain tumor diagnostics and stratified therapies: the requirement for a multidisciplinary approach. *Acta Neuropathol.* 2013;126(1):21-37.

9. Vitucci M, Hayes DN, Miller CR. Gene expression profiling of gliomas: merging genomic and histopathological classification for personalised therapy. *Br J Cancer.* 2011;104(4):545-553.

10. Chang SM, Barker FG, 2nd, Schmidt MH, et al. Clinical trial participation among patients enrolled in the Glioma Outcomes Project. *Cancer.* 2002;94(10):2681-2687.

11. Trippa L, Lee EQ, Wen PY, et al. Bayesian adaptive randomized trial design for patients with recurrent glioblastoma. *J Clin Oncol.* 2012;30(26):3258-3263.

12. Alexander BM, Wen PY, Trippa L, et al. Biomarker-based adaptive trials for patients with glioblastoma--lessons from I-SPY 2. *Neuro Oncol.* 2013;15(8):972-978.

13. Barth RF, Kaur B. Rat brain tumor models in experimental neuro-oncology: the C6, 9L, T9, RG2, F98, BT4C, RT-2 and CNS-1 gliomas. *J Neurooncol.* 2009;94(3):299-312.

14. Candolfi M, Curtin JF, Nichols WS, et al. Intracranial glioblastoma models in preclinical neuro-oncology: neuropathological characterization and tumor progression. *J Neurooncol.* 2007;85(2):133-148.

15. Garber K. From human to mouse and back: 'tumorgraft' models surge in popularity. *J Natl Cancer Inst.* 2009;101(1):6-8.

16. de Vries NA, Beijnen JH, van Tellingen O. High-grade glioma mouse models and their applicability for preclinical testing. *Cancer Treat Rev.* 2009;35(8):714-723.

17. Fomchenko EI, Holland EC. Mouse models of brain tumors and their applications in preclinical trials. *Clin Cancer Res.* 2006;12(18):5288-5297.

18. Gutmann DH, Stiles CD, Lowe SW, Bollag GE, Furnari FB, Charest AL. Report from the fifth National Cancer Institute Mouse Models of Human Cancers Consortium Nervous System Tumors Workshop. *Neuro Oncol.* 2011;13(7):692-699.

19. Huszthy PC, Daphu I, Niclou SP, et al. In vivo models of primary brain tumors: pitfalls and perspectives. *Neuro Oncol.* 2012;14(8):979-993.

20. Schmid RS, Vitucci M, Miller CR. Genetically engineered mouse models of diffuse gliomas. *Brain Res Bull.* 2012;88(1):72-79.

21. Chen J, McKay RM, Parada LF. Malignant glioma: lessons from genomics, mouse models, and stem cells. *Cell.* 2012;149(1):36-47.

22. Hambardzumyan D, Parada LF, Holland EC, Charest A. Genetic modeling of gliomas in mice: new tools to tackle old problems. *Glia.* 2011;59(8):1155-1168.

23. Huse JT, Holland EC. Genetically engineered mouse models of brain cancer and the promise of preclinical testing. *Brain Pathol.* 2009;19(1):132-143.

24. Westphal M, Lamszus K. The neurobiology of gliomas: from cell biology to the development of therapeutic approaches. *Nat Rev Neurosci.* 2011;12(9):495-508.

25. Walker MD, Alexander E, Jr., Hunt WE, et al. Evaluation of BCNU and/or radiotherapy in the treatment of anaplastic gliomas. A cooperative clinical trial. *J Neurosurg.* 1978;49(3):333-343.

26. Weir B, Band P, Urtasun R, et al. Radiotherapy and CCNU in the treatment of high-grade supratentorial astrocytomas. *J Neurosurg.* 1976;45(2):129-134.

27. Stewart LA. Chemotherapy in adult high-grade glioma: a systematic review and meta-analysis of individual patient data from 12 randomised trials. *Lancet.* 2002;359(9311):1011-1018.

28. Sausville EA, Burger AM. Contributions of human tumor xenografts to anticancer drug development. *Cancer Res.* 2006;66(7):3351-3354.

29. Dykes DJ, Waud WR. Murine L1210 and P388 leukemias. In: Teicher BA, ed. *Tumor Models in Cancer Research*. Totowa, NJ: Humana Press; 2011: pp.23-41.

30. Venditti JM, Kline I, Goldin A. Evaluation of antileukemic agents employing advanced leukemia L1210 in mice. 8. *Cancer Res.* 1964;24:827-879.

31. Zimmerman HM, Arnold H. Experimental brain tumors I. Tumors produced with methylcholanthrene. *Cancer Research.* 1941;1(12):919-938.

32. Ausman JI, Shapiro WR, Rall DP. Studies on the chemotherapy of experimental brain tumors: development of an experimental model. *Cancer Res.* 1970;30(9):2394-2400.

33. Barker M, Hoshino T, Gurcay O, et al. Development of an animal brain tumor model and its response to therapy with 1,3-bis(2-chloroethyl)-1-nitrosourea. *Cancer Res.* 1973;33(5):976-986.

34. Benda P, Lightbody J, Sato G, Levine L, Sweet W. Differentiated rat glial cell strain in tissue culture. *Science.* 1968;161(3839):370-371.

35. Ponten J, Macintyre EH. Long term culture of normal and neoplastic human glia. *Acta Pathol Microbiol Scand.* 1968;74(4):465-486.

36. Giard DJ, Aaronson SA, Todaro GJ, et al. In vitro cultivation of human tumors: establishment of cell lines derived from a series of solid tumors. *J Natl Cancer Inst.* 1973;51(5):1417-1423.

37. Owens RB, Smith HS, Nelson-Rees WA, Springer EL. Epithelial cell cultures from normal and cancerous human tissues. *J Natl Cancer Inst.* 1976;56(4):843-849.

38. Bigner SH, Bullard DE, Pegram CN, Wikstrand CJ, Bigner DD. Relationship of in vitro morphologic and growth characteristics of established human glioma-derived cell lines to their tumorigenicity in athymic nude mice. *J Neuropathol Exp Neurol.* 1981;40(4):390-409.

39. Rygaard J, Povlsen CO. Heterotransplantation of a human malignant tumour to "Nude" mice. *Acta Pathol Microbiol Scand.* 1969;77(4):758-760.

40. Amarasingh S, Macleod MR, Whittle IR. What is the translational efficacy of chemotherapeutic drug research in neuro-oncology? A systematic review and meta-analysis of the efficacy of BCNU and CCNU in animal models of glioma. *J Neurooncol.* 2009;91(2):117-125.

41. Stevens MF, Hickman JA, Langdon SP, et al. Antitumor activity and pharmacokinetics in mice of 8-carbamoyl-3-methyl-imidazo[5,1-d]-1,2,3,5-tetrazin-4(3H)-one (CCRG 81045; M & B 39831), a novel drug with potential as an alternative to dacarbazine. *Cancer Res.* 1987;47(22):5846-5852.

42. Newlands ES, Blackledge GR, Slack JA, et al. Phase I trial of temozolomide (CCRG 81045: M&B 39831: NSC 362856). *Br J Cancer.* 1992;65(2):287-291.

43. O'Reilly SM, Newlands ES, Glaser MG, et al. Temozolomide: a new oral cytotoxic chemotherapeutic agent with promising activity against primary brain tumours. *Eur J Cancer.* 1993;29A(7):940-942.

44. Bower M, Newlands ES, Bleehen NM, et al. Multicentre CRC phase II trial of temozolomide in recurrent or progressive high-grade glioma. *Cancer Chemother Pharmacol.* 1997;40(6):484-488.

45. Stupp R, Dietrich PY, Ostermann Kraljevic S, et al. Promising survival for patients with newly diagnosed glioblastoma multiforme treated with concomitant radiation plus temozolomide followed by adjuvant temozolomide. *J Clin Oncol.* 2002;20(5):1375-1382.

46. Stupp R, Mason WP, van den Bent MJ, et al. Radiotherapy plus concomitant and adjuvant temozolomide for glioblastoma. *N Engl J Med.* 2005;352(10):987-996.

47. Stupp R, Hegi ME, Mason WP, et al. Effects of radiotherapy with concomitant and adjuvant temozolomide versus radiotherapy alone on survival in glioblastoma in a randomised phase III study: 5-year analysis of the EORTC-NCIC trial. *Lancet Oncol.* 2009;10(5):459-466.

48. Plowman J, Waud WR, Koutsoukos AD, Rubinstein LV, Moore TD, Grever MR. Preclinical antitumor activity of temozolomide in mice: efficacy against human brain tumor xenografts and synergism with 1,3-bis(2-chloroethyl)-1-nitrosourea. *Cancer Res.* 1994;54(14):3793-3799.

49. Hirst TC, Vesterinen HM, Sena ES, Egan KJ, Macleod MR, Whittle IR. Systematic review and meta-analysis of temozolomide in animal models of glioma: was clinical efficacy predicted? *Br J Cancer.* 2013;108(1):64-71.

50. Margison GP, Santibanez Koref MF, Povey AC. Mechanisms of carcinogenicity/chemotherapy by O6-methylguanine. *Mutagenesis.* 2002;17(6):483-487.

51. Gerson SL. Clinical relevance of MGMT in the treatment of cancer. *J Clin Oncol.* 2002;20(9):2388-2399.

52. Hegi ME, Diserens AC, Gorlia T, et al. MGMT gene silencing and benefit from temozolomide in glioblastoma. *N Engl J Med.* 2005;352(10):997-1003.

53. Dinca EB, Sarkaria JN, Schroeder MA, et al. Bioluminescence monitoring of intracranial glioblastoma xenograft: response to primary and salvage temozolomide therapy. *J Neurosurg.* 2007;107(3):610-616.

54. Kitange GJ, Carlson BL, Mladek AC, et al. Evaluation of MGMT promoter methylation status and correlation with temozolomide response in orthotopic glioblastoma xenograft model. *J Neurooncol.* 2009;92(1):23-31.

55. Carlson BL, Grogan PT, Mladek AC, et al. Radiosensitizing effects of temozolomide observed in vivo only in a subset of O6-methylguanine-DNA methyltransferase methylated glioblastoma multiforme xenografts. *Int J Radiat Oncol Biol Phys.* 2009;75(1):212-219.

56. Wick W, Platten M, Weller M. New (alternative) temozolomide regimens for the treatment of glioma. *Neuro Oncol.* 2009;11(1):69-79.

57. Tolcher AW, Gerson SL, Denis L, et al. Marked inactivation of O6-alkylguanine-DNA alkyltransferase activity with protracted temozolomide schedules. *Br J Cancer.* 2003;88(7):1004-1011.

58. Gilbert MR, Wang M, Aldape KD, et al. Dose-dense temozolomide for newly diagnosed glioblastoma: a randomized phase III clinical trial. *J Clin Oncol.* 2013;31(32):4085-4091.

59. Kitange GJ, Carlson BL, Schroeder MA, et al. Induction of MGMT expression is associated with temozolomide resistance in glioblastoma xenografts. *Neuro Oncol.* 2009;11(3):281-291.

60. Cen L, Carlson BL, Pokorny JL, et al. Efficacy of protracted temozolomide dosing is limited in MGMT unmethylated GBM xenograft models. *Neuro Oncol.* 2013;15(6):735-746.

61. Brennan CW, Verhaak RG, McKenna A, et al. The somatic genomic landscape of glioblastoma. *Cell.* 2013;155(2):462-477.

62. Huang PH, Xu AM, White FM. Oncogenic EGFR signaling networks in glioma. *Sci Signal.* 2009;2(87):re6.

63. Cancer Genome Atlas Research Network. Comprehensive genomic characterization defines human glioblastoma genes and core pathways. *Nature.* 2008;455(7216):1061-1068.

64. Verhaak RG, Hoadley KA, Purdom E, et al. Integrated genomic analysis identifies clinically relevant subtypes of glioblastoma characterized by abnormalities in PDGFRA, IDH1, EGFR, and NF1. *Cancer Cell.* 2010;17(1):98-110.

65. Guillamo JS, Leuraud P, De Bouard S, et al. Anti-proliferative and anti-invasive EGFR amplification dependent and anti-angiogenic EGFR independent activity of ZD1839 ('Iressa') tyrosine kinase inhibitor on human glioblastomas [abstract]. *Proceedings of the American Association for Cancer Research.* 2003;44:1009.

66. Vogelbaum MA, Goldlust S, Kanner A. The EGFR tyrosine kinase inhibitor Tarceva (OSI-774) shows activity against both wild-type and mutant EGFR function [abstract]. *Neuro Oncol.* 2003;5(4):309.

67. Learn CA, Hartzell TL, Wikstrand CJ, et al. Resistance to tyrosine kinase inhibition by mutant epidermal growth factor receptor variant III contributes to the neoplastic phenotype of glioblastoma multiforme. *Clin Cancer Res.* 2004;10(9):3216-3224.

68. Sarkaria JN, Yang L, Grogan PT, et al. Identification of molecular characteristics correlated with glioblastoma sensitivity to EGFR kinase inhibition through use of an intracranial xenograft test panel. *Mol Cancer Ther.* 2007;6(3):1167-1174.

69. Guillamo JS, de Bouard S, Valable S, et al. Molecular mechanisms underlying effects of epidermal growth factor receptor inhibition on invasion, proliferation, and angiogenesis in experimental glioma. *Clin Cancer Res.* 2009;15(11):3697-3704.

70. Pao W, Chmielecki J. Rational, biologically based treatment of EGFR-mutant non-small-cell lung cancer. *Nat Rev Cancer.* 2010;10(11):760-774.

71. Rich JN, Reardon DA, Peery T, et al. Phase II trial of gefitinib in recurrent glioblastoma. *J Clin Oncol.* 2004;22(1):133-142.

72. Krishnan S, Brown PD, Ballman KV, et al. Phase I trial of erlotinib with radiation therapy in patients with glioblastoma multiforme: results of North Central Cancer Treatment Group protocol N0177. *Int J Radiat Oncol Biol Phys.* 2006;65(4):1192-1199.

73. Prados MD, Lamborn KR, Chang S, et al. Phase 1 study of erlotinib HCl alone and combined with temozolomide in patients with stable or recurrent malignant glioma. *Neuro Oncol.* 2006;8(1):67-78.

74. Franceschi E, Cavallo G, Lonardi S, et al. Gefitinib in patients with progressive high-grade gliomas: a multicentre phase II study by Gruppo Italiano Cooperativo di Neuro-Oncologia (GICNO). *Br J Cancer.* 2007;96(7):1047-1051.

75. Brandes AA, Franceschi E, Tosoni A, Hegi ME, Stupp R. Epidermal growth factor receptor inhibitors in neuro-oncology: hopes and disappointments. *Clin Cancer Res.* 2008;14(4):957-960.

76. Brown PD, Krishnan S, Sarkaria JN, et al. Phase I/II trial of erlotinib and temozolomide with radiation therapy in the treatment of newly diagnosed

glioblastoma multiforme: North Central Cancer Treatment Group Study N0177. *J Clin Oncol.* 2008;26(34):5603-5609.

77. Prados MD, Yung WK, Wen PY, et al. Phase-1 trial of gefitinib and temozolomide in patients with malignant glioma: a North American brain tumor consortium study. *Cancer Chemother Pharmacol.* 2008;61(6):1059-1067.

78. Prados MD, Chang SM, Butowski N, et al. Phase II study of erlotinib plus temozolomide during and after radiation therapy in patients with newly diagnosed glioblastoma multiforme or gliosarcoma. *J Clin Oncol.* 2009;27(4):579-584.

79. Peereboom DM, Shepard DR, Ahluwalia MS, et al. Phase II trial of erlotinib with temozolomide and radiation in patients with newly diagnosed glioblastoma multiforme. *J Neurooncol.* 2010;98(1):93-99.

80. Uhm JH, Ballman KV, Wu W, et al. Phase II evaluation of gefitinib in patients with newly diagnosed Grade 4 astrocytoma: Mayo/North Central Cancer Treatment Group Study N0074. *Int J Radiat Oncol Biol Phys.* 2011;80(2):347-353.

81. Mellinghoff IK, Wang MY, Vivanco I, et al. Molecular determinants of the response of glioblastomas to EGFR kinase inhibitors. *N Engl J Med.* 2005;353(19):2012-2024.

82. Vivanco I, Robins HI, Rohle D, et al. Differential sensitivity of glioma- versus lung cancer-specific EGFR mutations to EGFR kinase inhibitors. *Cancer Discov.* 2012;2(5):458-471.

83. Togashi Y, Masago K, Masuda S, et al. Cerebrospinal fluid concentration of gefitinib and erlotinib in patients with non-small cell lung cancer. *Cancer Chemother Pharmacol.* 2012;70(3):399-405.

84. de Vries NA, Buckle T, Zhao J, Beijnen JH, Schellens JH, van Tellingen O. Restricted brain penetration of the tyrosine kinase inhibitor erlotinib due to the drug transporters P-gp and BCRP. *Invest New Drugs.* 2012;30(2):443-449.

85. Thiessen B, Stewart C, Tsao M, et al. A phase I/II trial of GW572016 (lapatinib) in recurrent glioblastoma multiforme: clinical outcomes, pharmacokinetics and molecular correlation. *Cancer Chemother Pharmacol.* 2010;65(2):353-361.

86. MacDonald TJ, Taga T, Shimada H, et al. Preferential susceptibility of brain tumors to the antiangiogenic effects of an alpha(v) integrin antagonist. *Neurosurgery.* 2001;48(1):151-157.

87. Nabors LB, Mikkelsen T, Rosenfeld SS, et al. Phase I and correlative biology study of cilengitide in patients with recurrent malignant glioma. *J Clin Oncol.* 2007;25(13):1651-1657.

88. Reardon DA, Fink KL, Mikkelsen T, et al. Randomized phase II study of cilengitide, an integrin-targeting arginine-glycine-aspartic acid peptide, in recurrent glioblastoma multiforme. *J Clin Oncol.* 2008;26(34):5610-5617.

89. Mikkelsen T, Brodie C, Finniss S, et al. Radiation sensitization of glioblastoma by cilengitide has unanticipated schedule-dependency. *Int J Cancer.* 2009;124(11):2719-2727.

90. Stupp R, Hegi ME, Neyns B, et al. Phase I/IIa study of cilengitide and temozolomide with concomitant radiotherapy followed by cilengitide and temozolomide maintenance therapy in patients with newly diagnosed glioblastoma. *J Clin Oncol.* 2010;28(16):2712-2718.

91. Nabors LB, Mikkelsen T, Hegi ME, et al. A safety run-in and randomized phase 2 study of cilengitide combined with chemoradiation for newly diagnosed glioblastoma (NABTT 0306). *Cancer.* 2012;118(22):5601-5607.

92. Stupp R, Hegi ME, Gorlia T, et al. Cilengitide combined with standard treatment for patients with newly diagnosed glioblastoma and methylated O6-methylguanine-DNA methyltransferase (MGMT) gene promoter: Key results of the multicenter, randomized, open-label, controlled, phase III CENTRIC study [abstract]. *Proc Annu Meet Am Soc Clin Oncol.* 2013;31:LBA2009.

93. Becher OJ, Holland EC. Genetically engineered models have advantages over xenografts for preclinical studies. *Cancer Res.* 2006;66(7):3355-3358.

94. Agnihotri S, Gajadhar AS, Ternamian C, et al. Alkylpurine-DNA-N-glycosylase confers resistance to temozolomide in xenograft models of glioblastoma multiforme and is associated with poor survival in patients. *J Clin Invest.* 2012;122(1):253-266.

95. Kitange GJ, Mladek AC, Carlson BL, et al. Inhibition of histone deacetylation potentiates the evolution of acquired temozolomide resistance linked to MGMT upregulation in glioblastoma xenografts. *Clin Cancer Res.* 2012;18(15):4070-4079.

96. Oliva CR, Nozell SE, Diers A, et al. Acquisition of temozolomide chemoresistance in gliomas leads to remodeling of mitochondrial electron transport chain. *J Biol Chem.* 2010;285(51):39759-39767.

97. Nasser S, Kiefer J, Armstrong B, Berens ME, Kim S. Aligning xenograft models to glioblastoma patient tumors to assess chemovulnerability of patients [abstract]. *Proceedings of the American Association for Cancer Research.* 2012;52:4917.

98. Herter-Sprie GS, Kung AL, Wong KK. New cast for a new era: preclinical cancer drug development revisited. *J Clin Invest.* 2013;123(9):3639-3645.

99. Colman H, Zhang L, Sulman EP, et al. A multigene predictor of outcome in glioblastoma. *Neuro Oncol.* 2010;12(1):49-57.

100. Carro MS, Lim WK, Alvarez MJ, et al. The transcriptional network for mesenchymal transformation of brain tumours. *Nature.* 2010;463(7279):318-325.

101. Bhat KP, Balasubramaniyan V, Vaillant B, et al. Mesenchymal differentiation mediated by NF-kappaB promotes radiation resistance in glioblastoma. *Cancer Cell.* 2013;24(3):331-346.

102. Gilbert MR, Dignam JJ, Armstrong TS, et al. A randomized trial of bevacizumab for newly diagnosed glioblastoma. *N Engl J Med.* 2014;370(8):699-708.

103. Agarwal S, Sane R, Oberoi R, Ohlfest JR, Elmquist WF. Delivery of molecularly targeted therapy to malignant glioma, a disease of the whole brain. *Expert Rev Mol Med.* 2011;13:e17.

104. Huse JT, Holland E, Deangelis LM. Glioblastoma: molecular analysis and clinical implications. *Annu Rev Med.* 2013;64:59-70.

105. Cloughesy TF, Cavenee WK, Mischel PS. Glioblastoma: from molecular pathology to targeted treatment. *Annu Rev Pathol.* 2014;9:1-25.

106. Phillips HS, Kharbanda S, Chen R, et al. Molecular subclasses of high-grade glioma predict prognosis, delineate a pattern of disease progression, and resemble stages in neurogenesis. *Cancer Cell.* 2006;9(3):157-173.

107. Gorovets D, Kannan K, Shen R, et al. IDH mutation and neuroglial developmental features define clinically distinct subclasses of lower grade diffuse astrocytic glioma. *Clin Cancer Res.* 2012;18(9):2490-2501.

108. Noushmehr H, Weisenberger DJ, Diefes K, et al. Identification of a CpG island methylator phenotype that defines a distinct subgroup of glioma. *Cancer Cell.* 2010;17(5):510-522.

109. Dunn GP, Rinne ML, Wykosky J, et al. Emerging insights into the molecular and cellular basis of glioblastoma. *Genes Dev.* 2012;26(8):756-784.

110. Burrell RA, McGranahan N, Bartek J, Swanton C. The causes and consequences of genetic heterogeneity in cancer evolution. *Nature.* 2013;501(7467):338-345.

111. Sottoriva A, Spiteri I, Piccirillo SG, et al. Intratumor heterogeneity in human glioblastoma reflects cancer evolutionary dynamics. *Proc Natl Acad Sci U S A.* 2013;110(10):4009-4014.

112. Johnson BE, Mazor T, Hong C, et al. Mutational analysis reveals the origin and therapy-driven evolution of recurrent glioma. *Science.* 2014;343(6167):189-193.

113. Patel AP, Tirosh I, Trombetta JJ, et al. Single-cell RNA-seq highlights intratumoral heterogeneity in primary glioblastoma. *Science.* 2014;344(6190):1396-1401.

114. Snuderl M, Fazlollahi L, Le LP, et al. Mosaic amplification of multiple receptor tyrosine kinase genes in glioblastoma. *Cancer Cell.* 2011;20(6):810-817.

115. Stommel J, Kimmelman A, Ying H, et al. Coactivation of receptor tyrosine kinases affects the response of tumor cells to targeted therapies. *Science.* 2007;318(5848):287-290.

116. Zhou BB, Zhang H, Damelin M, Geles KG, Grindley JC, Dirks PB. Tumour-initiating cells: challenges and opportunities for anticancer drug discovery. *Nat Rev Drug Discov.* 2009;8(10):806-823.

117. Singh SK, Clarke ID, Terasaki M, et al. Identification of a cancer stem cell in human brain tumors. *Cancer Res.* 2003;63(18):5821-5828.

118. Yuan X, Curtin J, Xiong Y, et al. Isolation of cancer stem cells from adult glioblastoma multiforme. *Oncogene.* 2004;23(58):9392-9400.

119. Singh SK, Hawkins C, Clarke ID, et al. Identification of human brain tumour initiating cells. *Nature.* 2004;432(7015):396-401.

120. Bao S, Wu Q, McLendon RE, et al. Glioma stem cells promote radioresistance by preferential activation of the DNA damage response. *Nature.* 2006;444(7120):756-760.

121. Singh SK, Clarke ID, Hide T, Dirks PB. Cancer stem cells in nervous system tumors. *Oncogene.* 2004;23(43):7267-7273.

122. Nduom EK, Hadjipanayis CG, Van Meir EG. Glioblastoma cancer stem-like cells: implications for pathogenesis and treatment. *Cancer J.* 2012;18(1):100-106.

123. Huang Z, Cheng L, Guryanova OA, Wu Q, Bao S. Cancer stem cells in glioblastoma--molecular signaling and therapeutic targeting. *Protein Cell.* 2010;1(7):638-655.

124. Wang J, Ma Y, Cooper MK. Cancer stem cells in glioma: challenges and opportunities. *Transl Cancer Res.* 2013;2(5):429-441.

125. Yan K, Yang K, Rich JN. The evolving landscape of glioblastoma stem cells. *Curr Opin Neurol.* 2013;26(6):701-707.

126. Miller CR, Williams CR, Buchsbaum DJ, Gillespie GY. Intratumoral 5-fluorouracil produced by cytosine deaminase/5-fluorocytosine gene therapy is effective for experimental human glioblastomas. *Cancer Res.* 2002;62(3):773-780.

127. Vitucci M, Karpinich NO, Bash RE, et al. Cooperativity between MAPK and PI3K signaling activation is required for glioblastoma pathogenesis. *Neuro Oncol.* 2013;15(10):1317-1329.

128. Clark MJ, Homer N, O'Connor BD, et al. U87MG decoded: the genomic sequence of a cytogenetically aberrant human cancer cell line. *PLoS Genet.* 2010;6(1):e1000832.

129. Stein WD, Litman T, Fojo T, Bates SE. A Serial Analysis of Gene Expression (SAGE) database analysis of chemosensitivity: comparing solid tumors with cell lines and comparing solid tumors from different tissue origins. *Cancer Res.* 2004;64(8):2805-2816.

130. Szakacs G, Gottesman MM. Comparing solid tumors with cell lines: implications for identifying drug resistance genes in cancer. *Mol Interv.* 2004;4(6):323-325.

131. Li A, Walling J, Kotliarov Y, et al. Genomic changes and gene expression profiles reveal that established glioma cell lines are poorly representative of primary human gliomas. *Mol Cancer Res.* 2008;6(1):21-30.

132. Parrish KE, Pokorny JL, Mittapalli RK, K. B, Sarkaria JN, Elmquist WF. BBB efflux pump activity limits brain penetration of palbociclib (PD0332991) in glioblastoma [abstract]. *Mol Cancer Ther.* 2013;12(S11):C81.

133. Camphausen K, Purow B, Sproull M, et al. Influence of in vivo growth on human glioma cell line gene expression: convergent profiles under orthotopic conditions. *Proc Natl Acad Sci U S A.* 2005;102(23):8287-8292.

134. Camphausen K, Purow B, Sproull M, et al. Orthotopic growth of human glioma cells quantitatively and qualitatively influences radiation-induced changes in gene expression. *Cancer Res.* 2005;65(22):10389-10393.

135. Tentler JJ, Tan AC, Weekes CD, et al. Patient-derived tumour xenografts as models for oncology drug development. *Nat Rev Clin Oncol.* 2012;9(6):338-350.

136. Giannini C, Sarkaria JN, Saito A, et al. Patient tumor EGFR and PDGFRA gene amplifications retained in an invasive intracranial xenograft model of glioblastoma multiforme. *Neuro Oncol.* 2005;7(2):164-176.

137. Joo KM, Kim J, Jin J, et al. Patient-specific orthotopic glioblastoma xenograft models recapitulate the histopathology and biology of human glioblastomas in situ. *Cell Rep.* 2013;3(1):260-273.

138. Yost SE, Pastorino S, Rozenzhak S, et al. High-resolution mutational profiling suggests the genetic validity of glioblastoma patient-derived pre-clinical models. *PLoS One.* 2013;8(2):e56185.

139. Hodgson JG, Yeh RF, Ray A, et al. Comparative analyses of gene copy number and mRNA expression in glioblastoma multiforme tumors and xenografts. *Neuro Oncol.* 2009;11(5):477-487.

140. Lee J, Kotliarova S, Kotliarov Y, et al. Tumor stem cells derived from glioblastomas cultured in bFGF and EGF more closely mirror the phenotype and genotype of primary tumors than do serum-cultured cell lines. *Cancer Cell.* 2006;9(5):391-403.

141. Lottaz C, Beier D, Meyer K, et al. Transcriptional profiles of CD133+ and CD133- glioblastoma-derived cancer stem cell lines suggest different cells of origin. *Cancer Res.* 2010;70(5):2030-2040.

142. Rich JN, Guo C, McLendon RE, Bigner DD, Wang XF, Counter CM. A genetically tractable model of human glioma formation. *Cancer Res.* 2001;61(9):3556-3560.

143. Sonoda Y, Ozawa T, Aldape KD, Deen DF, Berger MS, Pieper RO. Akt pathway activation converts anaplastic astrocytoma to glioblastoma multiforme in a human astrocyte model of glioma. *Cancer Res.* 2001;61(18):6674-6678.

144. Sonoda Y, Ozawa T, Hirose Y, et al. Formation of intracranial tumors by genetically modified human astrocytes defines four pathways critical in the development of human anaplastic astrocytoma. *Cancer Res.* 2001;61(13):4956-4960.

145. Mao XG, Hutt-Cabezas M, Orr BA, et al. LIN28A facilitates the transformation of human neural stem cells and promotes glioblastoma tumorigenesis through a pro-invasive genetic program. *Oncotarget.* 2013;4(7):1050-1064.

146. Zhu H, Woolfenden S, Bronson RT, et al. The novel Hsp90 inhibitor NXD30001 induces tumor regression in a genetically engineered mouse model of glioblastoma multiforme. *Mol Cancer Ther.* 2010;9(9):2618-2626.

147. Pitter KL, Galban CJ, Galban S, et al. Perifosine and CCI 779 co-operate to induce cell death and decrease proliferation in PTEN-intact and PTEN-deficient PDGF-driven murine glioblastoma. *PLoS One.* 2011;6(1):e14545.

148. Jun HJ, Acquaviva J, Chi D, et al. Acquired MET expression confers resistance to EGFR inhibition in a mouse model of glioblastoma multiforme. *Oncogene.* 2012;31(25):3039-3050.

149. de Vries NA, Bruggeman SW, Hulsman D, et al. Rapid and robust transgenic high-grade glioma mouse models for therapy intervention studies. *Clin Cancer Res.* 2010;16(13):3431-3441.

150. Lau J, Schmidt C, Markant SL, Taylor MD, Wechsler-Reya RJ, Weiss WA. Matching mice to malignancy: molecular subgroups and models of medulloblastoma. *Childs Nerv Syst.* 2012;28(4):521-532.

151. Remke M, Ramaswamy V, Taylor MD. Medulloblastoma molecular dissection: the way toward targeted therapy. *Curr Opin Oncol.* 2013;25(6):674-681.

152. von Werder A, Seidler B, Schmid RM, Schneider G, Saur D. Production of avian retroviruses and tissue-specific somatic retroviral gene transfer in vivo using the RCAS/TVA system. *Nat Protoc.* 2012;7(6):1167-1183.

153. Chow LM, Endersby R, Zhu X, et al. Cooperativity within and among Pten, p53, and Rb pathways induces high-grade astrocytoma in adult brain. *Cancer Cell.* 2011;19(3):305-316.

154. Song Y, Zhang Q, Kutlu B, et al. Evolutionary etiology of high-grade astrocytomas. *Proc Natl Acad Sci U S A.* 2013;110(44):17933-17938.

155. Kim HS, Woolard K, Lai C, et al. Gliomagenesis arising from Pten- and Ink4a/Arf-deficient neural progenitor cells is mediated by the p53-Fbxw7/Cdc4 pathway, which controls c-Myc. *Cancer Res.* 2012;72(22):6065-6075.

156. McEllin B, Camacho CV, Mukherjee B, et al. PTEN loss compromises homologous recombination repair in astrocytes: implications for glioblastoma therapy with temozolomide or poly(ADP-ribose) polymerase inhibitors. *Cancer Res.* 2010;70(13):5457-5464.

157. Radke J, Bortolussi G, Pagenstecher A. Akt and c-Myc induce stem-cell markers in mature primary p53(-)/(-) astrocytes and render these cells gliomagenic in the brain of immunocompetent mice. *PLoS One.* 2013;8(2):e56691.

158. Yahanda AM, Bruner JM, Donehower LA, Morrison RS. Astrocytes derived from p53-deficient mice provide a multistep in vitro model for development of malignant gliomas. *Mol Cell Biol.* 1995;15(8):4249-4259.

159. Blouw B, Song H, Tihan T, et al. The hypoxic response of tumors is dependent on their microenvironment. *Cancer Cell.* 2003;4(2):133-146.

160. McNeill RS, Van Swearingen AED, Bash RE, et al. Efficacy of mono and dual PI3K and MAPK inhibition in glioblastoma and triple-negative breast cancer brain metastasis models [abstract]. *J Neuropath Exp Neuro.* 2014;73(6):587.

161. Frattini V, Trifonov V, Chan JM, et al. The integrated landscape of driver genomic alterations in glioblastoma. *Nat Genet.* 2013;45(10):1141-1149.

162. Shapiro WR, Basler GA, Chernik NL, Posner JB. Human brain tumor transplantation into nude mice. *J Natl Cancer Inst.* 1979;62(3):447-453.

163. Shannon P, Sabha N, Lau N, Kamnasaran D, Gutmann DH, Guha A. Pathological and molecular progression of astrocytomas in a GFAP:12 V-Ha-Ras mouse astrocytoma model. *Am J Pathol.* 2005;167(3):859-867.

164. Schmid RS, Irvin DM, Vitucci M, Bash RE, Werneke AM, Miller CR. The role of regional astrocyte identity in astrocytoma genomic heterogeneity [abstract]. *Neuro Oncol.* 2013;15(S3):iii213.

165. Huse JT, Wallace M, Aldape KD, et al. Where are we now? And where are we going? A report from the Accelerate Brain Cancer Cure (ABC2) Low-grade Glioma Research Workshop. *Neuro Oncol.* 2014;16(2):173-178.

166. Dang L, White DW, Gross S, et al. Cancer-associated IDH1 mutations produce 2-hydroxyglutarate. *Nature.* 2009;462(7274):739-744.

167. Zhao S, Lin Y, Xu W, et al. Glioma-derived mutations in IDH1 dominantly inhibit IDH1 catalytic activity and induce HIF-1alpha. *Science.* 2009;324(5924):261-265.

168. Ward PS, Patel J, Wise DR, et al. The common feature of leukemia-associated IDH1 and IDH2 mutations is a neomorphic enzyme activity converting alpha-ketoglutarate to 2-hydroxyglutarate. *Cancer Cell.* 2010;17(3):225-234.

169. Xu W, Yang H, Liu Y, et al. Oncometabolite 2-hydroxyglutarate is a competitive inhibitor of alpha-ketoglutarate-dependent dioxygenases. *Cancer Cell.* 2011;19(1):17-30.

170. Duncan CG, Barwick BG, Jin G, et al. A heterozygous IDH1R132H/WT mutation induces genome-wide alterations in DNA methylation. *Genome Res.* 2012;22(12):2339-2355.

171. Jin G, Pirozzi CJ, Chen LH, et al. Mutant IDH1 is required for IDH1 mutated tumor cell growth. *Oncotarget.* 2012;3(8):774-782.

172. Li S, Chou AP, Chen W, et al. Overexpression of isocitrate dehydrogenase mutant proteins renders glioma cells more sensitive to radiation. *Neuro Oncol.* 2013;15(1):57-68.

173. Lu C, Ward PS, Kapoor GS, et al. IDH mutation impairs histone demethylation and results in a block to cell differentiation. *Nature.* 2012;483(7390):474-478.

174. Turcan S, Rohle D, Goenka A, et al. IDH1 mutation is sufficient to establish the glioma hypermethylator phenotype. *Nature.* 2012;483(7390):479-483.

175. Piaskowski S, Bienkowski M, Stoczynska-Fidelus E, et al. Glioma cells showing IDH1 mutation cannot be propagated in standard cell culture conditions. *Br J Cancer.* 2011;104(6):968-970.

176. Jin G, Reitman ZJ, Duncan CG, et al. Disruption of wild-type IDH1 suppresses D-2-hydroxyglutarate production in IDH1-mutated gliomas. *Cancer Res.* 2013;73(2):496-501.

177. Kelly JJ, Blough MD, Stechishin OD, et al. Oligodendroglioma cell lines containing t(1;19)(q10;p10). *Neuro Oncol.* 2010;12(7):745-755.

178. Klink B, Miletic H, Stieber D, et al. A novel, diffusely infiltrative xenograft model of human anaplastic oligodendroglioma with mutations in FUBP1, CIC, and IDH1. *PLoS One.* 2013;8(3):e59773.

179. Luchman HA, Stechishin OD, Dang NH, et al. An in vivo patient-derived model of endogenous IDH1-mutant glioma. *Neuro Oncol.* 2012;14(2):184-191.

180. Sasaki M, Knobbe CB, Itsumi M, et al. D-2-hydroxyglutarate produced by mutant IDH1 perturbs collagen maturation and basement membrane function. *Genes Dev.* 2012;26(18):2038-2049.

181. McNeill RS, Schmid RS, Bash RE, et al. Modeling astrocytoma pathogenesis in vitro and in vivo using cortical astrocytes or neural stem cells from conditional, genetically engineered mice. *J Vis Exp.* 2014:DOI:10.3791/51763.

182. Northcott PA, Korshunov A, Pfister SM, Taylor MD. The clinical implications of medulloblastoma subgroups. *Nat Rev Neurol.* 2012;8(6):340-351.

183. Salphati L, Heffron TP, Alicke B, et al. Targeting the PI3K pathway in the brain--efficacy of a PI3K inhibitor optimized to cross the blood-brain barrier. *Clin Cancer Res.* 2012;18(22):6239-6248.

184. Duncan JS, Whittle MC, Nakamura K, et al. Dynamic reprogramming of the kinome in response to targeted MEK inhibition in triple-negative breast cancer. *Cell.* 2012;149(2):307-321.

185. Bash R, Karpinich NO, Vitucci M, et al. Concurrent temozolomide-external-beam radiation therapy is effective for experimental glioblastomas in an orthotopic, genetically engineered syngeneic mouse allograft model system [abstract]. *Neuro Oncology.* 2009;11(5):638.

186. Miller CR, Bash RE, Vitucci M, White KK. A genetically-defined, orthotopic allograft model system of glioblastoma: Pathological features and experimental therapeutics [abstract]. *J Neuropath Exp Neuro.* 2010;69(5):522.

187. Fulop GM, Phillips RA. The scid mutation in mice causes a general defect in DNA repair. *Nature.* 1990;347(6292):479-482.

188. Holmen SL, Williams BO. Essential role for Ras signaling in glioblastoma maintenance. *Cancer Res.* 2005;65(18):8250-8255.

189. Holland EC, Celestino J, Dai C, Schaefer L, Sawaya RE, Fuller GN. Combined activation of Ras and Akt in neural progenitors induces glioblastoma formation in mice. *Nat Genet.* 2000;25(1):55-57.

190. Liu C, Sage JC, Miller MR, et al. Mosaic analysis with double markers reveals tumor cell of origin in glioma. *Cell.* 2011;146(2):209-221.

191. Kim YW, Liu TJ, Koul D, et al. Identification of novel synergistic targets for rational drug combinations with PI3 kinase inhibitors using siRNA synthetic lethality screening against GBM. *Neuro Oncol.* 2011;13(4):367-375.

192. Piao Y, Liang J, Holmes L, Henry V, Sulman E, de Groot JF. Acquired resistance to anti-VEGF therapy in glioblastoma is associated with a mesenchymal transition. *Clin Cancer Res.* 2013;19(16):4392-4403.

193. Gruber Filbin M, Dabral SK, Pazyra-Murphy MF, et al. Coordinate activation of Shh and PI3K signaling in PTEN-deficient glioblastoma: new therapeutic opportunities. *Nat Med.* 2013;19(11):1518-1523.

194. Dinca EB, Lu KV, Sarkaria JN, et al. p53 Small-molecule inhibitor enhances temozolomide cytotoxic activity against intracranial glioblastoma xenografts. *Cancer Res.* 2008;68(24):10034-10039.

195. Clarke MJ, Mulligan EA, Grogan PT, et al. Effective sensitization of temozolomide by ABT-888 is lost with development of temozolomide resistance in glioblastoma xenograft lines. *Mol Cancer Ther.* 2009;8(2):407-414.

196. Taveras JM, Thompson HG, Jr., Pool JL. Should we treat glioblastoma multiforme? A study of survival in 425 cases. *Am J Roentgenol Radium Ther Nucl Med.* 1962;87:473-479.

197. Mealey J, Jr. Treatment of malignant cerebral astrocytomas by intra-arterial infusion of vinblastine. *Cancer Chemother Rep.* 1962;20:121-126.

198. Walker MD, Hurwitz BS. BCNU (1,3-bis(2-chloroethyl)-1-nitrosourea; NSC-409962) in the treatment of malignant brain tumor--a preliminary report. *Cancer Chemother Rep.* 1970;54(4):263-271.

199. Fine HA, Figg WD, Jaeckle K, et al. Phase II trial of the antiangiogenic agent thalidomide in patients with recurrent high-grade gliomas. *J Clin Oncol.* 2000;18(4):708-715.

200. Friedman HS, Prados MD, Wen PY, et al. Bevacizumab alone and in combination with irinotecan in recurrent glioblastoma. *J Clin Oncol.* 2009;27(28):4733-4740.

201. Kreisl TN, Kim L, Moore K, et al. Phase II trial of single-agent bevacizumab followed by bevacizumab plus irinotecan at tumor progression in recurrent glioblastoma. *J Clin Oncol.* 2009;27(5):740-745.

202. Caskey LS, Fuller GN, Bruner JM, et al. Toward a molecular classification of the gliomas: histopathology, molecular genetics, and gene expression profiling. *Histol Histopathol.* 2000;15(3):971-981.

203. Horten BC, Basler GA, Shapiro WR. Xenograft of human malignant glial tumors into brains of nude mice. A histopatholgical study. *J Neuropathol Exp Neurol.* 1981;40(5):493-511.

204. Ding H, Roncari L, Shannon P, et al. Astrocyte-specific expression of activated p21-ras results in malignant astrocytoma formation in a transgenic mouse model of human gliomas. *Cancer Res.* 2001;61(9):3826-3836.

CHAPTER III: COMBINATION THERAPY WITH POTENT PI3K AND MAPK INHIBITORS OVERCOMES ADAPTIVE KINOME RESISTANCE TO SINGLE AGENTS IN PRECLINICAL MODELS OF GLIOBLASTOMA[2]

Introduction

Glioblastoma (GBM) is the most common and aggressive adult primary brain tumor. Despite advances in diagnosis, specifically incorporation of both histological and molecular criteria in the 2016 classification, GBM is uniformly treated with surgery, radiation, and temozolomide chemotherapy.[1] Recurrence is inevitable and leads to ~15 month survival.[2] Molecular heterogeneity of GBM has been extensively characterized using genomics. Primary GBM that arise *de novo* without a lower grade antecedent have been stratified into four molecular subtypes characterized by mutations in three core signaling pathways: RB, TP53, and RTK/phosphoinositide 3-kinase (PI3K)/mitogen activated protein kinase (MAPK).[3,4]

---

[2]A version of this work was recently accepted in *Neuro-Oncology*. The original citation is as follows: McNeill RS, Canoutas DA, Stuhlmiller TJ, Dhruv HD, Irvin DM, Bash RE, Angus SP, Herring LE, Simon JM, Skinner KR, Limas JC, Chen X, Schmid RS, Siegel MB, Van Swearingen AED, Hadler MJ, Sulman EP, Sarkaria JN, Anders CK, Graves LM, Berens ME, Johnson GL, and Miller CR. Combination therapy with potent PI3K and MAPK inhibitors overcomes adaptive kinome resistance to single agents in preclinical models of glioblastoma. *Neuro Oncol*. 2017;doi:10.1093/neuonc/nox044.

The RTK/PI3K/MAPK pathways are mutated in 90% of GBM.[3] The PI3K and MAPK pathways promote many cancer hallmarks, including survival, proliferation, and migration.[5-7] PI3K is most frequently activated in GBM via mutations in its negative regulator, *PTEN*.[3,5,6] Activation of MAPK signaling is due either to activating mutations in RTK or *KRAS*, or inactivating mutations in its negative regulator *NF1*.[3,8,9] RTK/PI3K/MAPK pathways are attractive therapeutic targets because of their mutation frequency and role in tumorigenesis.

Kinase inhibitors targeting the PI3K or MAPK pathways are currently approved for non-glioma tumors or in clinical development.[10,11] However, single agent kinase inhibitors have had disappointing clinical results in gliomas due to limited brain penetrance and drug resistance.[12-14] Many kinase inhibitors, including the EGFR inhibitors gefitinib and erlotinib, have low brain penetrance, restricting their ability to reach and suppress their biologic target.[13] Additionally, intrinsic and acquired drug resistance has significantly limited the impact of kinase inhibitors in gliomas.[13,15]

Preclinical studies that define drug efficacy, elucidate resistance mechanisms, and confirm target modulation will aid in clinical drug development. Genetically engineered mouse (GEM) and patient-derived xenograft (PDX) models are valuable tools for these efforts because they enable direct genotype to phenotype comparisons and faithfully recapitulate the molecular heterogeneity of human tumors, respectively.[13] We and others have shown that activating PI3K and MAPK mutations cooperate to promote gliomagenesis in preclinical models.[16-20] We developed a series of nGEM models using cultured astrocytes immortalized via an N-terminal SV40 large T (T_{121}, T) mutant that ablates the Rb family of pocket proteins. MAPK and PI3K were activated

alone and in combination via oncogenic *Kras* ($Kras^{G12D}$, R) and *Pten* deletion (P), respectively.[20] We used these models to show that activated PI3K and MAPK cooperate to promote astrocyte proliferation, migration, and de-differentiation *in vitro* and malignant progression to rapidly fatal GBM *in vivo*. TRP astrocytes also displayed the phenotypic hallmarks of GBM stem cells (GSC) and molecularly recapitulated proneural GBM.[16,20] Here we utilized the TRP nGEM culture and allograft model system and GBM PDX to define the influence of drug potency on signaling dynamics, efficacy, and synergism of PI3K (PI3Ki) and MEK1/2 (MEKi) inhibitors.[16,20]

Materials and Methods

Murine astrocyte cultures. Cortical, genetically engineered mouse (GEM)-derived astrocytes were cultured as previously described.[16,20,21] Briefly, mice harboring conditional *TgGZT*$_{121}$ (T), *Kras*^{G12D} knock-in (R), and *Pten* knock-out (P) alleles were crossed to generate compound TRP mice.[20,22-24] Astrocytes harboring the floxed alleles (T/R, heterozygous; P, homozygous) were harvested from neonatal mice. Recombination was induced *in vitro* with a recombinant adenoviral vector encoding cytomegalovirus promoter-driven Cre recombinase (Ad5CMVCre, University of Iowa Gene Transfer Vector Core). TRP astrocytes expressing luciferase were generated as previously described.[16] Astrocytes were maintained as adherent cells at 37 °C and 5% CO_2 in Dulbecco's Modified Eagle Medium (DMEM) supplemented with 10% fetal bovine serum and 1% penicillin/streptomycin. The UNC Institutional Animal Care and Use Committee approved all animal studies (Protocol # 16-112).

Human ECL and PDX cultures. D32, D65, D54, U251, and U87 ECL were a kind gift from G. Yancey Gillespie at the University of Alabama at Birmingham. U373, LN229, and LN18 ECL were obtained from ATCC (Manassas, VA). ECL were maintained as adherent cells in DMEM supplemented with 10% fetal bovine serum and 1% penicillin/streptomycin at 37 °C and 5% CO_2 as previously described.[25,26] GSC20, GSC23, GSC6-27, GBM6, GBM12, GBM46, and GBM59 PDX were maintained at 37 °C and 5% CO_2 as non-adherent spheroids in DMEM/F12 supplemented with 1x B27 (ThermoFisher, Waltham, MA), 20 ng/ml epidermal growth factor (EGF), and basic fibroblast growth factor (bFGF) (Sigma-Aldrich, St. Louis, MO or ThermoFisher), with or

without N-2 supplement (ThermoFisher) and 1% penicillin/streptomycin, as previously described.[27,28] Subcutaneous PDX were maintained as previously described.[29]

Drugs. See **Table S3.1** for details on drugs used in this study.[30-37] For *in vitro* experiments, working stocks of buparlisib, LY, temsirolimus, everolimus, selumetinib, PD01, and trametinib were dissolved in dimethyl sulfoxide (DMSO), while dactolisib was dissolved in N,N-Dimethylformamide (DMF).

Dose response. To examine relative growth in response to drugs, TRP astrocytes were plated in technical replicates (N=3-6) in 96-well tissue culture plates and allowed to adhere overnight. Cells were treated the following day with increasing concentrations of drug or an equal concentration of solvent (control). Cell growth was assessed 5 days after treatment with the CellTiter 96 Aqueous One Solution Cell Proliferation Assay (MTS, Promega, Madison, WI) according to manufacturer's instructions. Absorbance was measured on an Emax plate reader (Molecular Devices, Chicago, IL) equipped with SoftMax Pro 5 software. Baseline absorbance (MTS reagent plus media) was subtracted from the absorbance in each well and relative growth was calculated as absorbance of treated relative to control cells.

Drug response of cultured PDX (GBM6, GBM12, GBM46, and GBM59) was performed as previously described with minor modifications.[38] Briefly, PDX were seeded (3000 cells/well) in technical replicates (N=7) in 96-well plates and cultured for 72 hours to form neurospheres. Increasing drug concentrations were added and treated cells were incubated for 96 hours. Vehicle only and staurosporine (a drug toxic to most cell lines at 5 μM) were included as negative and positive controls, respectively. CellTiterGlo® (Promega, San Luis Obispo, CA) was used to assess cell viability.

Luminescence was measured using a Perkin Elmer Envision 2104 Multilabel Reader. Raw values were normalized on a plate-by-plate basis such that 100% cell viability was equivalent to the mean of vehicle wells and 0% cell viability was equivalent to the mean of the staurosporine treated control.

Data from independent TRP (N=2-5) and PDX (N=1) drug treatment experiments were pooled and fit to a non-linear, log [inhibitor] versus response curves with variable slope. IC_{50}, GI_{50}, I_{max} and Hill slopes were calculated as previously described.[16,39,40] Genotype and drug potency effects on IC_{50} were calculated by two-way ANOVA. The pairwise effects of PDX model and drugs on IC_{50} were compared using the extra-sum-of-squares F test.

Cell cycle analysis. TRP astrocytes were plated in 12-well tissue culture plates, allowed to adhere overnight, and then treated with drugs or vehicle control. Cell cycle analysis was performed 2 days post-treatment using Guava Cell Cycle Reagent according to the manufacturer's instructions (EMD Millipore, Billerica, MA). Briefly, cells were harvested by trypsinization, fixed for >1 h in 70% ethanol on ice, and relative DNA content was determined on a Guava EasyCyte Plus. Percent cells in each cell cycle phase were analyzed using ModFit LT v3.2 (Verity, Topsham, ME). Mean percent cells in G_0/G_1, S, and G_2/M were calculated from 1-2 technical replicates from two independent experiments. Drug effects on cell cycle distribution were analyzed by two-way ANOVA.

Kinome profiling. For dynamic kinome profiling of TRP astrocytes, cells were treated with either 1 μM of buparlisib for 4, 24, and 48 h or DMSO (control) for ~20 min (0 h). Multiplexed inhibitor bead chromatography was performed as previously described for

astrocytes and untreated, snap-frozen GBM PDX samples.[41,42] Briefly, cells or frozen PDX samples were lysed in a HEPES/NaCl/Triton X-100 buffer and lysates gravity-flowed through columns containing inhibitor-conjugated beads (CTx-0294885, VI-16832, PP58, Purvalanol B, and two custom-synthesized compounds UNC-2147A and UNC-8088A). Beads were then washed and kinases eluted. Kinases were purified by chloroform/methanol extraction, suspended in 50 mM HEPES (pH 8), digested with trypsin, labeled with iTRAQ (AB SCIEX, Framingham, MA) or TMT (Thermo Scientific) according to manufacturer's instructions, and cleaned with PepClean C18 Spin Columns (Thermo Scientific). Peptide samples were analyzed by LC/MS/MS using an Easy nLC1000 coupled to a QExactive or QExactive HF mass spectrometer (Thermo Scientific). Peptides were injected onto an Easy Spray PepMap C18 column (75 µm x 25 cm, 2 µm particle size) (Thermo Scientific) and separated over a 300 min (QExactive) or 165 min (QExactive HF) gradient. The gradient for separation consisted of 5–40% mobile phase B at a 250 nl/min flow rate, where mobile phase A was 0.1% formic acid in water and mobile phase B consisted of 0.1% formic acid in acetonitrile. Mass spectrometer parameters were as follows: 3e6 AGC MS1, 80ms MS1 max inject time, 1e5 AGC MS2, 100ms MS2 max inject time, 20 loop count, 1.8 m/z isolation window, 45s dynamic exclusion. Spectra were searched against the Uniprot/Swiss-Prot database with Sequest HT on Proteome Discoverer software with 5% false discovery rate (FDR). Peptides with greater than 25%-coisolation interference were omitted. Multiplexed inhibitor beads (MIB)-binding of treated samples was set relative to controls and pooled from two independent experiments. For baseline PDX comparison, scaled abundance values in biological triplicate from Proteome Discoverer were used for

principal components analysis using Perseus software (Max Planck Institute of Biochemistry) and hierarchical clustering (one minus Pearson correlation) using GENE-E software (Broad Institute).

Baseline kinome profiling of ECL and human samples were performed as described above. Baseline spectra were searched with MaxQuant software using default parameters and Label Free Quantification (LFQ) intensity was used as the normalized level for each kinase. D54, U373, LN18, and LN229 were selected and pooled as a standard reference for MIB and mass spectrometry (MIB-MS) analysis of the human GBM samples based on their differentially enriched kinases. All kinome tree illustrations reproduced courtesy of Cell Signaling Technology, Inc. (www.cellsignal.com). One minus Pearson hierarchical clustering was performed on LFQ intensities using GENE-E software. Principal components analysis (PCA) was performed using Cluster 3.0. Human GBM samples were obtained from the UNC Tissue Procurement Facility in compliance with institutional guidelines under a protocol approved by the UNC Office of Human Research Ethics (Institutional Review Board [IRB], 15-0923).

Immunoblots. TRP astrocytes were treated with drug(s) or solvent (control). Cells were mechanically harvested 4 or 24 h after treatment, and proteins were extracted. Briefly, proteins (20 μg for immunoblots to detect PI3K and MAPK signaling and 50 μg for immunoblots to detect cleaved caspase-3) were resolved by gradient (8-16%) gel electrophoresis (SDS-PAGE, Bio-Rad, Hercules, CA) then transferred to PVDF membranes (EMD Millipore). Immunoblots were probed at 4 °C overnight using primary antibodies against Gapdh (#AB2302, EMD Millipore) and Akt (#2967), p-Akt (Ser473,

#9271), p-S6 (Ser240/244, #2215), p-Erk1/2 (Thr202/Tyr204, #9101), Erk1/2 (#4696), and cleaved caspase-3 (#9664) all from Cell Signaling Technology (Danvers, MA). Blots were incubated with species specific Alexa 488, 568, or 633 conjugated secondary antibodies at room temperature for 30 min, imaged on a GE Typhoon Trio (GE Healthcare), and band intensities were quantified using ImageJ (NIH, Bethesda, MD). Signaling levels were assessed by normalization of phosphoproteins to the corresponding total protein or Gapdh and then set relative to control-treated cells. Alternatively, normalized proteins from tumor samples were set relative to a TRP protein standard contained on all blots, and then were normalized to untreated tumors.

Whole Exome Sequencing. DNA from PDX tumors was isolated from subcutaneous tumor pieces using Qiagen's AllPrep Kit. Isolated DNA was used to generate whole exome sequencing libraries. Genomic tumor and normal DNAs (1.1 µg) for each sample were fragmented to a target size of 150–200 bp; 100 ng of fragmented product was run on TAE gel to verify fragmentation. The remaining 1 µg of fragmented DNA was prepared using Agilent's SureSelectXT Human All Exon 50 Mb kit (catalog# G7544C). Exome libraries were prepared with Agilent's SureSelectXT Human All Exon V4 library preparation kit (catalog# 5190-4632) and SureSelectXT Human All Exon V4+UTRs (catalog# 5190-4637) following the manufacturer's protocols. Libraries were paired-end sequenced on the Illumina HiSeq 2000 and analyzed after Fastq generation and alignment using the Burrows-Wheeler Alignment against the human reference genome and matched patient germline DNA sequence for identification of somatic events.[43]

Drug synergism. Relative growth of TRP astrocytes was determined for single agent and combination treatments at a constant molar ratio as described above and synergism was determined using the Chou-Talalay method.[44] Briefly, fraction affected (1 – relative growth, FA) was determined and the combination index was calculated using CompuSyn (ComboSyn, Inc., Paramus, NJ). Data were pooled from 2–4 independent experiments. Combination index (CI) values >1, 1–0.86, and <0.86 were considered antagonistic, additive, and synergistic, respectively.

EdU incorporation. EdU incorporation assays were performed as previously described with the following modifications.[45] TRP astrocytes were seeded on poly-D lysine (Sigma-Aldrich) coated Nunc Lab-Tek II chamber slides (ThermoFisher). Cells were allowed to adhere and at ~60% confluence were treated with vehicle control (DMSO), selumetinib (2.5 μM), buparlisib (1.5 μM) or both selumetinib (2.5 μM) + buparlisib (1.5 μM). At 24 h post-treatment, 10 μM 5-ethynyl-2′-deoxyuridine (EdU, Invitrogen, Grand Island, NJ) was supplemented to the culture + drug containing media and cells were incubated in the presence of EdU for 6 hr. Cells were then fixed with 4% para-formaldehyde for 5 min, blocked with 0.1% Triton X-100, 1% BSA, 5% horse serum, and 0.01 M glycine in PBS at 4 °C for 30 min. EdU was detected by labeling with Alexa 555 or 647 using the Click-iT EdU Imaging Kit (ThermoFisher) according to manufacturer's instructions. Cells were washed, counter-stained with DAPI, and coverslipped with PermaFluor (ThermoFisher). Three images per well were taken with a LSM 780 confocal microscope (Zeiss, Oberkochen, Germany) equipped with 20X objective and ZEN 2012 software. Percentage of EdU positive cells per image was quantified using ImageJ (NIH) and the mean (±SEM) percent EdU^+ cells was calculated from the three

images per two technical replicates from two independent experiments. Drug effects on EdU incorporation were analyzed by Students's t tests.

Apoptosis. TRP astrocytes were plated in 12-well tissue culture plates, allowed to adhere overnight, and then treated with vehicle control (DMSO), selumetinib (2.5 μM), buparlisib (1.5 μM) or both selumetinib (2.5 μM) + buparlisib (1.5 μM). Apoptosis was measured 24 h post-treatment by flow cytometry using the Guava Viacount Assay according to the manufacturer's instructions (EMD Millipore). Briefly, cells were harvested by trypsinization, stained with the Guava Viacount reagent and dye exclusion was determined on a Guava EasyCyte Plus. Gates for viable, apoptotic and dead cells were set according to the manufacture's instructions and percent apoptotic cells (mean ± SEM) was calculated from one technical replicate from four independent experiments. Drug effects on apoptosis were analyzed by Student's t tests.

Orthotopic TRP allografts. TRP astrocytes expressing luciferase were injected orthotopically into syngeneic C57Bl/6 mice as previously described.[20,21] Briefly, astrocytes were harvested by trypsinization, counted, and suspended in serum free DMEM with 5% methyl cellulose. Adult mice (mean ~6 months) were anesthetized with Avertin (250 mg/kg) and 10^5 astrocytes were injected into the right basal ganglia using the coordinates 1, -2, and -4 mm (A, L, D) from bregma. Beginning on day 3 post injection, isoflurane anesthetized mice were imaged bi-weekly by bioluminescence imaging (BLI) on an Ivis Kinetic (PerkinElmer, Waltham, MA) as previously described.[16,21] Briefly, mice were injected peritoneally with D-luciferin (PerkinElmer), images were acquired after 10-15 min, and bioluminescence flux (photons/sec/cm2) was quantified using PerkinElmer Living Image software. Mice were randomized 7 days

after cell injection into 4 groups (control, buparlisib, selumetinib, and buparlisib/selumetinib; 13-18 mice per group), and treatment on a 5 days on, 2 days off schedule (**Table S3.2**) was initiated via chow on day 10 and continued until signs of neurologic morbidity. BLI flux was expressed relative to initial flux (day 3). Relative flux from treatment initiation (day 10) through day 21 was fit to an exponential growth equation and the rate constant k and doubling time [ln(2)/k] were calculated. Animals were monitored for neurological symptoms and upon onset, mice were sacrificed, brains were harvested, and cut sagittally through the needle track. A portion of grossly visible tumor was harvested and snap frozen while the remaining brain was immersion fixed in 10% neutral buffered formalin overnight and stored in 70% ethanol prior to paraffin embedding. Immunoblots on frozen tumor lysates (N=3 per group) were performed as described above.

Orthotopic PDX. PDX were established in athymic mice (Taconic) as described previously.[29] Briefly, 3 x 10^5 glioma cells (GBM6, GBM12, and GBM46) were implanted in the right striatum and tumors established for 15 days. Mice were then randomized to receive vehicle control (n = 10) or 45 mg/kg dactolisib (n = 10) on a 5 days on/2 days off schedule every 28-day cycle. Mice were observed daily and euthanized upon neurological morbidity. Studies were approved by the Translational Drug Development Management Animal Care and Use Committee (Scottsdale, AZ).

Histopathology. Histopathological evaluation was conducted as previously described.[16] Briefly, formalin-fixed, paraffin-embedded brains were cut in serial 4-5 µm sections on a rotary microtome, placed on glass slides, and stained with hematoxylin and eosin (H&E) on a Leica Microsystems Autostainer XL (Buffalo Grove, IL). Stained

slides were scanned on an Aperio ScanScope XT (Vista, CA) using a 20X objective and svs files were imported into an Aperio eSlideManager web database. Histopathological analyses and tumor grading was conducted according to the WHO 2007 criteria for human astrocytomas for each mouse within the control (n=15) or selumetinib (n=13) cohorts.[46] Tumor area (mm^2) on scanned H&E-stained slides (2 sections per brain) was measured using the annotation tools in Aperio ImageScope v12.2.1.5005. Photomicrographs were taken on an Olympus BX41 microscope and DP70 digital camera (Center Valley, PA). Effects of treatment on diagnosis were compared by two-way ANOVA with Bonferroni multiple comparisons post-tests. Effects of treatment on tumor size were compared using unpaired t-tests.

Subcutaneous TRP allografts. TRP astrocytes expressing luciferase were harvested by trypsinization, counted, and suspended in serum free DMEM with 5% methyl cellulose. Adult syngeneic C57Bl/6 mice (mean ~9.5 months) were anesthetized with Avertin (250 mg/kg) and 5 x 10^6 astrocytes were injected into the right flank. Tumors were established for 14 days, volume (mm^3) was determined with calipers using the formula $(L*W^2)/2$, mice were randomized into treatment groups (**Table S3.2**) containing 4-6 mice each with statistically insignificant differences in tumor volume, and treatment via oral gavage was initiated and continued for five days (14–19) with the following exception. Dactolisib- and dactolisib/selumetinib-treated mice showed signs of drug-induced toxicity and were thus not treated on day 19. Tumor volume was measured 5 days per week from days 14–25 and expressed relative to treatment initiation (day 14). Tumor volume data were then fit to an exponential growth equation and the rate constant k and doubling time [ln(2)/k] were calculated. For pharmacokinetic

experiments, subcutaneous allografts and treatment were performed as described above, except that mice (n=2-3 per group) were treated for two days and then sacrificed 4 h following the second treatment. Subcutaneous tumors were harvested, snap frozen, and then lysed for immunoblots. Buparlisib, dactolisib, and selumetinib were dissolved in 10/90 V/V of N-methyl-2-pyrrolidone (NMP)/poly(ethylene glycol) 300 (PEG300) at 15 mg/ml, 15 mg/ml, and 10.8 mg/ml respectively. Trametinib was dissolved in 0.5% methylcellulose and 0.2% Tween-80 in deionized water at 0.3 mg/ml.

Statistics. Statistical analyses were conducted in GraphPad Prism 5 (La Jolla, CA). $P \leq 0.05$ were considered statistically significant unless otherwise stated. Error bars are SEM. Log_{10} (Log) IC_{50} was graphed unless otherwise stated. Effects of treatment on survival of allograft or xenograft mice were determined by Kaplan-Meier analyses and were compared by log-rank tests. The effects of treatment on orthotopic or subcutaneous allograft growth (k value) was compared using the extra sum of squares F test.

Results

PI3K and MAPK mutations are frequent in GBM and drive tumorigenesis in preclinical models.[3,4,8,9,47] We previously showed that activated PI3K and MAPK cooperated to promote gliomagenesis in TRP nGEM culture and allograft models.[16,20] However, it remained unclear if these models were sensitive to PI3Ki and MEKi. We addressed this issue by examining how drug potency influences target inhibition, adaptive kinome response, efficacy, and synergism of single agent and combination therapies *in vitro* and *in vivo*.

PI3Ki and MEKi block TRP astrocyte and PDX growth *in vitro*

A dose-dependent, sigmoidal growth reduction was evident for multiple PI3Ki in cultured TRP and PDX models (**Fig S3.1AB**), with the PI3Ki buparlisib inducing a G_2/M cell cycle arrest in TRP astrocytes (**Fig S3.2A**). Moreover, a direct association between potency (dactolisib > buparlisib > LY) and efficacy was evident, both for TRP astrocytes (**Figs 3.1A**, **S3.2B**) and PDX (**Figs 3.1B**, **S3.3**). The PI3Ki/mTORi dactolisib was the most potent, but its efficacy may be due, in part, to direct mTOR inhibition. Two mTORi reduced TRP astrocyte growth with IC_{50} in the low micro- to high nanomolar range (**Fig S3.2B**). However, both caused more gradual decreases in growth (Hill slope, $P \leq 0.03$) and were less potent than dactolisib ($P \leq 0.003$).

Next we assessed how MEKi potency (trametinib > PD01 > selumetinib) influences growth. Although PD01 and trametinib have similar IC_{50} for purified MEK, their mechanism of inhibition differ and trametinib is the more potent inhibitor of signaling and cell growth.[35] MEKi caused gradual, dose-dependent decreases in growth of cultured TRP and PDX (**Fig S3.1C**). Moreover, a direct association between

potency and efficacy was evident, both for TRP astrocytes (**Figs 3.1C, S3.2B**) and PDX (**Figs 3.1D**, **S3.3**). Selumetinib also induced a G_1/S cell cycle arrest in TRP astrocytes (**Fig S3.2C**). Taken together, these data showed that cultured TRP astrocytes and PDX were sensitive to PI3Ki and MEKi.

PI3Ki induces adaptive kinome reprogramming, **including alternate MAPK activation**

Among PI3Ki, mTORi, and MEKi, PI3Ki were generally the most effective at inhibiting TRP astrocyte growth (**Figs 3.1AC**, **S3.1**, **S3.2**). However, many targeted kinase inhibitors that were effective in preclinical settings have had disappointing results when used as single agents in GBM patients.[12,13] One reason for this may be compensatory signaling changes that manifest as drug resistance, suggesting that combination therapies will be necessary to improve outcomes.

We have previously used MIB-MS to show that adaptive kinome reprogramming promotes resistance to single agent kinase inhibitors.[41,42] We thus used this technique to examine the adaptive kinome response of TRP astrocytes to the PI3Ki buparlisib. Buparlisib induced widespread kinome changes, with alterations in multiple kinase families (**Fig S3.4A**). Kinome response was dynamic and the patterns of activity differed among kinases (**Figs 3.2A**, **S3.4B**, **Table S3.3**). Three major temporal patterns were discernible, as we have previously described (**Fig 3.2B**).[41,42] Buparlisib induced sustained inhibition of proximal PI3K signaling (e.g. Akt1, pattern 1) and transient inhibition of distal PI3K (e.g. mTor), followed by re-activation (pattern 2). Activation of alternative pathways such as MAPK (e.g. Erk1/2) was also apparent (pattern 3).

Immunoblots of TRP astrocytes treated with buparlisib for 4 h (data not shown) and 24 h (**Fig 3.2C-E**) showed that proximal (p-Akt) and distal (p-S6) PI3K signaling was inhibited at 4 h and sustained for 24 h, while MAPK signaling progressively increased over 24 h. Next we assessed how potency influenced PI3K inhibition and alternate MAPK activation. All PI3Ki caused dose-dependent inhibition of proximal and distal PI3K signaling, and inhibition was directly associated with drug potency (**Fig 3.2CD**). Moreover, both of the more potent PI3Ki, buparlisib and dactolisib, induced alternate MAPK activation (**Fig 3.2CE**). Taken together, these results suggested that alternate MAPK activation contributes to PI3Ki resistance.

MEKi induces MAPK inhibition and alternate PI3K activation *in vitro*

We found that PI3Ki induced MAPK activation (**Fig 3.2B-E**) and that multiple MEKi reduced TRP astrocyte growth (**Figs 3.1C, S3.1C, S3.2B**). MEKi have been shown to induce alternate PI3K activation in multiple cancer types.[48-50] We therefore performed immunoblots on TRP astrocytes 24 h after treatment with increasingly potent MEKi to determine their effects on MAPK and PI3K signaling (**Fig 3.2F**). All three MEKi caused dose-dependent decreases in MAPK signaling and dose/potency was directly associated with degree of inhibition (**Fig 3.2FG**). Activation of proximal, but not distal, PI3K signaling was evident at 24 h with all three MEKi, and activation was associated directly with dose/potency (**Fig 3.2FH**).

A subset of GBM and PDX models have hyperactive kinomes featuring MAPK activation

GBM has extensive genome and transcriptome heterogeneity.[3,4] However, details on the basal activation state of its kinome are limited. We therefore analyzed

baseline kinome profiles of human GBM-derived ECL (**Fig 3.3A**) and patient samples (**Fig 3.3B**) via MIB-MS. Hierarchical clustering showed kinome heterogeneity, with relative hyper-activation of unique kinases in each model and patient sample. Principal component analysis stratified patient tumors into two kinome subtypes (K1 and K2) (**Fig 3.3C**). Heatmaps (**Fig 3.3B**) and kinome tree views (**Figs 3.3DE**, **S3.5AB**) showed that K1 tumors had a relatively hyperactive kinome compared to K2. Among the hyper-activated K1 kinases were MAP2K1 (MEK1), RPS6KA2 (RSK3), MAPK3 (ERK2), and MAPK1 (ERK1) (**Fig 3.3F**), suggesting that MAPK hyper-activation may be an attractive therapeutic target in these tumors. Baseline kinome profiles of subcutaneous (**Figs 3.3GH, S3.5C**) and cultured (**Fig S3.6A**) PDX were also variable. GSC23 and GSC6-27 harbored acitvation of numerous kinases within the tyrosine kinase (TK) and CMGC families, similar to the K1 subtype of patient samples (**Figs S3.5A, S3.6B**). Moreover, the PDX GBM59, GBM46, and GBM12 had heterogenous genomes (**Fig S3.7**), but all harbored activation of numerous TK (**Fig S3.5C**, **Table S3.4**).

PI3Ki and MEKi are synergistic *in vitro*

Data from **Fig 3.2** suggested that PI3K and MAPK are reciprocal bypass pathways that promote cell survival when either pathway alone is inhibited. We therefore assessed whether dual PI3Ki/MEKi caused inhibition of both pathways. Immunoblots of TRP astrocytes 24 h after buparlisib plus selumetinib (**Fig 3.4A**) or trametinib (**Fig 3.4B**) showed a dose-dependent inhibition of both PI3K/MAPK signaling. The concentration of buparlisib required for PI3K inhibition was similar regardless of the MEKi used, but MEKi potency was directly associated with MAPK inhibition.

Next, we assessed whether PI3Ki/MEKi functioned synergistically. Buparlisib/selumetinib inhibited growth and was synergistic in TRP astrocytes (**Fig 3.4C**), likely due to the combinatorial effects of selumetinib-induced decreases in proliferation (**Fig S3.8AB**) and buparlisib-induced increases in apoptosis (**Fig S3.8C**). Buparlisib plus the more potent MEKi trametinib also inhibited growth and was synergistic (**Fig 3.4D**). However, the PI3Ki/MEKi concentrations required for synergism were dramatically reduced with buparlisib/trametinib, compared to buparlisib/selumetinib.

PI3Ki and MEKi are effective in subcutaneous TRP allografts

The blood-brain barrier can hinder drug penetrance and thus limit efficacy.[13] We therefore first tested PI3Ki/MEKi efficacy in subcutaneous TRP allografts to eliminate the variable of blood-brain barrier penetrance. Single agents were used at doses described in the literature (**Table S3.2**).[31,51,52] Both PI3Ki effectively reduced tumor growth (**Fig S3.9AB**) and inhibited PI3K (pAkt) signaling by ~50% (**Fig S3.10AB**), but neither extended survival (**Fig S3.9C**). Both MEKi also delayed tumor growth (**Fig S3.9DE**) and decreased MAPK (pErk) signaling >60% (**Fig S3.10AC**). However, trametinib, but not selumetinib, extended survival (**Fig S3.9F**).

Because PI3Ki/MEKi were synergistic *in vitro* (**Fig 3.4**), we hypothesized that combinations would be more effective than single agents *in vivo*. However, drug-induced toxicity can be amplified when combinations are used, necessitating dose reduction. We found that maximum tolerated dose (MTD) of buparlisib/selumetinib was achieved at 1.2-2.1-fold lower doses in non-tumor bearing mice (**Table S3.2**, data not shown). This combination was well-tolerated and effective in an intracranial xenograft

model of triple-negative breast cancer (TNBC) when used on a 5 days on/2 days off schedule.[53] Dactolisib/selumetinib doses were based on published literature.[51] For *in vivo* experiments with the PI3Ki buparlisib or dactolisib in combination with MEKi trametinib, we empirically kept the PI3Ki doses constant and empirically halved the trametinib dose, as we did with selumetinib (**Table S3.2**). Combination treatments, as well as most single agents, caused an increase in cleaved caspase-3, an indicator of apoptosis (**Fig S3.10DE**). Buparlisib/selumetinib caused tumor regression (**Fig 3.5AB**) and increased survival (**Fig 3.5C**). Buparlisib plus the more potent MEKi trametinib also significantly reduced growth (**Fig 3.5DE**) and extended survival (**Fig 3.5F**). Both combinations were more effective than either drug alone.

Similar results were obtained with the more potent PI3Ki dactolisib combined with MEKi. Dactolisib/selumetinib significantly reduced tumor growth (**Fig 3.5GH**), but did not extend survival (**Fig 3.5I**). However, mice treated with dactolisib ± selumetinib, but not the more potent dactolisib/trametinib combination, exhibited drug-induced toxicity as evidenced by a rapid onset of lethargy. Dactolisib/trametinib induced tumor regression (**Fig 3.5JK**) and increased survival (**Fig 3.5L**). Moreover, dactolisib/trametinib was more effective at growth inhibition than either drug alone. These results indicate that combination therapy with PI3Ki/MEKi are effective in subcutaneous TRP allografts, with the more potent inhibitors being particularly effective.

Selumetinib delays orthotopic TRP allograft growth

We found that TRP astrocytes were sensitive to single agent PI3Ki/MEKi (**Figs 3.1**, **S3.2**) and that dual treatment was synergistic (**Fig 3.4CD**) *in vitro*. Moreover, single agents delayed subcutaneous tumor growth, but dual treatment was more effective (**Fig**

3.5). We therefore hypothesized that these treatments might be effective in orthotopic TRP allografts. We thus tested the brain penetrant PI3Ki buparlisib and/or MEKi selumetinib in this model and found that selumetinib ± buparlisib transiently delayed tumor growth, but buparlisib alone did not (**Fig 3.6AB**). Selumetinib modestly, but significantly prolonged survival, but all mice eventually succumbed to recurrent disease. Buparlisib ± selumetinib failed to extend survival (**Fig 3.6C**).

Next, we defined the pharmacodynamic effects of treatment on PI3K/MAPK signaling *in vivo* by performing immunoblots on tumors harvested from terminal mice (**Fig 3.6D**). Buparlisib did not affect PI3K signaling (**Fig 3.6E**), either alone or in combination with selumetinib. In contrast, selumetinib caused a modest MAPK decrease (**Fig 3.6F**) when used alone, but not in combination with buparlisib, likely due to the ~2-fold increased dose. Because selumetinib was the most effective treatment, we next compared the histopathology of terminal control and selumetinib-treated mice (**Fig S3.11AB**). Tumor area was similar between groups (**Fig S3.11C**), but progression to GBM was more frequent in untreated tumors (**Fig S3.11D**). Taken together, these data suggest that selumetinib was effective due to inhibition of MAPK (~50%, **Fig 3.6F**) with minimal PI3K reactivation when used alone at ~2-fold higher dose. Moreover, they suggest that buparlisib alone was ineffective due to minimal PI3K inhibition despite favorable CNS pharmacokinetics. Finally, these data suggest that the reduced doses of both drugs required for combination therapy limited target inhibition as well as efficacy in orthotopic GBM models.

GBM PDX response to dactolisib is heterogeneous

Human GBM PDX are valuable models for preclinical drug development because they faithfully recapitulate the genotypic and phenotypic characteristics of their parent tumors.[54] Although dactolisib was the most effective PI3Ki in cultured TRP astrocytes and PDX models (**Fig 3.1AB**), its effectiveness an intracranial GBM model was limited.[52] To confirm this finding, we examined efficacy of the most potent PI3Ki/mTORi dactolisib in a panel of orthotopic xenograft models. Survival of mice harboring GBM46, but not GBM12 or GBM6, was extended by dactolisib, but its effects were modest in this model (17% increased survival, **Fig 3.6G**). This heterogeneous response of PDX to dactolisib highlights the importance of identifying predictive biomarkers for the development of kinase inhibitors.

Discussion

PI3K/MAPK mutations influence targeted inhibitor efficacy

GBM are molecularly heterogeneous, but the vast majority harbor activated MAPK and PI3K.[3,8] Core pathway mutations influence single agent kinase inhibitor efficacy in GBM ECL models.[4,48,55] However, preclinical drug studies with ECL correlate poorly with clinical outcomes.[13] PDX and nGEM are more genetically faithful and thus may be more predictive.[56] We found that cultured PDX and TRP nGEM were sensitive to PI3Ki or MEKi treatment, with increased potency directly associated with efficacy (**Figs 3.1, S3.1-3**).

Dual PI3Ki/MEKi therapies have shown efficacy in some preclinical GBM models and have demonstrated the importance of PI3K/MAPK crosstalk in GSC maintenance.[48,50,52] We have shown that both of these pathways are critical for astrocyte de-differentiation into GSC in TRP nGEM models.[16,20] We expanded these results here by determining that the PI3Ki/MEKi concentrations required for synergism in TRP astrocytes was dramatically reduced when a more potent MEKi was used (**Fig 3.4CD**).

Bypass pathways promote resistance to single agent kinase inhibitors

We and others have shown that PI3K/MAPK crosstalk is essential for GSC genesis, maintenance, and tumorigenicity, suggesting that dual inhibition of these pathways may be effective.[16,20,50] Additional evidence for the necessity of combination treatments comes from our own preclinical work in breast cancer, showing that dynamic kinome reprogramming promotes single agent kinase inhibitor resistance.[41,42] We extended this work to GBM here and found that buparlisib induces extensive kinome

reprogramming in TRP astrocytes (**Fig 3.2**). Although we focused primarily on alternate MAPK activation, dynamic kinome profiling showed that multiple pathways were altered in response to PI3Ki and may thus promote resistance. Future work will be required to investigate these pathways.

We and others have found that PI3K and MAPK are reciprocal, bypass pathways that promote resistance to drugs targeting either pathway alone (**Figs 3.2**, **3.4**).[48,50,52] However, these dynamic responses may be influenced by mutational activation of PI3K/MAPK signaling as well as by different mutations or tumor cells of origin. Here we found that sensitivity of PDX to MEKi or PI3Ki was variable (**Figs 3.1**, **3.6**, **S3.1**), but the reason for these differences were not readily apparent based on their genomic or baseline kinome profiles (**Figs 3.3**, **S3.7**, **Table S3.4**). Thus, systematic profiling of chemovulnerability in a large, integrated panel of PDX and nGEM with diverse mutations and cells of origin will be necessary to further elucidate the contours of GBM kinome dynamics and aid in the development of combination treatments tailored to specific tumor subsets.

We previously showed that genomic heterogeneity in breast cancer extends to its kinome.[41,57] Here we extend these findings by demonstrating that MIB-MS analysis can stratify human GBM samples and PDX/ECL models based on their kinome profiles (**Fig 3.3**). Based on our experience with an ongoing “window” trial of neoadjuvant kinase inhibitor therapy in breast cancer, we anticipate that MIB-MS-based kinome profiling of pre- and post-treated GBM patient samples will ultimately result in identification of novel resistance mechanisms and facilitate design of rational combination treatments.[57]

Drug potency influences single and dual agent efficacy

Increased potency facilitates target modulation at lower drug concentrations and dose reduction *in vivo*. We found that increased PI3Ki/MEKi potency enhanced growth inhibition and synergism *in vitro* (**Figs 3.1**, **3.4**, **S3.1-3**). Single agent PI3Ki buparlisib and dactolisib were equally effective in subcutaneous TRP allografts, while trametinib was more effective than the less potent MEKi selumetinib (**Fig S3.9**). Three of four dual treatments were more effective than their corresponding single agents, particularly the most potent combination, buparlisib/trametinib (**Fig 3.5**). However, dactolisib ± selumetinib induced systemic toxicity, likely limiting their effectiveness.

We investigated efficacy of the CNS penetrant PI3Ki/MEKi combination, buparlisib and selumetinib, in orthotopic TRP allografts. Selumetinib alone caused signaling inhibition and was most effective. Lack of buparlisib/selumetinib efficacy was likely due to dose reduction (~2-fold for selumetinib) required to prevent toxicity (**Fig 3.6**, **Table S3.2**), consistent with dose limiting toxicity for kinase inhibitor combinations found in clinical settings.[14] We have also tested selumetinib and/or buparlisib in intracranial TNBC xenografts and found that target inhibition occurred in sensitive, but not resistant models.[58] This suggests that drug levels within orthotopic TRP allografts were insufficient to cause signaling inhibition and affect outcomes; this limitation may be overcome using alternative delivery approaches (e.g. nanoparticles) that improve brain penetrance and reduce systemic toxicity.[59]

Conclusion

MIB-MS-based monitoring of the dynamic kinome *en masse* represents a valuable tool to identify bypass pathways and design rational drug combinations. Its

use in directing preclinical trials in genetically faithful models, such as the nGEM model used here, can aid development of these therapies as well as predictive biomarkers to guide their use. Our results suggest that highly-potent, brain-penetrant kinase inhibitor combinations designed to target resistance pathways will likely be required to design effective clinical trials in molecularly-defined GBM patients.

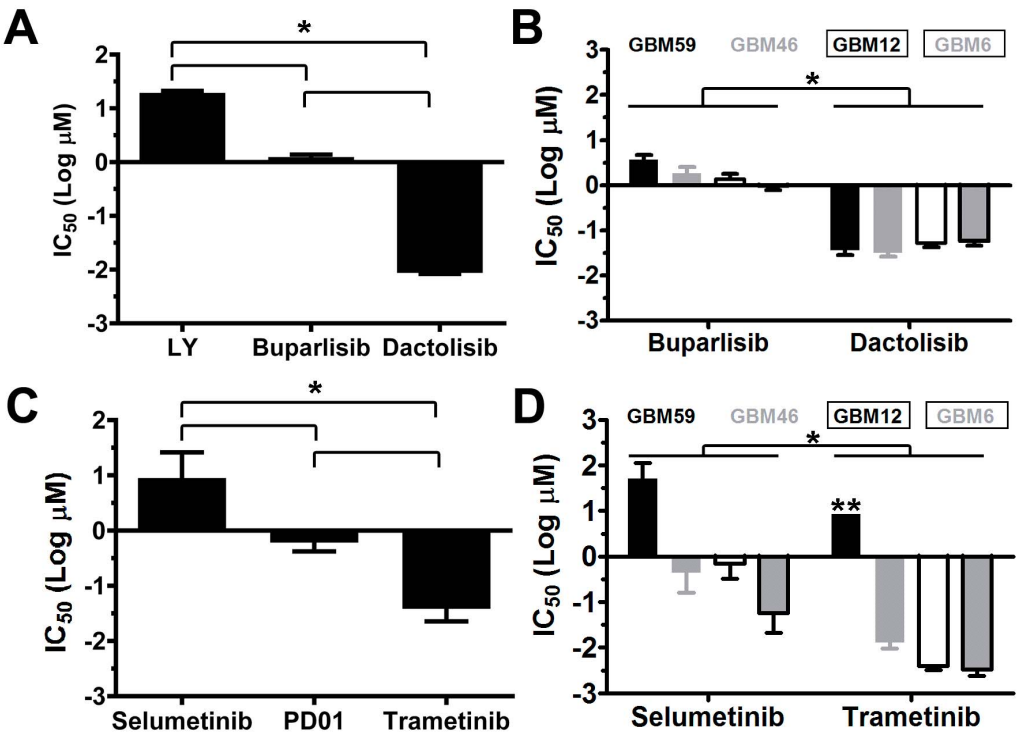

Figure 3.1. **Single agent PI3Ki or MEKi potency is directly associated with efficacy *in vitro***. PI3Ki (**A**,**B**) and MEKi (**C**,**D**) potency was inversely associated with IC_{50} in cultured TRP astrocytes (**A**,**C**) and PDX (**B**,**D**) (*, P<0.0001). **, ambiguous IC_{50}.

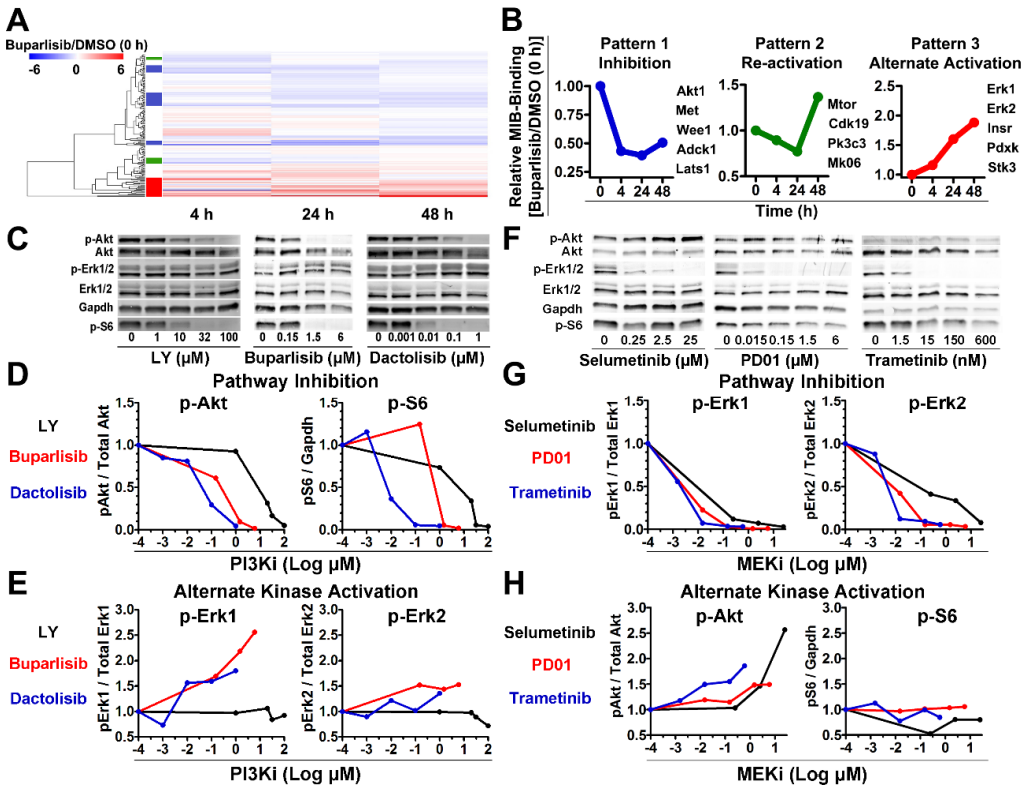

Figure 3.2. **Single agent PI3Ki/MEKi induces dynamic kinome changes in TRP astrocytes** A heatmap demonstrated temporal changes from 4-48 h after buparlisib (**A**). Dynamics of select kinases illustrated three response types: sustained inhibition (Pattern 1, blue), re-activation (Pattern 2, green), and alternate pathway activation (Pattern 3, red) (**B**). Graphs show the first kinase listed. Representative immunoblots (**C**) of PI3Ki-treated TRP astrocytes at 24 h showed that potency was directly associated with dose-dependent decreases of proximal (p-Akt) and distal (p-S6) PI3K (**D**), while the more potent PI3Ki, buparlisib and dactolisib, induced alternate MAPK (p-Erk1/2) activation (**E**). Immunoblots (**F**) performed on TRP astrocytes 24 h after selumetinib, PD01, or trametinib showed that MEKi potency directly associates with MAPK inhibition (**G**) and alternate activation of proximal, but not distal PI3K signaling (**H**). A representative immunoblot quantification is shown (N=1-5 biologic replicates, Mean=2.5).

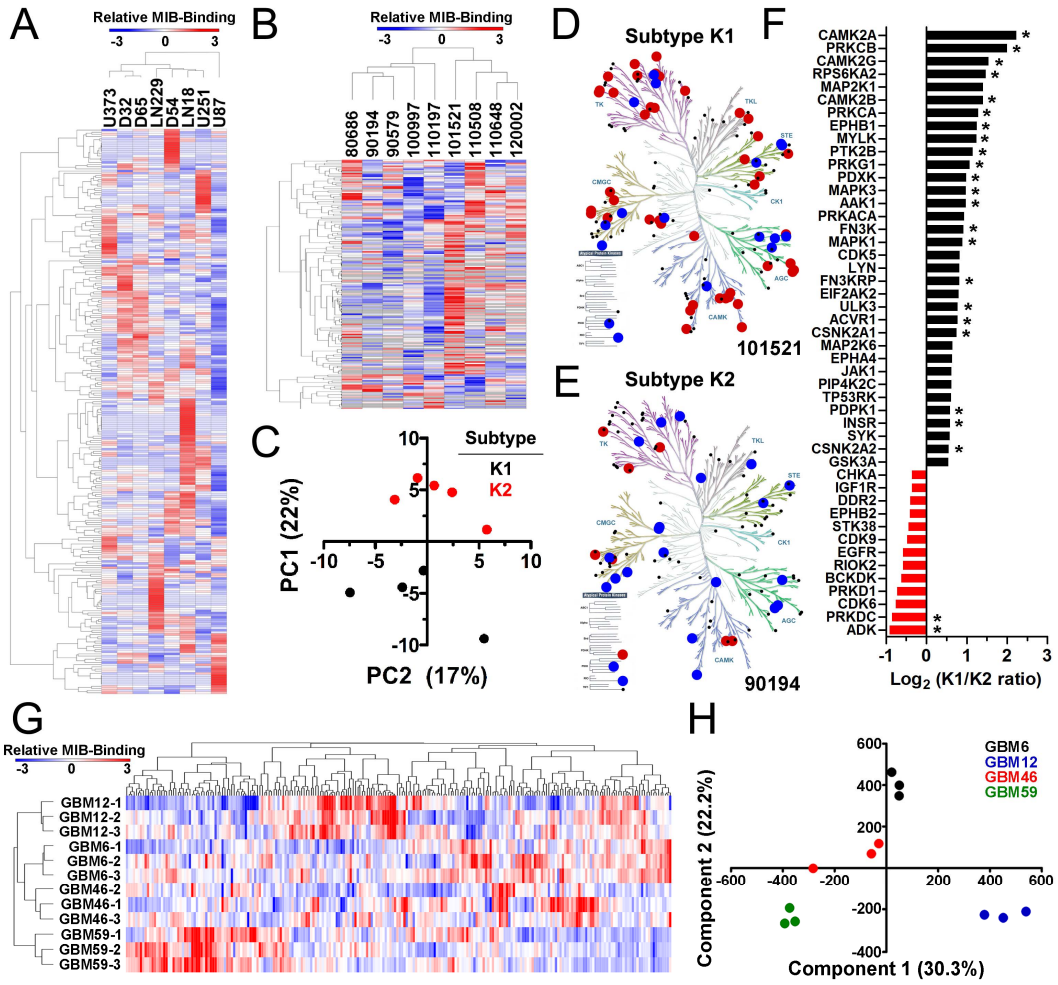

Figure 3.3. **GBM have heterogeneous kinomes**. Heterogeneous kinome activity was evident in ECL (**A**) and tumor samples from human GBM patients (**B**). PCA showed two kinome subtypes of human tumors (K1, K2) (**C**). K1 (**D**) had hyper-activation relative to K2 (**E**) tumors (**Fig S3.5AB**). Kinases with ≥2x (red) or ≤0.4x (blue) relative MIB-binding are indicated; other detected kinases (black). A waterfall plot shows the most differentially activated kinases (**F**). Kinases significantly (P<0.05) enriched in K1 (black) and K2 (red) are indicated (*). Heterogeneous kinome activity was also evident in subcutaneous GBM PDX (**G**, **Fig S3.5C**). PCA demonstrated that although variable, biologic replicates of subcutaneous GBM PDX were more similar to each other than to different PDX models (**H**).

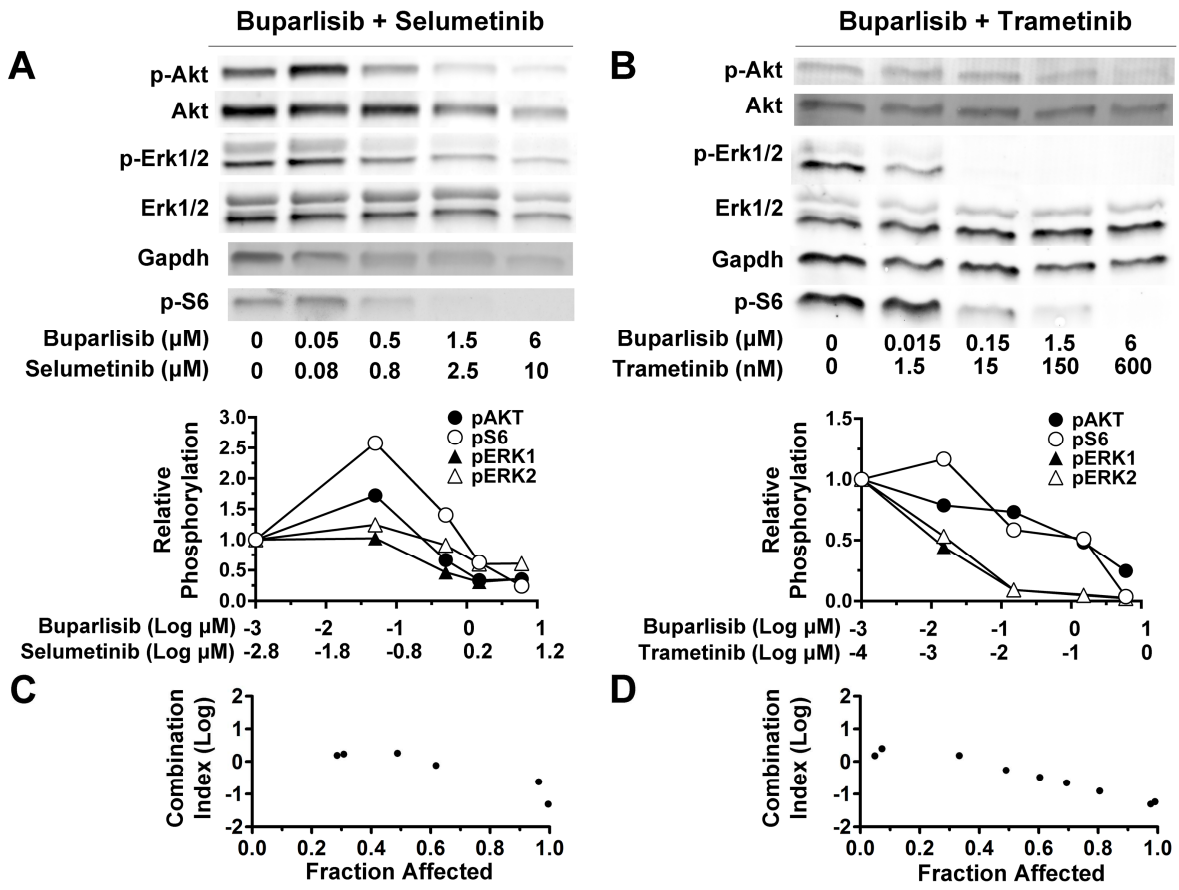

Figure 3.4. **PI3Ki/MEKi are synergistic and dual therapy inhibits alternate pathway activation**. Immunoblots of TRP astrocytes treated with buparlisib and either selumetinib (**A**) or trametinib (**B**) for 24 h showed that dual treatment blocks both PI3K and MAPK signaling. Buparlisib and selumetinib were synergistic in TRP astrocytes at 2-50 and 3.3-83 μM (≥0.6 fraction affected) (**C**). Buparlisib and trametinib were synergistic in TRP astrocytes at 0.75-50 and 0.08-5 μM (≥0.5 fraction affected) (**D**). A representative immunoblot quantification is shown (N=1-4 biologic replicates, Mean=2.5).

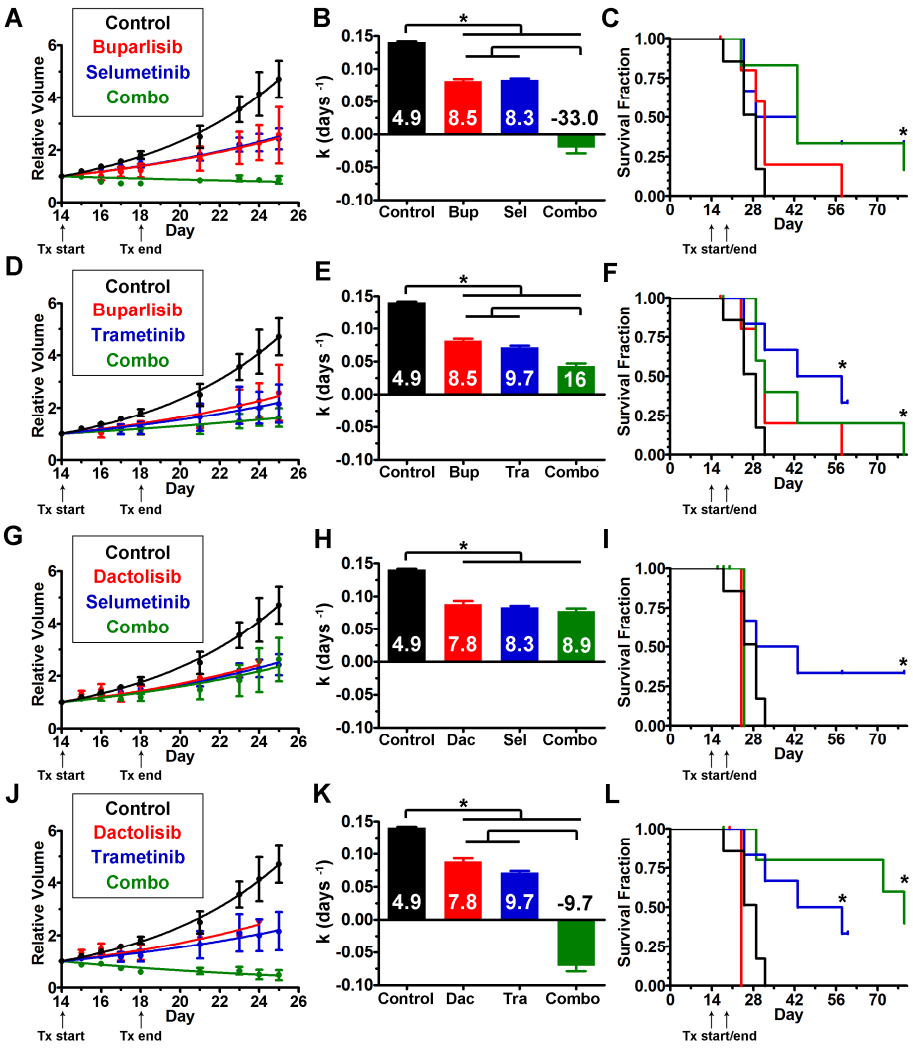

Figure 3.5. **PI3Ki and MEKi treatment inhibited growth of subcutaneous TRP tumors**. Buparlisib plus either selumetinib (**A-C**) or the more potent MEKi trametinib (**D-F**) delayed tumor growth more than either drug alone and improved survival compared to controls (*, P≤0.01). The more potent PI3Ki dactolisib plus either selumetinib (**G**,**H**) or the more potent MEKi trametinib (**J**,**K**) delayed tumor growth compared to controls (*, P<0.0001). Dactolisib/trametinib delayed growth more than either treatment alone (*, P<0.0001). Dactolisib/selumetinib did not improve survival compared to controls (**I**), but dactolisib/trametinib did (**L**) (*, P=0.01). Doubling times (days) are indicated (**B**,**E**,**H**,**K**).

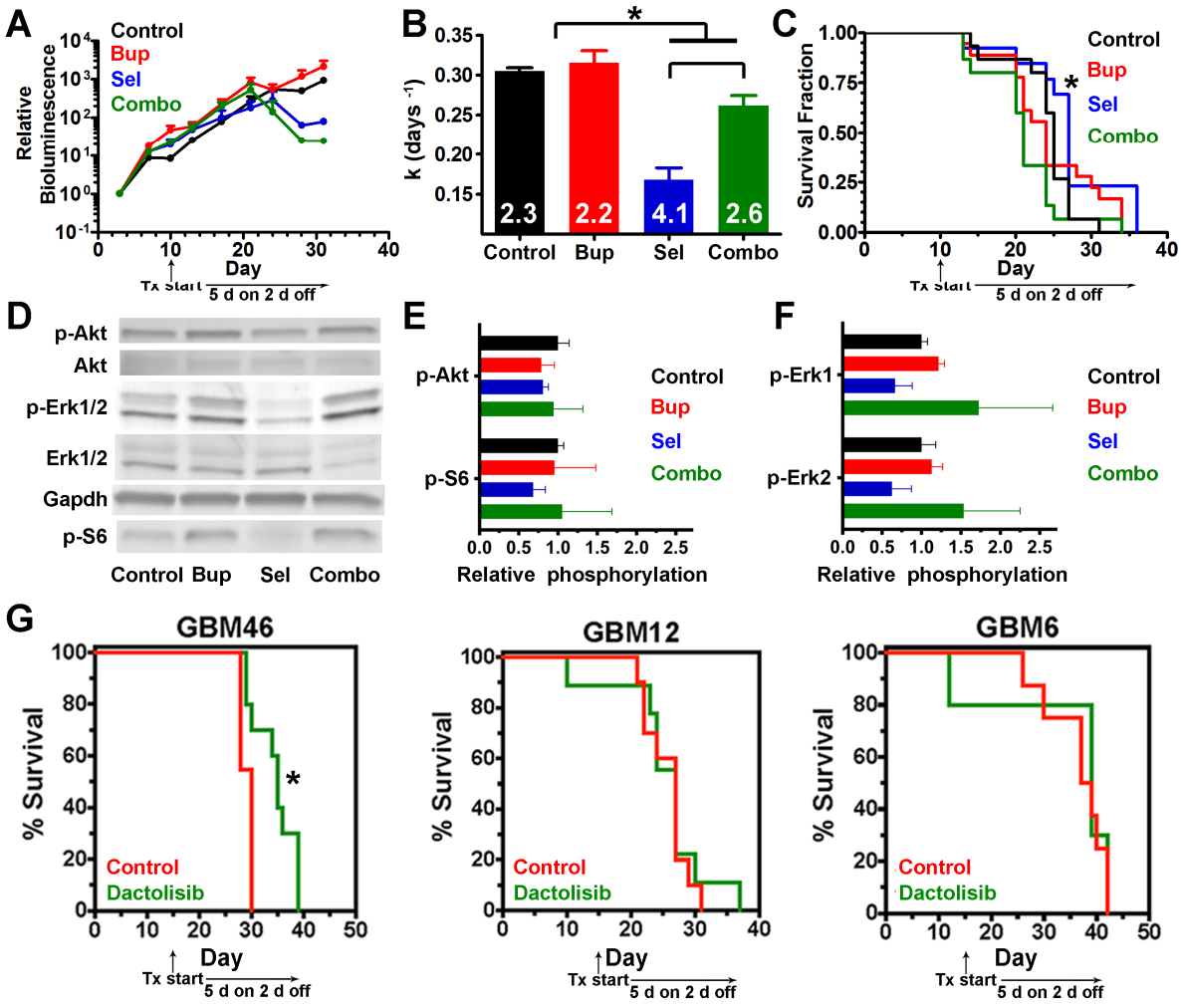

Figure 3.6. **Response of orthotopic TRP allografts and PDX to PI3Ki and MEKi**. In TRP allografts (**A**-**F**), selumetinib ± buparlisib delayed growth (*, P≤0.03) (**A**,**B**). Doubling times (days) are indicated (**B**). Selumetinib alone improved survival (*, P=0.03) (**C**). Representative immunoblot (**D**) and quantification showed no change in PI3K (**E**), but selumetinib trended towards decreased MAPK signaling (P=0.06) (N=3 biologic replicates) (**F**). In GBM PDX, dactolisib modestly improved GBM46 (*, P=0.003), but not GBM12 and GBM6 survival (**G**).

A

PDX	EGFR		PDGFRα	PTEN	PIK3CA	TP53	CDKN2A
	Amp	Mut	Amp	Mut	Mut	Mut	Del
GBM59	Y	vIII	N	HD		WT	Y
GBM46	Y	vIII	N	WT	WT	Q353K	
GBM12	Y	G719A	N	WT	WT	SPLICE	Y
GBM6	Y	vIII	Y	WT	WT	R273C	Y

**Amp = Amplification, Mut = Mutation, Del = Deletion, HD = Homozygous Deletion, WT = Wild Type, Y = Yes, and N = No*

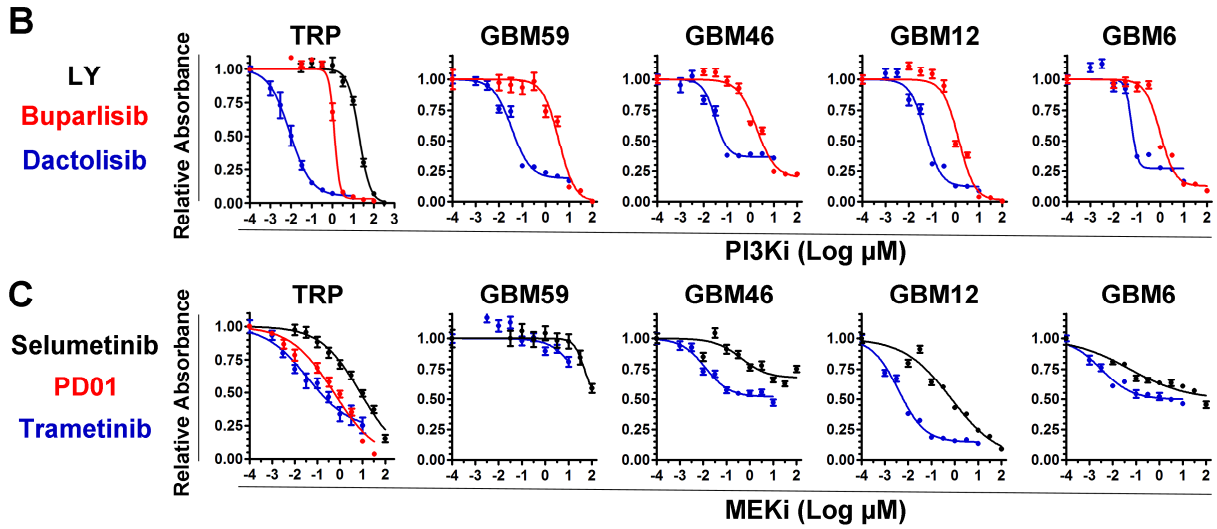

Figure S3.1. **Increased PI3Ki or MEKi potency potentiates growth inhibition *in vitro***. Mutations in core GBM signaling pathways in PDX (**A**).[28,60] Multiple PI3Ki reduced growth of cultured TRP astrocytes and PDX (R^2≥0.96) (**B**). Multiple MEKi reduced growth of cultured TRP astrocytes (R^2≥0.97) and PDX (R^2, 0.2-0.97) (**C**). IC_{50} calculated from these curves are graphed in **Fig 3.1**.

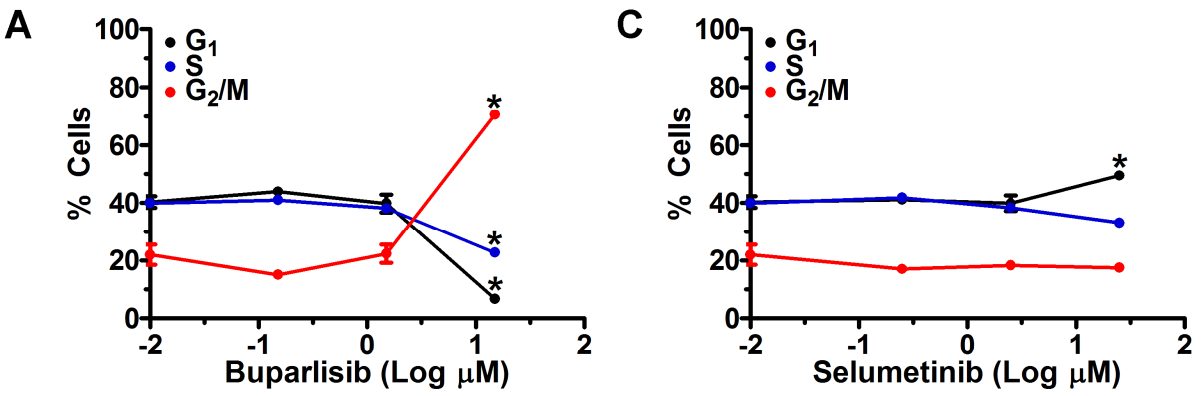

B

Class	Drug	IC_{50} (nM)	GI_{50} (nM)	I_{max} (%)	Hill slope	n
PI3Ki	LY	19,380	19,408	100	-1.6	3
	Buparlisib	1,240	1,264	97	-3.4	5
	Dactolisib	9	10	95	-0.9	2
MEKi	Selumetinib	7,973	9,743	85	-0.5	5
	PD01	543	754	96	-0.5	3
	Trametinib	38	134	78	-0.5	2
mTORi	Everolimus	199	57,016	56	-0.38	3
	Temsirolimus	1,372	2,130	85	-0.33	3

Figure S3.2. ***In vitro*** **efficacy of PI3Ki, MEKi, and mTORi in TRP astrocytes**. Micromolar doses of the PI3Ki buparlisib induced G_2/M cell cycle arrest within 48 h post-treatment (*, P≤0.001) (**A**). Summary of data from **Figs 3.1AC**, **S3.1BC**. N represents replicate biologic experiments (**B**). Micromolar doses of the MEKi selumetinib induced G1/S cell cycle arrest within 48 h post-treatment (*, P≤0.05) (**C**).

		GBM59				GBM46			
Class	Drug	IC_{50}	GI_{50}	I_{max}	Hill slope	IC_{50}	GI_{50}	I_{max}	Hill slope
		nM		%		nM		%	
PI3Ki	Buparlisib	3,650	3,682	100	-1.3	1,856	2,924	81	-1.1
	Dactolisib	36	56	81	-1.1	31	70	64	-1.6
MEKi	Selumetinib	51,050	NA	41	-1.9	438	NA	32	-0.8
	Trametinib	~ 923	NA	19	~ -13.85	13	~ 977	48	-0.8

		GBM12				GBM6			
Class	Drug	IC_{50}	GI_{50}	I_{max}	Hill slope	IC_{50}	GI_{50}	I_{max}	Hill slope
		nM		%		nM		%	
PI3Ki	Buparlisib	1,370	1,394	99	-1.3	979	1,212	87	-1.4
	Dactolisib	52	64	88	-1.3	59	74	73	-3.3
MEKi	Selumetinib	701	731	91	-0.4	58	11,194,379	51	-0.4
	Trametinib	4	6	86	-0.8	3	4,576	50	-0.7

Figure S3.3. ***In vitro*** **efficacy of PI3Ki and MEKi in PDX**. Summary of data from **Figs 3.1BD, S3.1BC**. P≤0.01 for all PI3Ki IC_{50} in GBM59 vs. GBM12 or GBM6. P<0.001 for selumetinib IC_{50} in GBM59 vs. GBM12. P≤0.02 for trametinib IC_{50} in GBM46 vs. GBM12 or GBM6. P≤0.0002 for all MEKi IC_{50} in GBM12 vs. GBM6. Some IC_{50}/GI_{50} could not be calculated (NA, not applicable) or were ambiguous (~).

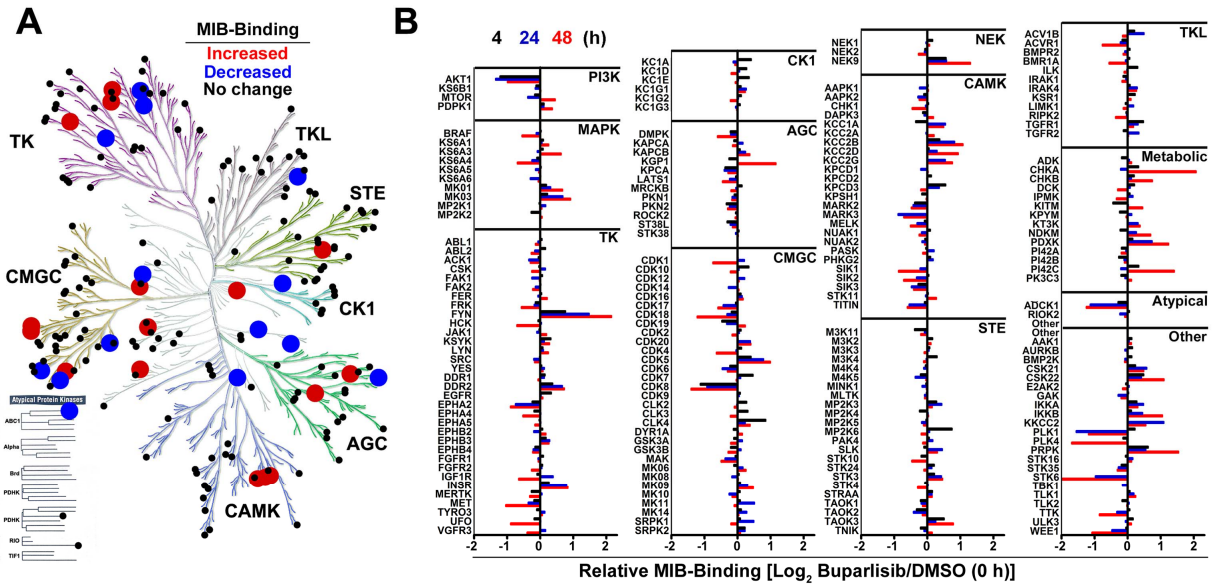

Figure S3.4. **Buparlisib induces dynamic kinome reprogramming in TRP astrocytes.** Buparlisib induced dynamic changes in numerous kinase families over 4-48 h (**A**,**B**). A kinome tree view of relative MIB-binding showed detected, but unchanged kinases (black) and those ≥1.5x (red) or ≤0.6x (blue) 48 h after buparlisib (**A**).

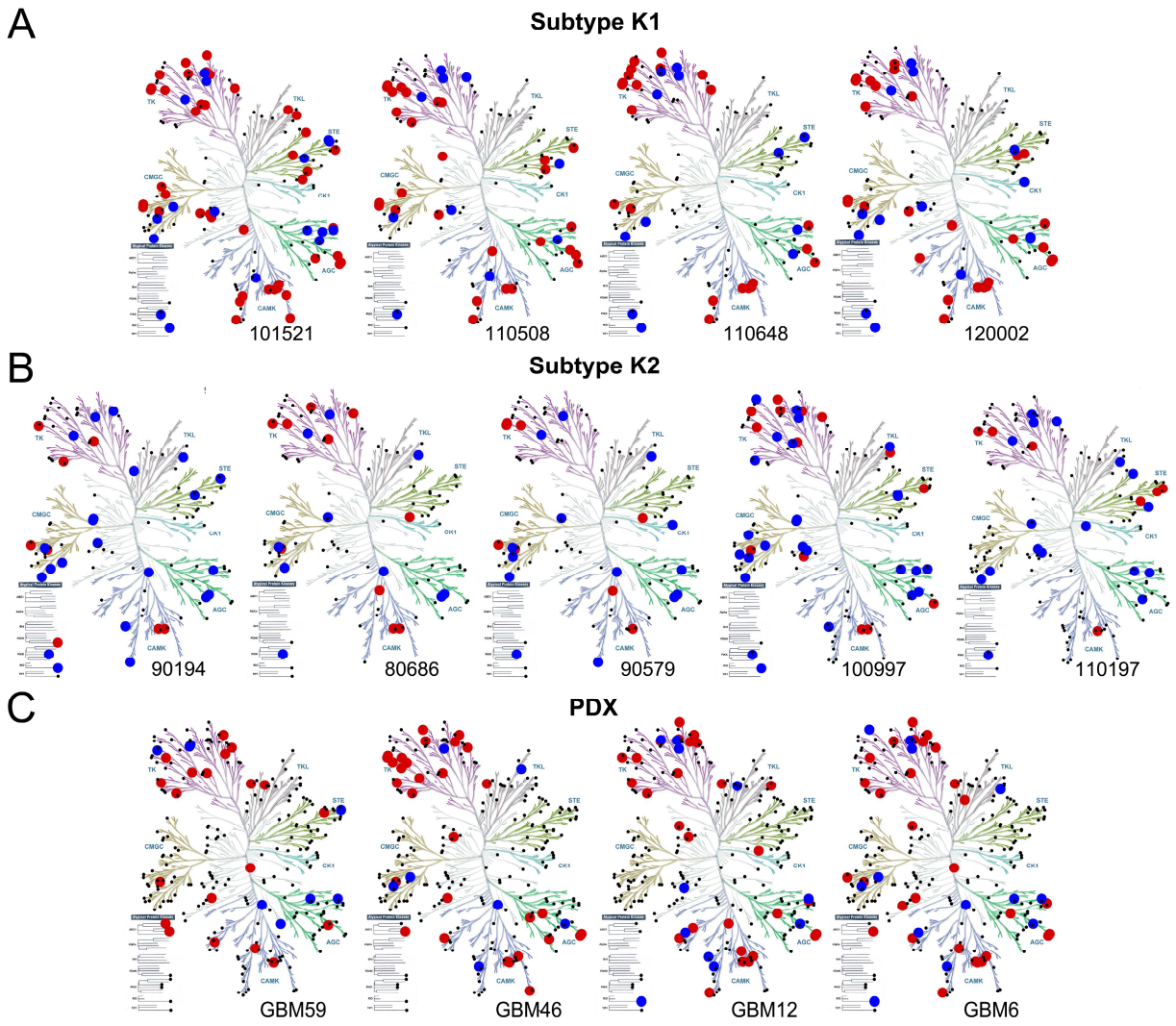

Figure S3.5. **Human GBM have diverse kinome profiles**. Tree views of all subtype K1 (**A**) and K2 (**B**) human GBM tumors from **Fig 3.3B-F** highlighted relative kinome hyper-activation of K1 vs. K2 tumors. Tree views of subcutaneous PDX models from **Fig 3.3GH** (**C**). Kinases with ≥2x (red) greater or ≤0.4x (blue) less MIB-binding relative to a pooled, standard reference consisting of established GBM cell lines are indicated. Other kinases detected by MIB-MS are indicated in black (**A**,**B**,**C**).

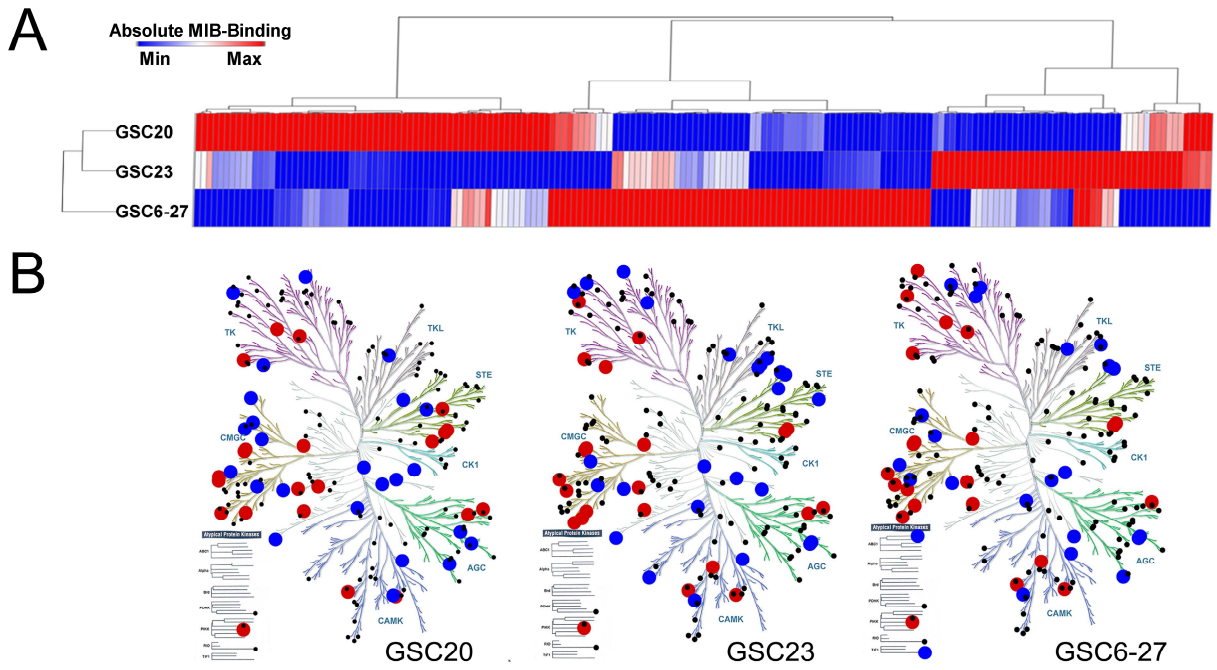

Figure S3.6. **PDX cultures have diverse kinome profiles**. Hierarchical clustering demonstrates heterogeneous kinome activity in cultured human GBM PDX (**A**). Tree views of the cultured PDX models, GSC20, GSC23, and GSC6-27 (**B**). The top (red) or bottom (blue) 25 kinases detected by MIB-binding in each model are indicated. Other kinases detected by MIB-MS are indicated in black.

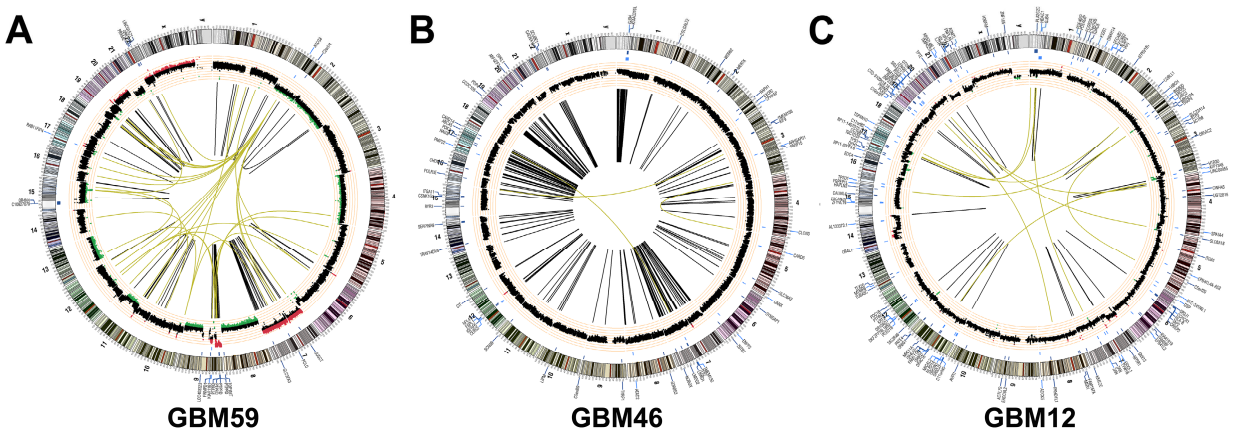

Figure S3.7. **Subcutaneous PDX have diverse genetic profiles**. Circos plots summarizing somatic events in GBM59 (**A**), GBM46 (**B**), and GBM12 (**C**). A summary of all identified somatic genomic alterations is shown. Translocations are marked by yellow (interchromosomal) and black (intrachromosomal translocations) lines; for intrachromosomal translocations, the gray connecting line may appear as a single line if the joined regions lie within 2000 kb. CNVs are shown along the thick black ring encircling the translocations (green, regions of loss; red, regions of gain; black, no change); on the ring encircling CNVs, somatic indels (insertion/deletions) are marked by light blue tick marks and on the ring encircling the indels, somatic point mutations are marked by dark blue tick marks. Gene labels associated with point mutations are shown along the outermost area of the plot.

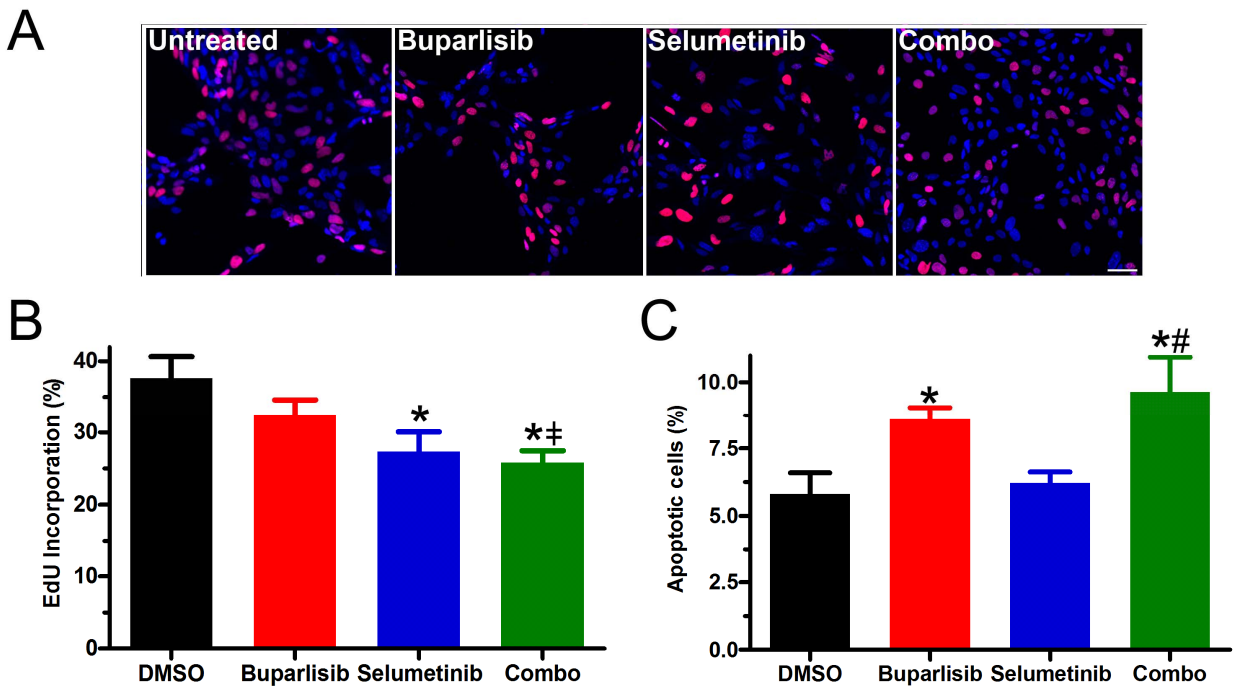

Figure S3.8. **Dual PI3Ki and MEKi treatment inhibits proliferation and induces apoptosis in TRP astrocytes *in vitro***. Representative images of EdU incorporation (red) in TRP astrocytes treated with vehicle (DMSO), selumetinib (2.5 μM), buparlisib (1.5 μM), or both (**A**). DAPI is shown in blue. Scale bars = 50 μm. Original magnifications 20X. Proliferation (EdU incorporation) was decreased by single agent selumetinib (*, P=0.02), but not buparlisib treatment (**B**). Combination treatment decreased proliferation compared to DMSO (*. P=0.003) or buparlisib alone (‡. P=0.02). Apoptosis was increased by single agent buparlisib (*, P=0.02), but not selumetinib (**C**). Combination treatment increased apoptosis compared to DMSO (*. P=0.05) or selumetinib alone (#. P=0.05).

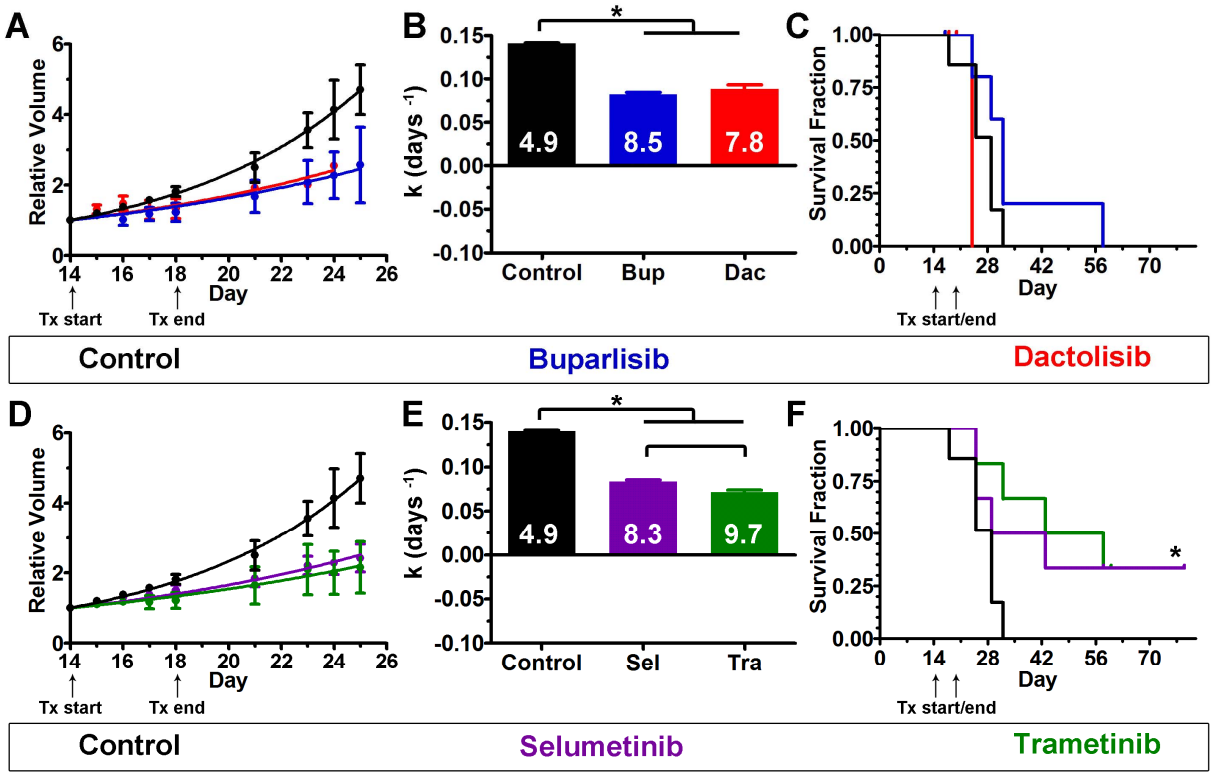

Figure S3.9. **Single agent PI3Ki or MEKi delayed growth of subcutaneous TRP allografts**. The PI3Ki buparlisib or dactolisib alone delayed tumor growth (*, P<0.0001) (**A**,**B**). Neither buparlisib nor dactolisib significantly improved median survival (**C**). The MEKi selumetinib or trametinib alone delayed tumor growth (*, P<0.0001) (**D**,**E**), but trametinib was more effective (P=0.0008). Trametinib improved median survival (*, P=0.01), but the less potent MEKi selumetinib did not (**F**). Doubling times (days) are indicated in white (**B**,**E**).

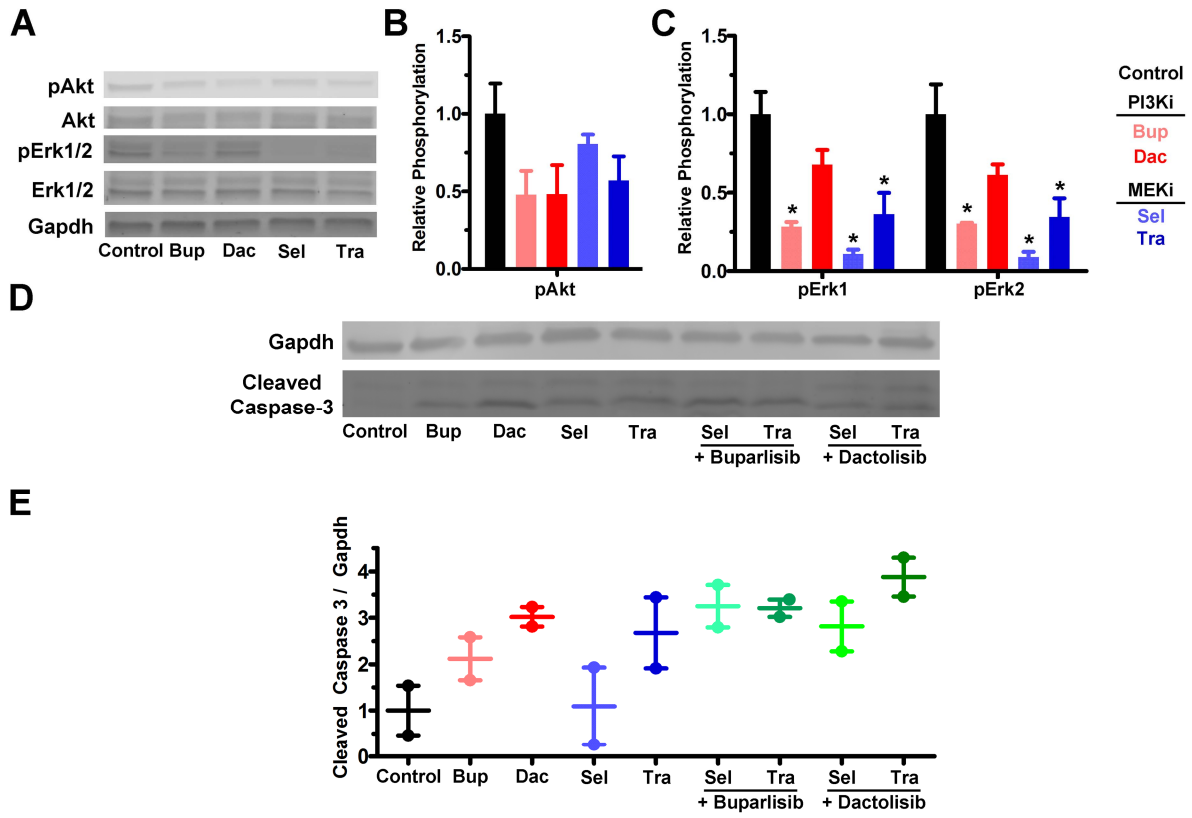

Figure S3.10. **PI3Ki and MEKi inhibit their targeted pathways in subcutaneous TRP allografts**. Representative immunoblots of acutely isolated bulk subcutaneous TRP tumors (**A**) and quantification showed a trend (~50%) towards PI3K inhibition in PI3Ki treated samples (P=0.10 - 0.13) (**B**) and a significant decrease (64-91%) in MAPK signaling in MEKi treated samples (*, P≤0.04) (**C**). While alternate pathway activation was not apparent in these bulk tumor samples (**B**,**C**), this may be due to either the kinetics of pathway inhibition and alternate activation *in vivo* and/or changes in cellular composition of the bulk tumor tested. Mean ± SEM of 3 biologic replicates are graphed. Representative immunoblots of acutely isolated bulk subcutaneous TRP tumors (**D**) and quantification (**E**) showed increased cleaved caspase-3 in most single agents and all combination treatments. Mean ± SEM of 2 biologic replicates are graphed.

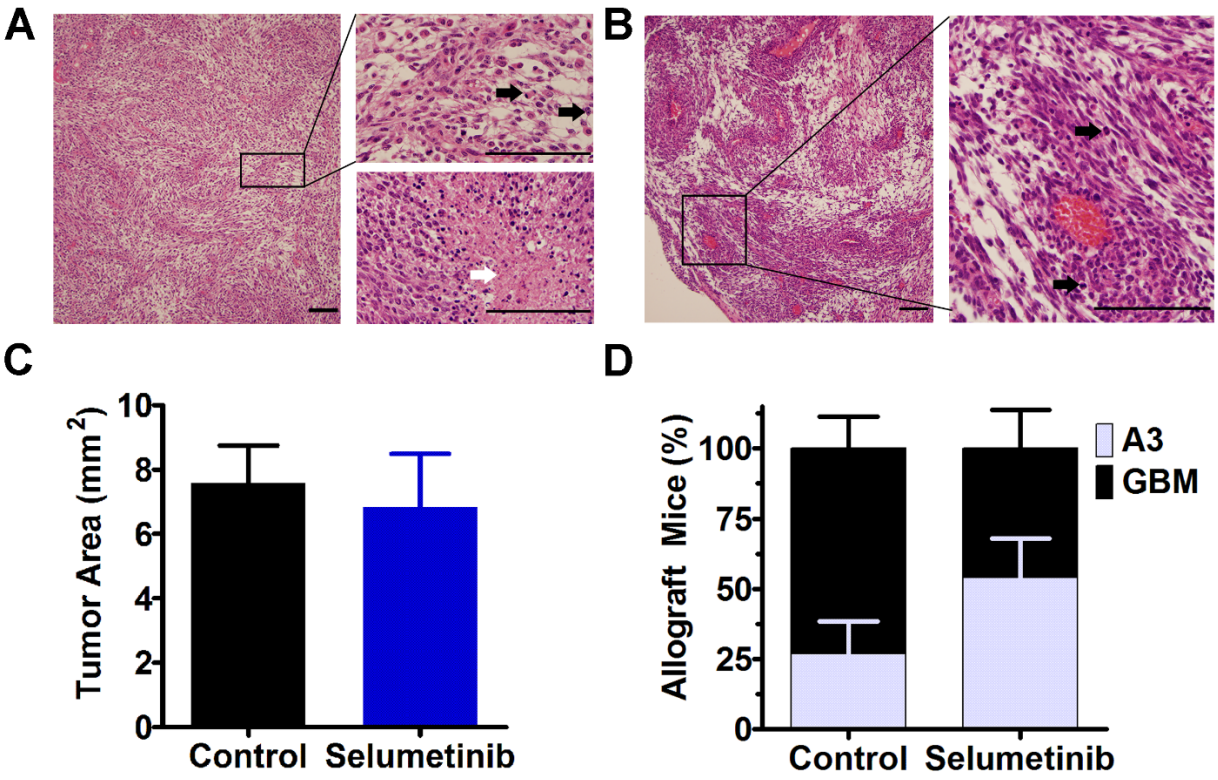

Figure S3.11. **Selumetinib influences malignant progression of orthotopic TRP allografts**. Histology of representative control (**A**) or selumetinib-treated (**B**) mice showed GBM and anaplastic astrocytoma (grade III, A3), respectively. Arrows indicate mitoses (black) and necrosis (white). No significant difference in tumor area was evident (**C**). Controls developed GBM more frequently than selumetinib-treated mice ($P<0.05$) (**D**). Original magnifications 40x (HI, left panels) or 10x (HI, right panels). Scale bars = 100 μm.

Table S3.1. **Drug names and purchasing information**

Class	Drug	Alternate name	Vendor(s)	Reference
PI3Ki	LY	LY294002	Cayman Chemicals	12
	Buparlisib	BKM120	MedChem Express Chemietek	13
	Dactolisib	BEZ235	MedChem Express	14
MEKi	Selumetinib	AZD6244	MedChem Express Chemietek	15
	PD01	PD0125901	Cayman Chemicals	16
	Trametinib	GSK1120212	MedChem Express Selleckchem	17
mTORi	Temsirolimus	CCI-779	Selleckchem	18
	Everolimus	RAD001	Selleckchem	19

Table S3.2. Drug doses and schedules

Treatment		Orthotopic	Subcutaneous
PI3Ki	**MEKi**	**Dose (mg/kg)**	
Buparlisib		30	30
Dactolisib		NA	50
	Selumetinib	37	37
	Trametinib	NA	1
Buparlisib	Selumetinib	25 + 18	25 + 18
	Trametinib	NA	25 + 0.5
Dactolisib	Selumetinib	NA	25 + 18
	Trametinib	NA	25 + 0.5
Schedule		5 d on/2 d off continuous	qd x5 (d 14-18)

Table S3.3. Summary of buparlisib-induced kinome changes

Kinase	4h	24h	48h
AURKA	1.000	0.511	0.161
PLK4	0.911	0.988	0.311
CDK8	0.460	0.528	0.379
ADCK1	0.821	0.458	0.422
CDK18	0.882	0.805	0.431
PLK1	1.162	0.342	0.442
WEE1	0.968	0.721	0.475
MET	0.881	0.782	0.487
AKT1	0.433	0.394	0.506
EPHA2	0.848	0.598	0.539
AXL	0.884	1.009	0.540
SIK1	0.991	0.863	0.550
TTK	1.043	0.800	0.555
ACVR1	0.894	0.862	0.591
CDK1	1.009	1.151	0.599
SIK2	1.028	0.801	0.612
MARK3	0.998	0.544	0.613
HCK	0.959	1.024	0.616
RPS6KA4	0.934	0.844	0.622
IGF1R	0.939	1.308	0.640
CDK4	1.085	0.973	0.645
DMPK	0.864	0.869	0.660
TTN	0.946	0.685	0.661
CDK17	0.964	0.743	0.666
FRK	0.907	0.886	0.676
BMPR1A	1.042	0.960	0.681
BRAF	1.016	0.924	0.686
EPHA4	0.882	1.010	0.699
MELK	0.947	0.809	0.705
MAK	0.955	0.773	0.711
MARK2	0.770	0.746	0.718
STK10	0.883	1.000	0.726
CHEK1	1.022	0.967	0.732
LATS1	0.966	0.849	0.733
SIK3	0.828	0.719	0.754
FLT4	1.006	1.117	0.763
RIPK2	0.972	0.982	0.780
IPMK	1.048	1.114	0.795
MERTK	0.835	1.034	0.806
STK35	0.879	0.827	0.808
CDK6	0.855	0.729	0.813

DCK	1.151	1.052	0.815
TNK2	0.966	0.791	0.816
PKN2	0.794	0.847	0.817
STK4	0.954	1.014	0.820
PRKCA	0.772	0.759	0.823
GSK3B	0.868	1.072	0.824
ABL2	1.115	0.896	0.833
NEK2	0.954	0.946	0.835
FGFR2	1.048	1.033	0.838
CSK	0.978	1.113	0.841
NUAK1	1.064	0.889	0.846
PRKAA2	0.934	0.824	0.847
PTK2B	1.010	0.907	0.858
EPHB4	0.899	0.866	0.858
CSNK1G2	1.079	1.016	0.864
CLK3	1.240	1.010	0.865
CDK10	1.264	1.028	0.865
GSK3A	0.928	1.104	0.870
SRPK1	1.058	1.402	0.874
GAK	1.017	0.823	0.875
CDC42BPB	1.094	0.969	0.876
PRKD3	1.466	1.283	0.876
MAP3K11	0.769	0.946	0.876
PIP4K2A	0.883	0.968	0.879
CSNK1D	1.207	1.041	0.879
MAP2K6	1.676	1.046	0.884
PKN1	0.937	0.896	0.892
IRAK1	0.912	0.965	0.894
SRC	0.991	0.876	0.894
CDK2	1.073	1.036	0.896
MAPK10	1.052	0.840	0.897
EPHA5	0.983	1.011	0.899
ACVR1B	1.153	1.404	0.903
STK38L	0.806	0.861	0.904
EIF2AK2	0.966	1.029	0.904
PRKACA	0.929	1.117	0.905
TAOK2	0.801	0.751	0.907
TAOK1	0.870	0.882	0.908
ABL1	1.035	0.958	0.910
PASK	0.973	1.148	0.912
PAK4	1.040	1.119	0.913
BMPR2	1.048	0.947	0.914
LIMK1	0.958	1.130	0.917

MAP2K5	0.977	0.891	0.927
MAP3K4	1.225	0.982	0.929
ILK	1.232	0.989	0.933
STK24	1.153	1.096	0.936
MAPK11	1.057	1.421	0.936
CLK2	1.206	0.989	0.938
PIP4K2B	0.833	0.931	0.939
MAP3K3	1.050	1.036	0.941
BMP2K	1.089	0.947	0.943
RIOK2	1.035	0.853	0.945
CSNK1A1	1.330	0.916	0.948
MLTK	0.986	0.949	0.948
NUAK2	0.953	0.898	0.949
ROCK2	0.964	0.991	0.955
CSNK1E	1.271	1.015	0.957
DDR1	1.105	1.086	0.959
FGFR1	1.067	0.959	0.963
RPS6KA6	1.009	0.817	0.964
PKM	0.847	1.086	0.973
MAP4K5	0.871	0.780	0.973
RPS6KA5	1.018	0.911	0.974
CDK7	1.379	1.065	0.977
PSKH1	0.895	1.000	0.982
MINK1	0.975	0.900	0.984
CSNK1G3	1.054	0.964	0.985
PTK2	1.045	0.844	0.986
TLK2	0.894	1.028	0.988
AURKB	1.104	0.948	0.991
MAP4K4	0.965	0.931	0.997
PRKD2	1.086	0.992	1.001
PHKG2	1.069	1.127	1.004
CDK9	1.056	1.033	1.005
TBK1	1.005	0.900	1.009
RPS6KB1	0.920	0.905	1.010
STK38	1.029	0.963	1.012
PRKD1	0.999	0.875	1.014
MAPK8	1.030	0.892	1.015
TGFBR2	0.919	1.261	1.018
PRKAA1	1.014	0.853	1.022
MAP2K4	0.853	1.015	1.023
MAPK14	1.080	1.209	1.026
CDK14	0.997	0.830	1.026
CDK12	1.007	1.157	1.032

MAP2K1	0.984	1.120	1.033
MAP2K2	0.831	1.004	1.037
TYRO3	0.933	1.099	1.043
NEK1	1.115	0.977	1.045
EGFR	1.260	1.017	1.054
YES1	1.029	1.089	1.058
SRPK2	1.166	1.167	1.059
KSR1	1.167	0.997	1.068
MAP3K2	1.116	0.997	1.078
ULK3	1.120	0.958	1.079
AAK1	1.088	1.031	1.079
PIK3C3	0.873	0.950	1.082
ADK	0.884	1.035	1.082
STK16	0.959	1.113	1.085
DYRK1A	0.921	1.014	1.103
STRADA	1.111	1.101	1.103
MAP2K3	1.213	1.349	1.106
TNIK	0.871	0.938	1.107
CDK16	1.073	1.099	1.121
EPHB2	1.050	0.878	1.124
TGFBR1	1.388	1.242	1.127
DAPK3	0.912	0.938	1.135
JAK1	0.981	0.936	1.140
CAMK2A	1.001	0.977	1.148
FER	1.027	0.957	1.155
CSNK1G1	1.074	1.197	1.175
CDK19	0.723	0.801	1.175
TLK1	1.047	1.138	1.180
LYN	1.057	1.068	1.184
RPS6KA1	1.066	1.036	1.191
MAPK6	0.929	1.117	1.191
EPHB3	1.129	1.217	1.197
IRAK4	1.051	1.220	1.200
STK11	1.017	0.968	1.206
SYK	1.247	1.086	1.213
SLK	0.935	1.367	1.231
CHUK	1.210	1.392	1.234
PDPK1	1.081	1.078	1.288
PRKACB	1.053	1.179	1.290
FN3KRP	1.009	1.242	1.294
CLK4	1.801	1.172	1.298
CDK20	1.009	1.306	1.318
TK2	0.737	1.013	1.366

MTOR	0.895	0.773	1.368
STK3	1.158	1.344	1.374
MAPK9	1.061	1.231	1.388
CSNK2A1	1.177	1.489	1.398
CAMK1	0.787	1.459	1.406
CAMKK2	0.013	2.128	1.459
RPS6KA3	1.060	0.945	1.546
MAPK1	1.138	1.241	1.593
NME4	0.857	1.198	1.615
DDR2	1.296	1.588	1.656
CHKB	1.144	1.079	1.674
CAMK2G	0.996	1.453	1.690
TAOK3	1.419	1.191	1.722
INSR	1.202	1.733	1.782
MAPK3	1.162	1.603	1.883
CAMK2D	1.036	1.225	1.906
CDK5	1.324	1.720	1.985
IKBKB	1.080	1.365	2.069
CAMK2B	1.295	1.767	2.109
CSNK2A2	1.396	1.333	2.135
PRKG1	0.839	1.000	2.228
PDXK	1.111	1.667	2.355
NEK9	1.479	1.493	2.461
PIP4K2C	1.259	0.871	2.655
TP53RK	1.534	1.460	2.903
CHKA	1.253	0.867	4.186
FYN	1.696	2.785	4.446

Table S3.4. Summary of PDX kinome profiles

GBM59			GBM46		
≥2	2-0.4	≤0.4	≥2	2-0.4	≤0.4
JNK3	NEK9	MSK1	FMS	EphA4	CDK7
PKCt	LRRK2	RSK1	IRAK3	GCK	MET
EGFR	PKG1	AurA	PKCb	ICK	PKCd
ADCK4	CaMK2a	MST3	LCK	CDK6	DLK
CaMK2d	CK1g2	SRC	SYK	PFTAIRE1	CDK4
IRAK3	STLK6	INSR	BTK	STLK6	NuaK2
NEK7	PFTAIRE1	IGF1R	JNK3	PIK3R4	AurA
EphA1	PKCb	YANK2	ADCK4	Erk2	
FMS	BCKDK		PKG1	ADCK1	
FYN	CLIK1		FGR	CLK2	
TIE2	CLK2		CaMK2a	PDGFRa	
PIK3R4	PHKg1		HCK	Erk1	
BTK	MAP2K6		NEK7	PKD1	
ADCK1	RSK3		CLIK1	BCKDK	
FES	IRAK1		BLK	NEK11	
GCK	YES		CaMK2d	TAO3	
SYK	CK1g1		FES	IRAK4	
LIMK1	CK2a1		FRK	PEK	
DRAK1	NEK11		DMPK1	QSK	
PKD1	DRAK2		FYN	LIMK1	
	MARK1		skMLCK	LKB1	
	STK33		PKCa	FGFR2	
	PKR		PHKg1	CK1g2	
	HCK		FLT4	CaMK1a	
	KHS1		LYN	TYRO3	
	CHK2		CaMK1d	p38b	
	EphB4		TRKB	RSK2	
	CaMK2g		EGFR	CaMK2b	
	Erk1		NDR2	NEK9	
	IRAK4		DDR1	MARK1	
	NuaK1			TAO1	
	FLT4			MAP2K6	
	CASK			Erk5	
	FGR			STK33	
	LKB1			BMPR2	
	MAP3K4			DRAK1	
	STLK5			LRRK2	
	PDK1			MAP3K1	
	TAO3			Wee1	
	PEK			PKCt	

p38b	TEC
ICK	STLK5
IRE1	DAPK2
AKT1	PDGFRb
CaMK1d	ATM
Erk2	MAP2K2
BMPR2	MER
Wee1	KHS2
JAK1	CASK
ATM	KHS1
PKN1	TIE2
GCN2	FAK
QSK	PKCe
PHKg2	BIKE
SRPK2	RET
MAP2K3	PRPK
TAO2	IRE1
MAP3K5	TESK1
EphA4	EphB3
DDR1	PASK
RIPK1	SRPK2
PRPK	CK2a1
CK2a2	MAP2K4
NDR2	ILK
BLK	BMPR1B
TEC	YES
EphA3	AKT2
MAP2K5	MARK4
DAPK2	HRI
ILK	CHK1
TAO1	PDK1
PASK	FER
CDK5	TAO2
PKCe	IRAK1
MARK3	NDR1
DMPK1	p38a
MAP3K7	RIPK1
PKD2	BRAF
CaMK2b	AKT1
TRKB	RSK3
TESK1	MLK2
FRK	MAPKAPK2
BRAF	TIF1b

p38a	DYRK1A
CLIK1L	PCTAIRE2
FER	ABL
RIPK2	MAP2K5
MER	PKACa
HRI	QIK
PKACa	PKR
PKN2	PKN1
PDGFRa	CHK2
MRCKb	CK2a2
CDK6	MAP3K5
TYRO3	FGFR1
CaMKK2	PHKg2
PKACb	MAP3K7
ZC2/TNIK	CDK5
TBK1	ROCK1
GSK3A	RSK1
MARK4	CDKL5
MAP3K6	CK1e
PCTAIRE3	PKN2
TIF1b	YSK1
TYK2	MAP2K3
CDK2	PYK2
AMPKa2	KDR
BIKE	GSK3B
MET	MRCKb
Erk5	MAP3K6
MYT1	IKKb
MST1	NEK3
AKT2	PKACb
YSK1	MST1
AAK1	TGFbR1
skMLCK	CDK11
PKD3	CDK2
MAP2K4	NuaK1
CK1a	MST2
TLK1	MAP2K1
RSK2	CaMK2g
CK1e	p70S6K
MLK2	PKD2
SgK496	CaMKK2
RET	EphB4
DYRK1A	CK1a

GSK3B	HIPK2
PKCa	CHED
MAP2K1	GSK3A
HIPK2	TGFbR2
CaMK1a	CK1g1
NDR1	JAK1
JNK2	DNAPK
ROCK1	CSK
MAP2K2	ZC1/HGK
QIK	NEK1
MAP3K1	DDR2
LYN	PKD3
FGFR2	ZC2/TNIK
PCTAIRE2	EphA1
ABL	CK1g3
MARK2	AKT3
KHS2	MAP3K4
PLK1	LATS1
SLK	MAP3K2
AMPKa1	MPSK1
MAP3K2	MARK2
NEK3	JNK2
NEK1	MARK3
MPSK1	CaMK4
NEK2	CRK7
CDC2	SgK496
BMPR1A	CLK1
AKT3	ACK
TLK2	TYK2
CDKL5	FRAP
MST2	TLK2
CLK1	ROCK2
CHK1	PAK4
CLK3	ULK3
IKKb	CLIK1L
ROCK2	TLK1
DDR2	LIMK2
PCTAIRE1	ZC3/MINK
CHED	TBK1
p70S6K	GAK
CDK8	AMPKa2
KDR	SRC
CK1g3	AMPKa1

IKKa	BMPR1A
TTK	TTK
FRAP	TTN
ZC3/MINK	PLK1
DNAPK	MYT1
FGFR1	CDK8
TGFbR2	GCN2
LATS1	CDK9
MELK	RIPK2
IKKe	MAP3K3
PAK4	DRAK2
FAK	ARG
ACK	AAK1
CRK7	EphA5
CDK10	AurB
PKCd	CDC2
LCK	CDK10
EphA5	PCTAIRE1
ZC1/HGK	IKKe
ARG	EphB2
BUB1	PCTAIRE3
GAK	PLK4
CDK9	CLK3
MSK2	MLK3
MAPKAPK2	EphA3
JNK1	NEK2
AurB	LOK
PLK4	ZAK
PKN3	PKN3
RIOK2	JNK1
BMPR1B	SLK
TGFbR1	IGF1R
ZAK	DAPK3
CK1d	INSR
CaMK4	ALK2
EphB3	IKKa
PDGFRb	AXL
MAP3K3	SRPK1
TTN	BUB1
DAPK3	MSK1
EphB2	MELK
PYK2	CK1d
SRPK1	RIOK2

LIMK2
smMLCK
ULK3
CSK
CDK11
DLK
ALK2
LOK
AXL
CDK4
NuaK2
MLK3
CDK7

smMLCK
MST3
YANK2
MSK2

GBM15		
≥2	2-0.4	≤0.4
skMLCK	FGFR1	smMLCK
PDGFRa	PRPK	NuaK2
IRAK3	ATM	AMPKa2
CaMK2a	TYRO3	RIOK2
MER	QSK	RSK1
SYK	PKD1	DDR2
CaMK2b	LRRK2	PKCd
BTK	DNAPK	LIMK2
TTN	GCK	AXL
PKCb	YES	MET
MARK1	PKACb	CaMKK2
FMS	CK1e	
RSK2	PIK3R4	
PKG1	CDC2	
FYN	CLK2	
HCK	NDR2	
PKCa	ABL	
FLT4	CaMK2d	
FGFR2	MAP3K4	
PEK	CK1g2	
PHKg1	BMPR2	
FES	KHS2	
CASK	PFTAIRE1	
STK33	ADCK4	
CLIK1	BLK	
BMPR1A	PKACa	

GBM6		
≥2	2-0.4	≤0.4
RET	CLIK1	CDK4
skMLCK	TIE2	MSK1
CaMK2b	IRAK4	smMLCK
JNK3	DRAK2	PKCd
IRAK3	CaMK1d	AurA
PKG1	PRPK	ALK2
FLT4	QSK	CDK7
PHKg1	EphA4	RSK1
PKCa	LKB1	NuaK2
FYN	NDR2	RIOK2
ADCK4	ATM	EphB2
BTK	CK1g2	AXL
FES	STK33	MET
FMS	YES	
CaMK2a	CDK6	
SYK	BMPR2	
EGFR	Wee1	
CaMK2d	MAP3K5	
PKD1	FGR	
LRRK2	HCK	
NEK11	CHK2	
FGFR2	IKKb	
Erk2	STLK5	
AKT2	MAP2K6	
PKCb	p38b	
DDR1	ADCK1	

Wee1	LKB1	NEK7	JAK1
DDR1	MLK2	PEK	LYN
	TAO3	PIK3R4	RSK2
	KHS1	MARK1	PKR
	NEK3		TAO3
	SLK		PFTAIRE1
	IRE1		NEK9
	MST1		MAP2K2
	NuaK1		CK2a1
	QIK		GCK
	AKT1		FAK
	MAP2K6		DNAPK
	TAO1		MAP3K6
	DYRK1A		CASK
	STLK5		FER
	TRKB		PDGFRa
	PKCt		CLK2
	AKT2		STLK6
	ZC2/TNIK		BIKE
	Erk2		CDK2
	LATS1		MER
	TIE2		PKN1
	CK1g1		TAO1
	MARK4		GSK3A
	DAPK2		SRPK2
	TIF1b		TLK1
	YANK2		NEK3
	CSK		GSK3B
	CDK2		ABL
	BIKE		BLK
	PKCe		PKD2
	CHK1		ICK
	SRPK2		LCK
	TAO2		RIPK1
	MAP3K1		PKD3
	ILK		BRAF
	GSK3B		MLK2
	SgK496		PKCt
	FAK		EphB3
	FGR		BCKDK
	HRI		BMPR1B
	BCKDK		LIMK1
	MAP2K4		MAP2K5

JNK3	TRKB
PDGFRb	MAP3K1
MAP2K5	Erk1
MARK2	DAPK2
p38b	CK2a2
CDK10	PCTAIRE2
MAP2K2	RSK3
LYN	TAO2
ROCK1	FGFR1
TYK2	IRAK1
ZC1/HGK	DYRK1A
CDK11	PASK
CHK2	MAP3K4
MST2	CK1e
CDK6	ILK
RIPK1	TIF1b
CLK1	YANK2
Erk5	FRK
TESK1	ULK3
CRK7	PKCe
TEC	Erk5
NEK7	FRAP
IRAK1	ZC1/HGK
TLK1	KHS2
YSK1	YSK1
GSK3A	HRI
IGF1R	ROCK1
JAK1	TYK2
NEK9	ROCK2
AurB	TEC
ADCK1	CDK5
CaMK1d	TYRO3
PKD3	TESK1
CK2a1	AKT1
EGFR	LATS1
NDR1	MAP2K1
PASK	NDR1
STLK6	PDK1
ULK3	MARK4
CLIK1L	p70S6K
IKKb	MAP2K4
FRAP	QIK
PCTAIRE2	CDK11

DRAK1	CaMKK2
CK1a	DMPK1
PKD2	CK1a
ARG	ZC2/TNIK
p38a	PKACa
LCK	BUB1
FRK	SgK496
MARK3	CDC2
TGFbR1	CK1g3
BUB1	PHKg2
Erk1	PKN2
MAPKAPK2	CHK1
CaMK2g	AMPKa1
EphA5	PCTAIRE3
CaMK4	MARK3
PKN2	IRE1
MAP2K3	EphA1
EphB2	CK1g1
PDK1	RIPK2
HIPK2	p38a
MRCKb	MRCKb
RSK3	PKACb
PKN3	CaMK2g
EphB4	DRAK1
CaMK1a	EphB4
JNK1	PKN3
IRAK4	CSK
PKN1	TBK1
TLK2	JNK2
PAK4	MST2
CK1g3	NEK1
RET	GAK
PLK1	PAK4
FER	PDGFRb
PHKg2	MST1
MAP3K3	KHS1
MAP3K7	HIPK2
LIMK1	AKT3
BRAF	CHED
MAP3K6	TTK
TTK	PYK2
MELK	MARK2
MAP2K1	MAP2K3

AurA	MAP3K2
NEK11	EphA5
CHED	ZC3/MINK
PYK2	TTN
EphB3	AMPKa2
MAP3K2	ARG
ACK	MPSK1
CK2a2	NEK2
PKR	NuaK1
TGFbR2	AurB
JNK2	PCTAIRE1
RIPK2	BMPR1A
ROCK2	CLK3
NEK2	KDR
ZAK	IGF1R
ZC3/MINK	ZAK
p70S6K	CaMK1a
CDKL5	MAPKAPK2
MLK3	AAK1
TBK1	CDK9
AKT3	TLK2
CLK3	TGFbR2
GCN2	CaMK4
ICK	MAP3K7
DRAK2	CDK10
CK1d	PLK1
CDK5	MLK3
AMPKa1	DDR2
MYT1	CLIK1L
CDK9	MYT1
PLK4	CLK1
EphA1	CDK8
DMPK1	MELK
BMPR1B	LIMK2
NEK1	SRPK1
AAK1	PLK4
MAP3K5	CRK7
EphA4	DLK
IKKa	TGFbR1
LOK	MAP3K3
PCTAIRE1	GCN2
SRPK1	CK1d
DAPK3	IKKe

MPSK1
GAK
CDK7
MSK2
DLK
IKKe
EphA3
SRC
CDK8
KDR
MST3
PCTAIRE3
MSK1
ALK2
CDK4
INSR

IKKa
JNK1
SLK
ACK
DAPK3
CDKL5
INSR
LOK
EphA3
MSK2
SRC
MST3

REFERENCES

1. Louis DN, Perry A, Reifenberger G, et al. The 2016 World Health Organization Classification of Tumors of the Central Nervous System: a summary. *Acta Neuropathol.* 2016;131(6):803-820.

2. Stupp R, Mason WP, van den Bent MJ, et al. Radiotherapy plus concomitant and adjuvant temozolomide for glioblastoma. *N Engl J Med.* 2005;352(10):987-996.

3. Brennan CW, Verhaak RG, McKenna A, et al. The somatic genomic landscape of glioblastoma. *Cell.* 2013;155(2):462-477.

4. Verhaak RG, Hoadley KA, Purdom E, et al. Integrated genomic analysis identifies clinically relevant subtypes of glioblastoma characterized by abnormalities in PDGFRA, IDH1, EGFR, and NF1. *Cancer Cell.* 2010;17(1):98-110.

5. Hanahan D, Weinberg RA. Hallmarks of cancer: the next generation. *Cell.* 2011;144(5):646-674.

6. Thorpe LM, Yuzugullu H, Zhao JJ. PI3K in cancer: divergent roles of isoforms, modes of activation and therapeutic targeting. *Nat Rev Cancer.* 2015;15(1):7-24.

7. Yoon S, Seger R. The extracellular signal-regulated kinase: multiple substrates regulate diverse cellular functions. *Growth Factors.* 2006;24(1):21-44.

8. Guha A, Feldkamp MM, Lau N, Boss G, Pawson A. Proliferation of human malignant astrocytomas is dependent on Ras activation. *Oncogene.* 1997;15(23):2755-2765.

9. Jeuken J, van den Broecke C, Gijsen S, Boots-Sprenger S, Wesseling P. RAS/RAF pathway activation in gliomas: the result of copy number gains rather than activating mutations. *Acta Neuropathol.* 2007;114(2):121-133.

10. Dienstmann R, Rodon J, Serra V, Tabernero J. Picking the point of inhibition: a comparative review of PI3K/AKT/mTOR pathway inhibitors. *Mol Cancer Ther.* 2014;13(5):1021-1031.

11. Roberts PJ, Der CJ. Targeting the Raf-MEK-ERK mitogen-activated protein kinase cascade for the treatment of cancer. *Oncogene.* 2007;26(22):3291-3310.

12. Cloughesy TF, Cavenee WK, Mischel PS. Glioblastoma: from molecular pathology to targeted treatment. *Annu Rev Pathol.* 2014;9:1-25.

13. McNeill RS, Vitucci M, Wu J, Miller CR. Contemporary murine models in preclinical astrocytoma drug development. *Neuro Oncol.* 2015;17(1):12-28.

14. Prados MD, Byron SA, Tran NL, et al. Toward precision medicine in glioblastoma: the promise and the challenges. *Neuro Oncol.* 2015;17(8):1051-1063.

15. Akhavan D, Cloughesy TF, Mischel PS. mTOR signaling in glioblastoma: lessons learned from bench to bedside. *Neuro Oncol.* 2010;12(8):882-889.

16. Schmid RS, Simon JM, Vitucci M, et al. Core pathway mutations induce de-differentiation of murine astrocytes into glioblastoma stem cells that are sensitive to radiation but resistant to temozolomide. *Neuro Oncol.* 2016;18(7):962-973.

17. Uhrbom L, Dai C, Celestino JC, Rosenblum MK, Fuller GN, Holland EC. Ink4a-Arf loss cooperates with KRas activation in astrocytes and neural progenitors to generate glioblastomas of various morphologies depending on activated Akt. *Cancer Res.* 2002;62(19):5551-5558.

18. Sonoda Y, Ozawa T, Aldape KD, Deen DF, Berger MS, Pieper RO. Akt pathway activation converts anaplastic astrocytoma to glioblastoma multiforme in a human astrocyte model of glioma. *Cancer Res.* 2001;61(18):6674-6678.

19. Chow LM, Endersby R, Zhu X, et al. Cooperativity within and among Pten, p53, and Rb pathways induces high-grade astrocytoma in adult brain. *Cancer Cell.* 2011;19(3):305-316.

20. Vitucci M, Karpinich NO, Bash RE, et al. Cooperativity between MAPK and PI3K signaling activation is required for glioblastoma pathogenesis. *Neuro Oncol.* 2013;15(10):1317-1329.

21. McNeill RS, Schmid RS, Bash RE, et al. Modeling astrocytoma pathogenesis in vitro and in vivo using cortical astrocytes or neural stem cells from conditional, genetically engineered mice. *J Vis Exp.* 2014(90):e51763.

22. Jackson EL, Willis N, Mercer K, et al. Analysis of lung tumor initiation and progression using conditional expression of oncogenic K-ras. *Genes Dev.* 2001;15(24):3243-3248.

23. Xiao A, Wu H, Pandolfi PP, Louis DN, Van Dyke T. Astrocyte inactivation of the pRb pathway predisposes mice to malignant astrocytoma development that is accelerated by PTEN mutation. *Cancer Cell.* 2002;1(2):157-168.

24. Xiao A, Yin C, Yang C, Di Cristofano A, Pandolfi PP, Van Dyke T. Somatic induction of Pten loss in a preclinical astrocytoma model reveals major roles in disease progression and avenues for target discovery and validation. *Cancer Res.* 2005;65(12):5172-5180.

25. Miller CR, Buchsbaum DJ, Reynolds PN, et al. Differential susceptibility of primary and established human glioma cells to adenovirus infection: targeting via

the epidermal growth factor receptor achieves fiber receptor-independent gene transfer. *Cancer Res.* 1998;58(24):5738-5748.

26. Miller CR, Williams CR, Buchsbaum DJ, Gillespie GY. Intratumoral 5-fluorouracil produced by cytosine deaminase/5-fluorocytosine gene therapy is effective for experimental human glioblastomas. *Cancer Res.* 2002;62(3):773-780.

27. Bhat KP, Balasubramaniyan V, Vaillant B, et al. Mesenchymal differentiation mediated by NF-kappaB promotes radiation resistance in glioblastoma. *Cancer Cell.* 2013;24(3):331-346.

28. Gupta SK, Kizilbash SH, Carlson BL, et al. Delineation of MGMT Hypermethylation as a Biomarker for Veliparib-Mediated Temozolomide-Sensitizing Therapy of Glioblastoma. *J Natl Cancer Inst.* 2016;108(5).

29. Carlson BL, Pokorny JL, Schroeder MA, Sarkaria JN. Establishment, maintenance and in vitro and in vivo applications of primary human glioblastoma multiforme (GBM) xenograft models for translational biology studies and drug discovery. *Curr Protoc Pharmacol.* 2011;52(14):1-14.

30. Vlahos CJ, Matter WF, Hui KY, Brown RF. A specific inhibitor of phosphatidylinositol 3-kinase, 2-(4-morpholinyl)-8-phenyl-4H-1-benzopyran-4-one (LY294002). *J Biol Chem.* 1994;269(7):5241-5248.

31. Maira SM, Pecchi S, Huang A, et al. Identification and characterization of NVP-BKM120, an orally available pan-class I PI3-kinase inhibitor. *Mol Cancer Ther.* 2012;11(2):317-328.

32. Maira SM, Stauffer F, Brueggen J, et al. Identification and characterization of NVP-BEZ235, a new orally available dual phosphatidylinositol 3-kinase/mammalian target of rapamycin inhibitor with potent in vivo antitumor activity. *Mol Cancer Ther.* 2008;7(7):1851-1863.

33. Yeh TC, Marsh V, Bernat BA, et al. Biological characterization of ARRY-142886 (AZD6244), a potent, highly selective mitogen-activated protein kinase kinase 1/2 inhibitor. *Clin Cancer Res.* 2007;13(5):1576-1583.

34. Sebolt-Leopold JS, Merriman R, Omer C, et al. The biological profile of PD 0325901: A second generation analog of CI-1040 with improved pharmaceutical potential. *Cancer Research.* 2004;64(7 Supplement):925.

35. Yoshida T, Kakegawa J, Yamaguchi T, et al. Identification and characterization of a novel chemotype MEK inhibitor able to alter the phosphorylation state of MEK1/2. *Oncotarget.* 2012;3(12):1533-1545.

36. Shor B, Zhang WG, Toral-Barza L, et al. A new pharmacologic action of CCI-779 involves FKBP12-independent inhibition of mTOR kinase activity and profound repression of global protein synthesis. *Cancer Res.* 2008;68(8):2934-2943.

37. Sedrani R, Cottens S, Kallen J, Schuler W. Chemical modification of rapamycin: the discovery of SDZ RAD. *Transplant Proc.* 1998;30(5):2192-2194.

38. Barretina J, Caponigro G, Stransky N, et al. The Cancer Cell Line Encyclopedia enables predictive modelling of anticancer drug sensitivity. *Nature.* 2012;483(7391):603-607.

39. Reinhold WC, Sunshine M, Liu H, et al. CellMiner: a web-based suite of genomic and pharmacologic tools to explore transcript and drug patterns in the NCI-60 cell line set. *Cancer Res.* 2012;72(14):3499-3511.

40. Pawaskar DK, Straubinger RM, Fetterly GJ, Ma WW, Jusko WJ. Interactions of everolimus and sorafenib in pancreatic cancer cells. *AAPS J.* 2013;15(1):78-84.

41. Duncan JS, Whittle MC, Nakamura K, et al. Dynamic reprogramming of the kinome in response to targeted MEK inhibition in triple-negative breast cancer. *Cell.* 2012;149(2):307-321.

42. Stuhlmiller TJ, Miller SM, Zawistowski JS, et al. Inhibition of lapatinib-induced kinome reprogramming in ERBB2-positive breast cancer by targeting BET family bromodomains. *Cell Rep.* 2015;11(3):390-404.

43. Li H, Durbin R. Fast and accurate short read alignment with Burrows-Wheeler transform. *Bioinformatics.* 2009;25(14):1754-1760.

44. Chou TC. Drug combination studies and their synergy quantification using the Chou-Talalay method. *Cancer Res.* 2010;70(2):440-446.

45. Irvin DM, McNeill RS, Bash RE, Miller CR. Intrinsic Astrocyte Heterogeneity Influences Tumor Growth in Glioma Mouse Models. *Brain Pathol.* 2017;27(1):36-50.

46. Louis DN, Ohgaki H, Wiestler OD, Cavenee WK, eds. *WHO classification of tumours of the central nervous system.* 4th ed. Lyon: IARC; 2007. WHO Classification of Tumours.

47. Schmid RS, Vitucci M, Miller CR. Genetically engineered mouse models of diffuse gliomas. *Brain Res Bull.* 2012;88(1):72-79.

48. See WL, Tan IL, Mukherjee J, Nicolaides T, Pieper RO. Sensitivity of glioblastomas to clinically available MEK inhibitors is defined by neurofibromin 1 deficiency. *Cancer Res.* 2012;72(13):3350-3359.

49. Turke AB, Song Y, Costa C, et al. MEK inhibition leads to PI3K/AKT activation by relieving a negative feedback on ERBB receptors. *Cancer Res.* 2012;72(13):3228-3237.

50. Sunayama J, Matsuda K, Sato A, et al. Crosstalk between the PI3K/mTOR and MEK/ERK pathways involved in the maintenance of self-renewal and tumorigenicity of glioblastoma stem-like cells. *Stem Cells.* 2010;28(11):1930-1939.

51. Roberts PJ, Usary JE, Darr DB, et al. Combined PI3K/mTOR and MEK inhibition provides broad antitumor activity in faithful murine cancer models. *Clin Cancer Res.* 2012;18(19):5290-5303.

52. El Meskini R, Iacovelli AJ, Kulaga A, et al. A preclinical orthotopic model for glioblastoma recapitulates key features of human tumors and demonstrates sensitivity to a combination of MEK and PI3K pathway inhibitors. *Dis Model Mech.* 2015;8(1):45-56.

53. Swearingen AEDV, Siegel MB, Bash R, et al. Abstract 5449A: PI3K and MEK inhibition in intracranial triple negative breast cancer: Efficacy of BKM120 and AZD6244 in preclinical mouse models. *Cancer Res.* 2014;74(19 Supplement):5449A.

54. Huszthy PC, Daphu I, Niclou SP, et al. In vivo models of primary brain tumors: pitfalls and perspectives. *Neuro Oncol.* 2012;14(8):979-993.

55. Koul D, Fu J, Shen R, et al. Antitumor activity of NVP-BKM120--a selective pan class I PI3 kinase inhibitor showed differential forms of cell death based on p53 status of glioma cells. *Clin Cancer Res.* 2012;18(1):184-195.

56. Herter-Sprie GS, Kung AL, Wong KK. New cast for a new era: preclinical cancer drug development revisited. *J Clin Invest.* 2013;123(9):3639-3645.

57. Stuhlmiller TJ, Earp HS, Johnson GL. Adaptive reprogramming of the breast cancer kinome. *Clin Pharmacol Ther.* 2014;95(4):413-415.

58. Van Swearingen AED, Siegel MB, Sambade MJ, et al. Abstract 2579: Combination therapy with MEK inhibition is efficacious in intracranial triple negative breast cancer models. *Cancer Research.* 2015;75(15 Supplement):2579.

59. Zamboni WC, Torchilin V, Patri AK, et al. Best practices in cancer nanotechnology: perspective from NCI nanotechnology alliance. *Clin Cancer Res.* 2012;18(12):3229-3241.

60. Cancer Genome Atlas Research Network. Comprehensive genomic characterization defines human glioblastoma genes and core pathways. *Nature.* 2008;455(7216):1061-1068.

CHAPTER IV: PI3K AND MAPK PATHWAY MUTATIONS IN GLIOBLASTOMA INFLUENCE RESPONSE TO KINASE INHIBITORS TARGETING THESE PATHWAYS

Introduction

Diffuse gliomas are a histologically and genetically diverse group of malignant primary brain tumors.[1-3] Gliomas have traditionally been classified based on their histologic resemblance to normal brain cells, specifically astrocytomas resemble astrocytes, while oligodendrogliomas resemble oligodendrocytes.[4] Molecular characterization of these diseases have improved diagnostics via the inclusion of both histological and genomic criteria in the new WHO 2016 classification.[1] Glioblastoma (GBM) is the most common and aggressive diffuse glioma in adults. The majority of GBM arise *de novo* without a clinically detectable lower grade antecedent (primary GBM).[5] Standard-of-care consists of surgical resection followed by radiation with concurrent and adjuvant temozolomide.[6] Median survival is only 12-15 months, due to the inevitable recurrence of this devastating disease.

Efforts such as TCGA have characterized the molecular heterogeneity of primary GBM (hereafter just GBM) using genomics.[3,7] GBM has been stratified into four molecular subtypes based on transcriptome profiles: classical, neural, proneural, and mesenchymal. GBM is also characterized by co-occurring mutations in the RB, TP53,

and receptor tyrosine kinase (RTK)/phosphoinositide 3-kinase (PI3K)/mitogen activated protein kinase (MAPK) pathways.[3,7]

PI3K signaling is most frequently activated via inactivating mutations in its negative regulator, *PTEN*.[3,8] MAPK signaling is activated in the majority of GBM, most frequently due to deletions/inactivating mutations in its negative regulator *NF1* or amplifications/activating mutations of RTK or *KRAS*.[3,9,10] Kinase inhibitors targeting the PI3K and MAPK pathways are in clinical development or approved for non-glioma tumors.[11,12] Moreover, the RTK/PI3K/MAPK pathways are appealing therapeutic targets in GBM because they are mutated in 90% of patients and have well-established roles in disease pathogenesis.[3,8,13,14] Nevertheless, clinical investigations of single agent kinase inhibitors have had disappointing results in GBM.[15-18] Defining how individual mutations influence efficacy and resistance to targeted inhibitors may aid in the identification of predictive biomarkers and the design rational combination therapies.

Preclinical studies can aid in clinical drug development by prospectively identifying potential resistance mechanisms and predictive biomarkers. Genetically engineered mouse (GEM) models are valuable tools for these efforts because they enable direct genotype to phenotype comparisons.[16] Activating PI3K and MAPK pathway mutations cooperate to promote tumorigenesis in preclinical glioma models.[19-23] For instance, we developed a series of non-germline GEM (nGEM) models in which astrocytes were immortalized by ablation of the Rb family of pocket proteins via expression of an N-terminal SV40 large T mutant (T_{121}, T).[23] PI3K and MAPK signaling were activated alone and in combination in T astrocytes via knock-in of a constitutively active *Kras* mutant ($Kras^{G12D}$, R) and homozygous *Pten* deletion (P), respectively. We

previously used T, TP, TR, and TRP astrocytes (hereafter the T(RP) series) to show that *Pten* deletion and mutant *Kras* cooperated to activate PI3K/MAPK signaling, promote proliferation and de-differentiation *in vitro*, and potentiate formation of GBM *in vivo*.[19,23] In Chapter III we showed that while triple mutant TRP astrocytes were sensitive to single agent pan-PI3K, mTOR, and MEK1/2 inhibitors (PI3Ki, mTORi, and MEKi), dual treatment with PI3Ki/MEKi were most effective *in vitro* and *in vivo*.[24] However, it remained unclear whether *Pten*/*Kras* mutations influenced efficacy of single agent and combination treatments. We therefore used the T(RP) nGEM series to define how PI3K/MAPK mutation status and drug potency interact to influence response single agent and combination treatments with PI3Ki, mTORi, and/or MEKi *in vitro.*[19,23]

Materials and Methods

Murine astrocyte cultures. Cortical astrocytes were harvested from GEM and maintained as previously described.[19,23,25] Briefly, mice containing conditional alleles (*TgGZT*$_{121}$, *Kras*^{G12D} knock-in, and/or *Pten* knock-out) were crossed to generate compound T(RP) mice.[23,26-28] Astrocytes harboring floxed, heterozygous T ± R and/or floxed, homozygous P alleles were harvested from neonatal mice, and recombination was induced *in vitro* with an adenoviral vector encoding Cre recombinase (Ad5CMVCre, University of Iowa Gene Transfer Vector Core). Astrocytes were maintained at 37 °C and 5% CO_2 as adherent cells in Dulbecco's Modified Eagle Medium (DMEM) supplemented with 10% fetal bovine serum and 1% penicillin/streptomycin. The UNC Institutional Animal Care and Use Committee approved all animal studies.

Drugs. LY294002 (LY) and PD0125901 (PD01) were purchased from Cayman Chemicals (Ann Arbor, MI). Temsirolimus (CCI-779) was purchased from Selleckchem (Houston, TX). Dactolisib (BEZ235) was purchased from MedChem Express (Monmouth Junction, NJ). Buparlisib (BKM120) and selumetinib (AZD6244) were purchased from MedChem Express and Chemietek (Indianapolis, IN). Trametinib was purchased from MedChem Express and Selleckchem. Dactolisib was dissolved in N,N-Dimethylformamide (DMF). All other drugs were dissolved in dimethyl sulfoxide (DMSO).

Immunoblots. The T(RP) astrocyte series were plated on tissue culture treated plates, and at ~60 confluence they were treated with buparlisib, selumetinib, or DMSO (control). Cells were mechanically harvested 4 or 24 h after treatment, lysed, and then protein concentration was quantified using Pierce BCA Protein Assay Kit (Thermo

Scientific, Waltham, MA). Immunoblots were performed as previously described.[19] Briefly, 20 µg of proteins were resolved by SDS-PAGE (gradient 8-16%) gel electrophoresis (Bio-Rad, Hercules, CA), transferred to PVDF membranes (EMD Millipore), then probed overnight at 4 °C using primary antibodies against Gapdh (#AB2302, EMD Millipore) and p-Erk1/2 (Thr202/Tyr204, #9101), Erk1/2 (#4696), Akt (#2967), p-Akt (Ser473, #9271), and p-S6 (Ser240/244, #2215) all from Cell Signaling Technology (Danvers, MA). Species specific Alexa 488, 568, and 633 conjugated secondary antibodies were incubated with the membranes at room temperature for 30 min. Immunoblots were imaged on a GE Typhoon Trio (GE Healthcare, Marlborough, MA), band intensities were quantified using ImageJ (NIH, Bethesda, MD), and intensities of phosphoproteins (p) were normalized to the corresponding total protein or Gapdh then set relative to control cells.

Dose response. The T(RP) astrocyte series were plated in 96-well tissue culture plates with 3-6 technical replicates per condition. The following day, cells were treated with solvent or drug(s). Effects of drugs on growth was assessed 5 days after treatment with the CellTiter 96 Aqueous One Solution Cell Proliferation Assay (MTS, Promega, Madison, WI) according to manufacturer's instructions. Absorbance at 490nm was measured with an Emax plate reader (Molecular Devices, Chicago, IL) equipped with SoftMax Pro 5 software. Absorbance in each well was subtracted by baseline absorbance (MTS reagent plus culture media) and then set relative to cells treated with solvent.

Data from 1-6 independent experiments were pooled, fit to a non-linear, log [inhibitor] versus response curves with variable slope, and Hill slopes, GI_{50}, IC_{50}, and

I_{max} were calculated as previously described.[19,24,29,30] Effects of PI3Ki and MEKi potency and genotype on IC_{50} and GI_{50} were calculated by two-way ANOVA. Effects of genotype on temsirolimus IC_{50} and GI_{50} were calculated by one-way ANOVA. The pairwise effects of genotype (T vs. TP, TR, and TRP; TP vs. TRP; and TR vs. TRP) and drugs on IC_{50}, GI_{50} and Hill slopes were compared using the extra-sum-of-squares F test. Log_{10} (Log) IC_{50} and GI_{50} were graphed unless otherwise stated.

Drug synergism. PI3Ki/MEKi synergism was determined using the Chou-Talalay method.[31] Briefly, relative absorbance was determined for single agents and the corresponding combinations at a constant molar ratio using MTS (Promega) as described above. Fraction affected (1 – relative growth, FA) was calculated, and the combination index (CI) was determined using CompuSyn (ComboSyn, Inc., Paramus, NJ). Data were pooled from 2–4 independent experiments. Combination index (CI) values <0.86, 1–0.86, and >1 were considered synergistic, additive, and antagonistic, respectively.

Statistics. Statistical analyses were conducted in GraphPad Prism (La Jolla, CA). Error bars are SEM. $P \leq 0.05$ were considered statistically significant.

Results

The PI3K and MAPK pathways are frequently activated in GBM, and drive gliomagenesis in preclinical models.[3,7,9,10,32,33] Using our T(RP) series of nGEM models, we showed that *Pten* deletion and mutant *Kras* cooperate to promote gliomagenesis.[19,23] We recently found that TRP astrocytes were sensitive to pharmacological inhibition of PI3K and MAPK signaling.[24] Whether mutations that activated PI3K/MAPK signaling influenced response to their inhibition remained unclear. To address this issue, we used a combinatorial experimental approach to determine how *Pten*/*Kras* mutation status and drug potency interact to influence efficacy, synergism, and alternate pathway activation *in vitro*.

PI3Ki-induced alternate MAPK activation is independent of *Pten* and *Kras* mutation status

The PI3K pathway is a potential therapeutic target in GBM.[18] We previously found that the PI3Ki buparlisib inhibited PI3K signaling and induced dynamic kinome reprogramming of TRP astrocytes, including alternate activation of MAPK signaling.[24] Here, we determined whether buparlisib-induced changes in PI3K and MAPK signaling were influenced by *Pten* and/or *Kras* mutation status. Immunoblots showed that proximal (p-Akt) and distal (p-S6) PI3K signaling was inhibited within 4 h (**Fig S4.1AB**) and sustained for 24 h (**Fig 4.1AB**) in all four genotypes of T(RP) astrocytes. Although buparlisib caused minimal changes in MAPK signaling at four h (**Fig S4.1AC**), it increased MAPK signaling by 24 h post-treatment regardless of *Pten*/*Kras* mutation status (**Fig 4.1AC**). Thus, buparlisib-induced PI3K inhibition and alternate MAPK activation was independent of mutational activation of either PI3K or MAPK signaling.

PI3Ki efficacy is potentiated by *Pten* and/or *Kras* mutations

Pten/*Kras* mutation status did not affect PI3Ki-induced changes in signaling (**Figs 4.1**, **S4.1**), but these mutations may modulate drug efficacy. We previously found a direct association between PI3Ki potency (dactolisib > buparlisib > LY) and efficacy in TRP astrocytes.[24] We therefore determined the effects of these three PI3Ki on T(RP) astrocyte growth *in vitro*. Dactolisib, buparlisib, and LY all caused dose-dependent decreases in growth, and a direct association between PI3Ki potency and efficacy (IC_{50} and GI_{50}) was evident in all four genotypes (**Fig 4.2**, **S4.2**). Furthermore, *Pten* and/or *Kras* mutations increased PI3Ki efficacy, especially for the most potent inhibitor dactolisib.

Dactolisib is a dual PI3Ki/mTORi, and it was the most effective inhibitor in all four T(RP) genotypes. Moreover, dactolisib was the only PI3Ki in which efficacy was increased in T astrocytes with both *Pten* deletion and mutant *Kras* compared to those with either mutation alone (TRP vs. TP or TR) (**Fig 4.2BC**). These data suggested that mTORi efficacy might also be influenced by *Pten/Kras* mutation status. The mTORi temsirolimus caused dose-dependent decreases in growth of all four T(RP) astrocyte genotypes (**Fig S4.3A**). Compared to dactolisib, temsirolimus was less effective in all genotypes ($P \leq 0.01$), and caused more gradual decreases in growth of TP, TR, and TRP astrocytes (Hill slope, $P \leq 0.001$) (**Fig S4.2**, **S4.3**). Temsirolimus IC_{50} were similar among T, TP, and TR astrocytes (**Fig S4.3B**). In contrast, temsirolimus IC_{50} was lower in TRP than T astrocytes (**Fig S4.3B**), and its GI_{50} was lower in TRP than TP and TR astrocytes (**Fig S4.3C**). Thus, *Pten* deletion and mutant *Kras* sensitized T astrocytes to mTORi more than either mutation alone.

Mutant *Kras* modulates MEKi-induced alternate activation of PI3K signaling

Consistent with other preclinical models, we previously found that multiple MEKi reduced TRP astrocyte growth, inhibited MAPK signaling, and induced proximal PI3K signaling.[24,34-37] Data from **Fig 4.1** demonstrated that PI3Ki ablated PI3K signaling and potentiated MAPK activation regardless of genotype. However, the effects of *Pten*/*Kras* mutation status on MEKi-induced signaling changes remained unclear. We therefore assessed MAPK/PI3K signaling in the T(RP) astrocyte series 4 h (**Fig 4.S4**) and 24 h (**Fig 4.3**) after treatment with the MEKi selumetinib. Immunoblots showed that MAPK signaling was reduced at 4 h, and inhibition was sustained for 24 h in all four genotypes. Ablation of MAPK signaling was more pronounced at 24 h in T astrocytes with *Pten* deletion (TP, TRP) than those without (T, TR) (**Fig 4.3AB**). Selumetinib increased proximal PI3K signaling in T, TR, and TRP astrocytes at 4 h (**Fig S4.4AC**), and this potentiation progressively increased over 24 h, particularly in astrocytes with mutant *Kras* (TR, TRP) (**Fig 4.3AC**). However, distal PI3K signaling was generally not activated in any genotype at either time. Taken together, these results indicate that *Pten* deletion influences MEKi-induced MAPK inhibition, while mutant *Kras* modulates MEKi-induced alternate PI3K activation.

MEKi efficacy is increased by *Pten* deletion

Because *Pten*/*Kras* mutation status influenced MEKi-induced changes in signaling (**Fig 4.3**), we hypothesized that these mutations would also influence MEKi efficacy. We therefore determined how increasingly potent MEKi (trametinib > PD01 > selumetinib) influenced T(RP) astrocyte growth *in vitro*.[38-40] All three MEKi caused dose-dependent decreases in growth, and potency was directly associated with efficacy

in all four genotypes (**Figs 4.4A**, **S4.2**). Moreover, MEKi sensitivity was influenced by *Pten*/*Kras* mutation status. TR astrocytes tended to have lower IC_{50} (P≥0.11) (**Fig 4.4B**) and had significantly lower GI_{50} (**Fig 4.4C**) than T astrocytes for the more potent MEKi (PD01 and trametinib). *Pten*-deleted astrocytes (TP and TRP) had significantly lower IC_{50} and GI_{50} than T astrocytes for all MEKi (**Fig 4.4BC**). Furthermore, TRP astrocytes also had decreased IC_{50} and GI_{50} compared to TR astrocytes. Thus, *Pten* deletion sensitizes T astrocytes to MEKi regardless of *Kras* status.

PI3Ki/MEKi synergism is influenced by drug potency and *Pten*/*Kras* mutation status

We previously found that dual PI3Ki/MEKi treatment was synergistic in TRP astrocytes.[24] However, *Pten*/*Kras* mutation status influenced MEKi-induced signaling changes, and efficacy of single agent PI3Ki and MEKi (**Figs 4.2**, **4.4**). We therefore determined whether *Pten*/*Kras* mutation status also influenced synergism of dual PI3Ki/MEKi treatment *in vitro*. Buparlisib/selumetinib treatment inhibited growth and was synergistic in all four T(RP) genotypes (**Fig 4.5A**). However, the buparlisib/selumetinib concentrations required for synergism were lower in TP, TR, and TRP than in T astrocytes. Because MEKi potency influenced the effects of mutant *Kras* on efficacy (**Fig 4.4C**), MEKi potency may also alter the effects of *Pten*/*Kras* mutations PI3Ki/MEKi synergism. To address this issue, we assessed drug synergism in cultured T(RP) astrocytes treated with buparlisib/trametinib. This inhibitor combination also reduced growth in all four genotypes, and the buparlisib/trametinib concentrations required for synergism were dramatically reduced compared to buparlisib/selumetinib treatment (**Fig 4.5AB**). Interestingly, the effects of *Pten*/*Kras* mutation status on

PI3Ki/MEKi synergism was blunted with dual buparlisib/trametinib treatment (**Fig 4.5B**). Thus, increased MEKi potency lowered the PI3Ki/MEKi concentrations required for synergism and abrogated the effects of *Pten* deletion and mutant *Kras*.

Discussion

PI3K and MAPK mutations influence efficacy of single agent targeted inhibitors

GBM are genetically heterogeneous, but recurrent mutations commonly converge on three "core" pathways: RB, TP53, and RTK/PI3K/MAPK.[3,41] Moreover, the vast majority of GBM harbor activated PI3K and MAPK signaling.[3,9] Preclinical models may aid in the clinical development of targeted inhibitors by defining how frequent mutations influence drug efficacy and resistance. To this end, the influence of "core" pathway mutations on sensitivity to single agent kinase inhibitors has been investigated using GBM established cell lines (ECL) and patient derived xenografts (PDX).[7,34,42,43] Nevertheless, ECL models poorly correlate with clinical outcomes.[16] Additionally, these preclinical studies were generally designed to correlate specific mutations with drug efficacy. In contrast, nGEM models enable direct genotype/phenotype comparisons and thus may be more predictive.[44,45]

Because *PTEN* deletion activates PI3K signaling, it may promote sensitivity to inhibitors of this pathway. However, the utility of *PTEN* status as a predictive biomarker remains unclear, and preclinical studies which sought to answer this question in a variety of cancer types, including GBM, have had variable results.[42,43,46-51] We previously showed that TRP astrocytes were sensitive to PI3Ki.[24] Here we found that *Pten* deletion and/or mutant *Kras* resulted in biologically marginal, but statistically significant increases in efficacy of the less potent PI3Ki LY and buparlisib (**Fig 4.2**). This finding is consistent with the lack of correlation between *PTEN* status and buparlisib efficacy in GBM ECL.[42] The influence of *Pten*/*Kras* mutation status on inhibitor efficacy was much more pronounced with the most potent, dual PI3Ki/mTORi

dactolisib (**Fig 4.2**). *Pten*/*Kras* mutations resulted in 5-15 fold decreases in IC_{50} and 10-34 fold decreases in GI_{50} compared to T astrocytes. Furthermore, T astrocytes with both *Pten* deletion and mutant *Kras* (TRP) were more sensitive to dactolisib than those with either mutation alone (TP, TR). These data suggest that *Pten*/*Kras* mutation status has a greater impact on PI3Ki efficacy when a more potent PI3Ki and/or a dual mTOR/PI3Ki is used. Similar to the finding that *PTEN* loss does not predict efficacy of mTORi in GBM PDX, we found that *Pten* deletion alone did not alter sensitivity to the mTORi temsirolimus (**Figs S4.2**, **S4.3**).[43] However, mTORi efficacy was greatest in TRP astrocytes, suggesting that *Pten* deletion and mutant *Kras* cooperate to promote sensitivity to mTORi.

We previously found that mutant *Kras* activated MAPK signaling, and promoted tumorigenesis.[23] We therefore hypothesized that *Kras* status would increase MEKi efficacy. Nevertheless, the effects of mutant *Kras* were relatively minor, and only decreased GI_{50} for the more potent MEKi (PD01 and trametinib) (**Fig 4.4**). This indicates that MEKi potency influences the impact of MAPK mutations on efficacy. See et al. found that only a subset of *NF1*-null GBM ECL were sensitive to MEKi.[34] Taken together, these results suggest that MAPK mutations alone may not accurately predict MEKi efficacy in GBM.

We found that *Pten* deletion had a far more dramatic effect on MEKi sensitivity than mutant *Kras* (**Fig 4.4**). While surprising, there is a precedent for this result in the literature. Similar to our previous finding that *Pten* deletion and mutant *Kras* cooperate to potentiate MAPK signaling and gliomagenesis, Ebbesen et al. showed that *Pten* knock-down increased PI3K and MAPK signaling and promoted malignant progression

of HER2/neu driven breast carcinomas.[23,52] Interestingly, MEKi treatment phenocopied *Pten* restoration in this model, and was more effective than either PI3K or AKT inhibitors at inhibiting tumor growth. Taken together, these results demonstrate that *PTEN* loss increases sensitivity to MEKi, suggesting that GBM patients with *PTEN*-null tumors may be uniquely sensitive to MEKi.

Activation of bypass pathways promote resistance to single agent kinase inhibitors

There is extensive cross talk between the PI3K and MAPK pathways.[53] We and others have found that pharmacologic inhibition of either PI3K or MAPK signaling induces compensatory activation of the alternate arm of RTK signaling (**Figs 4.1**, **4.3**).[34,37,54] We expanded these findings here by demonstrating that *Pten* deletion potentiated MEKi-induced MAPK inhibition, while mutant *Kras* enhanced MEKi-induced PI3K activation (**Fig 4.3**). In contrast, we found that *Pten*/*Kras* mutation status did not influence PI3Ki-induced signaling changes, suggesting that they are intrinsic to astrocyte biology (**Fig 4.1**). However, the specific PI3K/MAPK mutations and cellular origin may influence the signaling changes characterized here. Future work will be required to investigate how cellular origin and additional PI3K/MAPK pathway mutations interact to impact the dynamic kinome response to PI3Ki/MEKi.

We and others have shown that cooperativity between PI3K and MAPK signaling is important for glioma stem cell biology and tumorigenicity.[19,23,37] Moreover, PI3K and MAPK are reciprocal bypass pathways that promote resistance to inhibition of either pathway alone.[34,37,54] We expanded these results here by determining how *Pten*/*Kras* mutations affect PI3Ki/MEKi synergism *in vitro*. *Pten* deletion and/or mutant *Kras*

increased the concentration range in which buparlisib/selumetinib were synergistic (**Fig 4.5A**). We also found that increased MEKi potency (trametinib vs. selumetinib) expanded the range of synergistic concentrations for both PI3Ki and MEKi in all four genotypes. Moreover, the effects of *Pten*/*Kras* mutation status on synergism were blunted with dual trametinib/buparlisib treatment (**Fig 4.5B**). Taken together, these results suggest that both MEKi potency and *Pten*/*Kras* mutation status interact to influence PI3Ki/MEKi synergism.

Conclusion

Defining mechanisms of drug resistance and characterizing predictive biomarkers in preclinical studies may aid in the design and use of rational drug combinations in GBM patients likely to respond. Here we used a series of nGEM models to determine the influence of *Pten* deletion and mutant *Kras* on response to single agent and combination treatments with PI3Ki and MEKi *in vitro*. These results indicate that PI3Ki/MEKi single agent efficacy and synergism are influenced by drug potency and PI3K/MAPK mutations. Moreover, our results demonstrate how mutations in cooperating pathways interact to enhance efficacy of single agent PI3Ki/mTORi, suggesting that prospective screening for multiple mutations may be necessary to accurately predict drug efficacy.

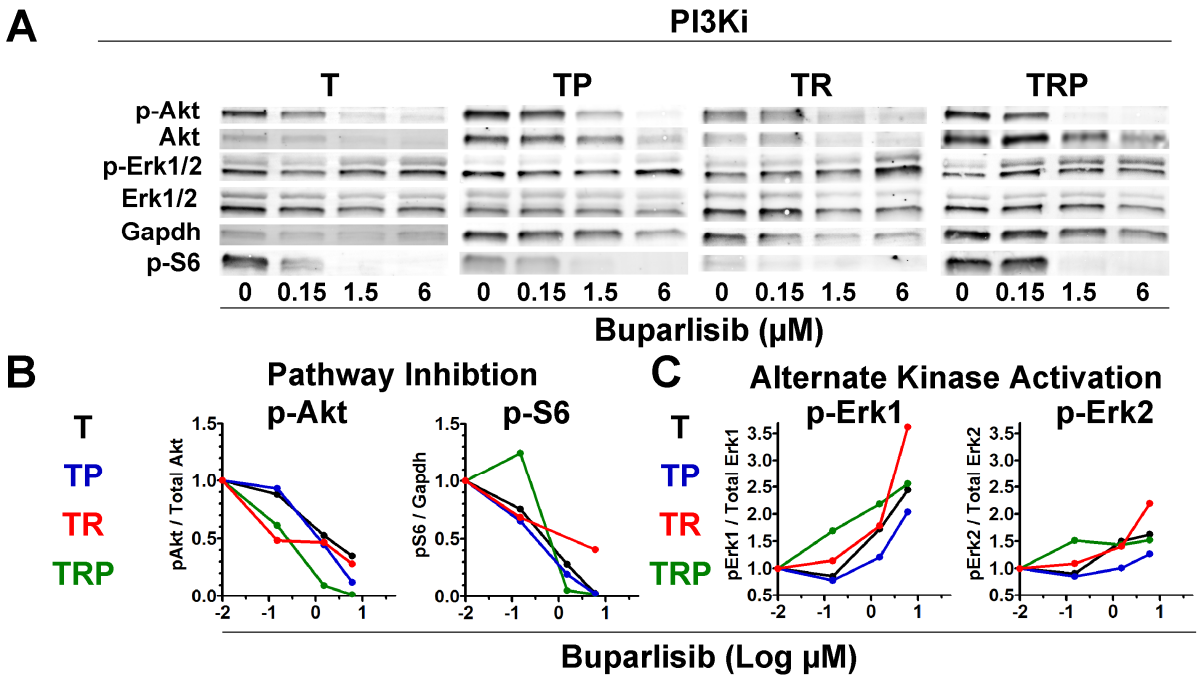

Figure 4.1. **Buparlisib inhibits PI3K signaling and induces MAPK signaling regardless of *Pten*/*Kras* mutation status**. Immunoblots (**A**) of the T(RP) astrocyte series 24 h after buparlisib treatment showed that buparlisib caused dose-dependent decreases in proximal (p-AKT) and distal (p-S6) PI3K (**B**), and increases in MAPK (p-Erk1/2) (**C**) signaling regardless of *Pten*/*Kras* mutation status.

.

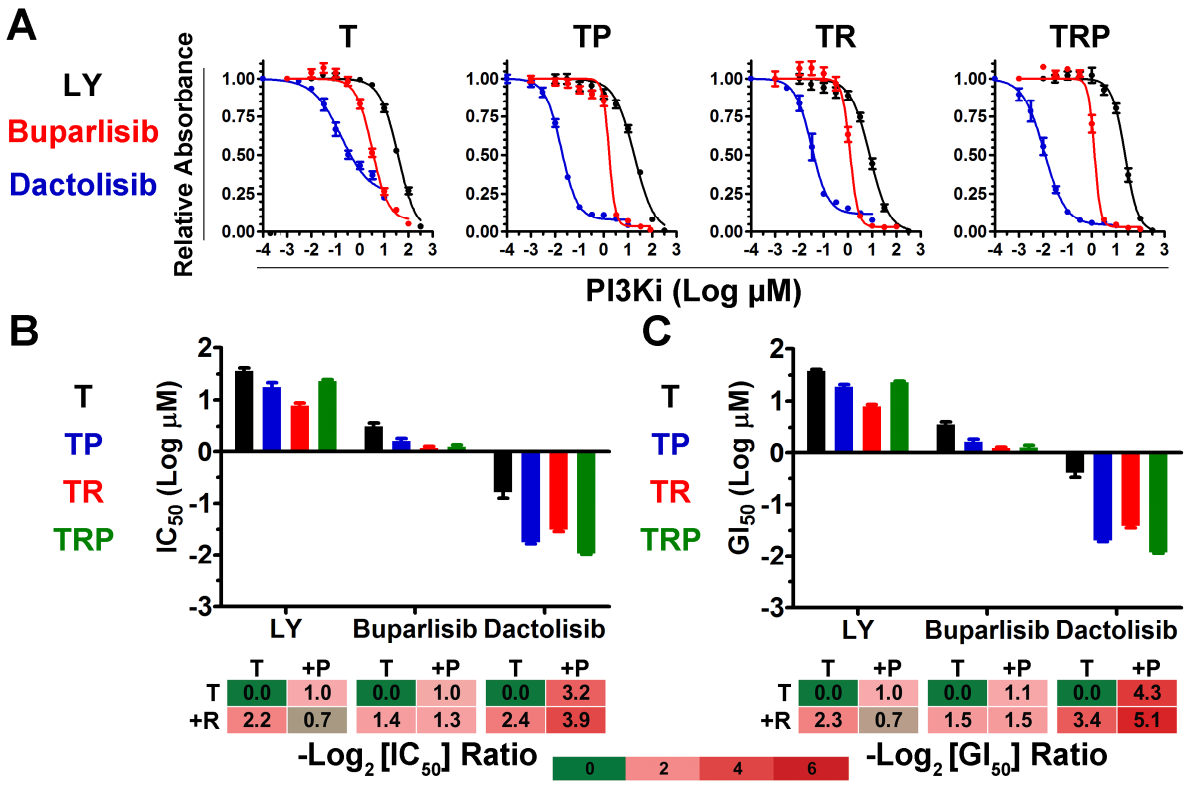

Figure 4.2. **PI3Ki efficacy is influenced by *Pten*/*Kras* mutation status**. Multiple PI3Ki reduced growth of the T(RP) astrocyte series ($R^2 \geq 0.99$) (**A**), and both drug potency and *Pten*/*Kras* mutation status influenced IC_{50} (**B**) and GI_{50} (**C**) (ANOVA, $P<0.0001$). $P \leq 0.003$ for all PI3Ki IC_{50}/GI_{50} in T vs. TP, TR, or TRP. $P \leq 0.001$ for LY IC_{50}/GI_{50} in TR vs. TRP. $P \leq 0.001$ for dactolisib IC_{50}/GI_{50} in TP/TR vs. TRP. IC_{50}/GI_{50} fold decreases for T(RP) relative to T astrocytes are shown as heatmaps.

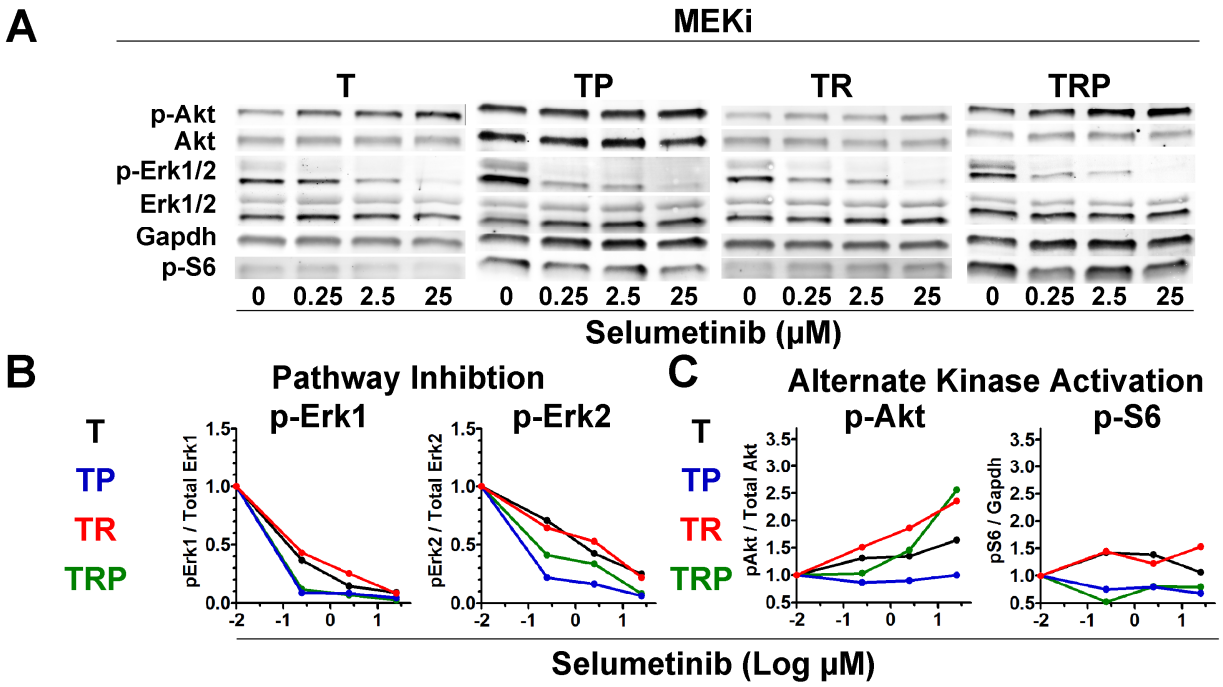

Figure 4.3. **MEKi-induced MAPK inhibition and PI3K activation is influenced by *Pten*/*Kras* mutation status**. Immunoblots (**A**) of the T(RP) astrocyte series 24 h after selumetinib treatment showed that selumetinib inhibited MAPK signaling at lower concentrations in *Pten*-null (TP, TRP) astrocytes (**B**). They also showed that selumetinib-induced alternate activation of proximal, but not distal, PI3K signaling was most pronounced in *Kras* mutant (TR and TRP) astrocytes (**C**).

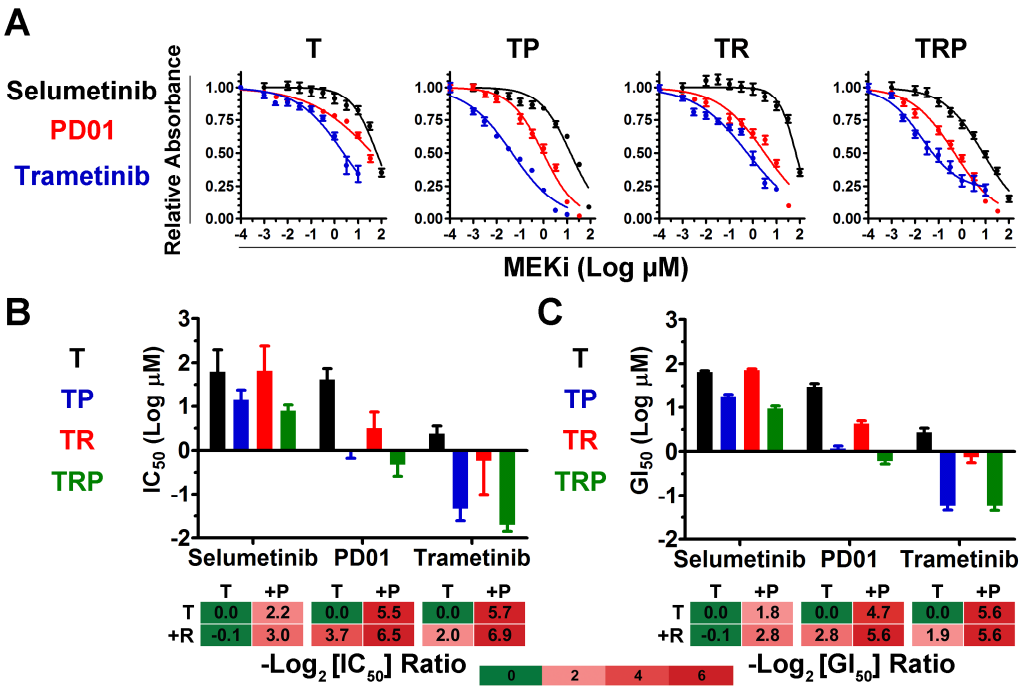

Figure 4.4. **MEKi efficacy is increased by *Pten* deletion**. Multiple MEKi reduced growth of the T(RP) astrocyte series (R^2≥0.93) (**A**), and both drug potency and *Pten*/*Kras* mutation status influenced IC_{50} (**B**) and GI_{50} (**C**) (ANOVA, P<0.0001). P≤0.03 for all MEKi IC_{50}/GI_{50} in T vs. TP and TRP, and TR vs. TRP. P≤0.002 for PD01/trametinib GI_{50} in T vs. TR. P≤0.04 for PD01 IC_{50}/GI_{50} and selumetinib GI_{50} in TP vs. TRP. IC_{50}/GI_{50} fold decreases for T(RP) relative to T astrocytes are shown as heatmaps.

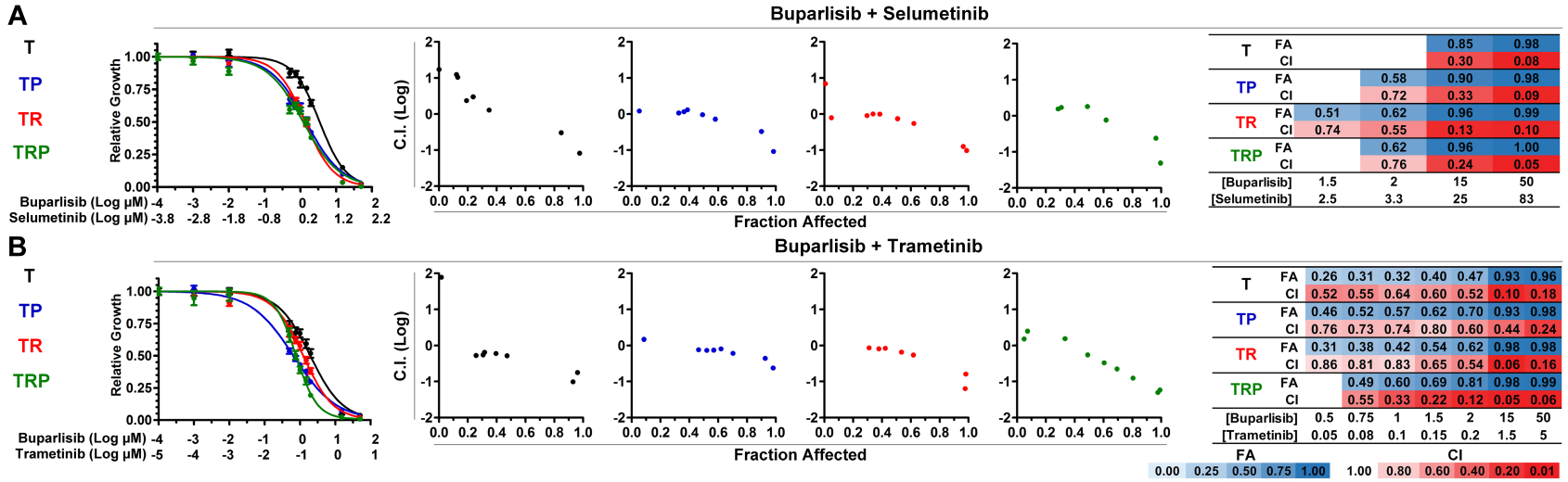

Figure 4.5. **PI3Ki/MEKi synergism is influenced by *Pten*/*Kras* mutation status and drug potency**.

Buparlisib/selumetinib treatment reduced growth of the T(RP) astrocyte series (R^2≥0.97) and were synergistic at ≥7.5x lower concentrations in TP, TR, and TRP compared to T astrocytes (**A**). Buparlisib/trametinib treatment reduced growth of T(RP) astrocytes (R^2≥0.99) (**B**). The concentration ranges in which PI3Ki and MEKi were synergistic was increased when the more potent MEKi trametinib was used, but the effects of *Pten*/*Kras* mutation status on PI3Ki/MEKi synergism were blunted. Combination index (CI) and corresponding fraction affected (FA) for synergistic PI3Ki/MEKi concentrations in the T(RP) astrocyte series are shown as heatmaps.

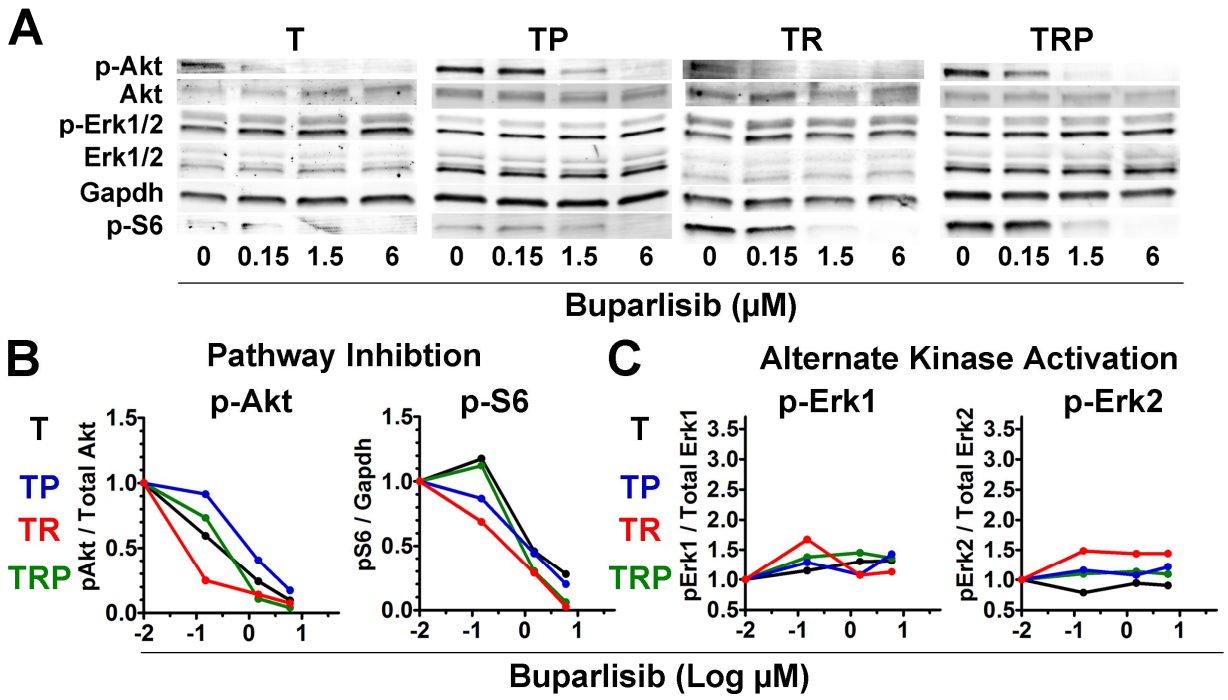

Figure S4.1. **The PI3Ki buparlisib ablates PI3K signaling within 4 h post-treatment**. Immunoblots performed on the T(RP) astrocyte series 4 h after buparlisib (**A**) showed dose-dependent decreases in proximal (p-Akt) and distal (p-S6) PI3K signaling (**B**) and little to no increases in MAPK signaling (p-Erk1/2) (**C**). These results, in combination with those in **Fig 4.1**, demonstrated that the dynamic changes in PI3K inhibition and alternate activation of MAPK signaling was independent of *Pten*/*Kras* mutation status.

		T					TP				
Class	Drug	IC_{50} nM	GI_{50} nM	I_{max} %	Hill slope	n	IC_{50} nM	GI_{50} nM	I_{max} %	Hill slope	n
PI3Ki	LY	36,190	38,019	100	-1.2	2	17,650	18,967	100	-1.1	2
	Buparlisib	3,166	3,592	92	-1.3	4	1,638	1,675	96	-3.4	2
	Dactolisib	165	409	75	-0.7	2	18	20	92	-1.3	2
MEKi	Selumetinib	62,510	64,863	65	-0.8	2	13,880	18,072	91	-0.7	1
	PD01	41,900	29,854	54	-0.3	3	950	1,179	98	-0.6	3
	Trametinib	2,389	2,716	66	-0.4	2	45	56	97	-0.4	1
mTORi	Temsirolimus	82,650	NA	43	-0.5	3	12,660	12,106	63	-0.3	2

		TR					TRP				
Class	Drug	IC_{50} nM	GI_{50} nM	I_{max} %	Hill slope	n	IC_{50} nM	GI_{50} nM	I_{max} %	Hill slope	n
PI3Ki	LY	7,756	7,962	100	-1.1	2	23,030	23,121	100	-1.6	4
	Buparlisib	1,206	1,237	97	-2.6	4	1,273	1,299	97	-3.4	6
	Dactolisib	31	38	88	-1.3	2	11	12	95	-1.0	3
MEKi	Selumetinib	66,250	71,945	65	-1.2	2	7,838	9,451	85	-0.5	6
	PD01	31,920	4,271	90	-0.4	3	478	605	94	-0.5	4
	Trametinib	580	744	77	-0.4	2	20	57	78	-0.6	3
mTORi	Temsirolimus	55,330	28,973	64	-0.3	3	1,372	2,130	85	-0.33	4

Figure S4.2. ***In vitro* efficacy of PI3Ki, MEKi, and mTORi in T(RP) astrocytes**. Summary of data from **Figures 4.2**, **4.4**, and **S4.3.** N represents replicate biologic experiments.

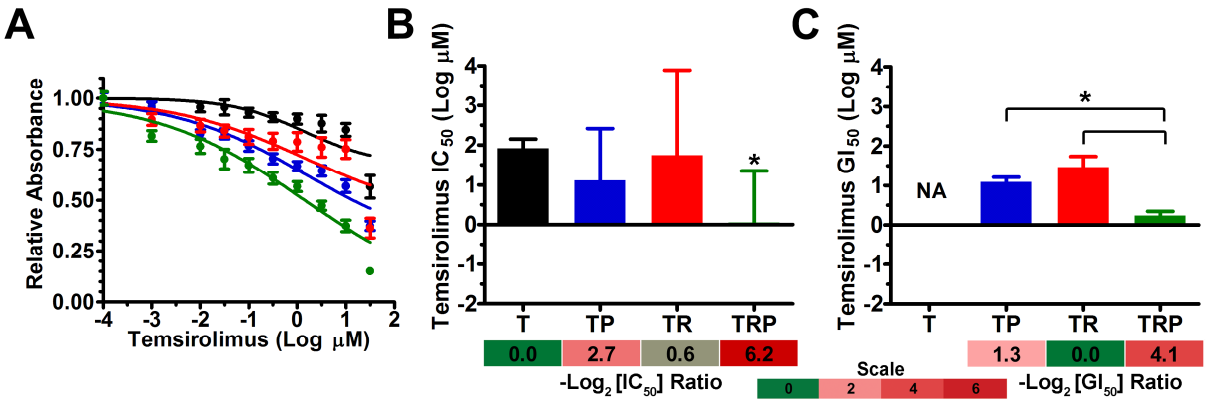

Figure S4.3. **mTORi sensitivity is increased in triple mutant TRP astrocytes**.

Temsirolimus reduced growth of the T(RP) astrocyte series ($R^2 \geq 0.74$) (**A**). Only triple mutant TRP astrocytes had a significantly lower IC_{50} compared to T astrocytes (*, P=0.02) (**B**). TRP also had a significantly lower GI_{50} compared to TP and TR astrocytes (*, P≤0.0003) (**C**). GI_{50} of temsirolimus could not be calculated in T astrocytes (NA, not applicable). IC_{50} fold decreases for the T(RP) astrocyte series relative to T astrocytes and GI_{50} fold decreases for T(RP) relative to TR astrocytes are shown as heatmaps.

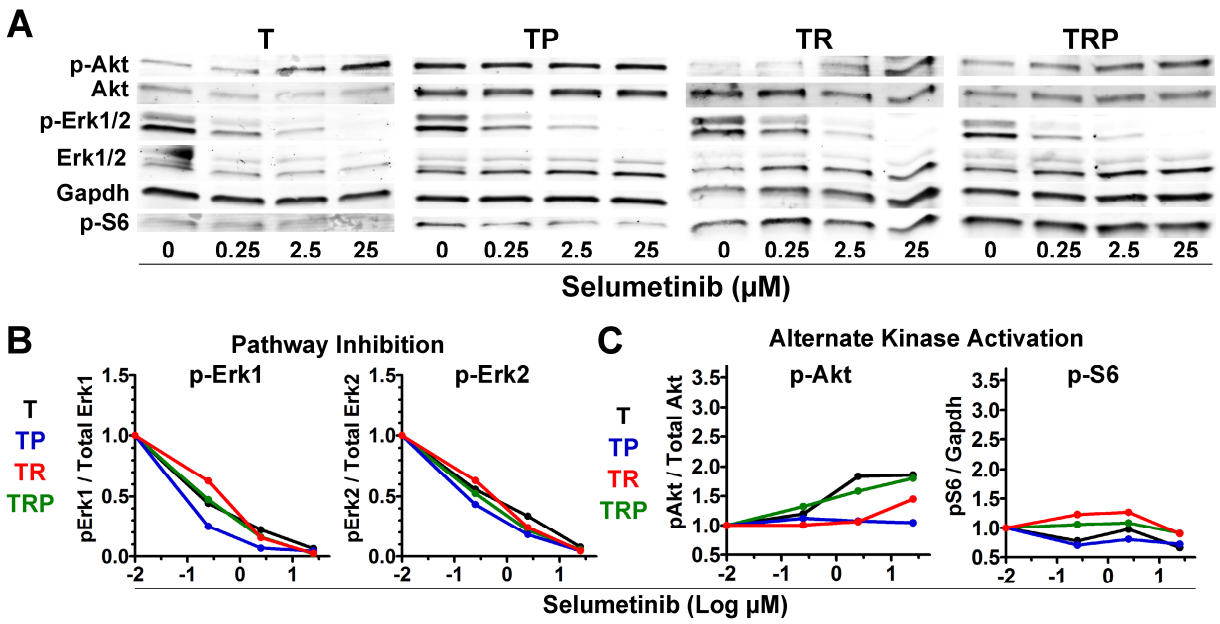

Figure S4.4. **MEKi ablates MAPK signaling and induces alternate activation of proximal PI3K signaling**. Immunoblots (**A**) performed on the T(RP) astrocyte series 4 h after selumetinib treatment showed dose-dependent decreases in MAPK signaling in all four T(RP) genotypes (**B**) and modest alternate activation of proximal, but not distal PI3K signaling in T, TR, and TRP astrocytes (**C**). These results, in combination with those in **Fig 4.3**, demonstrated that alternate activation of PI3K begins shortly after treatment (within 4 h) and increases over time (24 h).

REFERENCES

1. Louis DN, Perry A, Reifenberger G, et al. The 2016 World Health Organization classification of tumors of the central nervous system: a summary. *Acta Neuropathol.* 2016;131(6):803-820.

2. Cancer Genome Atlas Research Network, Brat DJ, Verhaak RG, et al. Comprehensive, integrative genomic analysis of diffuse lower-grade gliomas. *N Engl J Med.* 2015;372(26):2481-2498.

3. Brennan CW, Verhaak RG, McKenna A, et al. The somatic genomic landscape of glioblastoma. *Cell.* 2013;155(2):462-477.

4. Louis DN, Ohgaki H, Wiestler OD, Cavenee WK, eds. *WHO classification of tumours of the central nervous system.* 4th ed. Lyon: IARC; 2007. WHO Classification of Tumours.

5. Miller CR, Perry A. Glioblastoma. *Arch Pathol Lab Med.* 2007;131(3):397-406.

6. Stupp R, Mason WP, van den Bent MJ, et al. Radiotherapy plus concomitant and adjuvant temozolomide for glioblastoma. *N Engl J Med.* 2005;352(10):987-996.

7. Verhaak RG, Hoadley KA, Purdom E, et al. Integrated genomic analysis identifies clinically relevant subtypes of glioblastoma characterized by abnormalities in PDGFRA, IDH1, EGFR, and NF1. *Cancer Cell.* 2010;17(1):98-110.

8. Thorpe LM, Yuzugullu H, Zhao JJ. PI3K in cancer: divergent roles of isoforms, modes of activation and therapeutic targeting. *Nat Rev Cancer.* 2015;15(1):7-24.

9. Guha A, Feldkamp MM, Lau N, Boss G, Pawson A. Proliferation of human malignant astrocytomas is dependent on Ras activation. *Oncogene.* 1997;15(23):2755-2765.

10. Jeuken J, van den Broecke C, Gijsen S, Boots-Sprenger S, Wesseling P. RAS/RAF pathway activation in gliomas: the result of copy number gains rather than activating mutations. *Acta Neuropathol.* 2007;114(2):121-133.

11. Dienstmann R, Rodon J, Serra V, Tabernero J. Picking the point of inhibition: a comparative review of PI3K/AKT/mTOR pathway inhibitors. *Mol Cancer Ther.* 2014;13(5):1021-1031.

12. Roberts PJ, Der CJ. Targeting the Raf-MEK-ERK mitogen-activated protein kinase cascade for the treatment of cancer. *Oncogene.* 2007;26(22):3291-3310.

13. Hanahan D, Weinberg RA. Hallmarks of cancer: the next generation. *Cell.* 2011;144(5):646-674.

14. Yoon S, Seger R. The extracellular signal-regulated kinase: multiple substrates regulate diverse cellular functions. *Growth Factors.* 2006;24(1):21-44.

15. Cloughesy TF, Cavenee WK, Mischel PS. Glioblastoma: from molecular pathology to targeted treatment. *Annu Rev Pathol.* 2014;9:1-25.

16. McNeill RS, Vitucci M, Wu J, Miller CR. Contemporary murine models in preclinical astrocytoma drug development. *Neuro Oncol.* 2015;17(1):12-28.

17. Prados MD, Byron SA, Tran NL, et al. Toward precision medicine in glioblastoma: the promise and the challenges. *Neuro Oncol.* 2015;17(8):1051-1063.

18. Akhavan D, Cloughesy TF, Mischel PS. mTOR signaling in glioblastoma: lessons learned from bench to bedside. *Neuro Oncol.* 2010;12(8):882-889.

19. Schmid RS, Simon JM, Vitucci M, et al. Core pathway mutations induce de-differentiation of murine astrocytes into glioblastoma stem cells that are sensitive to radiation but resistant to temozolomide. *Neuro Oncol.* 2016;18(7):962-973.

20. Uhrbom L, Dai C, Celestino JC, Rosenblum MK, Fuller GN, Holland EC. Ink4a-Arf loss cooperates with KRas activation in astrocytes and neural progenitors to generate glioblastomas of various morphologies depending on activated Akt. *Cancer Res.* 2002;62(19):5551-5558.

21. Sonoda Y, Ozawa T, Aldape KD, Deen DF, Berger MS, Pieper RO. Akt pathway activation converts anaplastic astrocytoma to glioblastoma multiforme in a human astrocyte model of glioma. *Cancer Res.* 2001;61(18):6674-6678.

22. Chow LM, Endersby R, Zhu X, et al. Cooperativity within and among Pten, p53, and Rb pathways induces high-grade astrocytoma in adult brain. *Cancer Cell.* 2011;19(3):305-316.

23. Vitucci M, Karpinich NO, Bash RE, et al. Cooperativity between MAPK and PI3K signaling activation is required for glioblastoma pathogenesis. *Neuro Oncol.* 2013;15(10):1317-1329.

24. McNeill RS, Canoutas DA, Stuhlmiller TJ, et al. Combination therapy with potent PI3K and MAPK inhibitors overcomes adaptive kinome resistance to single agents in preclinical models of glioblastoma. *Neuro Oncol.* 2017. doi:10.1093/neuonc/nox044.

25. McNeill RS, Schmid RS, Bash RE, et al. Modeling astrocytoma pathogenesis in vitro and in vivo using cortical astrocytes or neural stem cells from conditional, genetically engineered mice. *J Vis Exp.* 2014(90):e51763.

26. Jackson EL, Willis N, Mercer K, et al. Analysis of lung tumor initiation and progression using conditional expression of oncogenic K-ras. *Genes Dev.* 2001;15(24):3243-3248.

27. Xiao A, Wu H, Pandolfi PP, Louis DN, Van Dyke T. Astrocyte inactivation of the pRb pathway predisposes mice to malignant astrocytoma development that is accelerated by PTEN mutation. *Cancer Cell.* 2002;1(2):157-168.

28. Xiao A, Yin C, Yang C, Di Cristofano A, Pandolfi PP, Van Dyke T. Somatic induction of Pten loss in a preclinical astrocytoma model reveals major roles in disease progression and avenues for target discovery and validation. *Cancer Res.* 2005;65(12):5172-5180.

29. Reinhold WC, Sunshine M, Liu H, et al. CellMiner: a web-based suite of genomic and pharmacologic tools to explore transcript and drug patterns in the NCI-60 cell line set. *Cancer Res.* 2012;72(14):3499-3511.

30. Pawaskar DK, Straubinger RM, Fetterly GJ, Ma WW, Jusko WJ. Interactions of everolimus and sorafenib in pancreatic cancer cells. *AAPS J.* 2013;15(1):78-84.

31. Chou TC. Drug combination studies and their synergy quantification using the Chou-Talalay method. *Cancer Res.* 2010;70(2):440-446.

32. Huszthy PC, Daphu I, Niclou SP, et al. In vivo models of primary brain tumors: pitfalls and perspectives. *Neuro Oncol.* 2012;14(8):979-993.

33. Schmid RS, Vitucci M, Miller CR. Genetically engineered mouse models of diffuse gliomas. *Brain Res Bull.* 2012;88(1):72-79.

34. See WL, Tan IL, Mukherjee J, Nicolaides T, Pieper RO. Sensitivity of glioblastomas to clinically available MEK inhibitors is defined by neurofibromin 1 deficiency. *Cancer Res.* 2012;72(13):3350-3359.

35. Turke AB, Song Y, Costa C, et al. MEK inhibition leads to PI3K/AKT activation by relieving a negative feedback on ERBB receptors. *Cancer Res.* 2012;72(13):3228-3237.

36. Hoeflich KP, O'Brien C, Boyd Z, et al. In vivo antitumor activity of MEK and phosphatidylinositol 3-kinase inhibitors in basal-like breast cancer models. *Clin Cancer Res.* 2009;15(14):4649-4664.

37. Sunayama J, Matsuda K, Sato A, et al. Crosstalk between the PI3K/mTOR and MEK/ERK pathways involved in the maintenance of self-renewal and tumorigenicity of glioblastoma stem-like cells. *Stem Cells.* 2010;28(11):1930-1939.

38. Yoshida T, Kakegawa J, Yamaguchi T, et al. Identification and characterization of a novel chemotype MEK inhibitor able to alter the phosphorylation state of MEK1/2. *Oncotarget.* 2012;3(12):1533-1545.

39. Yeh TC, Marsh V, Bernat BA, et al. Biological characterization of ARRY-142886 (AZD6244), a potent, highly selective mitogen-activated protein kinase kinase 1/2 inhibitor. *Clin Cancer Res.* 2007;13(5):1576-1583.

40. Sebolt-Leopold JS, Merriman R, Omer C, et al. The biological profile of PD 0325901: A second generation analog of CI-1040 with improved pharmaceutical potential [abstract]. *Cancer Research.* 2004;64(7 Supplement):925.

41. Cancer Genome Atlas Research Network. Comprehensive genomic characterization defines human glioblastoma genes and core pathways. *Nature.* 2008;455(7216):1061-1068.

42. Koul D, Fu J, Shen R, et al. Antitumor activity of NVP-BKM120--a selective pan class I PI3 kinase inhibitor showed differential forms of cell death based on p53 status of glioma cells. *Clin Cancer Res.* 2012;18(1):184-195.

43. Yang L, Clarke MJ, Carlson BL, et al. PTEN loss does not predict for response to RAD001 (Everolimus) in a glioblastoma orthotopic xenograft test panel. *Clin Cancer Res.* 2008;14(12):3993-4001.

44. Sharpless NE, Depinho RA. The mighty mouse: genetically engineered mouse models in cancer drug development. *Nat Rev Drug Discov.* 2006;5(9):741-754.

45. Herter-Sprie GS, Kung AL, Wong KK. New cast for a new era: preclinical cancer drug development revisited. *J Clin Invest.* 2013;123(9):3639-3645.

46. Meric-Bernstam F, Akcakanat A, Chen H, et al. PIK3CA/PTEN mutations and Akt activation as markers of sensitivity to allosteric mTOR inhibitors. *Clin Cancer Res.* 2012;18(6):1777-1789.

47. Weigelt B, Warne PH, Downward J. PIK3CA mutation, but not PTEN loss of function, determines the sensitivity of breast cancer cells to mTOR inhibitory drugs. *Oncogene.* 2011;30(29):3222-3233.

48. Seront E, Pinto A, Bouzin C, Bertrand L, Machiels JP, Feron O. PTEN deficiency is associated with reduced sensitivity to mTOR inhibitor in human bladder cancer through the unhampered feedback loop driving PI3K/Akt activation. *Br J Cancer.* 2013;109(6):1586-1592.

49. Luchman HA, Stechishin OD, Nguyen SA, Lun XQ, Cairncross JG, Weiss S. Dual mTORC1/2 blockade inhibits glioblastoma brain tumor initiating cells in vitro and in vivo and synergizes with temozolomide to increase orthotopic xenograft survival. *Clin Cancer Res.* 2014;20(22):5756-5767.

50. Spoerke JM, O'Brien C, Huw L, et al. Phosphoinositide 3-kinase (PI3K) pathway alterations are associated with histologic subtypes and are predictive of sensitivity to PI3K inhibitors in lung cancer preclinical models. *Clin Cancer Res.* 2012;18(24):6771-6783.

51. Sangai T, Akcakanat A, Chen H, et al. Biomarkers of response to Akt inhibitor MK-2206 in breast cancer. *Clin Cancer Res.* 2012;18(20):5816-5828.

52. Ebbesen SH, Scaltriti M, Bialucha CU, et al. Pten loss promotes MAPK pathway dependency in HER2/neu breast carcinomas. *Proc Natl Acad Sci U S A.* 2016;113(11):3030-3035.

53. Mendoza MC, Er EE, Blenis J. The Ras-ERK and PI3K-mTOR pathways: cross-talk and compensation. *Trends Biochem Sci.* 2011;36(6):320-328.

54. El Meskini R, Iacovelli AJ, Kulaga A, et al. A preclinical orthotopic model for glioblastoma recapitulates key features of human tumors and demonstrates sensitivity to a combination of MEK and PI3K pathway inhibitors. *Dis Model Mech.* 2015;8(1):45-56.

CHAPTER V: *PIK3CA* MISSENSE MUTATIONS PROMOTE GLIOBLASTOMA PATHOGENESIS, BUT DO NOT ENHANCE PI3K INHIBITOR EFFICACY

Introduction

Glioblastoma (GBM) is the most common malignant primary brain tumor in adults. It is also the most aggressive, with a median survival of only 12-15 months.[1-3] The molecular heterogeneity of GBM has been extensively characterized in order to better understand the biology of this devastating disease.[4-6] The vast majority of GBM arise *de novo* and harbor frequent mutations in three "core" signaling pathways: RB, TP53, and receptor tyrosine kinase (RTK)/mitogen activated protein kinase (MAPK)/phosphoinositide 3-kinase (PI3K). GBM can be stratified into four molecular subtypes based on gene expression. However, this knowledge has yet to impact GBM standard-of-care. First line therapy consists of surgical resection followed by radiation with concurrent and adjuvant temozolomide, a DNA damaging chemotherapeutic.[3] Clinical investigations of inhibitors targeting the pathways frequently mutated in GBM have had disappointing results for a variety of reasons, including drug resistance and inclusion of genetically heterogeneous patients.[7,8] Preclinical modeling can aid in the development of novel therapies by defining whether mutations associated with GBM drive disease pathogenesis and are predictive of drug response.

The PI3K pathway promotes many cancer hallmarks, including survival, proliferation, and migration.[9-11] PI3K is a heterodimeric lipid kinase composed of a

catalytic and regulatory subunit encoded by genes such as *PIK3CA* and *PIK3R1* respectively.[12] Pathway activation is mediated by the conversion of PIP_2 to PIP_3 by the catalytic subunit of PI3K, resulting in recruitment and activation of effector proteins, including AKT. PI3K signaling is antagonized by the tumor suppressor *PTEN*.[12] PI3K signaling is an attractive therapeutic target in GBM because mutually exclusive mutations in *PIK3CA*, *PIK3R1*, and *PTEN* occur in 46% of pateints.[13-15]

Activation of PI3K signaling via *Pten* deletion, *PIK3R1* mutations, or constitutively active *AKT* promotes tumorigenesis in multiple preclinical GBM models.[16-21] For example, we found that *Pten* deletion cooperates with mutant *Kras* in immortalized mouse astrocytes to activate PI3K signaling and potentiate malignant progression.[17,22] Similarly, in cultured normal human astrocytes that were immortalized by expression of the HPV oncogenes E6 and E7 to inhibit the TP53 and RB pathways respectively, and by expression of hTERT to maintain telomere length (NHA), constitutively active *AKT* cooperated with mutant *RAS* (NHA^{RAS}) to promote gliomagenesis.[20,23] However, the role of *PIK3CA* mutations in gliomagenesis has not been experimentally investigated.

PIK3CA is altered in 10% of GBM, mostly via missense mutations.[4,13,14] These missense mutations are generally restricted to three of its functional protein domains (adaptor binding (ABD), helical, and kinase) and are predicted to activate PI3K signaling via distinct mechanisms.[24] Some *PIK3CA* missense mutations that occur in GBM promote tumorigenesis in non-brain tissues, particularly the most prevalent E542K and E545K helical mutations, and H1047R kinase mutation.[25-27] However, their role in gliomagenesis has yet to be determined. Here we used NHA with and without mutant *RAS* to define the role of *PIK3CA* missense mutations in GBM pathogenesis.

Furthermore, we determined if *PIK3CA* missense mutations influenced response to single agent and combination treatments with PI3K/MEK inhibitors in order to elucidate the utility of *PIK3CA* mutation status as a predictive biomarker.

Materials and Methods

***PIK3CA* mutagenesis**. Third generation lentiviral gateway destination vector (pLenti-PGK-Hygro-DEST, #19066), pENTR4 vector (pENTR4-no-ccDB, #17424), hemagglutinin (HA)-tagged wild-type (WT) *PIK3CA* (*PIK3CA*^{WT}, pBabe-puro-HAPIK3CA, #12522), and HA-tagged *GFP* (GFP, pDEST-Flag-HA-GFP, #22612) plasmids were purchased from Addgene (Cambridge, MA). *PIK3CA*^{WT} was excised from the pBabe backbone by sequential restriction digests with SalI and BamHI (New England BioLabs, Ipswich, MA). The pENTR4 vector was digested with BamHI and EcoRV, then *PIK3CA*^{WT} was inserted into this vector by ligation. Alternatively, both pDEST-Flag-HA-GFP and pENTR4 vectors were digested with NcoI and EcoRI (New England BioLabs) followed by insertion of *GFP* into the pENTR4 vector by ligation. Six *PIK3CA* missense mutations (*PIK3CA*^{mut}: R88Q, C90Y, E542K, E545K, M1043V, or H1047R) were generated by point mutagenesis of *PIK3CA*^{WT} within the pENTR4 vector using the Q5 Site-Directed Mutagenesis Kit (New England Biolabs) according to manufacturer's instructions. *GFP*, *PIK3CA*^{WT}, and the *PIK3CA*^{mut} genes were transferred from their pENTR4 vectors to pLenti-PGK-Hygro-DEST vectors by recombination as previously described.[28] Subsequent point mutagenesis of *PIK3CA*^{WT}- and *PIK3CA*^{mut}-pLenti-PGK-Hygro-DEST vectors were performed using the Q5 Site-Directed Mutagenesis Kit to substitute an adenine to a guanine within an upstream ATG start codon in the NcoI restriction site from the pENTR4 vector. All point mutations were confirmed by Sanger sequencing (Genewiz, South Plainfield, NJ).

Lentivirus production. Lentiviral particles encoding *GFP*, *PIK3CA*^{WT}, or individual *PIK3CA*^{mut} were generated using 293FT cells (Invitrogen, Grand Island, NY) according to manufacturer's instructions. Briefly, 5 x 10^5 cells were plated on 10 cm tissue culture plates in Dulbecco's Modified Eagle's Medium (DMEM) supplemented with 10% FBS, 1% Penn/Strep, 2 mM GlutaMAX (Invitrogen), 0.1 mM MEM Non-Essential Amino Acids (Invitrogen), and 1 mM sodium pyruvate (Invitrogen) (293FT media). The next day medium was replaced with fresh 293FT medium without penicillin/streptomycin, and 9 µg *GFP*-, *PIK3CA*^{wt}-, or *PIK3CA*^{mut}-pDEST, plus 9 µg pMDL/pRRE (Addgene, #12251), 3.6 µg pRSV-Rev (Addgene, #12253), and 1.89 µg pMD2.G (Addgene, #12259) plasmids were transfected into these cells using Lipofectamine 2000 (Invitrogen) according to the manufacturer's instructions. Medium was exchanged for new 293FT medium supplemented with 1 M HEPES (Invitrogen) after 24 hours. Supernatants containing lentiviruses were collected and fresh 293FT medium supplemented with 1M HEPES was added to cells 48 h and 72 h post-transfection. Viral supernatants from each time point were filtered through a 45 µm PES filter, and stored at 4 ºC until all time points could be pooled, aliquoted, and stored at -80 ºC.

Cell culture. NHA and NHA^{RAS} lines were a kind gift from Dr. Russell O. Pieper.[9] All cells were maintained as adherent cultures at 37 ºC and 5% CO_2 in DMEM supplemented with 5% FBS and 1% penicillin/streptomycin (complete DMEM). All *in vitro* experiments were performed in DMEM supplemented with 2.5% FBS and 1% penicillin/streptomycin (low serum medium) unless otherwise stated. To create NHA and NHA^{RAS} lines expressing GFP, *PIK3CA*^{WT}, or *PIK3CA*^{mut}, 135,000 and 120,000 cells respectively were plated on 60 cm^2 tissue culture plates. Lentiviral vectors were

added two days after plating, and then incubated with the cells overnight in complete DMEM containing 8 μg/ml polybrene (Sigma-Aldrich, St. Louis, MO) at 37ºC and 5% CO_2. Two days post-infection, transduced cells were selected by culture in complete DMEM supplemented with 300 μg/ml hygromycin B (Gold Biotechnology, St. Louis, MO) for 14 days. Stable gene expression was confirmed by immunoblot for the HA tag on *PIK3CA*^{wt} and *PIK3CA*^{mut}.

Drugs. The PI3K inhibitor (PI3Ki) buparlisib (BKM120) and the MEK inhibitor (MEKi) selumetinib (AZD6244) were purchased from MedChem Express and Chemietek (Indianapolis, IN) and dissolved in dimethyl sulfoxide (DMSO).

Immunoblots. Control (parental, GFP, and *PIK3CA*^{WT}) and *PIK3CA*^{mut} NHA and NHA^{RAS} were plated on 60 or 100 cm^2 tissue culture plates. At ~60% confluence, cells were washed with Hank's Balance Salt Solution (HBSS), then serum-starved in DMEM supplemented with 0.5% FBS and 1% penicillin/streptomycin. Alternatively, cells were washed with HBSS, low serum medium was added, and then cells were treated with vehicle control (DMSO), buparlisib, or selumetinib. Twenty-four h after serum starvation or drug treatment, cells were mechanically harvested and snap frozen. Cell pellets were lysed, and protein concentration was quantified using Pierce BCA Protein Assay Kit (Thermo Scientific, Waltham, MA) according to manufacturer's instructions. Immunoblots were performed as previously described.[22] Briefly, protein samples (20 μg) were separated by gradient (4-15% or 8-16%) gel electrophoresis (SDS-PAGE, Bio-Rad, Hercules, CA) and transferred to PDVF membranes (EMD Millipore Corp, Billerica, MA). Membranes were probed with primary antibodies against GAPDH (EMD Millipore Corp, Billerica, MA, MAB374), AKT (#2920S), phospho (p)AKT (Ser473, #4060), pS6

(Ser240/244, #2215), ERK1/2 (#4696), or pERK1/2 (Thr202/Tyr204, #4370) all from Cell Signaling Technology (Danvers, MA). Blots were then probed with species specific Alexa 488, 555, or 647 conjugated secondary antibodies (Life Technologies, Grand Island, NY) and imaged on a Typhoon Trio (GE Healthcare, Pittsburgh, PA). Alternatively, membranes were probed with an anti-HA-peroxidase antibody (Roche Applied Science, Penzberg, Germany, #12013819001) and imaged using enhanced chemiluminescence (Clarity Western ECL Substrate, Bio-Rad) on an Image Quant LAS 4000 (GE Healthcare). Band intensities were quantified using ImageJ (NIH, Bethesda, MD). Phospho-proteins were normalized to their respective total protein or GAPDH. Normalized band intensities from serum-starved immunoblots were set relative to an external standard and then normalized to parental and *PIK3CA*^{WT} cells. Normalized band intensities from drug-treated samples were set relative to vehicle control cells. Differences between groups were determined by one-way ANOVA. Pairwise comparisons were performed by unpaired t-tests.

Cell growth. NHA and NHA^{RAS} lines were plated in triplicate or quadruplicate in 96-well tissue culture plates at 1000 cells/well and 675 cells/well respectively. Changes in absorbance (cell growth) was assessed using CellTiter 96 Aqueous One Solution Cell Proliferation Assay (MTS, Promega, Madison, WI) according to manufacturer's instructions. Briefly, absorbance at 490 nm was measured daily for 4-5 days using an Emax 96-well plate reader (Molecular Devices, Chicago, IL) equipped with SoftMax Pro 5 software. Absorbance of experimental samples were subtracted by baseline absorbance (low serum media + MTS), then set relative to day 0. Data (mean ± SEM) from 2-4 independent experiments (mean=3) were fit to an exponential growth equation

and the rate constant k and doubling time [ln(2)/k] were calculated. Differences in growth rates (k) were compared using the extra-sum-of-squares F test.

Cell migration. Migration rate across a cell-free gap was determined using culture inserts (Ibidi, Munich, Germany) according to manufacturer's instructions. Briefly, inserts were attached to individual wells of a 6-well tissue culture plate. Twenty-six thousand cells were seeded into each well of the insert and allowed to adhere overnight. The following morning inserts were lifted to create a cell free gap that was imaged at 3 non-overlapping locations every 2 hours for 12 hours using a VistaVision inverted microscope (Model #82026-630, VWR, Radnor, PA) equipped with a DV-300 digital camera. The area of the gap between the cell fronts was analyzed using ImageJ (NIH). Gap area was normalized to time 0 at each image location, and data from hours 2-12 were fit to a linear regression equation to calculate and compare rates of gap closure.

Colony formation in soft agar. Colony formation was determined in 6-well tissue cultured treated plates as previously described with minor modifications.[23,29] Briefly, a base layer of a low serum DMEM/0.5% low melting temperature agarose (Denville Scientific INC., Holliston, MA) mixture was added to each well and allowed to solidify. Cells were harvested by trypsinization, placed in a mixture of low serum DMEM/0.35% low melting temperature agarose, and plated (14,000 per well) in duplicate or triplicate. Cells were maintained at 37 ºC and 5% CO_2 for 4 weeks, then fixed and stained with 0.005% crystal violet in 70% ethanol for ≥1 hr. Wells were washed with PBS, and colonies were imaged on a Typhoon Trio (GE Healthcare). Colonies ≥ 30 μm^2 were automatically counted using ImageJ (NIH). Mean (± SEM) colonies per well was

calculated from 2 independent experiments and data were compared using unpaired t-tests.

Orthotopic xenografts. Control and *PIK3CA*^{mut} NHA^{RAS} lines were harvested by trypsinization, counted, and suspended in serum free DMEM with 5% methyl cellulose. Adult athymic nude mice (mean ~3 months) were anesthetized with Avertin (250 mg/kg) and 2 x 10^5 GFP, *PIK3CA*^{WT}, *PIK3CA*^{R88Q}, *PIK3CA*^{E542K}, or *PIK3CA*^{H1047R} NHA^{RAS} cells were injected the right basal ganglia of mice (N=5-10 per group, mean=9) using the coordinates 1, -2, and -4 mm (A, L, D) from bregma as previously described.[22] Animals were monitored for the onset of neurological symptoms and were then sacrificed. Survival was determined by Kaplan-Meier analyses and was compared by log-rank tests. The UNC Institutional Animal Care and Use Committee approved all animal studies (protocol # 16-112).

Drug response. Dose response assays were performed as previously described.[22] Briefly, cells were plated in triplicate in 96-well plates and maintained at 37˚C and 5% CO_2. The following day they were treated with vehicle control (DMSO) or increasing concentrations of buparlisib and/or selumetinib. Effects of drugs on cell growth was determined with CellTiter 96 Aqueous One Solution Cell Proliferation Assay (MTS, Promega) according to manufacturer's instructions. Briefly, absorbance at 490 nm was measured 5 days post-treatment as described above. Absorbance of experimental wells was subtracted by baseline absorbance and then set relative to vehicle control. Data (mean ± SEM) were pooled from 2-4 (mean=3) independent experiments and fit to a non-linear, log [inhibitor] versus response curves with variable slopes, and IC_{50} were calculated. Differences in IC_{50} were compared using the extra-sum-of-squares F test.

Synergism between MEKi and PI3Ki was determined by the BLISS method in Combenefit v1.31.[30]

Cell cycle. Control and *PIK3CA*^{mut} NHA^{RAS} were plated in 12-well tissue culture plates, and were treated with buparlisib or vehicle control the following day. Cell cycle analysis was performed 2 days post-treatment on a Guava EasyCyte Plus using Guava Cell Cycle Reagent according to the manufacturer's instructions (EMD Millipore, Billerica, MA). Cell cycle distribution was determined using ModFit LT v3.2 (Verity, Topsham, ME). Percent cells in G_0/G_1, S, and G_2/M were calculated from one experiment.

Statistics. Statistical analyses were performed in GraphPad Prism (La Jolla, CA) unless otherwise stated. $P \leq 0.05$ were considered significant. Error bars are SEM unless otherwise stated.

Results

PIK3CA missense mutations frequently occur in GBM and are heterogeneously distributed across multiple of the encoded protein domains, particularly the ABD, helical, and kinase domains (**Fig S5.1A**).[13,14] *PTEN* deletion or activating AKT mutations, cooperate with activated MAPK signaling to promote tumorigenesis in preclinical glioma models.[17,20] However, the role of *PIK3CA* mutations in gliomagenesis has not been experimentally determined. To this end, we selected the missense mutations that most frequently occur in the helical (E542K and E545K) and kinase (M1043V and H1047R) domains of *PIK3CA* in GBM, as well as other cancer types (**Fig S5.1A-C**). Individual missense mutations in the ABD of *PIK3CA* are less prevalent in most cancers than the hotspot helical (E542K and E545K) and kinase (H1047R) domain mutations. R88Q is generally the most common ABD mutation in *PIK3CA*-mutated cancers, and it is the only recurrent ABD mutation in GBM. We therefore selected R88Q as well as one other ABD (C90Y) mutation to evaluate here. We transduced NHA and NHA^{RAS} with lentiviral vectors encoding each individual *PIK3CA^{mut}*. Parental lines and those transduced with either GFP or *PIK3CA^{WT}* were used as controls. We then used these cells to define the role of *PIK3CA* missense mutations in both tumorigenesis and response to kinase inhibitors.

PIK3CA^{mut} increase PI3K signaling *in vitro*

Immunoblots showed that *PIK3CA^{WT}* and all *PIK3CA^{mut}* were expressed at similar levels in NHA and NHA^{RAS} (**Fig S5.2**), suggesting that any phenotypic differences are a consequence of the *PIK3CA* missense mutation. Next, we performed immunoblots to determine whether these mutations activate PI3K signaling in serum-

starved NHA. Neither *PIK3CA*^{WT} nor ABD *PIK3CA*^{mut} significantly increased activation of proximal (pAKT) or distal (pS6) PI3K signaling (**Fig 5.1A-C**). In contrast, helical and kinase *PIK3CA*^{mut} induced proximal and distal PI3K signaling compared to parental and *PIK3CA*^{WT} NHA respectively. Moreover, E542K and H1047R *PIK3CA*^{mut} increased proximal PI3K signaling more than *PIK3CA*^{WT}.

We previously found that mutant *Kras* cooperated with *Pten* deletion to activate PI3K signaling in immortalized mouse astrocytes.[17] We therefore determined the effects of *PIK3CA*^{mut} on PI3K signaling in NHA^{RAS} via immunoblots. *PIK3CA*^{WT} and all *PIK3CA*^{mut} increased proximal PI3K signaling compared to parental NHA^{RAS} (**Fig 5.1DE**). Furthermore, helical and kinase *PIK3CA*^{mut} potentiated proximal PI3K signaling more than *PIK3CA*^{WT}. However, distal PI3K signaling was only increased by the M1043V *PIK3CA*^{mut} in NHA^{RAS} (**Fig 5.1DF**). Taken together, these results suggest that mutant *RAS* cooperated with ectopic expression of both *PIK3CA*^{WT} and *PIK3CA*^{mut} to increase proximal PI3K signaling.

There is extensive cross-talk between the PI3K and MAPK pathways.[31] We therefore determined the effects of the *PIK3CA*^{mut} on MAPK signaling. Neither *PIK3CA*^{WT} nor any of the *PIK3CA*^{mut} significantly altered MAPK (pERK1/2) signaling in NHA and NHA^{RAS} (**Fig S5.3**). Thus, *PIK3CA* missense mutations activated PI3K signaling, without affecting the MAPK pathway.

PIK3CA^{mut} increase NHA proliferation *in vitro*

PIK3CA^{mut}, particularly those in the helical and kinase domains, activated PI3K signaling, suggesting that they may also promote cell growth (**Fig 5.1**). MTS assays at high-serum concentrations (10% FBS) showed that *PIK3CA*^{WT} and a subset of

PIK3CA^{mut} increased proliferation of NHA (**Fig S5.4**). However, these changes were relatively minor (≤15%), and all lines were rapidly proliferating with doubling times ≤1 day. We therefore hypothesized that the growth factor concentration within the high-serum media was masking the effects of the *PIK3CA*^{mut} on NHA growth. We therefore performed MTS assays in low-serum medium (2.5% FBS) in order to reduce the concentration of mitogenic growth factors. Proliferation was increased in both GFP and *PIK3CA*^{WT} NHA compared to parental cells (**Figs 5.2A**, **S5.5A**), indicating that lentiviral transduction and antibiotic selection caused enrichment for a more proliferative subset of cells. Moreover, all *PIK3CA*^{mut}, except C90Y, increased proliferation compared to parental and *PIK3CA*^{WT} NHA. In contrast, proliferation rates were similar in NHA^{RAS} lines, regardless of *PIK3CA*^{mut} status (**Figs 5.2B**, **S5.5B**). Taken together, these data suggest that *PIK3CA* missense mutations promote astrocyte growth in the absence of mutant *RAS*.

PIK3CA* mutations increase migration *in vitro

Complete surgical resection of GBM is precluded by its diffuse infiltration of the brain.[32] The PI3K pathway has an established role in migration.[33] Indeed, we previously showed that *Pten* deletion increased migration of immortalized mouse astrocytes.[17] We therefore determined the effects of *PIK3CA*^{mut} on migration using a gap closure assay *in vitro*. GFP, *PIK3CA*^{WT} and all *PIK3CA*^{mut} increased migration compared to parental NHA (**Figs 5.2C**, **S5.5C**). These increases were greater in *PIK3CA*^{WT} and all *PIK3CA*^{mut}, except C90Y, than GFP NHA (P≤0.04). Similarly, all *PIK3CA*^{mut}, except C90Y, increased migration compared to GFP and parental NHA^{RAS}

(P≤0.006, **Figs 5.2D**, **S5.5D**). Moreover, E542K and H1047R *PIK3CA*^{mut} increased migration compared to *PIK3CA*^{WT} in NHA and NHA^{RAS} (**Fig 5.2CD**).

***PIK3CA* mutations potentiate tumorigenesis**

Anchorage-independent growth is an established marker of cellular transformation.[23,29] Mutant *RAS* promotes colony formation and tumorigenicity of NHA.[23] To determine whether *PIK3CA*^{mut} also promote anchorage independent growth of NHA, we selected the most potent *PIK3CA*^{mut} per domain based on induction of proximal PI3K signaling, proliferation, and migration (**Figs 5.1**, **5.2**). We then assessed colony formation in soft agar. *PIK3CA*^{WT}, and both R88Q and E542K *PIK3CA*^{mut} did not increase colony formation compared to GFP and parental NHA (**Fig 5.3A**). In contrast, H1047R *PIK3CA*^{mut} increased colony formation of NHA to an extent similar to mutant *RAS*. Because H1047R was the only *PIK3CA*^{mut} to potentiate colony formation of NHA, we also tested whether it potentiated colony formation of NHA^{RAS}. However, no significant differences in colony formation between H1047R *PIK3CA*^{mut} and parental NHA^{RAS} was evident (**Fig 5.3A**).

We next performed orthotopic xenografts of GFP, *PIK3CA*^{WT}, and *PIK3CA*^{mut} NHA^{RAS} lines to determine whether *PIK3CA*^{mut} potentiate tumorigenesis *in vivo*. All xenograft mice eventually succumbed to disease, but *PIK3CA*^{WT} tended to decrease survival (P=0.08), while the R88Q *PIK3CA*^{mut} significantly decreased survival compared to GFP controls (**Fig 5.3BC**). E542K and H1047R *PIK3CA*^{mut} were more potent and resulted in decreased survival compared to GFP, *PIK3CA*^{WT}, and R88Q *PIK3CA*^{mut} NHA^{RAS} (P≤0.0002). Taken together, these results indicate that both the domain

mutated, and the presence of mutant *RAS* influence the role of *PIK3CA*^{mut} in gliomagenesis *in vitro* and *in vivo*.

PI3Ki efficacy is similar regardless of *PIK3CA*^{mut} status

Cancer treatments are transitioning away from broadly cytotoxic chemotherapies towards precision medicine, in which the mutation profiles of patients are utilized to tailor treatment with targeted inhibitors.[8,34] However, successful implementation of precision medicine requires knowing which oncogenic drivers influence response targeted inhibitors. To this end, we determined to effects of *PIK3CA*^{mut} on PI3Ki efficacy *in vitro*. The PI3Ki buparlisib caused dose-dependent decreases in growth of control and *PIK3CA*^{mut} NHA (**Fig S5.6A**), with high nanomolar IC_{50} regardless of *PIK3CA*^{mut} status (**Fig 5.4A**). Similar results were obtained with control and *PIK3CA*^{mut} NHA^{RAS}, except that buparlisib IC_{50} tended to be slightly higher (**Figs 5.4B**, **S5.6BC**). Moreover, buparlisib induced G_2/M cell cycle arrest in NHA^{RAS} lines, regardless of *PIK3CA*^{mut} status (**Fig**. **S5.7**).

PI3Ki treatment ablates PI3K signaling and potentiates MAPK signaling

PIK3CA^{mut} in NHA and NHA^{RAS} did not alter efficacy of PI3Ki *in vitro* (**Fig 5.4AB**). However, they differentially activated PI3K signaling (**Fig 5.1**). We therefore investigated whether *PIK3CA*^{mut} influence PI3Ki-induced changes in PI3K signaling by immunoblots. Buparlisib caused dose-dependent decreases in proximal (**Fig 5.4CD**) and distal (**Fig S5.8**) PI3K signaling in control and *PIK3CA*^{mut} NHA. We and others have shown that PI3K inhibition induces alternate activation of MAPK signaling in preclinical GBM models.[31,35] Immunoblots of NHA lines showed that buparlisib induced

dose-dependent increases in MAPK signaling, regardless of *PIK3CA*^{mut} status (**Fig 5.4CE**).

Mutant *RAS* cooperated with *PIK3CA*^{WT} and *PIK3CA*^{mut} to potentiate activation of proximal PI3K signaling (**Fig 5.1**). We therefore performed immunoblots of buparlisib-treated control and *PIK3CA*^{mut} NHA^{RAS} to determine whether *RAS* status influences PI3Ki-induced changes in PI3K and MAPK signaling. Buparlisib caused PI3K inhibition and dose-dependent increases in MAPK activation in control and *PIK3CA*^{mut} NHA^{RAS} (**Figs 5.4F-H**, **S5.8CD**, **S5.9**). Furthermore, inhibition of proximal PI3K signaling was least pronounced in the helical and kinase *PIK3CA*^{mut} lines at the lowest buparlisib concentration. These results demonstrate that a higher PI3Ki concentration is required to ablate PI3K signaling in the presence of activating *PIK3CA*^{mut} in NHA^{RAS}. Furthermore, they indicate that *PIK3CA*^{mut} status does not influence alternate activation of MAPK signaling.

MEKi efficacy is similar in NHA regardless of *PIK3CA*^{mut}

Because we found that PI3Ki promoted MAPK signaling regardless of *PIK3CA*/*RAS* mutation status, we determined efficacy of the MEKi selumetinib in control and *PIK3CA*^{mut} NHA and NHA^{RAS} lines *in vitro*. Selumetinib caused gradual, dose-dependent decreases in growth (**Fig S5.10AB**). *PIK3CA*^{mut} status did not influence selumetinib IC_{50} in NHA (**Fig 5.5A**). Selumetinib IC_{50} were also similar between parental NHA and NHA^{RAS}. However, *PIK3CA*^{WT} and all *PIK3CA*^{mut} NHA^{RAS}, except C90Y and H1047R, had slightly higher selumetinib IC_{50} than parental cells (**Figs 5.5B**, **S5.10C**). Thus, *PIK3CA* missense mutations and mutant *RAS* had little to no effect on MEKi sensitivity.

PIK3CA^{WT} and *PIK3CA*^{mut} influence MEKi-induced activation of PI3K signaling in NHA^{RAS}

We next performed immunoblots to confirm MAPK inhibition in control and *PIK3CA*^{mut} NHA treated with selumetinib (**Fig 5.5C**). Selumetinib induced dose-dependent decreases in pERK, regardless of *PIK3CA*^{mut} status (**Fig 5.5CD**). We and others have shown that MEKi induced alternate activation of PI3K signaling in preclinical GBM models.[31,36,37] We extended these findings here by demonstrating that selumetinib potentiated proximal PI3K signaling by 1.4-5 fold in control and *PIK3CA*^{mut} NHA (**Fig 5.5CE**). Interestingly, this induction was least pronounced in E542K and H1047R *PIK3CA*^{mut} NHA.

Mutant *RAS* cooperated with *PIK3CA*^{WT} and *PIK3CA*^{mut} to promote activation of proximal PI3K signaling (**Fig 5.1**). We therefore investigated whether *PIK3CA*^{mut} influence MEKi-induced changes in MAPK and PI3K signaling in NHA^{RAS}. *PIK3CA*^{mut} status did not affect MAPK inhibition in selumetinib treated NHA^{RAS} lines (**Fig 5.5FG**, **S5.11AB**). Similar to NHA, selumetinib caused alternate activation of proximal PI3K signaling in GFP and parental NHA^{RAS} (**Fig 5.5FH**, **S5.11AC**). However, induction of proximal PI3K signaling was ablated in *PI3KCA*^{WT} and all *PIK3CA*^{mut} NHA^{RAS}. Taken together, these results indicate that ectopic expression of *PIK3CA* in combination with mutant *RAS* prevents MEKi-induced alternate activation of the PI3K pathway.

Dual PI3Ki/MEKi treatment is synergistic in control and *PIK3CA*^{mut} NHA and NHA^{RAS}

We and others have shown that efficacy of PI3Ki/MEKi is increased by dual treatment.[31,35-37] However, the effects of GBM-associated mutations on PI3Ki/MEKi

synergism remain unclear. To this end, we determined whether *PIK3CA*^{mut} influence the effects of dual PI3Ki/MEKi treatment on growth of NHA *in vitro*. Treatment with buparlisib/selumetinib inhibited growth and functioned synergistically in control and *PIK3CA*^{mut} NHA (**Fig 5.6A**). Moreover, synergy was greatest in R88Q and E542K *PIK3CA*^{mut} NHA compared to *PIK3CA*^{WT} and H1047R *PIK3CA*^{mut} lines.

PIK3CA^{WT} and *PIK3CA*^{mut} in NHA^{RAS} marginally decreased efficacy of MEKi (**Figs 5.5B**, **S5.10BC**). They also cooperated with mutant *RAS* to prevent MEKi-induced potentiation of proximal PI3K signaling (**Figs 5.5F-H**, **S5.11**). Therefore, *PIK3CA*^{WT} and *PIK3CA*^{mut} in combination with mutant *RAS* may alter PI3Ki/MEKi synergism. Dual buparlisib/selumetinib treatment inhibited growth of all NHA^{RAS} lines and functioned synergistically (**Figs 5.6B**). However, synergism between buparlisib and selumetinib was most pronounced at higher concentrations of both drugs in NHA^{RAS} lines compared to NHA. Furthermore, buparlisib/selumetinib synergy was greatest in R88Q and E542K *PIK3CA*^{mut} NHA^{RAS}. Taken together, these data suggest that mutant *RAS* and *PIK3CA*^{mut} alter synergism between PI3Ki/MEKi.

Discussion

PIK3CA^{mut} differentially activate PI3K signaling and promote gliomagenesis

The vast majority of GBM harbor mutations in core PI3K pathway genes and/or upstream RTK.[4] Activation of PI3K signaling via *Pten* deletion, *PIK3R1* mutations, or constitutively active *AKT* mutants, promotes tumorigenesis in glioma models.[17-20] Here, we determined the effects of ABD, helical, and kinase *PIK3CA* missense mutations on gliomagenesis. Both helical and kinase *PIK3CA*^{mut} potentiated PI3K signaling, proliferation, and migration of NHA compared to parental and *PIK3CA*^{WT} lines (**Figs 5.1**, **5.2**). In contrast, only the H1047R kinase *PIK3CA*^{mut} potentiated colony formation of NHA (**Fig 5.3A**). Similarly, H1047R *PIK3CA*^{mut} induced tumors with a shorter latency than the E545K helical mutation in a mammary carcinoma model.[38]

We and others have shown that *Pten* deletion and constitutively active AKT cooperates with activated MAPK signaling to potentiate PI3K signaling and gliomagenesis.[17,20-22] We extended these finding here by demonstrating that mutant *RAS* promoted *PIK3CA*^{WT}- and *PIK3CA*^{mut}-induced proximal PI3K signaling (**Fig 5.1**). Unlike in NHA, *PIK3CA*^{mut} did not increase proliferation of NHA^{RAS}, likely due to the rapid proliferation rate of parental cells (**Fig 5.2AB**). H1047R *PIK3CA*^{mut} also did not potentiate colony formation of NHA^{RAS} (**Fig 5.3A**). However, compared to GFP and*PIK3CA*^{WT}, the E542K and H1047R *PIK3CA*^{mut} potentiated malignancy of NHA^{RAS} *in vivo* (**Fig 5.3BC**). These results are consistent with the previous findings that constitutively active AKT does not enhance proliferation or colony formation of NHA^{RAS} *in vitro*, but promoted tumorigenesis *in vivo*.[20] Taken together, these data suggest that

the E542K and H1047R *PIK3CA*^{mut} equally promote gliomagenesis in the presence of mutant *RAS*, but not in its absence.

In contrast to helical and kinase *PIK3CA* mutations, ABD *PIK3CA*^{mut} did not increase PI3K signaling, migration, or colony formation of NHA more than *PIK3CA*^{WT} (**Figs 5.1-3**). Similar results were obtained with ABD *PIK3CA*^{mut} in NHA^{RAS}. Moreover, R88Q *PIK3CA*^{mut} did not promote malignancy of NHA^{RAS} more than *PIK3CA*^{WT} *in vivo* (**Fig 5.3BC**). Taken together, these results demonstrate that the phenotypic consequences of ABD *PIK3CA*^{mut} are similar to ectopic over-expression of *PIK3CA*^{WT}. Furthermore, they suggest that mutations in the ABD of *PIK3CA* are passenger mutations in GBM. However, ectopic expression of *PIK3CA*^{WT} and *PIK3CA*^{mut} may not fully recapitulate the effects of *PIK3CA* missense mutations when expressed under its endogenous promoter. Furthermore, other cooperating mutations and/or cellular origin may influence the role of *PIK3CA* missense mutations in gliomagenesis. Future work will be required to investigate the role of *PIK3CA*^{mut} in other cellular/genetic contexts.

PIK3CA^{mut} do not influence PI3Ki efficacy

The precision medicine initiative seeks to direct treatment with targeted inhibitors based on the mutation profiles of patients.[8,34] However, this requires an understanding of how oncogenic mutations influence drug response. Mutational activation of kinases can cause oncogene addiction, in which tumor cells become reliant upon the activated signaling pathway(s), and are thus highly sensitive to their inhibition.[39] Additionally, kinase mutations can alter drug affinity, thereby altering efficacy.[40] Buparlisib inhibits purified PIK3CA^{WT} and the most common PIK3CA^{mut}, E542K, E545K, and H1047R, with similar IC_{50}.[41,42] Because these helical and kinase domain *PIK3CA*^{mut} activated PI3K

signaling and promoted gliomagenesis, we hypothesized that they would also increase PI3Ki efficacy. Activating *PIK3CA*^{mut}, particularly those in the helical and kinase domains, increased the buparlisib concentration required to ablate PI3K signaling (**Fig 5.4**). However, they did not influence efficacy of PI3Ki treatment *in vitro*. These results suggest that *PIK3CA* missense mutations do not induce oncogene addiction and do not enhance sensitivity to PI3Ki. Whether they influence efficacy of isoform specific PI3Ki or inhibitors of downstream kinases, such as mTOR, remains to be determined.

PIK3CA^{mut} influence MEKi-induced activation of PI3K signaling and PI3Ki/MEKi synergism

We previously found that buparlisib induced widespread kinome changes, including MAPK activation, in immortalized murine astrocytes with *Pten* deletion and mutant *Kras*.[37] We expanded these findings here by demonstrating that buparlisib potentiated MAPK signaling regardless of *RAS*/*PIK3CA* mutation status (**Fig 5.4C-H**). *PIK3CA*^{mut} also had minimal to no effect on sensitivity of NHA and NHA^{RAS} to MEKi *in vitro* (**Figs 5.5AB**).

We and others have also shown that MEKi promote PI3K signaling in preclinical GBM models.[31,36,37] We found that selumetinib increased proximal PI3K signaling in control and *PIK3CA*^{mut} NHA, and in GFP and parental NHA^{RAS} (**Fig 5.5C-H**). Interestingly, this increase was not apparent in *PIK3CA*^{WT} and *PIK3CA*^{mut} NHA^{RAS} (**Figs 5.5FH**, **S5.11AC**). The mechanism by which ectopic *PIK3CA* expression in combination with mutant *RAS* alters MEKi response is unclear. A mutually inhibitory crosstalk between PI3K and MAPK signaling is mediated by p70S6K in glioma stem cells.[31] MAPK inhibition induces PI3K signaling in non-GBM cell lines via removal of a negative

feedback loop on RTK.[43] Similarly, selumetinib induces widespread kinome changes in breast cancer models, including increased expression and activity of multiple RTK.[44] Taken together, these results suggest that *PIK3CA*^{WT} and *PIK3CA*^{mut} may cooperate with mutant *RAS* to alter MEKi-induced dynamic kinome changes, particularly as it pertains to PI3K activation.

Dual PI3Ki/MEKi treatment is effective in multiple preclinical GBM models.[31,35-37] It remained unclear whether the underlying genetics of these models influenced drug synergism. We therefore determined if *PIK3CA*^{mut} affected PI3Ki/MEKi synergism in the presence and absence of mutant *RAS*. Consistent with other GBM models, we found that dual buparlisib/selumetinib treatment was synergistic in NHA and NHA^{RAS} lines (**Fig 5.6**). However, *RAS*/*PIK3CA*^{mut} status influenced drug response. A higher concentration of buparlisib and selumetinib was required to maximize synergism in NHA^{RAS} lines compared to NHA. Furthermore, synergy was generally greater in R88Q and E542K *PIK3CA*^{mut} NHA and NHA^{RAS} compared to those with either *PIK3CA*^{WT} or H1047R PIK3CA^{mut}. Taken together, these results suggest that GBM patients with ABD or helical *PIK3CA* missense mutations may be most sensitive to dual PI3Ki/MEKi treatment.

Conclusion

Defining the role of frequently occurring mutations on GBM pathogenesis and drug response can aid in the identification of predictive biomarkers. Our results demonstrate that *PIK3CA* missense mutations differentially promote gliomagenesis. Furthermore, they suggest that *PIK3CA* mutations do not predict PI3Ki sensitivity, but they do impact PI3Ki/MEKi synergism.

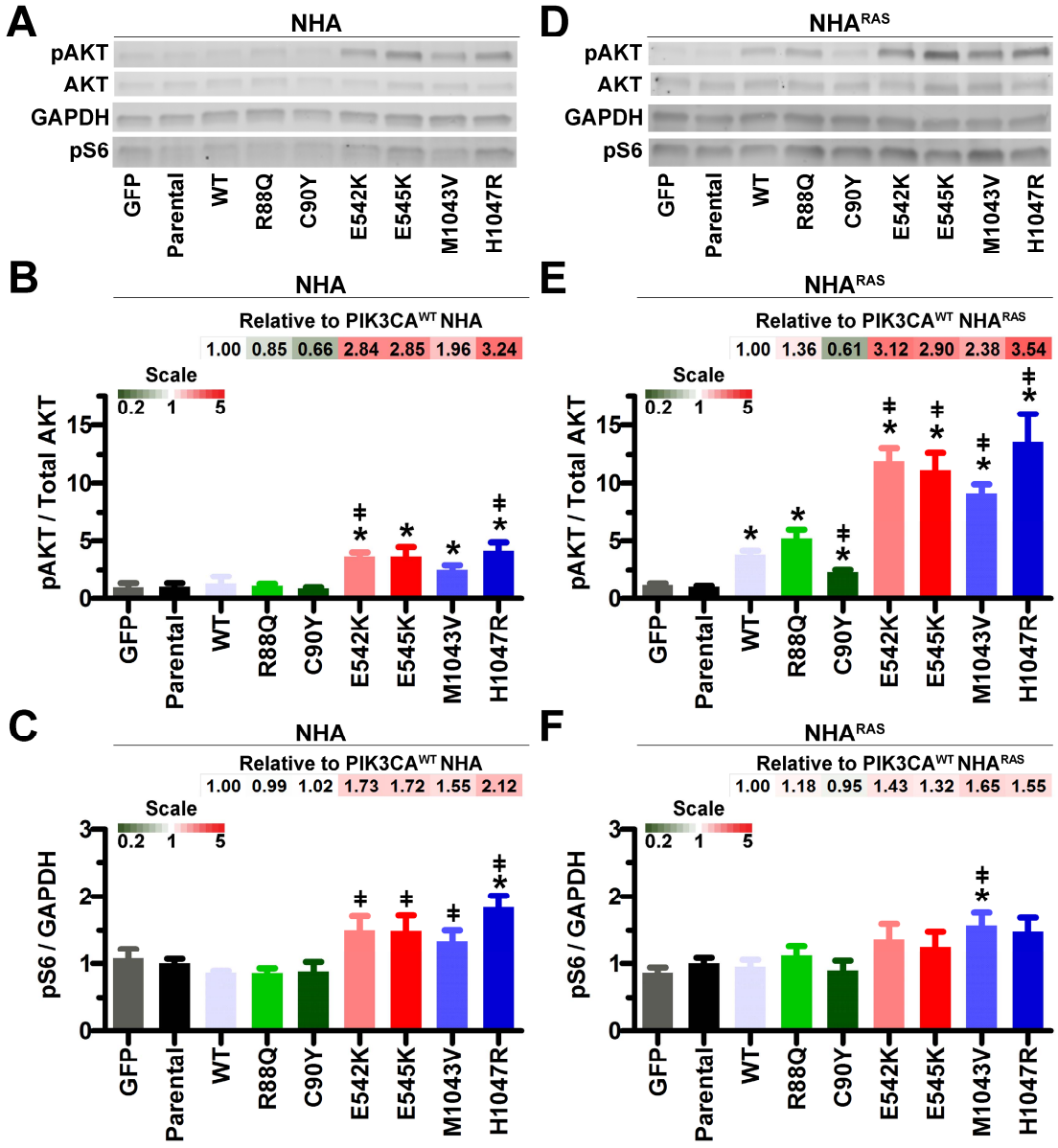

Figure 5.1. Helical and kinase *PIK3CA*^{mut} activate proximal PI3K signaling.

Representative immunoblots (**A**) and quantification showed that compared to parental NHA, proximal PI3K signaling (pAKT) was increased by helical and kinase *PIK3CA*^{mut} (**B**), while distal PI3K signaling (pS6) was only increased by H1047R (**C**) (*, P≤0.02). Compared to *PIK3CA*^{WT} NHA, E542K and H1047R *PIK3CA*^{mut} increased proximal PI3K

signaling and all helical and kinase *PIK3CA*^{mut} increased distal PI3K signaling (‡, P≤0.04). Representative immunoblots (**D**) and quantification showed that proximal PI3K signaling was increased by *PIK3CA*^{WT} and all *PIK3CA*^{mut} compared to parental NHA^{RAS} (**E**). Helical and kinase *PIK3CA*^{mut} also increased proximal PI3K signaling compared to *PIK3CA*^{WT} *NHA*^{RAS} (‡, P≤0.007). Only M1043V *PIK3CA*^{mut} increased distal PI3K signaling compared to parental (*, P=0.03) and *PIK3CA*^{WT} (‡, P=0.03) NHA^{RAS} (**F**). Bar graph data are set relative to parental lines (N=4 biologic replicates). Fold changes in pAKT and pS6 relative to *PIK3CA*^{WT} lines are shown as heatmaps.

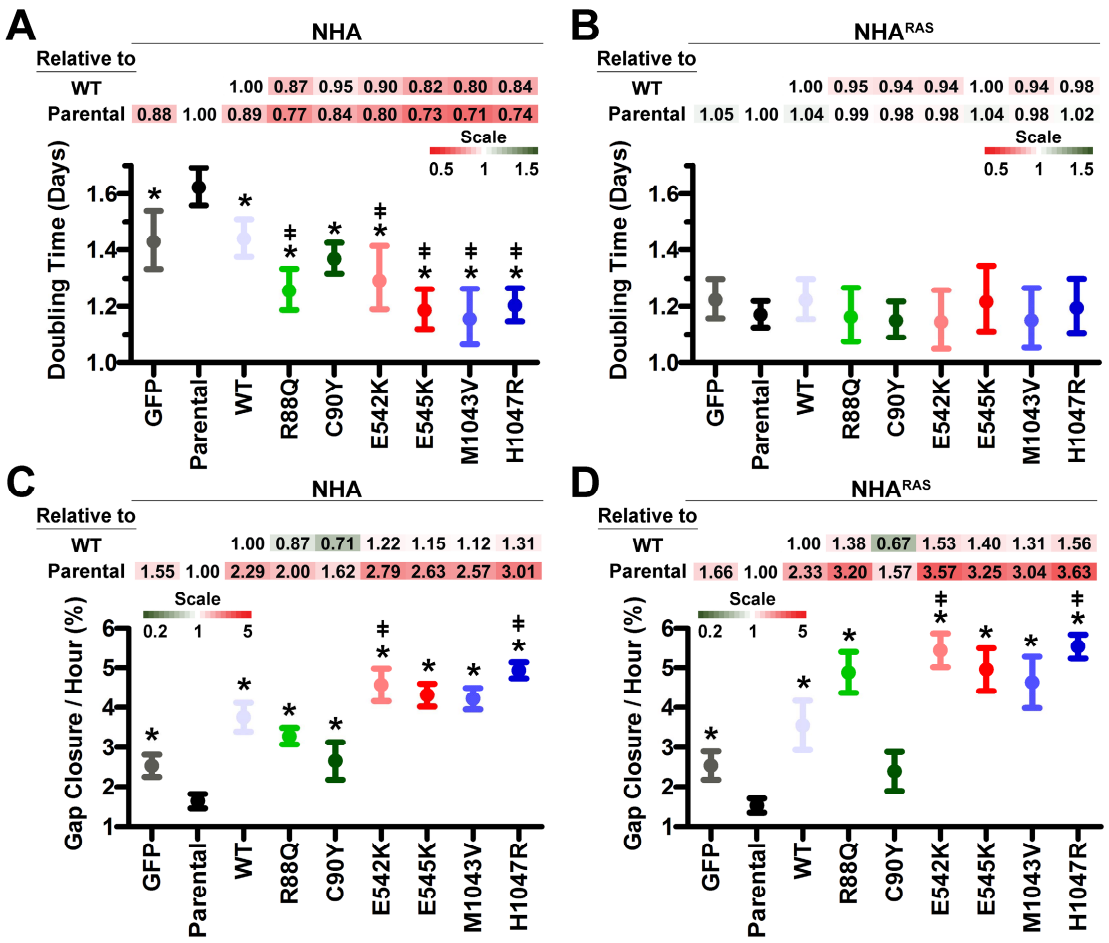

Figure 5.2. ***PIK3CA*^{mut} potentiate proliferation and migration *in vitro***. MTS assays showed that *PIK3CA*^{WT} and all *PIK3CA*^{mut} decreased doubling times of parental NHA (**A**), but not parental NHA^{RAS} (**B**) (*, P≤0.02. See **Fig. S5.5AB**). All *PIK3CA*^{mut}, except C90Y, decreased doubling times compared to *PIK3CA*^{WT} NHA (‡, P≤0.03). Statistical analyses of growth rates were performed by comparing k values. Error bars are 95% confidence intervals. *PIK3CA*^{WT} and all *PIK3CA*^{mut}, except C90Y, increased migration of both NHA (**C**) and NHA^{RAS} (**D**) (*, P≤0.04. See **Fig. S5.5CD**). E542K and H1047R *PIK3CA*^{mut} also potentiated migration compared to *PIK3CA*^{WT} NHA and NHA^{RAS} (‡, P≤0.005). Fold changes in doubling times and migration rates relative to parental and *PIK3CA*^{WT} lines are shown as heatmaps.

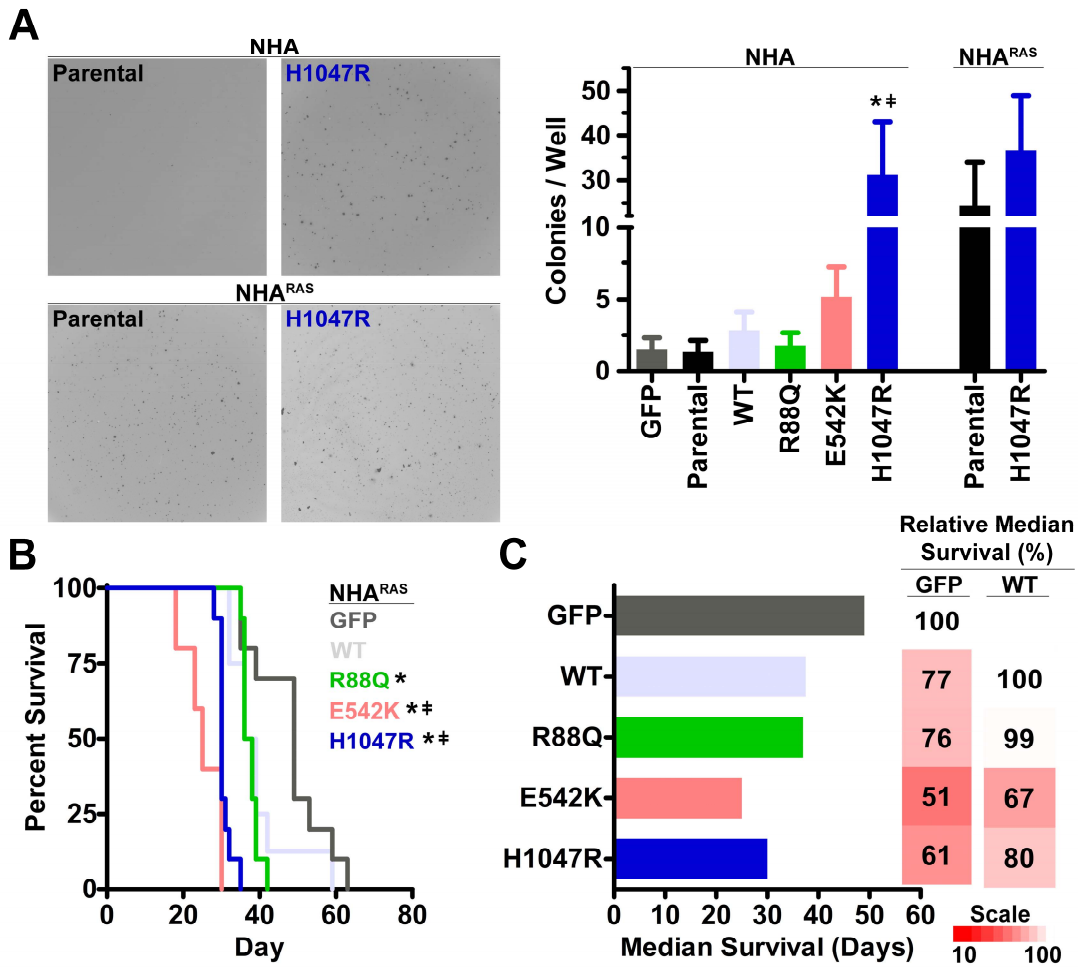

Figure 5.3. **Helical and kinase *PIK3CA*^{mut} potentiate tumorigenesis**. Only H1047R *PIK3CA*^{mut} increased colony formation compared to parental (*, P=0.03) and *PIKCA*^{WT} (‡, P=0.04) NHA (**A**). H1047R *PIK3CA*^{mut} did not affect colony formation of NHA^{RAS} (P=0.5). Representative images of parental and H1047R *PIK3CA*^{mut} NHA and NHA^{RAS} are shown. Orthotopic xenografts of GFP, *PIK3CA*^{WT}, and *PIK3CA*^{mut} NHA^{RAS} (**B**,**C**). Median survival of mice injected with R88Q, E542K, or H1047R *PIK3CA*^{mut} NHA^{RAS} was decreased compared to GFP controls (*, P≤0.003). E542K and H1047R *PIK3CA*^{mut} also decreased survival compared to *PIK3CA*^{WT} (‡, P≤0.002) and R88Q *PIK3CA*^{mut} (P<0.0001). Fold changes in median survival relative to GFP and *PIK3CA*^{WT} NHA^{RAS} are shown as heatmaps.

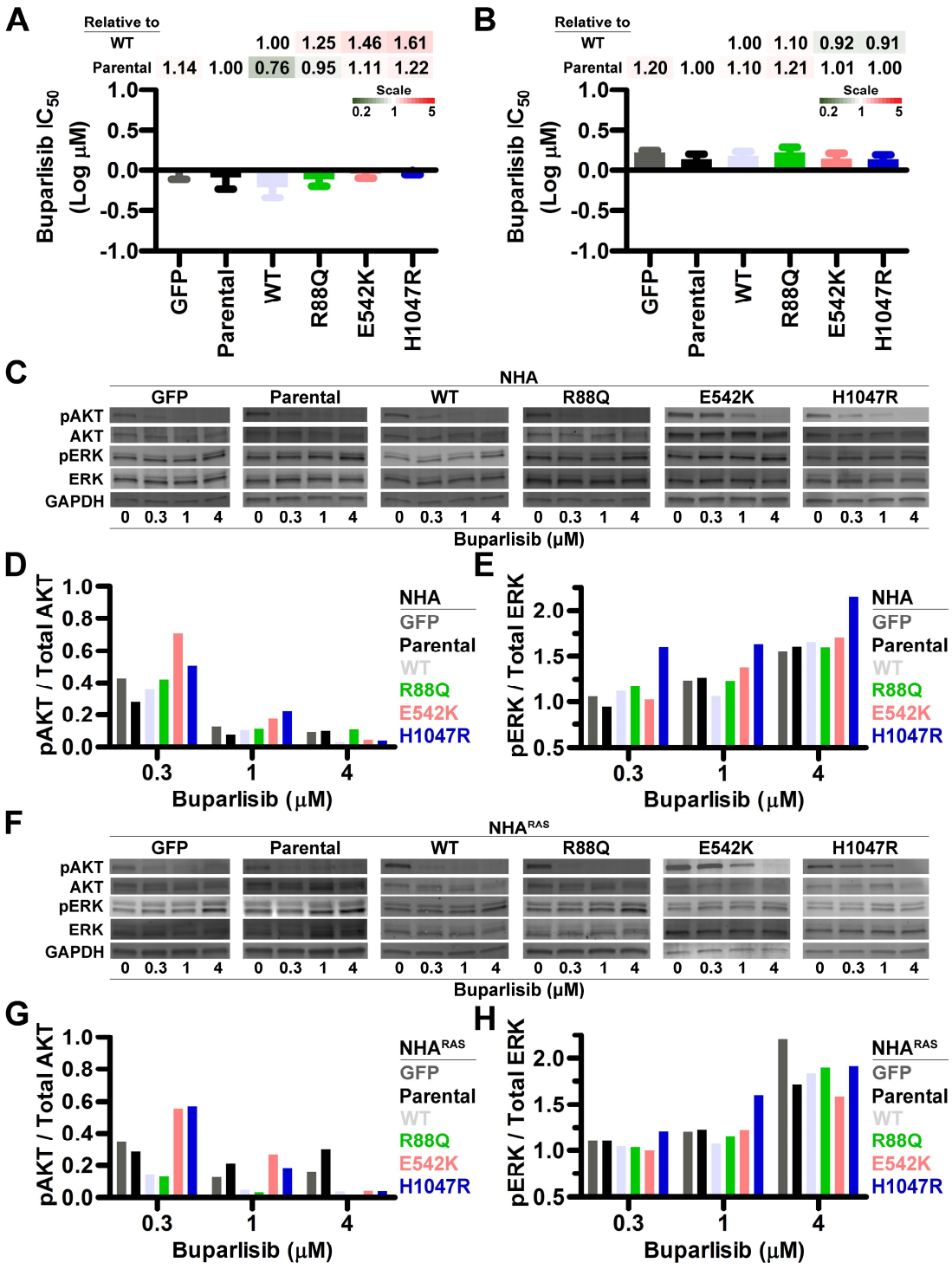

Figure 5.4. PI3Ki inhibits growth and ablates PI3K signaling regardless of *PIK3CA*^{mut} status. Buparlisib IC_{50} were similar regardless of *PIK3CA*^{mut} status in NHA (**A**) and NHA^{RAS} (**B**) (See **Fig S5.6**). Fold changes in IC_{50} relative to parental and

PIK3CA^{WT} lines are shown as heatmaps. Representative immunoblots of control and *PIK3CA*^{mut} NHA (**C**) and NHA^{RAS} (**F**) treated with buparlisib for 24 h. Immunoblot quantification (**D**,**E**,**G**,**H**) demonstrated dose-dependent decreases in proximal PI3K signaling (**D**,**G**), with corresponding increases in MAPK signaling (**E**,**H**) in all NHA (**D**,**E**) and NHA^{RAS} (**G**,**H**) lines (See **Fig S5.9**). Immunoblot data were pooled from 1-3 biologic replicates (Mean=2.3).

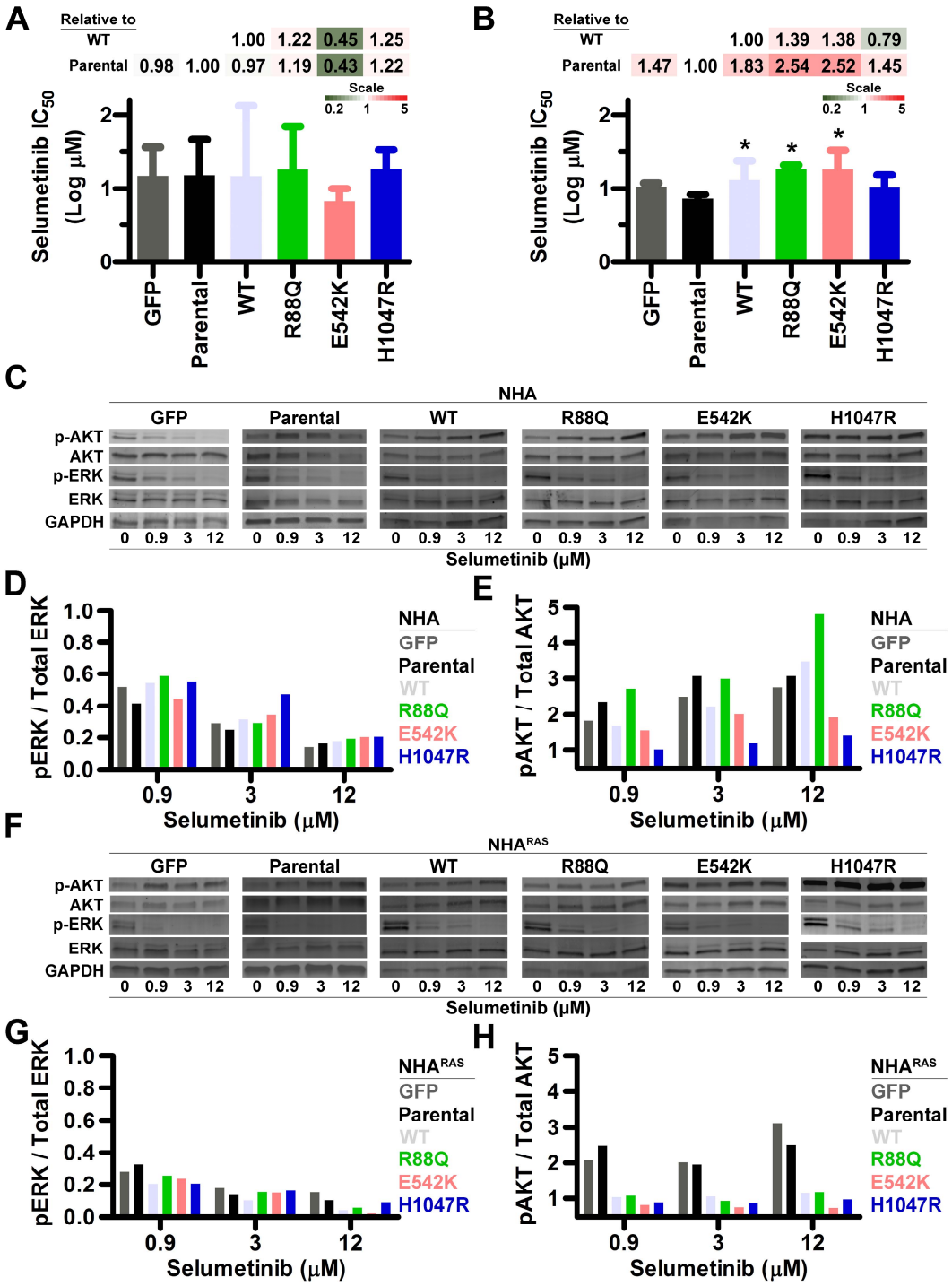

Figure 5.5. MEKi inhibits growth and ablates MAPK signaling regardless of *PIK3CA*^{mut} status. Selumetinib IC_{50} were similar regardless of *PIK3CA*^{mut} status in NHA (**A**). Selumetinib IC_{50} were slightly higher in most *PIK3CA*^{mut} NHA^{RAS}, compared

to parental cells (*, P≤0.03) (**B**) (See **Fig S5.10**). Fold changes in IC_{50} relative to parental and *PIK3CA*^{WT} lines are shown as heatmaps. Representative immunoblots of control and *PIK3CA*^{mut} NHA (**C**) and NHA^{RAS} (**F**) treated with selumetinib for 24 h. Immunoblot quantification (**D**,**E**,**G**,**H**) demonstrated dose-dependent decreases in MAPK signaling in all NHA (**D**) and NHA^{RAS} (**G**) lines. Although proximal PI3K signaling was induced in all control and *PIK3CA*^{mut} NHA (**E**), it was only potentiated in GFP and parental NHA^{RAS} (**H**) (See **Fig S5.11**). Immunoblot data were pooled from 1-2 biologic replicates (Mean=1.8)

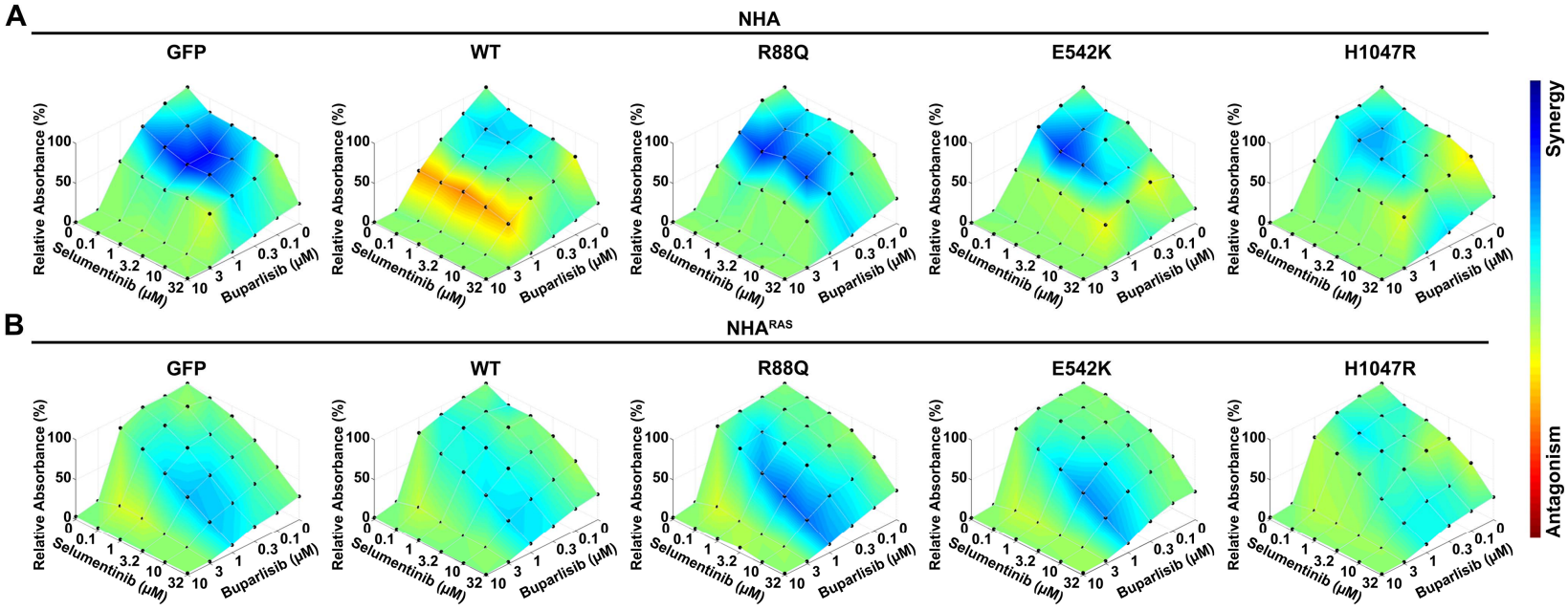

Figure 5.6. **PI3Ki/MEKi synergism *in vitro* is influenced by *PIK3CA*^{mut} and mutant *RAS***. Buparlisib and selumetinib inhibited growth and were synergistic in control and PIK3CA^{mut} NHA (**A**) and NHA^{RAS} (**B**). BLISS analyses showed that synergy was most pronounced at high nanomolar concentrations of buparlisib when used with low micromolar- high nanomolar concentrations of selumetinib in NHA lines. In contrast, synergistic concentrations in NHA^{RAS} lines were generally most pronounced at low micromolar concentrations of both buparlisib and selumetinib.

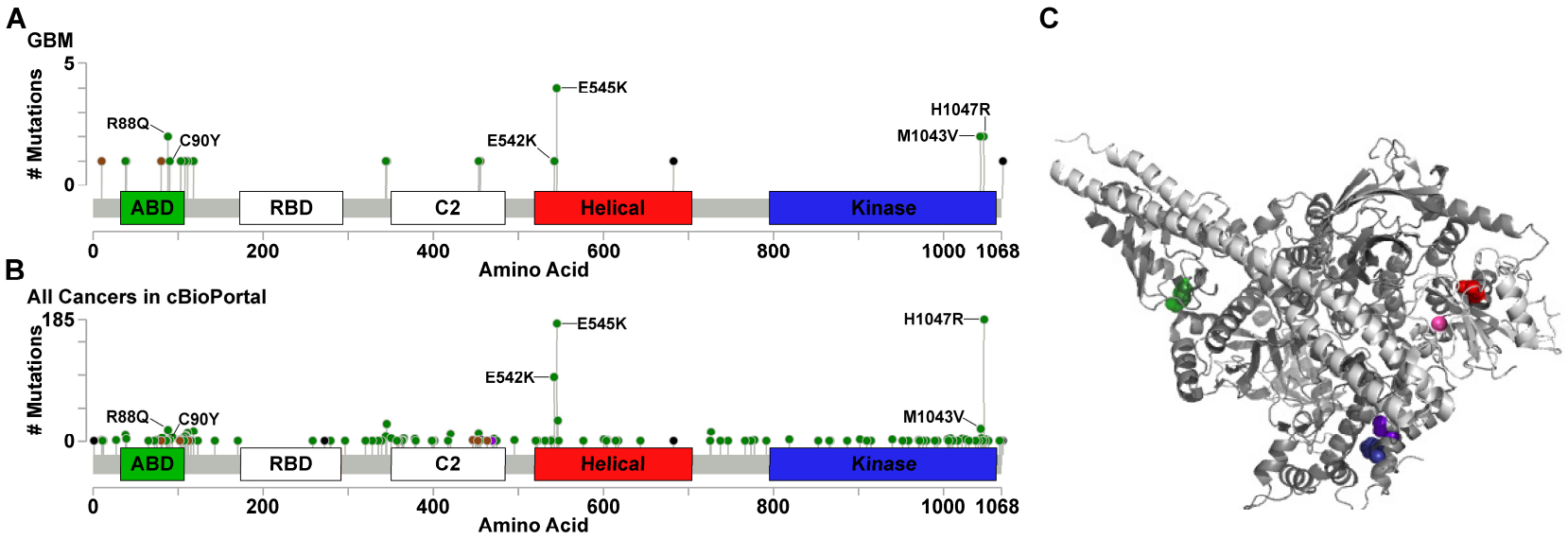

Figure S5.1. **Distribution of *PIK3CA* missense mutations across the protein**. Lollipop diagram showing the frequency and distribution of *PIK3CA* missense mutations (green), in-frame deletions (brown), and truncating mutations (black) in GBM (**A**) and all published TCGA datasets (**B**). The *PIK3CA* missense mutations investigated here are indicated. Data were downloaded from cBioPortal (http://www.cbioportal.org/) on March 10th, 2017. Ribbon diagram of *PIK3CA* with the mutations investigated highlighted (**C**) (R88Q = light green; C90Y = dark green; E542K = pink; E545K = red; M1043V = purple; H1047R = blue). Model was generated in PyMOL. (Schrödinger, New York City, NY) using a script downloaded from cBioPortal.[13,14]

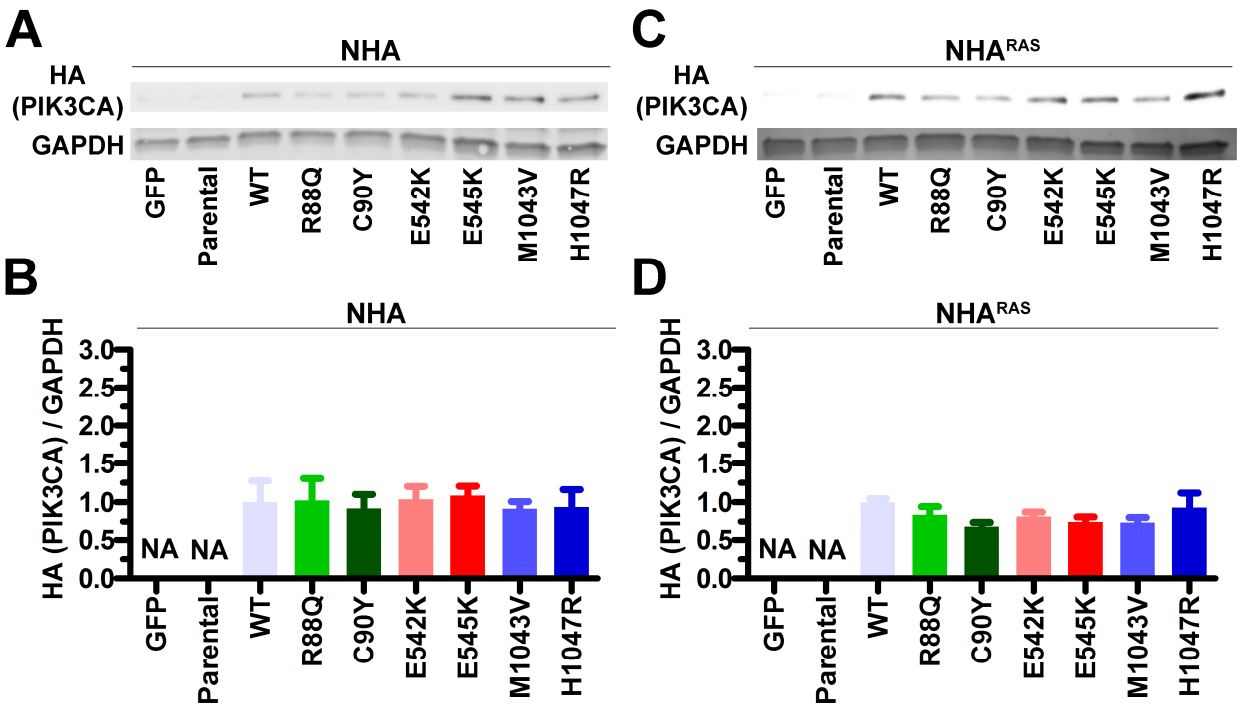

Figure S5.2. ***PIK3CA^{WT}* and *PIK3CA^{mut}* are expressed at similar levels**.

Representative immunoblots (**A**,**C**) and quantification (**B**,**D**) of HA-tagged PIK3CA showed that *PIK3CA^{WT}* and all *PIK3CA^{mut}* are expressed at similar levels in NHA (**B**,**C**) and NHA^{RAS} (**C**,**D**) (ANOVA, P≥0.3). Bar graph data are set relative to *PIK3CA^{WT}* lines (N=3-4 biologic replicates, Mean=3.5).

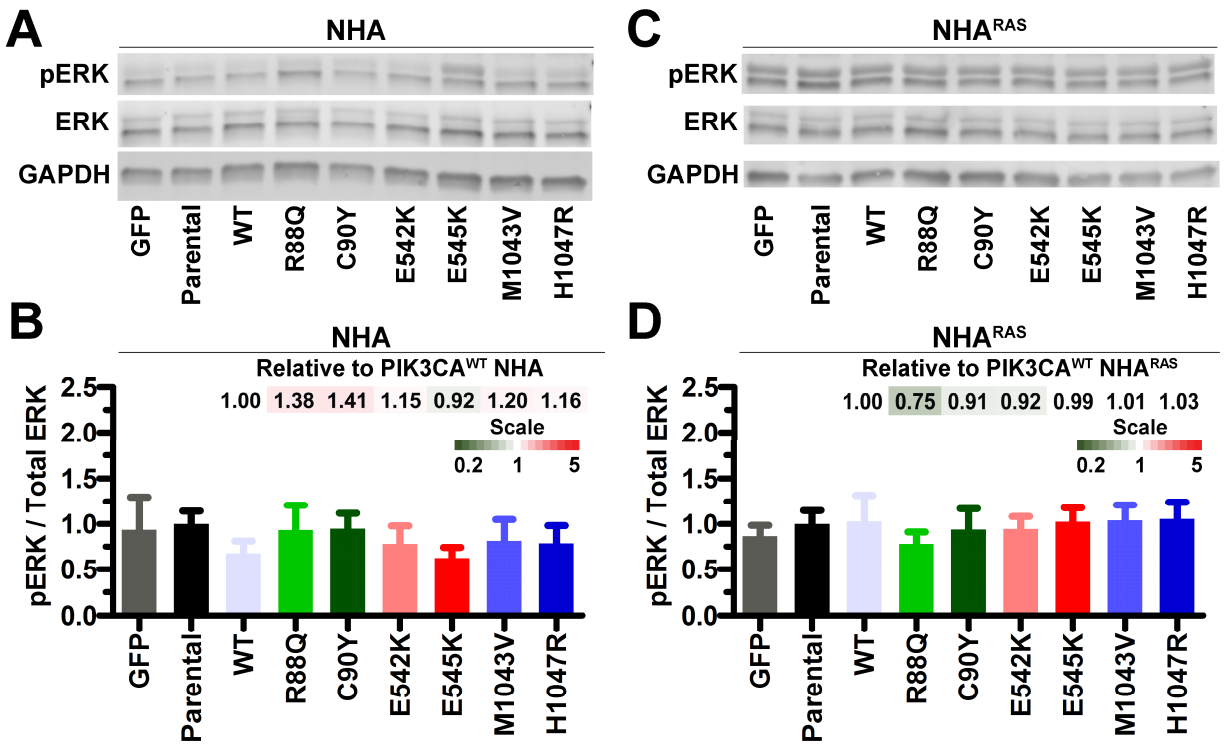

Figure S5.3. ***PIK3CA*^{mut} do not alter MAPK signaling**. Representative immunoblots (**A**,**C**) and quantification (**B**,**D**) showed that *PIK3CA*^{mut} did not alter MAPK signaling (phosphorylation of ERK1/2, pERK) in either NHA (**A**,**B**) or NHA^{RAS} (**C**,**D**) (P≥0.93). Bar graph data are set relative to parental lines (N=3-4 biologic replicates, Mean=3.5). Fold changes in pERK relative to PIK3CA^{WT} lines are shown as heatmaps.

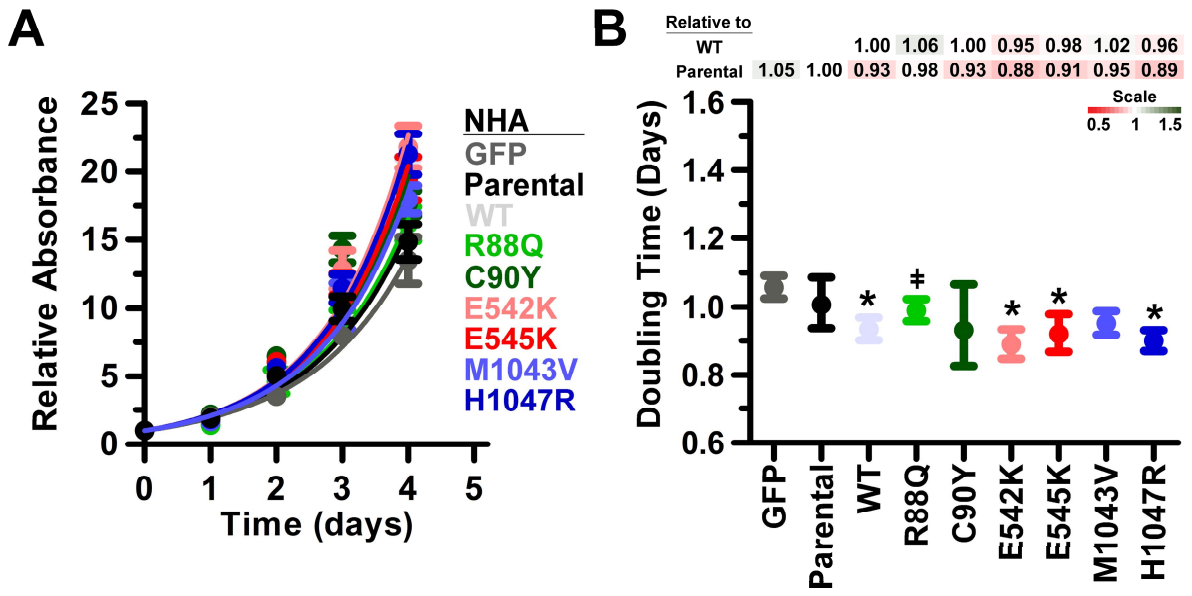

Figure S5.4. ***PIK3CA* mutations have minor effects of on growth in high-serum culture**. MTS assays (**A**) showed that, when grown in media containing high (10% FBS) serum concentrations, *PIK3CA*^{WT} and a subset of *PIK3CA*^{mut} slightly reduced doubling times compared to parental NHA (*, P≤0.03) (**B**). Growth of R88Q *PIK3CA*^{mut} was slightly less than *PIK3CA*^{WT} NHA (‡, P=0.01). Statistical analyses of growth rates were performed by comparing k values. Fold changes in doubling times relative to parental and *PIK3CA*^{WT} lines are shown as heatmaps. Error bars in **B** are 95% confidence intervals.

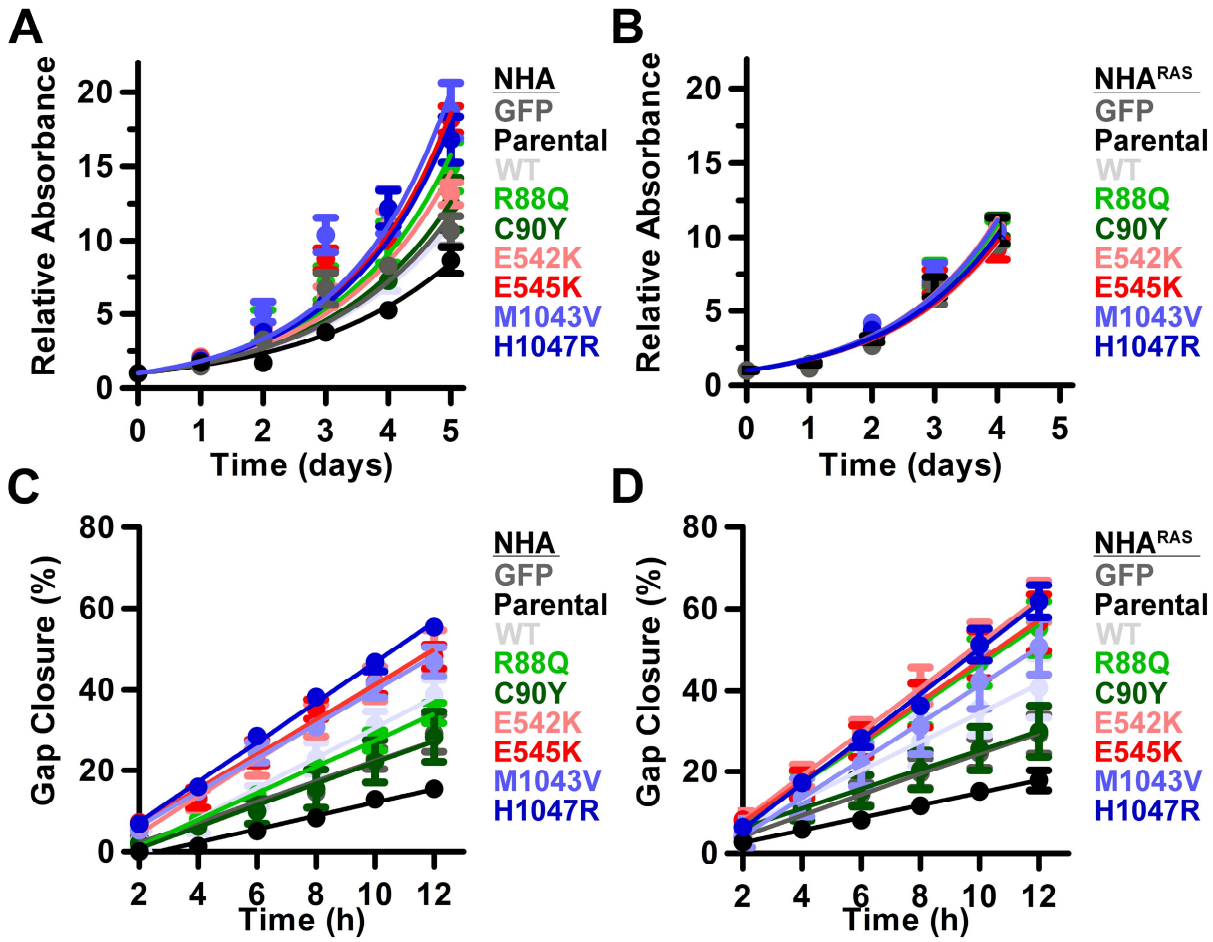

Figure S5.5. **Mutant *RAS* affects the impact of *PIK3CA*^{mut} on proliferation, but not migration *in vitro***. Growth of control and *PIK3CA*^{mut} NHA (**A**) and NHA^{RAS} (**B**) (See **Fig 5.2AB**). Growth was determined by assessing changes in relative absorbance daily by MTS. Migration of control and *PIK3CA* mutant NHA (**C**) and NHA^{RAS} (**D**) across a gap (See **Fig 5.2CD**).

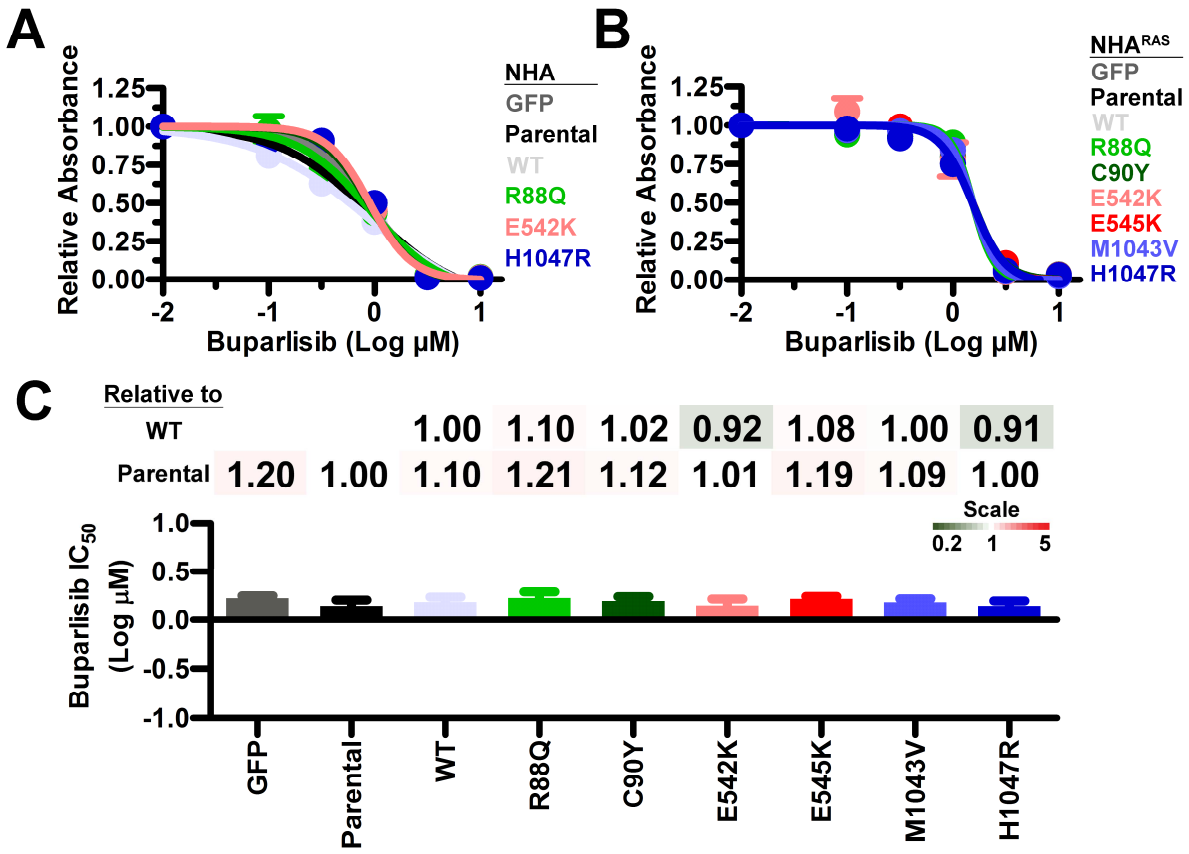

Figure S5.6. **PI3Ki inhibits *in vitro* growth independent of *PIK3CA*^{mut} status**. MTS assays showed that buparlisib caused dose-dependent decreases in growth of control and *PIK3CA*^{mut} NHA (**A**) and NHA^{RAS} (**B**). Buparlisib IC_{50} were similar between control and all 6 *PIK3CA*^{mut} NHA^{RAS} (**C**).

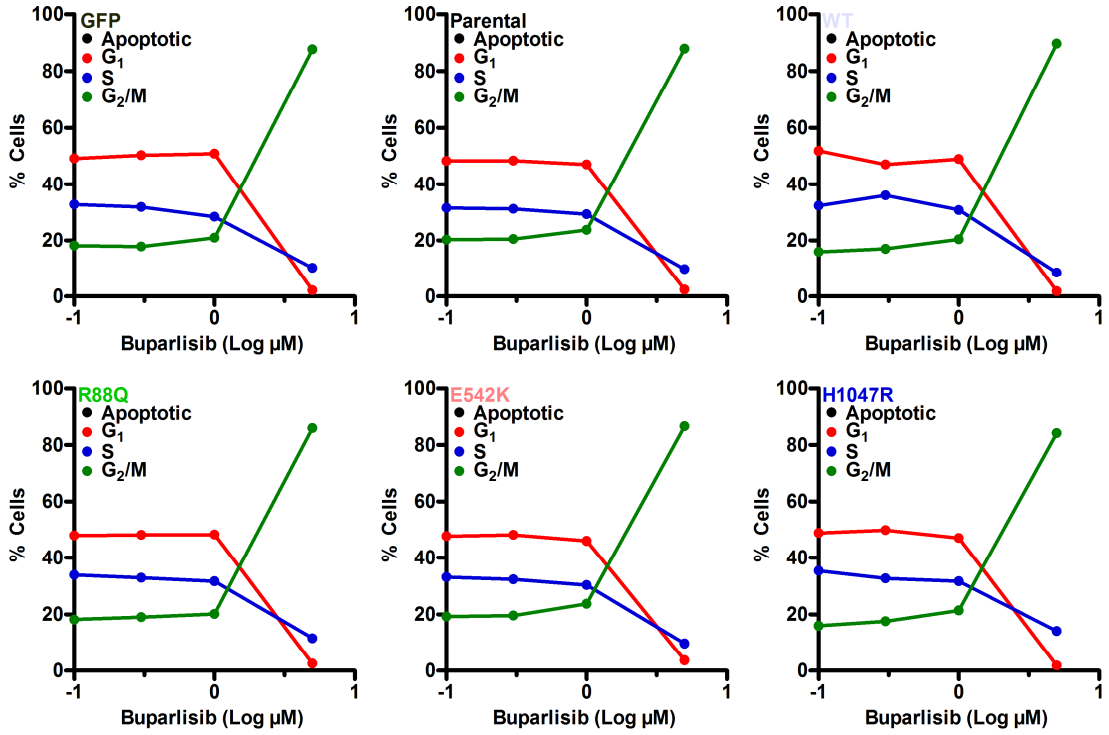

Figure S5.7. **PI3Ki induces G_2/M cell cycle arrest in NHA^{RAS} cells regardless of *PIK3CA^{mut}* status**. Micromolar doses of buparlisib induced G_2/M cell cycle arrest within 48 h post-treatment in control and PIK3CA^{mut} NHA^{RAS}.

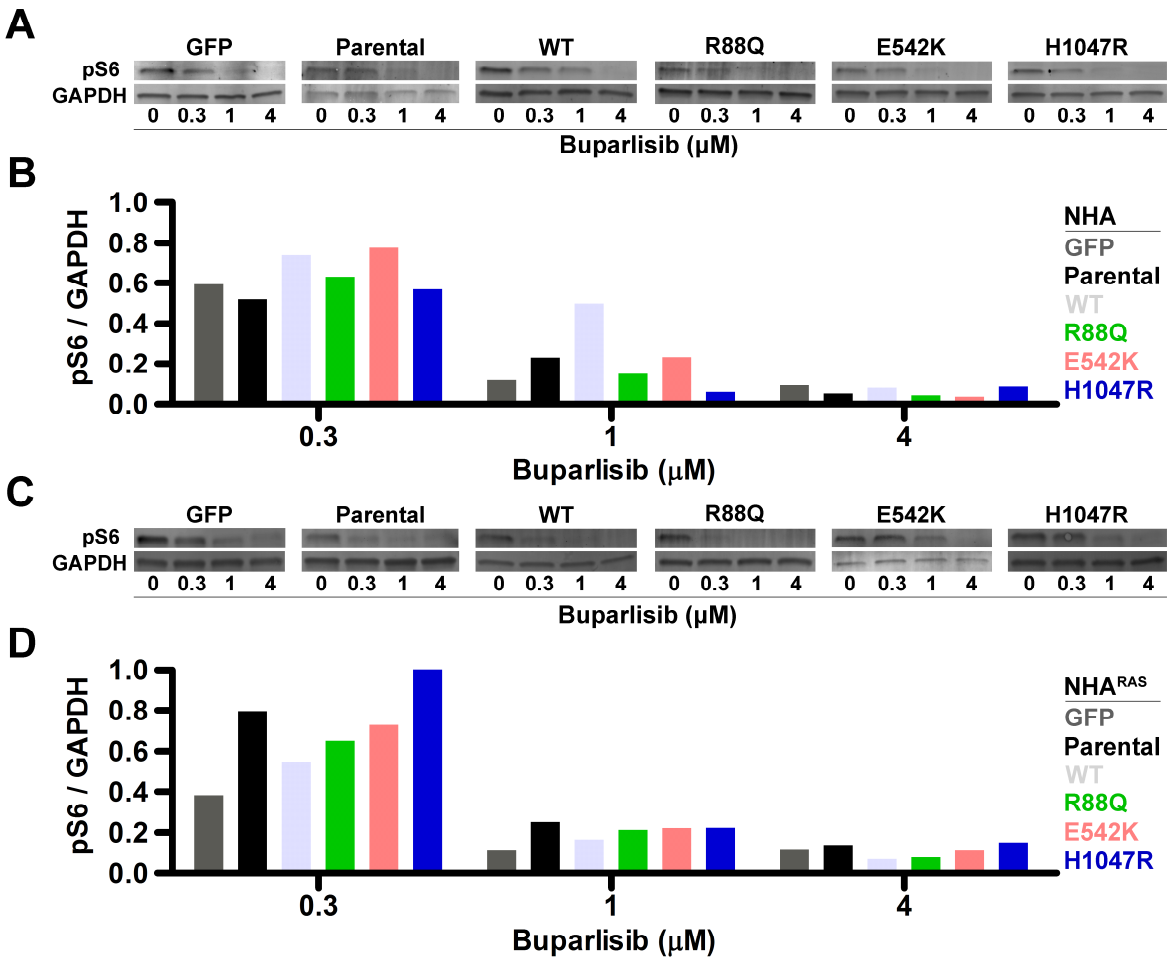

Figure S5.8. **PI3Ki inhibits distal PI3K signaling regardless of *PIK3CA*^{mut} status**. Representative immunoblots of control and *PIK3CA*^{mut} NHA (**A**) and NHA^{RAS} (**C**) 24 h after buparlisib treatment. Immunoblot quantification demonstrated dose-dependent decreases in distal PI3K signaling in all NHA (**B**) and NHA^{RAS} (**D**) lines (N=1-3 biologic replicates, Mean=1.7).

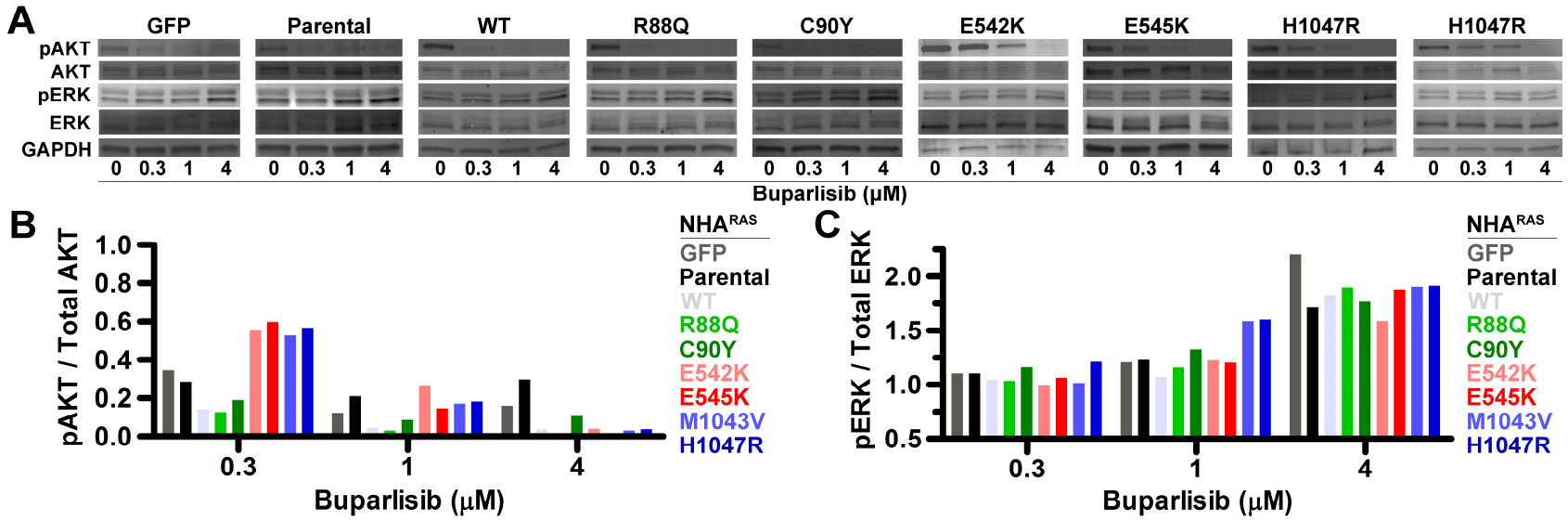

Figure S5.9. **PI3Ki inhibits proximal PI3K signaling and induces MAPK signaling in all control and *PIK3CA*^{mut} NHA^{RAS}.** Representative immunoblots (**A**) and quantification of proximal PI3K (**B**) and MAPK (**C**) signaling showed that within 24 h, buparlisib induced dose-dependent decreases in PI3K signaling, with concurrent increases in MAPK signaling in parental, GFP, PIK3CA^{WT}, and all 6 PIK3CA^{mut} NHA^{RAS} lines (N=2-3 biologic replicates, Mean=2.7).

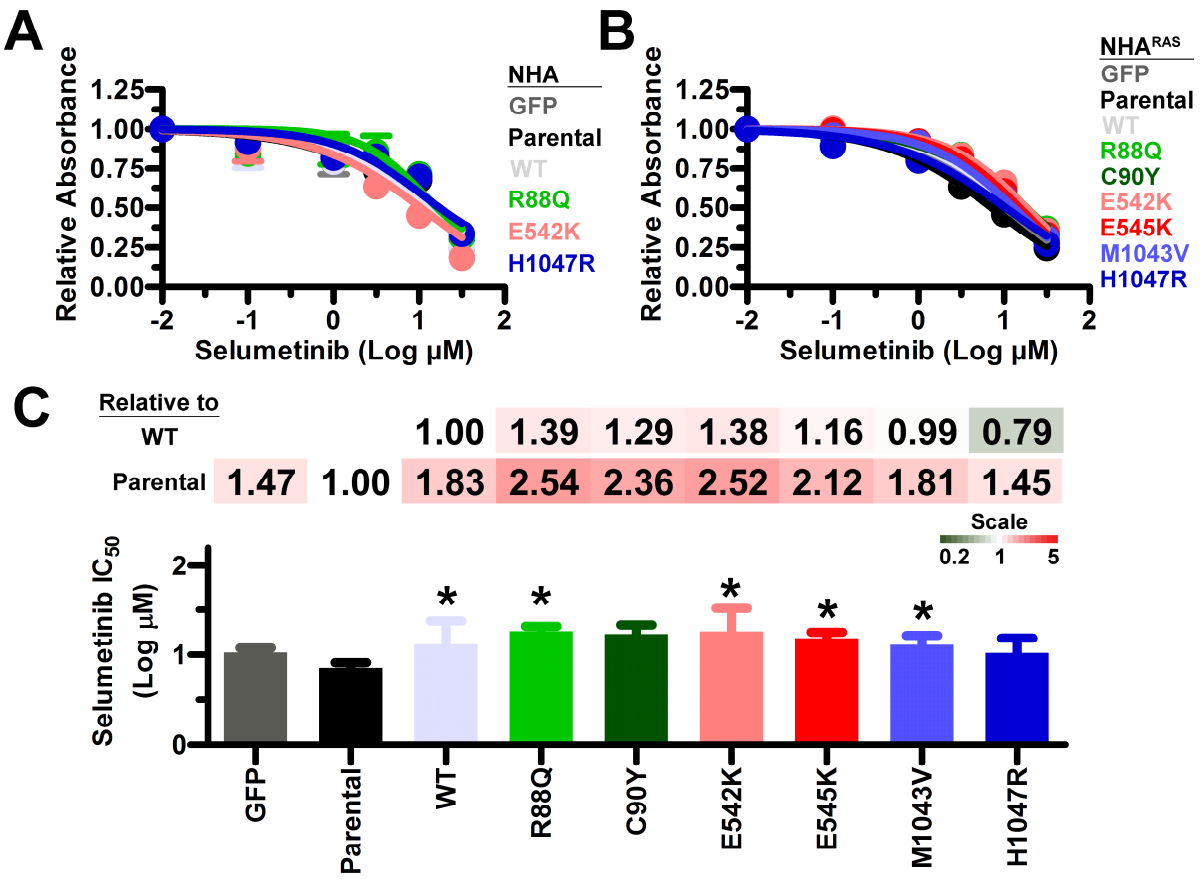

Figure S5.10. **MEKi inhibits *in vitro* growth in all *PIK3CA*^{mut} lines.** MTS assays showed that selumetinib caused dose-dependent decreases in growth of control and *PIK3CA*^{mut} NHA (**A**) and NHA^{RAS} (**B**). Selumetinib IC_{50} were slightly increased by *PIK3CA*^{WT} and all *PIK3CA*^{mut}, except C90Y and H1047R, compared to parental NHA^{RAS} (*, P≤0.03) (**C**).

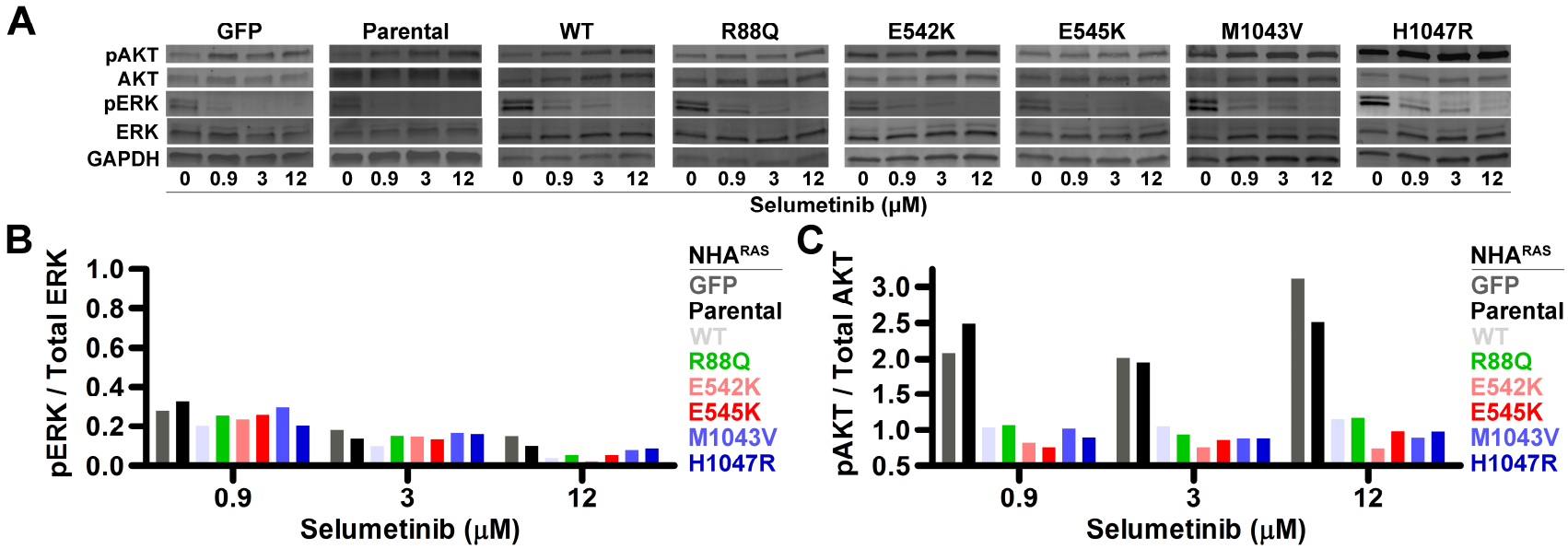

Figure S5.11. **MEKi-induced potentiation of proximal PI3K signaling is abrogated in *PIK3CA^{WT}* and *PIK3CA^{mut}* NHA^{RAS}**. Representative immunoblots (**A**) and quantification of MAPK (**B**) and proximal PI3K (**C**) signaling showed that selumetinib caused dose-dependent decreases in MAPK signaling regardless of *PIKCA^{WT}* or *PIK3CA^{mut}* status, but concurrent increases in proximal PI3K signaling only occurred in parental and GFP NHA^{RAS} (N=2-3 biologic replicates, Mean=2.7).

REFERENCES

1. Louis DN, Perry A, Reifenberger G, et al. The 2016 World Health Organization Classification of Tumors of the Central Nervous System: a summary. *Acta Neuropathol.* 2016;131(6):803-820.

2. Ostrom QT, Gittleman H, Fulop J, et al. CBTRUS Statistical Report: Primary Brain and Central Nervous System Tumors Diagnosed in the United States in 2008-2012. *Neuro Oncol.* 2015;17 Suppl 4:iv1-iv62.

3. Stupp R, Mason WP, van den Bent MJ, et al. Radiotherapy plus concomitant and adjuvant temozolomide for glioblastoma. *N Engl J Med.* 2005;352(10):987-996.

4. Brennan CW, Verhaak RG, McKenna A, et al. The somatic genomic landscape of glioblastoma. *Cell.* 2013;155(2):462-477.

5. Cancer Genome Atlas Research Network. Comprehensive genomic characterization defines human glioblastoma genes and core pathways. *Nature.* 2008;455(7216):1061-1068.

6. Verhaak RG, Hoadley KA, Purdom E, et al. Integrated genomic analysis identifies clinically relevant subtypes of glioblastoma characterized by abnormalities in PDGFRA, IDH1, EGFR, and NF1. *Cancer Cell.* 2010;17(1):98-110.

7. Cloughesy TF, Cavenee WK, Mischel PS. Glioblastoma: from molecular pathology to targeted treatment. *Annu Rev Pathol.* 2014;9:1-25.

8. Mendelsohn J. Personalizing oncology: perspectives and prospects. *J Clin Oncol.* 2013;31(15):1904-1911.

9. Hanahan D, Weinberg RA. Hallmarks of cancer: the next generation. *Cell.* 2011;144(5):646-674.

10. Courtney KD, Corcoran RB, Engelman JA. The PI3K pathway as drug target in human cancer. *J Clin Oncol.* 2010;28(6):1075-1083.

11. Fruman DA, Rommel C. PI3K and cancer: lessons, challenges and opportunities. *Nat Rev Drug Discov.* 2014;13(2):140-156.

12. Thorpe LM, Yuzugullu H, Zhao JJ. PI3K in cancer: divergent roles of isoforms, modes of activation and therapeutic targeting. *Nat Rev Cancer.* 2015;15(1):7-24.

13. Cerami E, Gao J, Dogrusoz U, et al. The cBio cancer genomics portal: an open platform for exploring multidimensional cancer genomics data. *Cancer Discov.* 2012;2(5):401-404.

14. Gao J, Aksoy BA, Dogrusoz U, et al. Integrative Analysis of Complex Cancer Genomics and Clinical Profiles Using the cBioPortal. *Sci Signal*. 2013;6(269):pl1.

15. Wen PY, Lee EQ, Reardon DA, Ligon KL, Alfred Yung WK. Current clinical development of PI3K pathway inhibitors in glioblastoma. *Neuro Oncol.* 2012;14(7):819-829.

16. Chow LM, Endersby R, Zhu X, et al. Cooperativity within and among Pten, p53, and Rb pathways induces high-grade astrocytoma in adult brain. *Cancer Cell.* 2011;19(3):305-316.

17. Vitucci M, Karpinich NO, Bash RE, et al. Cooperativity between MAPK and PI3K signaling activation is required for glioblastoma pathogenesis. *Neuro Oncol.* 2013;15(10):1317-1329.

18. Song Y, Zhang Q, Kutlu B, et al. Evolutionary etiology of high-grade astrocytomas. *Proc Natl Acad Sci U S A.* 2013;110(44):17933-17938.

19. Quayle SN, Lee JY, Cheung LW, et al. Somatic mutations of PIK3R1 promote gliomagenesis. *PLoS One.* 2012;7(11):e49466.

20. Sonoda Y, Ozawa T, Aldape KD, Deen DF, Berger MS, Pieper RO. Akt pathway activation converts anaplastic astrocytoma to glioblastoma multiforme in a human astrocyte model of glioma. *Cancer Res.* 2001;61(18):6674-6678.

21. Holland EC, Celestino J, Dai C, Schaefer L, Sawaya RE, Fuller GN. Combined activation of Ras and Akt in neural progenitors induces glioblastoma formation in mice. *Nat Genet.* 2000;25(1):55-57.

22. Schmid RS, Simon JM, Vitucci M, et al. Core pathway mutations induce de-differentiation of murine astrocytes into glioblastoma stem cells that are sensitive to radiation but resistant to temozolomide. *Neuro Oncol.* 2016;18(7):962-973.

23. Sonoda Y, Ozawa T, Hirose Y, et al. Formation of intracranial tumors by genetically modified human astrocytes defines four pathways critical in the development of human anaplastic astrocytoma. *Cancer Res.* 2001;61(13):4956-4960.

24. Huang CH, Mandelker D, Schmidt-Kittler O, et al. The structure of a human p110alpha/p85alpha complex elucidates the effects of oncogenic PI3Kalpha mutations. *Science.* 2007;318(5857):1744-1748.

25. Bader AG, Kang S, Vogt PK. Cancer-specific mutations in PIK3CA are oncogenic in vivo. *Proc Natl Acad Sci U S A.* 2006;103(5):1475-1479.

26. Hanker AB, Pfefferle AD, Balko JM, et al. Mutant PIK3CA accelerates HER2-driven transgenic mammary tumors and induces resistance to combinations of anti-HER2 therapies. *Proc Natl Acad Sci U S A.* 2013;110(35):14372-14377.

27. Koren S, Bentires-Alj M. Mouse models of PIK3CA mutations: one mutation initiates heterogeneous mammary tumors. *FEBS J.* 2013;280(12):2758-2765.

28. Campeau E, Ruhl VE, Rodier F, et al. A versatile viral system for expression and depletion of proteins in mammalian cells. *PLoS One.* 2009;4(8):e6529.

29. Borowicz S, Van Scoyk M, Avasarala S, et al. The soft agar colony formation assay. *J Vis Exp.* 2014(92):e51998.

30. Di Veroli GY, Fornari C, Wang D, et al. Combenefit: an interactive platform for the analysis and visualization of drug combinations. *Bioinformatics.* 2016;32(18):2866-2868.

31. Sunayama J, Matsuda K, Sato A, et al. Crosstalk between the PI3K/mTOR and MEK/ERK pathways involved in the maintenance of self-renewal and tumorigenicity of glioblastoma stem-like cells. *Stem Cells.* 2010;28(11):1930-1939.

32. Giese A, Bjerkvig R, Berens ME, Westphal M. Cost of migration: invasion of malignant gliomas and implications for treatment. *J Clin Oncol.* 2003;21(8):1624-1636.

33. Vanhaesebroeck B, Guillermet-Guibert J, Graupera M, Bilanges B. The emerging mechanisms of isoform-specific PI3K signalling. *Nat Rev Mol Cell Biol.* 2010;11(5):329-341.

34. Prados MD, Byron SA, Tran NL, et al. Toward precision medicine in glioblastoma: the promise and the challenges. *Neuro Oncol.* 2015;17(8):1051-1063.

35. El Meskini R, Iacovelli AJ, Kulaga A, et al. A preclinical orthotopic model for glioblastoma recapitulates key features of human tumors and demonstrates sensitivity to a combination of MEK and PI3K pathway inhibitors. *Dis Model Mech.* 2015;8(1):45-56.

36. See WL, Tan IL, Mukherjee J, Nicolaides T, Pieper RO. Sensitivity of glioblastomas to clinically available MEK inhibitors is defined by neurofibromin 1 deficiency. *Cancer Res.* 2012;72(13):3350-3359.

37. McNeill RS, Canoutas DA, Stuhlmiller TJ, et al. Combination therapy with potent PI3K and MAPK inhibitors overcomes adaptive kinome resistance to single agents in preclinical models of glioblastoma. *Neuro Oncol.* 2017. doi:10.1093/neuonc/nox044

38. Meyer DS, Koren S, Leroy C, et al. Expression of PIK3CA mutant E545K in the mammary gland induces heterogeneous tumors but is less potent than mutant H1047R. *Oncogenesis.* 2013;2:e74.

39. Torti D, Trusolino L. Oncogene addiction as a foundational rationale for targeted anti-cancer therapy: promises and perils. *EMBO Mol Med.* 2011;3(11):623-636.

40. Barouch-Bentov R, Sauer K. Mechanisms of drug resistance in kinases. *Expert Opin Investig Drugs.* 2011;20(2):153-208.

41. Koul D, Fu J, Shen R, et al. Antitumor activity of NVP-BKM120--a selective pan class I PI3 kinase inhibitor showed differential forms of cell death based on p53 status of glioma cells. *Clin Cancer Res.* 2012;18(1):184-195.

42. Maira SM, Pecchi S, Huang A, et al. Identification and characterization of NVP-BKM120, an orally available pan-class I PI3-kinase inhibitor. *Mol Cancer Ther.* 2012;11(2):317-328.

43. Turke AB, Song Y, Costa C, et al. MEK inhibition leads to PI3K/AKT activation by relieving a negative feedback on ERBB receptors. *Cancer Res.* 2012;72(13):3228-3237.

44. Duncan JS, Whittle MC, Nakamura K, et al. Dynamic reprogramming of the kinome in response to targeted MEK inhibition in triple-negative breast cancer. *Cell.* 2012;149(2):307-321.

CHAPTER VI: DISCUSSION

The results described in the previous chapters provide significant insight that should inform future preclinical drug development. They determined how drug potency influences efficacy of single agent and combination treatments with targeted inhibitors of PI3K and MAPK signaling. Furthermore, they helped define how PI3K and MAPK pathway mutations influence response to their inhibition.

In Chapter III, we used a non-germline genetically engineered mouse (nGEM) model of GBM in which PI3K and MAPK signaling are activated in immortalized (T) astrocytes via *Pten* deletion (R) and a constitutively active mutant *Kras* (R, $Kras^{G12D}$) (TRP) and a panel of *EGFR*-amplified patient derived xenografts (PDX). We found that cultured TRP astrocytes and PDX were sensitive to single agent PI3K and MEK inhibitors (PI3Ki and MEKi), and drug potency directly associated with efficacy in these models. However, the extent of sensitivity to MEKi was variable between GBM PDX. We showed that the kinomes of GBM established cell lines (ECL), PDX, and patient samples were highly variable. A subset of GBM patient samples was characterized by widespread of hyper-activation of numerous kinase families, and extensive activation of MAPK signaling. The PI3Ki buparlisib induced dynamic kinome reprogramming of cultured TRP astrocytes, including alternate activation of MAPK signaling. Similarly, multiple MEKi inhibited MAPK and induced PI3K signaling *in vitro*, indicating that PI3K and MAPK signaling are alternative bypass pathways that promote resistance to

inhibition of either pathway alone. Indeed, we found that dual PI3Ki/MEKi treatment was synergistic *in vitro* and effective in subcutaneous TRP allografts, especially when the most potent PI3Ki/MEKi combination (buparlisib/trametinib) was used. However, drug-induced toxicity necessitated a reduction in dose for combination treatments compared to the corresponding single agents, and toxicity was still apparent with the more potent PI3Ki dactolisib. Furthermore, efficacy of the brain penetrant PI3Ki and MEKi, buparlisib and selumetinib alone and in combination was limited in orthotopic TRP allografts, likely due to inefficient target inhibition within the brain. Taken together, these results suggest that increased PI3Ki/MEKi potency enhances efficacy and synergy *in vitro* and *in vivo*, but limited brain penetrance and systemic toxicity reduces the effectiveness of kinase inhibitors when used alone and in combination.

In Chapter IV, we extended the findings described in Chapter III by defining how activation of PI3K and MAPK signaling via deletion of *Pten* and mutant *Kras* influence response to PI3Ki and MEKi *in vitro*. We found that buparlisib induced PI3K inhibition and alternate activation of MAPK signaling regardless of *Pten*/*Kras* mutation status. However, *Pten* deletion and/or mutant *Kras* marginally (<5 fold) increased sensitivity to the PI3Ki LY or buparlisib, but dramatically (5-34 fold) increased sensitivity to the more potent dual PI3Ki/mTORi dactolisib. Furthermore, sensitivity to dactolisib and the mTORi temsirolimus was enhanced in T astrocytes with both *Pten* and *Kras* mutations compared to either alone. *Pten*/*Kras* mutation status also influenced response to MEKi. Mutant *Kras* potentiated MEKi-induced alternate activation of PI3K signaling, and decreased GI_{50}, but not IC_{50}, of the more potent MEKi, PD01 and trametinib. In contrast, *Pten* deletion enhanced MEKi-induced MAPK inhibition, and dramatically increased

MEKi sensitivity independent of *Kras* status. *Pten* deletion and/or mutant *Kras* also enhanced synergy between PI3Ki and MEKi when a less potent MEKi (selumetinib) was used. These results demonstrate that drug potency and activating mutations in PI3K and MAPK signaling interact to influence response to inhibitors of these pathways.

In Chapter V, we used immortalized human astrocytes with (NHA^{RAS}) and without (NHA) mutant *RAS* to define whether *PIK3CA* missense mutations promote gliomagenesis and influence PI3Ki/MEKi response. *PIK3CA* missense mutations, particularly those in the helical and kinase domains, potentiated proximal PI3K signaling and migration of NHA *in vitro*. Furthermore, they cooperated with mutant *RAS* to further promote proximal PI3K signaling *in vitro* and tumorigenesis *in vivo*. $PIK3CA^{mut}$ had little to no effect on PI3Ki or MEKi efficacy in NHA and NHA^{RAS}. We confirmed the findings in the previous chapters by showing that single agent PI3Ki or MEKi caused inhibition of their targeted pathway, activation of the alternate arm of RTK signaling, and functioned synergistically *in vitro*. Interestingly, MEKi-induced PI3K activation was not apparent in $PIK3CA^{WT}$ and $PIK3CA^{mut}$ NHA^{RAS}, suggesting that the combination of ectopic *PIK3CA* expression and mutant RAS may alter the dynamic kinome response to MEKi. Taken together, these results demonstrate that mutations in the helical and kinase domains of *PIK3CA* promote gliomagenesis, but do not enhance sensitivity to single agent PI3Ki.

Multiple PI3K pathway mutations promote gliomagenesis

Large scale sequencing projects, such as TCGA, predict oncogenic drivers based on the frequency of alterations in a given gene.[1-3] These studies are invaluable in identifying the most frequently altered genes and pathways in a disease, and in

characterizing inter-tumor heterogeneity. However, they are correlative by nature and experimental validation of putative driver mutations in animal models is necessary.

The RTK/MAPK/PI3K pathways are mutated in 90% of GBM, and their activation promotes gliomagenesis in mouse models.[2,4-6] RTK activate PI3K and MAPK signaling in normal and tumor cells.[7] The most frequent RTK mutation in GBM, EGFRvIII, preferentially activates PI3K signaling, and EGFR activation cooperates with other "core" pathway mutations to promote gliomagenesis.[8-12] Mutations in canonical PI3K signaling genes, particularly *PIK3R1*, *AKT*, and *PTEN,* have also been validated as oncogenic drivers in gliomas. *PIK3R1* mutations were shown to activate PI3K signaling and promote tumorigenesis in orthotopic xenografts.[13] Although mutations in *AKT* are infrequent in GBM, constitutively active *AKT* mutants are commonly used to model PI3K activation in preclinical glioma models.[14-19] For instance, Sonoda et al. determined that constitutively active *AKT* alone was insufficient to transform NHA, but it cooperated with mutant *RAS* to promote malignant progression.[16,17] *PTEN* is the most frequently mutated canonical PI3K signaling gene, and we and others have extensively characterized its role in gliomagenesis using GEM and nGEM models.[2,4,12,20-23] *Pten* deletion alone does not induce gliomas in adult mice, but cooperates with other "core" pathway mutations, such as mutant *Kras* and ablation of the Rb family members, or deletion of *Rb1* and *TP53*, to promote tumorigenesis.[21,24,25]

Missense mutations in *PIK3CA* frequently occur in GBM. These mutations are heterogeneously distributed across multiple of its protein domains.[2,26,27] Mutations in the helical (E542K and E545K) and kinase (H1047R) domains of *PIK3CA* are the most prevalent in *PIK3CA*-mutated cancers, and they drive tumorigenesis in non-brain

tissues.[26-31] However, the role of *PIK3CA* missense mutations in gliomagenesis had not been experimentally investigated until now. In Chapter V, we found that helical and kinase domain *PIK3CA* missense mutations activate PI3K signaling *in vitro* and cooperate with mutant RAS to promote gliomagenesis in orthotopic xenografts. Interestingly, while both helical and kinase domain *PIK3CA* mutations promoted malignancy of NHA^{RAS} *in vivo*, only kinase mutations induced colony formation of NHA *in vitro*. These results suggest that helical mutations require MAPK activation to promote gliomagenesis. Moreover, they are consistent with the observation that helical *PIK3CA* (p110α) mutants must interact with RAS to activate PI3K signaling and transform chicken embryonic fibroblasts.[32]

We also found that the infrequent R88Q and C90Y mutations in the adaptor-binding domain (ABD) of *PIK3CA* did not activate PI3K signaling or promote gliomagenesis more than ectopic expression of wild-type *PIK3CA* ($PIK3CA^{WT}$) alone.[26,27] However, introduction of the *PIK3CA* mutants into NHA and NHA^{RAS} via lentiviral vectors likely does not fully recapitulate the phenotypic consequences of expression of *PIK3CA* missense mutants under the control of its endogenous promoter. Thus, future studies utilizing CRISPR/Cas9 and GEM with *PIK3CA* missense mutations knocked into its endogenous promoter will be important in further defining the role of individual *PIK3CA* missense mutations in gliomagenesis. Moreover, cellular origin and associating mutations may influence the effects of *PIK3CA* mutations on gliomagenesis, and future work will be focused on answering these questions.

Drug delivery, resistance, and toxicity hinder the development of targeted therapies in GBM

The advent of targeted therapies has led to the rapid expansion of FDA approved cancer treatments.[33] Some of these targeted agents have revolutionized the standard-of-care for certain cancers and greatly improved prognoses, such as imatinib in Philadelphia chromosome-positive chronic myelogenous leukemia (CML).[34,35] However, no targeted therapies have effectively improved survival of GBM patients. One unique challenge in the development of beneficial drugs for brain tumors, including GBM, is the blood-brain barrier (BBB).[36,37] The BBB precludes many anti-cancer agents from accumulating within the brain, leading to poor pharmacodynamics, particularly in diffusely infiltrating GBM cells, and limiting their efficacy.[33,36-38]

In Chapter III, we found that TRP astrocytes and PDX were sensitive to single agent PI3Ki and MEKi *in vitro*.[39] We also found that 5 consecutive days of treatment with PI3Ki or MEKi dramatically reduced growth of subcutaneous TRP tumors for at least 2 weeks. Nevertheless, even the brain penetrant PI3Ki and MEKi, buparlisib and selumetinib respectively, had minor effects on growth of orthotopic TRP allografts.[39-42] Buparlisib and selumetinib poorly inhibited their respective targets within the brain tumors, indicating that there was an insufficient accumulation of these drugs. Thus, even though PI3K/MAPK signaling are effective therapeutic targets in TRP astrocytes, the benefits of PI3Ki and MEKi in the intracranial allografts were likely masked by their limited brain penetrance. Taken together, these results highlight that a major obstacle in preclinical and clinical development of novel therapies for GBM is determining

whether targeted agents have limited efficacy due to ineffective targets or poor pharmacokinetics in the brain.

Intrinsic drug resistance is also a barrier in the development of novel treatments. Preclinical studies demonstrate that single agent kinase inhibitors induce adaptive kinome changes that promote drug resistance.[43-46] Moreover, GBM harbor extensive genetic and phenotypic intratumor heterogeneity, suggesting that divergent subpopulations of cells within a tumor may have different drug sensitivies.[2,38,47-50] Thus, combination therapies will likely be required to effectively treat GBM.[38,51]

In Chapters III-V, we determined that single agent PI3Ki and MEKi treatment inhibited PI3K and MAPK signaling respectively, and potentiated activation of the alternate arm of RTK signaling.[39] We also found that PI3Ki/MEKi were synergistic *in vitro*, and that dual treatment was most effective at inhibiting growth of subcutaneous TRP tumors. However, a frequent challenge in the clinical development of targeted inhibitors, particularly when used in combination, is systemic toxicity.[52,53] In order to avoid toxicity of dual treatments in mice, we reduced the doses of individual PI3Ki/MEKi by up to 50%.[39] Even with this precaution, the PI3Ki/mTORi dactolisib was toxic alone and in combination with the MEKi selumetinib. Furthermore, dual buparlisib/selumetinib treatment was less effective than selumetinib alone in intracranial TRP allografts, likely due to the requisite dose reductions. Toxicity induced by dual PI3Ki/MEKi treatment is also a problem in patients. Clinical investigations showed that the long-term tolerability of dual PI3Ki/MEKi treatment was limited by toxicity in patients with *RAS* or *BRAF* mutant cancers.[52] Taken together, these results suggest that the clinical implementation of targeted drugs in GBM will likely require the development of highly-

brain penetrant drug combinations that do not cause dose-limiting toxicity. Going forward, the achievability of this requirement could be enhanced by using alternate drug delivery methods, such as nanoparticles, or drugs that disrupt the BBB to improve the pharmacokinetics of targeted agents within the brain, while limiting adverse advents.[38,54]

Using mutation status to guide treatment with targeted inhibitors

Predictive biomarkers such as *HER2*, Philadelphia-chromosome, and *BRAF* status in breast cancer, CML, and melanoma respectively, guide the use of many of the most beneficial targeted therapies.[34,35] However, clinical investigations of targeted inhibitors in GBM were largely done in genetically diverse patients.[33,38,55] Even clinical trials evaluating kinase inhibitors in rationally selected GBM patients, such as the mTORi temsirolimus in *PTEN*-null GBM, have had disappointing results.[56]

Preclinical studies may aid in the identification of predictive biomarkers by defining how mutations associated with GBM influence response to targeted kinase inhibitors.[33] We therefore used our previously developed series of nGEM astrocyte cultures in Chapter IV, to determine whether PI3K and MAPK activation via *Pten* deletion and mutant *Kras* influence response to PI3Ki and MEKi.[25] Similar to the observation that *PTEN* status did not correlate with buparlisib efficacy in GBM ECL, we found that *Pten* deletion modestly increased efficacy of the PI3Ki LY and buparlisib. Mutant *Kras* also had minor effects on sensitivity to these drugs. However, *Pten* deletion cooperated with mutant *Kras* to increase efficacy of the dual PI3Ki/mTORi dactolisib and the mTORi temsirolimus. Additionally, *Pten* deletion, but not mutant *Kras*, dramatically increased MEKi efficacy, and the influence of *Pten*/*Kras* mutation status on sensitivity to MEKi was potentiated by increased drug potency. Taken

together, these results demonstrate that drug potency and cooperativity between multiple mutations can influence the impact of oncogenic mutations on drug sensitivity. They also suggest that accounting for both drug potency and cooperating mutations may be advantageous in the design of studies seeking to identify predictive biomarkers.

Our findings in Chapter IV represent a valuable addition to the GBM field by defining how *Pten* deletion and mutant *Kras* influence PI3Ki/MEKi efficacy, but questions remain. Only TRP astrocytes form tumors with high penetrance, short latencies, and uniform growth kinetics when injected into mice.[25] The poor tumorigenicity of T, TP, and TR astrocytes precluded us from determining whether *Pten* deletion increased sensitivity PI3Ki/MEKi in *vivo*. Furthermore, our series of nGEM models are all derived from astrocytes.[25] However, human GBM likely arise from multiple cellular origins. The transcriptomes of the four molecular subtypes defined by TCGA resemble different purified brain cell types.[47] Multiple brain cell types, particularly neural stem cells (NSC), oligodendrocyte precursor cells (OPC), and astrocytes, can be transformed by GBM-associated mutations, and give rise gliomas in GEM.[11,25,57-61] Moreover, cellular origin can affect the impact of oncogenic mutations on tumorigenesis, and thus may influence the role of *Pten* deletion and mutant *Kras* on PI3Ki/MEKi sensitivity. An ongoing project in the Miller lab is the establishment of a large panel of nGEM models in which combinations of frequently occurring GBM mutations, including deletion of *Pten*, *Nf1*, *Cdkn2a*, and *Trp53*, and/or expression of constitutively active *Kras*, *Pik3ca*, *Pdgfra*, and *Egfr* mutants are induced in nGEM astrocytes, OPC, and NSC.[2] Once established, this panel can be used to determine how diverse oncogenic mutations and cellular origins influence PI3Ki/MEKi response.

Using kinome activity to guide treatment with targeted inhibitors

Novel clinical trials designs, such as adaptive and basket trials, utilize the mutation status of one or more genes to guide treatment with targeted inhibitors.[62] One goal of these designs is to increase the efficiency of clinical drug development by prospectively enriching for likely responders.[33,62] However, comparative analyses between genetic mutations and pathway activation in GBM have demonstrated a non-linear relationship between mutation status and protein signaling.[2] This highlights the complex and dynamic signaling in GBM. Moreover, it suggests that analyses of kinome activity will aid in guiding treatment with targeted inhibitors, and could potentially prove more predictive than genomics based assays. Our collaborators in the Johnson lab are testing these hypotheses in a window trial of triple-negative breast cancer patients.[63] They are using multiplexed inhibitor beads-mass spectrometry (MIB-MS) and comparative genomics in the hopes of identifying kinome based biomarkers that predict response to therapy.

In Chapter III, we used MIB-MS based profiling to demonstrate that human GBM samples as well as PDX and ECL models have heterogeneous kinomes. Moreover, we showed that GBM tissue samples can be stratified based on kinome activity, with a subset of patients having hyper-activation of their kinomes, including an enrichment in MAPK signaling. This suggests that these patients will be uniquely sensitive inhibitors of MAPK signaling. Furthermore, we will be evaluating the utility of MIB-MS analyses in predicting drug response by kinome profiling of an integrated panel of nGEM and PDX models with diverse mutations. We will then use the kinome activity of these preclinical models to direct treatment of single agent and combination therapies in specific disease

subsets. Taken together, the results of this project will help validate the utility of kinome activation status to predict drug response, and aid in the development of rationally designed treatments.

Predicting PI3Ki/MEKi efficacy based on the specific PI3K pathway mutation

As discussed above, in Chapter IV, we utilized our T(RP) series of nGEM astrocyte cultures to determine how *Pten* deletion and mutant *Kras* influence response to PI3Ki/MEKi. We expanded these finding in Chapter V by defining whether *PIK3CA* missense mutations influence response of NHA and NHA^{RAS} to PI3Ki/MEKi *in vitro*. *Pten* deletion minimally increased buparlisib efficacy in the T(RP) astrocyte series, while *PIK3CA* missense mutations in NHA and NHA^{RAS} did not. Wild-type *TP53,* but not loss of *PTEN*, has been shown to correlate with a slight increase in sensitivity to buparlisib in GBM ECL.[64] *TP53* is inhibited in NHA and NHA^{RAS} lines, but not in the T(RP) series.[17,25] Therefore, differences in *TP53* status may be affecting PI3Ki response in these model systems, and thus causing the differential effects between *Pten* deletion and *PIK3CA* mutations on buparlisib efficacy that we observed. Moreover, we found that *Pten* deletion and mutant *Kras* cooperated to increase efficacy of the dual PI3Ki/mTORi dactolisib and the mTORi temsirolimus. Whether *PIK3CA* missense mutations increase sensitivity to dactolisib or temsirolimus is unknown and is currently under investigation within the Miller lab.

In Chapters IV and V, we also showed that mutant *RAS* did not affect efficacy of the MEKi selumetinib in T astrocytes and NHA. In contrast, *Pten* deletion dramatically increased sensitivity to MEKi in the T(RP) astrocyte series, while *PIK3CA* missense mutations in NHA and NHA^{RAS} ($NHA^{\pm RAS}$) did not. There are a few potential reasons for

this disparity between *Pten* deletion and *PIK3CA* missense mutations in the T(RP) and NHA$^{\pm RAS}$ models, respectively. One reason may be species-specific differences in the effects of PI3K activation on MEKi efficacy.

Another reason may be that activating *PIK3CA* mutations and deletion of *Pten* have divergent impacts on PI3K signaling. The p110α and p110β isoforms of the catalytic subunit of PI3K (encoded by *PIK3CA* and *PIK3CB* respectively), differentially respond to upstream proteins, particularly RTK, GPCR, and RAS.[7] In preclinical models of multiple cancer types, including GBM, *Pten* deletion activates PI3K signaling and promotes tumorigenesis via p110β, not p110α.[7,65-67] However, the reliance on p110β in *Pten*-null cells is influenced by cellular origin and cooperating mutations.[68,69] *PIK3CA* mutations and deletion of *Pten* can also have divergent effects on downstream signaling. Vasudevan et al. showed that AKT is highly activated in *PTEN*-null cells from multiple cancer types and breast tumors.[70] They also demonstrated that *Pten*-null cells rely on AKT activation for tumorigenicity. In contrast, AKT activation was generally less robust in *PIK3CA*-mutant cells and tumors, and *PIK3CA* mutant cells were less dependent on AKT.[70] Moreover, *PIK3CA*-mutant cells highly expressed PDK1 and were reliant upon PDK1-dependent singling for tumorigenicity. Taken together, these data suggest that *PTEN* deletion and mutant *PIK3CA* may have divergent effects on PI3K signaling, and thus may differentially affect sensitivity to targeted inhibitors.

PTEN deletion and *PIK3CA* mutations could also have divergent impacts on response to targeted inhibitors due to the PI3K-independent nuclear functions of *PTEN*. Besides *PTEN*'s well characterized cytoplasmic role in antagonizing PI3K signaling, it also has important nuclear functions in chromosome stability, DNA repair, and cell cycle

arrest.[71] At this time, it is unclear whether the PI3K-dependent or independent functions of *Pten* contribute to the increased efficacy of MEKi in the T(RP) astrocyte series.

Future work will seek to answer the important mechanistic questions discussed above. To this end, we will knockout-*PTEN* using shRNA in NHA and NHA^{RAS}, and introduce constitutively active *PIK3CA* missense mutations into T and TR astrocytes. Comparisons between the effects of *Pten* deletion and *PIK3CA* mutations in both of these model systems will enable us to determine whether our disparate findings on MEKi efficacy were due to species-specific differences or divergent consequences of these PI3K pathway mutations. Furthermore, if *PTEN*-loss uniquely sensitives the T(RP) astrocyte series and NHA$^{\pm RAS}$ to MEKi, we will then assess MEKi efficacy in *PTEN*-null cells reconstituted with *PTEN* mutants lacking either phosphatase or nuclear activity.[71] Comparisons of MEKi efficacy in these cells will enable us to determine whether *PTEN*-loss influences response to MAPK inhibition via PTEN's PI3K-dependent or independent functions.

Conclusions

In the work above, we use PDX, genetically modified normal human astrocytes, and nGEM to evaluate efficacy to single agent and combination treatments with PI3Ki/MEKi. Furthermore, we defined how PI3K and MAPK pathway mutations influence response to these drugs. These studies provide a valuable platform to functionally validate whether cellular origin and other PI3K/MAPK mutations influence response to targeted inhibitors. Additionally, the knowledge gained here will facilitate future preclinical testing of combination therapies and predictive biomarkers.

REFERENCES

1. Tomczak K, Czerwinska P, Wiznerowicz M. The Cancer Genome Atlas (TCGA): an immeasurable source of knowledge. *Contemp Oncol (Pozn).* 2015;19(1A):A68-77.

2. Brennan CW, Verhaak RG, McKenna A, et al. The somatic genomic landscape of glioblastoma. *Cell.* 2013;155(2):462-477.

3. Ciriello G, Gatza ML, Beck AH, et al. Comprehensive molecular portraits of invasive lobular breast cancer. *Cell.* 2015;163(2):506-519.

4. Schmid RS, Vitucci M, Miller CR. Genetically engineered mouse models of diffuse gliomas. *Brain Res Bull.* 2012;88(1):72-79.

5. Huszthy PC, Daphu I, Niclou SP, et al. In vivo models of primary brain tumors: pitfalls and perspectives. *Neuro Oncol.* 2012;14(8):979-993.

6. Chow LM, Baker SJ. Capturing the molecular and biological diversity of high-grade astrocytoma in genetically engineered mouse models. *Oncotarget.* 2012;3(1):67-77.

7. Thorpe LM, Yuzugullu H, Zhao JJ. PI3K in cancer: divergent roles of isoforms, modes of activation and therapeutic targeting. *Nat Rev Cancer.* 2015;15(1):7-24.

8. Li B, Yuan M, Kim IA, Chang CM, Bernhard EJ, Shu HK. Mutant epidermal growth factor receptor displays increased signaling through the phosphatidylinositol-3 kinase/AKT pathway and promotes radioresistance in cells of astrocytic origin. *Oncogene.* 2004;23(26):4594-4602.

9. Choe G, Horvath S, Cloughesy TF, et al. Analysis of the phosphatidylinositol 3'-kinase signaling pathway in glioblastoma patients in vivo. *Cancer Res.* 2003;63(11):2742-2746.

10. Gan HK, Cvrljevic AN, Johns TG. The epidermal growth factor receptor variant III (EGFRvIII): where wild things are altered. *FEBS J.* 2013;280(21):5350-5370.

11. Bachoo RM, Maher EA, Ligon KL, et al. Epidermal growth factor receptor and Ink4a/Arf: convergent mechanisms governing terminal differentiation and transformation along the neural stem cell to astrocyte axis. *Cancer Cell.* 2002;1(3):269-277.

12. Li L, Dutra A, Pak E, et al. EGFRvIII expression and PTEN loss synergistically induce chromosomal instability and glial tumors. *Neuro Oncol.* 2009;11(1):9-21.

13. Quayle SN, Lee JY, Cheung LW, et al. Somatic mutations of PIK3R1 promote gliomagenesis. *PLoS One.* 2012;7(11):e49466.

14. Holland EC, Celestino J, Dai C, Schaefer L, Sawaya RE, Fuller GN. Combined activation of Ras and Akt in neural progenitors induces glioblastoma formation in mice. *Nat Genet.* 2000;25(1):55-57.

15. Hu X, Pandolfi PP, Li Y, Koutcher JA, Rosenblum M, Holland EC. mTOR promotes survival and astrocytic characteristics induced by Pten/AKT signaling in glioblastoma. *Neoplasia.* 2005;7(4):356-368.

16. Sonoda Y, Ozawa T, Aldape KD, Deen DF, Berger MS, Pieper RO. Akt pathway activation converts anaplastic astrocytoma to glioblastoma multiforme in a human astrocyte model of glioma. *Cancer Res.* 2001;61(18):6674-6678.

17. Sonoda Y, Ozawa T, Hirose Y, et al. Formation of intracranial tumors by genetically modified human astrocytes defines four pathways critical in the development of human anaplastic astrocytoma. *Cancer Res.* 2001;61(13):4956-4960.

18. Uhrbom L, Dai C, Celestino JC, Rosenblum MK, Fuller GN, Holland EC. Ink4a-Arf loss cooperates with KRas activation in astrocytes and neural progenitors to generate glioblastomas of various morphologies depending on activated Akt. *Cancer Res.* 2002;62(19):5551-5558.

19. Lindberg N, Jiang Y, Xie Y, et al. Oncogenic signaling is dominant to cell of origin and dictates astrocytic or oligodendroglial tumor development from oligodendrocyte precursor cells. *J Neurosci.* 2014;34(44):14644-14651.

20. Schmid RS, Simon JM, Vitucci M, et al. Core pathway mutations induce de-differentiation of murine astrocytes into glioblastoma stem cells that are sensitive to radiation but resistant to temozolomide. *Neuro Oncol.* 2016;18(7):962-973.

21. Chow LM, Endersby R, Zhu X, et al. Cooperativity within and among Pten, p53, and Rb pathways induces high-grade astrocytoma in adult brain. *Cancer Cell.* 2011;19(3):305-316.

22. Song Y, Zhang Q, Kutlu B, et al. Evolutionary etiology of high-grade astrocytomas. *Proc Natl Acad Sci U S A.* 2013;110(44):17933-17938.

23. Kim HS, Woolard K, Lai C, et al. Gliomagenesis arising from Pten- and Ink4a/Arf-deficient neural progenitor cells is mediated by the p53-Fbxw7/Cdc4 pathway, which controls c-Myc. *Cancer Res.* 2012;72(22):6065-6075.

24. Song MS, Salmena L, Pandolfi PP. The functions and regulation of the PTEN tumour suppressor. *Nat Rev Mol Cell Biol.* 2012;13(5):283-296.

25. Vitucci M, Karpinich NO, Bash RE, et al. Cooperativity between MAPK and PI3K signaling activation is required for glioblastoma pathogenesis. *Neuro Oncol.* 2013;15(10):1317-1329.

26. Cerami E, Gao J, Dogrusoz U, et al. The cBio cancer genomics portal: an open platform for exploring multidimensional cancer genomics data. *Cancer Discov.* 2012;2(5):401-404.

27. Gao J, Aksoy BA, Dogrusoz U, et al. Integrative Analysis of Complex Cancer Genomics and Clinical Profiles Using the cBioPortal. Sci Signal. 2013;6(269):pl1.

28. Bader AG, Kang S, Vogt PK. Cancer-specific mutations in PIK3CA are oncogenic in vivo. *Proc Natl Acad Sci U S A.* 2006;103(5):1475-1479.

29. Hanker AB, Pfefferle AD, Balko JM, et al. Mutant PIK3CA accelerates HER2-driven transgenic mammary tumors and induces resistance to combinations of anti-HER2 therapies. *Proc Natl Acad Sci U S A.* 2013;110(35):14372-14377.

30. Koren S, Bentires-Alj M. Mouse models of PIK3CA mutations: one mutation initiates heterogeneous mammary tumors. *FEBS J.* 2013;280(12):2758-2765.

31. Meyer DS, Koren S, Leroy C, et al. Expression of PIK3CA mutant E545K in the mammary gland induces heterogeneous tumors but is less potent than mutant H1047R. *Oncogenesis.* 2013;2:e74.

32. Zhao L, Vogt PK. Helical domain and kinase domain mutations in p110alpha of phosphatidylinositol 3-kinase induce gain of function by different mechanisms. *Proc Natl Acad Sci U S A.* 2008;105(7):2652-2657.

33. McNeill RS, Vitucci M, Wu J, Miller CR. Contemporary murine models in preclinical astrocytoma drug development. *Neuro Oncol.* 2015;17(1):12-28.

34. Torti D, Trusolino L. Oncogene addiction as a foundational rationale for targeted anti-cancer therapy: promises and perils. *EMBO Mol Med.* 2011;3(11):623-636.

35. Pagliarini R, Shao W, Sellers WR. Oncogene addiction: pathways of therapeutic response, resistance, and road maps toward a cure. *EMBO Rep.* 2015;16(3):280-296.

36. van Tellingen O, Yetkin-Arik B, de Gooijer MC, Wesseling P, Wurdinger T, de Vries HE. Overcoming the blood-brain tumor barrier for effective glioblastoma treatment. *Drug Resist Updat.* 2015;19:1-12.

37. Agarwal S, Sane R, Oberoi R, Ohlfest JR, Elmquist WF. Delivery of molecularly targeted therapy to malignant glioma, a disease of the whole brain. *Expert Rev Mol Med.* 2011;13:e17.

38. Prados MD, Byron SA, Tran NL, et al. Toward precision medicine in glioblastoma: the promise and the challenges. *Neuro Oncol.* 2015;17(8):1051-1063.

39. McNeill RS, Canoutas DA, Stuhlmiller TJ, et al. Combination therapy with potent PI3K and MAPK inhibitors overcomes adaptive kinome resistance to single agents in preclinical models of glioblastoma*. Neuro Oncol*. 2017. doi:10.1093/neuonc/nox044

40. Maira SM, Pecchi S, Huang A, et al. Identification and characterization of NVP-BKM120, an orally available pan-class I PI3-kinase inhibitor. *Mol Cancer Ther.* 2012;11(2):317-328.

41. El Meskini R, Iacovelli AJ, Kulaga A, et al. A preclinical orthotopic model for glioblastoma recapitulates key features of human tumors and demonstrates sensitivity to a combination of MEK and PI3K pathway inhibitors. *Dis Model Mech.* 2015;8(1):45-56.

42. Chen HY, Yang YM, Han R, Noble M. MEK1/2 inhibition suppresses tamoxifen toxicity on CNS glial progenitor cells. *J Neurosci.* 2013;33(38):15069-15074.

43. Duncan JS, Whittle MC, Nakamura K, et al. Dynamic reprogramming of the kinome in response to targeted MEK inhibition in triple-negative breast cancer. *Cell.* 2012;149(2):307-321.

44. Stuhlmiller TJ, Miller SM, Zawistowski JS, et al. Inhibition of lapatinib-induced kinome reprogramming in ERBB2-positive breast cancer by targeting BET family bromodomains. *Cell Rep.* 2015;11(3):390-404.

45. Turke AB, Song Y, Costa C, et al. MEK inhibition leads to PI3K/AKT activation by relieving a negative feedback on ERBB receptors. *Cancer Res.* 2012;72(13):3228-3237.

46. Sunayama J, Matsuda K, Sato A, et al. Crosstalk between the PI3K/mTOR and MEK/ERK pathways involved in the maintenance of self-renewal and tumorigenicity of glioblastoma stem-like cells. *Stem Cells.* 2010;28(11):1930-1939.

47. Verhaak RG, Hoadley KA, Purdom E, et al. Integrated genomic analysis identifies clinically relevant subtypes of glioblastoma characterized by abnormalities in PDGFRA, IDH1, EGFR, and NF1. *Cancer Cell.* 2010;17(1):98-110.

48. Sottoriva A, Spiteri I, Piccirillo SG, et al. Intratumor heterogeneity in human glioblastoma reflects cancer evolutionary dynamics. *Proc Natl Acad Sci U S A.* 2013;110(10):4009-4014.

49. Snuderl M, Fazlollahi L, Le LP, et al. Mosaic amplification of multiple receptor tyrosine kinase genes in glioblastoma. *Cancer Cell.* 2011;20(6):810-817.

50. Huang Z, Cheng L, Guryanova OA, Wu Q, Bao S. Cancer stem cells in glioblastoma--molecular signaling and therapeutic targeting. *Protein Cell.* 2010;1(7):638-655.

51. Wen PY, Lee EQ, Reardon DA, Ligon KL, Alfred Yung WK. Current clinical development of PI3K pathway inhibitors in glioblastoma. *Neuro Oncol.* 2012;14(7):819-829.

52. Bedard PL, Tabernero J, Janku F, et al. A phase Ib dose-escalation study of the oral pan-PI3K inhibitor buparlisib (BKM120) in combination with the oral MEK1/2 inhibitor trametinib (GSK1120212) in patients with selected advanced solid tumors. *Clin Cancer Res.* 2015;21(4):730-738.

53. Rodon J, Dienstmann R, Serra V, Tabernero J. Development of PI3K inhibitors: lessons learned from early clinical trials. *Nat Rev Clin Oncol.* 2013;10(3):143-153.

54. Zamboni WC, Torchilin V, Patri AK, et al. Best practices in cancer nanotechnology: perspective from NCI nanotechnology alliance. *Clin Cancer Res.* 2012;18(12):3229-3241.

55. Cloughesy TF, Cavenee WK, Mischel PS. Glioblastoma: from molecular pathology to targeted treatment. *Annu Rev Pathol.* 2014;9:1-25.

56. Cloughesy TF, Yoshimoto K, Nghiemphu P, et al. Antitumor activity of rapamycin in a Phase I trial for patients with recurrent PTEN-deficient glioblastoma. *PLoS Med.* 2008;5(1):e8.

57. Galvao RP, Kasina A, McNeill RS, et al. Transformation of quiescent adult oligodendrocyte precursor cells into malignant glioma through a multistep reactivation process. *Proc Natl Acad Sci U S A.* 2014;111(40):E4214-4223.

58. Irvin DM, McNeill RS, Bash RE, Miller CR. Intrinsic astrocyte heterogeneity influences tumor growth in glioma mouse models. *Brain Pathol.* 2017;27(1):36-50.

59. Chen J, McKay RM, Parada LF. Malignant glioma: lessons from genomics, mouse models, and stem cells. *Cell.* 2012;149(1):36-47.

60. Uhrbom L, Kastemar M, Johansson FK, Westermark B, Holland EC. Cell type-specific tumor suppression by Ink4a and Arf in Kras-induced mouse gliomagenesis. *Cancer Res.* 2005;65(6):2065-2069.

61. Alcantara Llaguno S, Chen J, Kwon CH, et al. Malignant astrocytomas originate from neural stem/progenitor cells in a somatic tumor suppressor mouse model. *Cancer Cell.* 2009;15(1):45-56.

62. Renfro LA, Mallick H, An MW, Sargent DJ, Mandrekar SJ. Clinical trial designs incorporating predictive biomarkers. *Cancer Treat Rev.* 2016;43:74-82.

63. Stuhlmiller TJ, Earp HS, Johnson GL. Adaptive reprogramming of the breast cancer kinome. *Clin Pharmacol Ther.* 2014;95(4):413-415.

64. Koul D, Fu J, Shen R, et al. Antitumor activity of NVP-BKM120--a selective pan class I PI3 kinase inhibitor showed differential forms of cell death based on p53 status of glioma cells. *Clin Cancer Res.* 2012;18(1):184-195.

65. Chen H, Mei L, Zhou L, et al. PTEN restoration and PIK3CB knockdown synergistically suppress glioblastoma growth in vitro and in xenografts. *J Neurooncol.* 2011;104(1):155-167.

66. Wee S, Wiederschain D, Maira SM, et al. PTEN-deficient cancers depend on PIK3CB. *Proc Natl Acad Sci U S A.* 2008;105(35):13057-13062.

67. Jia S, Liu Z, Zhang S, et al. Essential roles of PI(3)K-p110beta in cell growth, metabolism and tumorigenesis. *Nature.* 2008;454(7205):776-779.

68. Berenjeno IM, Guillermet-Guibert J, Pearce W, Gray A, Fleming S, Vanhaesebroeck B. Both p110alpha and p110beta isoforms of PI3K can modulate the impact of loss-of-function of the PTEN tumour suppressor. *Biochem J.* 2012;442(1):151-159.

69. Schmit F, Utermark T, Zhang S, et al. PI3K isoform dependence of PTEN-deficient tumors can be altered by the genetic context. *Proc Natl Acad Sci U S A.* 2014;111(17):6395-6400.

70. Vasudevan KM, Barbie DA, Davies MA, et al. AKT-independent signaling downstream of oncogenic PIK3CA mutations in human cancer. *Cancer Cell.* 2009;16(1):21-32.

71. Planchon SM, Waite KA, Eng C. The nuclear affairs of PTEN. *J Cell Sci.* 2008;121(Pt 3):249-253.